Production of fungal lipids

Kinetic modeling and process design

Thesis committee

Thesis supervisor
Prof. dr. ir. J. Tramper
Professor, Bioprocess Engineering, Wageningen University

Thesis co-supervisor
Dr. ir. A. Rinzema
Assistant professor, Bioprocess Engineering, Wageningen University

Other members
Prof. dr. J.P.M. Sanders
Wageningen University

Dr. S. Papanikolaou
Agricultural University of Athens, Greece

Prof. dr. J.J. Heijnen
Delft University of Technology

Dr. R.P. de Vries
Utrecht University and CBS Fungal Biodiversity Center, Utrecht

This research was conducted under the auspices of the Graduate school VLAG

Production of fungal lipids

Kinetic modeling and process design

Petra Meeuwse

Submitted in fulfillment of the requirements for the degree of doctor
at Wageningen University
by the authority of the Rector Magnificus
Prof. dr. M.J. Kropff,
in the presence of the
Thesis committee appointed by the Academic Board
to be defended in public
on Wednesday 30 November 2011
at 4 p.m. in the Aula.

Petra Meeuwse
Production of fungal lipids – Kinetic modeling and process design
240 pages

PhD Thesis, Wageningen University, Wageningen, The Netherlands (2011)
With propositions and summaries in Dutch and English

ISBN: 978-94-6173-093-0

Contents

Chapter 1

Introduction

Transport fuels from renewable sources

The search for alternatives for fossil fuels is currently a hot topic. This search is initiated for different reasons, such as a possible scarcity of fossil fuels in the future, becoming independent from oil-producing countries, or reduction of the CO_2-concentration in the atmosphere. For the production of transport fuels, biomass such as plant material or microorganisms is considered as most important raw material. First-generation biofuels are produced from feedstock such as corn, grain or vegetable oil, and therefore compete with food applications. Second-generation biofuels use non-edible biomass or agricultural waste as feedstock.

The two most studied biofuels are bioethanol and biodiesel. First-generation bioethanol is already produced on a large scale in different parts of the world (Walker 2011). Second-generation bioethanol production, however, still struggles with problems. Firstly because wild-type yeast cannot utilize all sugars in many of the substrates, and secondly because the high content of lignin in many of the substrates reduces biodegradability. Both problems are currently addressed by research on genetically modified yeasts and substrate pretreatment (Walker 2011). First-generation biodiesel is currently produced from vegetable oil and waste fats by transesterification. Second-generation biodiesel can be produced from oils accumulated by microorganisms such as yeasts, fungi or algae (Li et al. 2008, Feofilova et al. 2009, Meng et al. 2009). Production of biodiesel from algae is an important research topic now, and development towards large-scale production has started (Wijffels and Barbosa 2010). Production of biodiesel from yeasts and fungi is mentioned in literature as being promising (Angerbauer et al. 2008, Zhu et al. 2008), but an integrated approach towards an efficient process is not available yet. This thesis provides some essential steps of this approach by focusing on growth and lipid accumulation kinetics of the oleaginous fungus *Umbelopsis isabellina* in submerged and solid-state fermentation.

Lipids from lipid-accumulating fungi

Many organisms can store carbon in the form of lipids as a reserve energy source, among which plants, algae, yeasts, fungi, bacteria and animals. Microorganisms that store more than 20% of their cell dry weight in lipids are called oleaginous microorganisms; accumulation up to 80% has been observed (Ratledge and Wilkinson, 1989). The focus in this thesis is on lipid accumulation in fungi, because

filamentous fungi are among the microorganisms with the highest lipid fractions, and because they are the most suitable for the solid-state fermentation system we studied.

Lipid accumulation in fungi occurs when the C-source is available while growth is limited by another substrate. Usually the N-source is limited, although lipid accumulation because of limitation of other nutrients has also been described (Gill et al. 1977). A chain of biochemical events leads to lipid accumulation in oleaginous fungi during N-limitation, as was described in detail by Wynn et al. (2001). Some key enzymes in this process were identified (Wynn et al. 2001), but this did not lead so far to creation of high producing strains by genetic modification (Beopoulos et al. 2011).

Lipid accumulation in yeasts and fungi has mainly been studied because these organisms often produce poly-unsaturated fatty acids (Certik and Shimizu 1999). For example, the only commercially available process to produce arachidonic acid (C20:4), used in infant nutrition, uses the fungus *Mortierella alpina* (Ratledge 2004). Only recently, lipids from fungi have gained interest for biodiesel production (Li et al. 2008, Feofilova et al. 2009, Meng et al. 2009). Also the use of renewable substrates has become more important in research (Papanikolaou et al. 2007, Angerbauer et al. 2008, Peng and Chen 2008, Vamvakaki et al. 2010). Both submerged fermentation and solid-state fermentation can be used for fungal culture; both culture systems are explained below.

Submerged fermentation

In submerged fermentation (SmF), microorganisms are cultured in a liquid medium. SmF is used widely because the process is easy to handle. Control of temperature, pH and concentrations is easy as mass and heat transport are fast. Because most fungi need oxygen to grow and produce lipids, oxygen has to be transferred to the liquid to reach the fungi. This is usually done by shaking (in shake flasks at very small scale) or by stirring and aeration. When using fungi in SmF, the hyphae can cause the viscosity to increase dramatically, thereby decreasing mass transfer rates and increasing energy requirements for oxygen transfer (Van 't Riet and Tramper 1991). This can be prevented by growing the fungus in pellets, although this causes oxygen transfer problems inside the pellets.

Submerged fermentation can be carried out in different modes of operation. In batch culture, all substrate is added at the start of the culture. In continuous culture, a substrate solution is added continuously, while broth is removed continuously at the same rate, thereby keeping the volume of the culture constant. When this is done for a certain time with the same feed rate, the culture reaches a steady state, in which the contents of the culture do not change in time. In that case, the continuous culture is called a chemostat.

Solid-state fermentation

Solid-state fermentation (SSF) is the cultivation of a microorganism, usually a filamentous fungus, on wet solid particles without free flowing water. The fungus grows on the surface of the substrate particles, and produces enzymes to break down the substrate to release monomers. Both the enzymes as well as the monomers are transported by diffusion in the solid particles; oxygen is directly taken up from the air. Solid-state fermentation has several advantages compared to submerged fermentation. Many fungi grow and produce better in SSF because it is their 'natural' habitat, products are easier to recover because they are not diluted, less waste water is produced and SSF processes are often cheaper than their SmF counterparts (Pandey 2003, Holker and Lenz 2005, Bhargav et al. 2008). However, SSF also has disadvantages. Because the substrate consists of particles, transport by diffusion can cause gradients inside the particles, which can slow down reactions. Furthermore, heat generated during the cultivation is hard to remove because the solid particles with air in-between usually conduct heat very poorly.

SSF is usually carried out as a batch culture. There are different bioreactor types available, both on small scale and large scale. The simplest type is a tray reactor, which is simply a layer of solid substrate in a tray. Because no active aeration is applied, the layer can only be thin to avoid overheating in the layer. Therefore, the aerated packed bed reactor is more commonly used, in which heat is removed by active aeration. Also different mixed bioreactors are available, such as rotating drums and stirred beds (Mitchell et al. 2006).

Outline of the thesis

The aim of this thesis is to provide the first steps in the development of a process for fungal lipid production on renewable substrates. The focus of the work is on gaining insight in the kinetics of growth and lipid production of oleaginous fungi under different circumstances. Solid-state fermentation was chosen for the production process to be developed, because most available substrates are solid and it is less expensive than submerged fermentation.

The development of this process was started by choosing a model fungus that is not necessarily the best fungus for this process, but that can produce lipids and is capable of utilizing different polymer materials that can be used as substrate for this process. **Chapter 2** describes the research on two lipid-producing fungi, *Mortierella alpina* and *Umbelopsis isabellina*, that were tested for growth on different monomer and polymer substrates, and on the agricultural waste product sugar beet pulp. Because *U. isabellina* appeared to grow best on the tested substrates, it was chosen as model organism in this thesis.

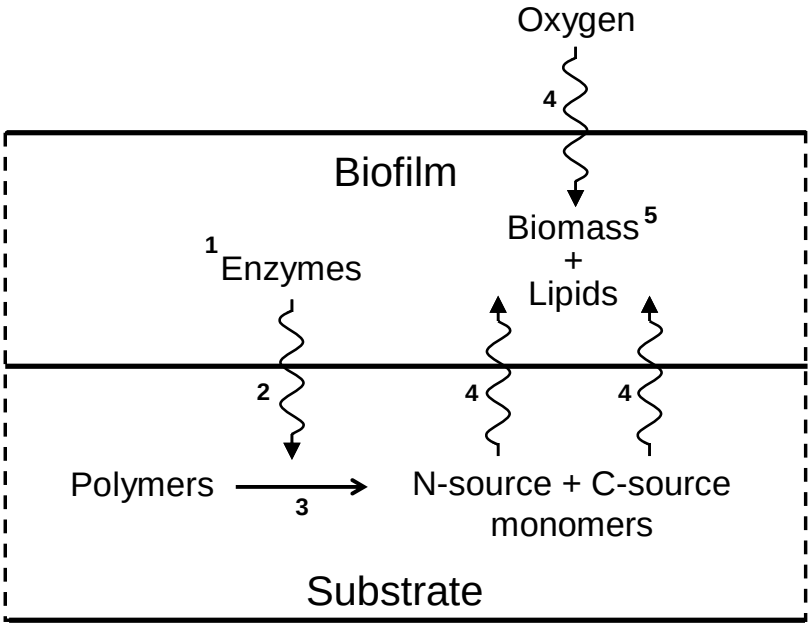

Figure 1: Schematic overview of a fungal biofilm growing on a solid substrate with the main chemical and physical processes outlined.

The next step in this research was to try to understand the complete process of lipid production by fungi in solid-state fermentation. We tried to achieve this by developing mathematical models that describe the physiology of the fungal cells as well as the physical and chemical properties of the substrate and the fungal biofilm. Figure 1 shows the different steps that are present in the process. These steps are:

1. production of hydrolyzing enzymes by the fungus
2. diffusion of enzymes to the substrate
3. hydrolysis of the substrate polymers to monomers
4. diffusion of monomers to the fungus and diffusion of oxygen to the fungus
5. conversion of the substrates into biomass and lipids

Although it is the last step of the process, the first focus was on step 5, because this is the step where the actual product formation is accomplished. Figure 2 shows a schematic overview of a fungal cell with the physiological processes considered in our models on metabolism. The influence of the availability of the C-source and N-source was first studied in submerged fermentation in a steady-state situation (chemostat culture) with constant supply of both substrates (Chapter 3 and 4) and subsequently in a dynamic situation (batch culture) with depletion of the substrates (Chapter 5). In a model SSF system, the influence of oxygen was considered together with step 4 from Figure 1 (Chapter 6). Steps 1-3 are only theoretically discussed in Chapter 7.

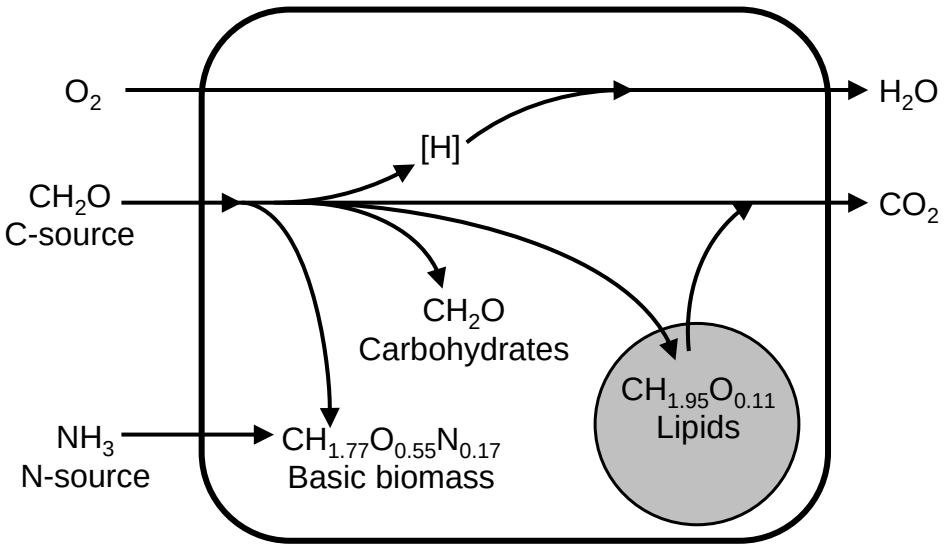

Figure 2: Schematic overview of the physiological processes inside the fungal cell considered during modeling of the metabolism.

Chapter 3 describes a model for growth and lipid production in submerged chemostat culture, in which oxygen was present in abundance, but the C-source and the N-source supply rates were varied by varying the dilution rate as well as the substrate concentrations in the feed. Because of practical problems such as formation of aggregates at low dilution rates, not all combinations of C-source and N-source supply rates could be used in our experiments with *U. isabellina*; therefore, the model was also validated with several data sets for oleaginous yeasts from literature, which is shown in **Chapter 4**.

Chapter 5 describes a dynamic model for submerged batch culture, in which the N-source becomes exhausted before the C-source. In this case, growth and lipid production do not occur simultaneously as in chemostat culture, but consequently. The model and the described experiments show that this leads to metabolic differences between chemostat and batch culture.

In **Chapter 6**, step 4 from Figure 1 was also included. κ-Carrageenan gel plates with glucose and alanine as C-source and N-source monomers were used as a model system. Diffusion of these substrates as well as oxygen was included in the developed model. Different substrate limitations occurred not only in time, but also in space in the growing biofilm. Steps 1, 2 and 3 were not included in this model, but are based on the same diffusion principles and can be added in a similar model.

In **Chapter 7**, the models from Chapters 3, 5 and 6 were combined with basic engineering principles to calculate lipid yield and energy consumption in lipid production processes in both submerged and solid-state fermentation with sugar beet pulp as substrate. This process design shows that still quite some work has to be done to make microbial lipids tomorrow's source of biodiesel, but that the possibilities look promising.

Chapter 2

Utilization of agro-industrial waste components by *Mortierella alpina* and *Umbelopsis isabellina*

Abstract

Lipid accumulating fungi may offer possibilities to convert organic wastes to lipids, which can be converted to biodiesel. Efficient conversion of a range of waste components is a prerequisite. We cultivated the oleaginous fungi *M. alpina* and *U. isabellina* on agar plates containing glucose, xylose, starch, cellulose or pectin, and on sugar beet pulp in a packed bed. *M. alpina* did not utilize xylose, cellulose and pectin, utilized starch much slower than glucose and only consumed approximately 40% of the sugar beet pulp in 20 days. This shows that *M. alpina* is not a suitable organism for lipid production. *U. isabellina* utilized pectin and xylose with the same rate as glucose, but used starch slower and pure cellulose not at all. It consumed approximately 75% of the sugar beet pulp after 8 days and approximately 100% after 20 days. Also, it accumulated some lipids (3% of remaining dry mass) in the culture on sugar beet pulp; optimization of this process increased the lipid content to 9% of remaining dry mass. This shows that *U. isabellina* is a promising strain for lipid production from agro-industrial waste.

Introduction

Lipid accumulating fungi may offer possibilities to convert organic wastes to lipids, which can be converted to biodiesel. They have been studied for years (Certik and Shimizu 1999), aiming primarily at poly-unsaturated fatty acids. Most research was done in submerged fermentation (SmF) with easily degradable carbon sources and limited supply of nitrogen source. This approach is suitable for the production of high-value products, but cheaper processes and substrates are needed to produce biodiesel precursors. One possibility is to use solid-state fermentation (SSF) with agro-industrial waste. This would require fungi capable of converting various sugars and other monomers present in organic waste, and preferably also of hydrolyzing the corresponding biopolymers.

In this chapter, we describe the cultivation of the lipid-accumulating fungi *Mortierella alpina* and *Umbelopsis isabellina* (formerly known as *Mortierella isabellina* (Meyer and Gams 2003)) on several polymers and monomers, and on sugar beet pulp. Both fungi can accumulate lipids up to high percentages of their cell dry weight: *M. alpina* can reach up to 50% (Shinmen et al. 1989) and *U. isabellina* up to 55% (Papanikolaou et al. 2004a). In SmF, *M. alpina* converted several hexose monomers, oligomers and polymers successfully (Shinmen et al. 1989, Stredanska and Sajbidor 1993, Botha et al. 1997, Chen et al. 1997, Jang et al. 2005), but ribose was converted slowly and arabinose and xylose were not converted (Botha et al. 1997). *M. alpina* has been tested in SSF on grain (Stredanska et al. 1993) and agro-industrial waste (Jang et al. 2000), but the results do not clearly show its potential for growth, efficient substrate conversion and lipid accumulation. *U. isabellina* has been shown to grow on a large diversity of substrates in submerged culture, among which starch, pectin, xylose, fructose, saccharose, and the mixtures molasses and sweet sorghum extract, although with different biomass and lipid yields (Papanikolaou et al. 2007, Fakas et al. 2009b, Chatzifragkou et al. 2010, Economou et al. 2011). It has also successfully been cultivated in SSF on pear pomace and sweet sorghum (Economou et al. 2010, Fakas et al. 2009a).

Preliminary results obtained in our lab (Meeuwse, not published) showed poor growth of *M. alpina* on a highly concentrated starch gel, which initiated the research described in this paper. This was in contradiction with published results (Stredanska and Sajbidor 1993, Botha et al. 1997). The results reported for *U.*

isabellina were carried out with a different strain than we used, and were published after we carried out our experiments described in this chapter. The research described in this chapter can be used to check published results for both fungi.

M. alpina and *U. isabellina* were cultivated on agar plates containing starch, cellulose, pectin, glucose or xylose, plus an organic nitrogen source (protein hydrolysate). CO_2 production was used as growth indicator as described before (Sugama and Okazaki 1979, Desgranges et al. 1991, Nagel et al. 2001). In addition to the test with single carbon sources, both strains were cultivated on sugar beet pulp in an aerated packed bed. Sugar beet pulp consists mainly of cellulose, hemicellulose and pectin (Phyllis database). These experiments give the indication that *M. alpina* is not suitable for lipid production in SSF, but that *M. isabellina* might be a good choice for lipid production in SSF.

Materials and methods

Inoculum

Mortierella alpina ATCC 3222 and Umbelopsis *isabellina* CBS 194.28 were cultured on potato dextrose agar (Oxoid CM139) for 14-20 days at 25 °C. The spores were harvested by adding 10 mL PFS-Tween (containing 1 g neutral bacterial peptone (Oxoid L34), 8.5 g NaCl and 0.5 g Tween-80 per litre water) per plate and scraping with a glass spatula. The obtained spore suspension was filtered through sterile glass wool to remove mycelium. Glycerol was added up to 23% v/v and the suspension was frozen at –80°C in 1-mL aliquots. The spores were counted on plate count agar (Oxoid CM325) after thawing by diluting the spore suspension. The vials contained $4 \cdot 10^4$ CFU mL^{-1} for *M. alpina* and $3 \cdot 10^7$ CFU/mL^{-1} for *U. isabellina.*

Agar plate experiments

Medium contained 20 g C-source, 6 g Hypep 4601 (Kerry Bioscience, The Netherlands), 0.5 g KCl, 0.5 g $MgSO_4 \cdot 7H_2O$, 1.5 g $Na_2HPO_4 \cdot 2H_2O$, 1 mL trace metal solution as described by Vishniac and Santer (1957) and 15 g agar per liter water. The pH was adjusted to 6 using 3M H_2SO_4. The medium was autoclaved and poured into agar-plates (Ø 53 mm, approximately 23 mL medium). After cooling, plates were inoculated with spore suspension (200 µl/plate for *M. alpina*, 100 µl/plate for *U. isabellina*).

Eight plates containing the same C-source were placed on a rack in an aerated (50 mL min^{-1}) closed jar (Ø 200 mm, height 250 mm) inside a temperature-controlled cabinet at 25 °C. A small layer of water was present at the bottom of the jar to prevent dehydration. The incoming air flow was controlled with a mass flow controller (Brooks Instrument BV, The Netherlands), passed through soda-lime pellets to remove CO_2, through a PTFE-filter (0.2 µm Whatman Polyvent 16) to sterilize it and through a washing bottle filled with water (at 25°C) to humidify it. The outgoing air was dehumidified using a condenser (at 4°C) and analysed with an infrared CO_2 analyser (Servomex 1440, The Netherlands).

The C-sources tested were D-glucose, unmodified wheat starch (Sigma), cellulose (Solka-Floc 200 NF, IFC, U.S.A.), D-xylose and pectin from citrus peel (Fluka). Medium with all ingredients except the C-source was used as a blank. All media

contained abundant nitrogen compared to carbon (C/N < 12 g/g) because we wanted to test the ability to grow, not the ability to accumulate lipids. Growth is a prerequisite for lipid accumulation, because lipids are accumulated inside the fungal cells.

Sugar beet pulp in packed beds

Dried beet pulp pellets (CSM, Breda, the Netherlands) were grinded to pieces of 1-5 mm. 2.33 g water was added per g dry beet pulp and the substrate was autoclaved. After cooling, inoculum was added (6×10^5 spores/g dry weight for *U.* isabellina and 4×10^3 spores/g dry weight for *M. alpina*). The inoculated substrate was incubated at 25°C in aerated (50 mL min^{-1}) fermentation tubes of approximately 23 cm^3, 2 tubes for each strain. The incoming and used air flows were handled as described for the agar cultures. At the start and at the end of the fermentation, the dry weight of the substrate was measured by drying samples in an oven at 80°C.

Optimization experiments were carried out by adding sterilized hemp (Hemparade, HempFlax bv., The Netherlands) up to 50% of the total dry weight of the substrate and 8 – 40 µl/g dry sugar beet pulp of an enzyme mixture consisting of Pectinex Ultra SPL and Celluclast 1.5L (Novozymes, Denmark) in a ratio 1:3, together with the inoculum. The fermentation was carried out in the same way as described above.

Radial growth rates

Small pieces of mycelium were placed in the center of Petri-dishes (Ø 86 mm) containing 20 mL PDA (Oxoid CM139). The plates were incubated in temperature-controlled cabinets at 20, 25, 30 and 35 °C (5 plates per strain per temperature). The colony diameters were measured several times per day along two perpendicular lines drawn on the bottom of the plate. The radial growth rate was calculated using linear regression analysis.

Lipid determination

Lipid determination was carried out as described in Meeuwse et al. (2011).

Results

Optimum growth temperature

The incubation temperature should be close to optimal, to allow comparison of the substrate conversion capacities of both fungi. Based on radial growth rates, the optimum temperature is 25 °C for *M. alpina* and 30 °C for *U. isabellina* (Figure 1). The growth rate of *U. isabellina* decreased only slightly at lower temperatures. Therefore, both strains were incubated at 25 °C.

Utilization of glucose

M. alpina and *U. isabellina* were grown on agar plates containing glucose, protein hydrolysate and minerals; results are shown in Figure 2 and Table 1. Both fungi had almost the same specific growth rate during their exponential growth phase (Figure 2b, Table 1). *M. alpina* exhibited a longer apparent lag time; considering the analyzer accuracy, we defined this as the time needed to reach a CO_2 production rate of 0.2 mmol h^{-1} m^{-2}; indicated with an arrow in Figure 2b. This can be explained largely by the difference in inoculum density, which would give a difference of 23 h.

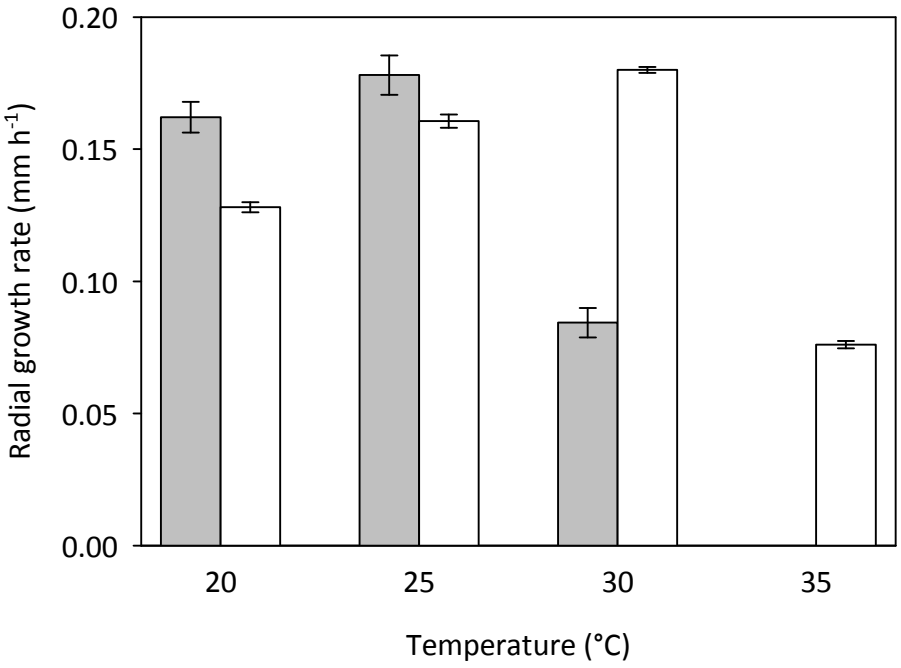

Figure 1: Radial growth rates (mm h^{-1}) of *M. alpina* (grey) and *U. isabellina* (white) colonies at different temperatures. Error bars indicate 95%-confidence intervals (n=5). For *M. alpina*, no growth was observed at 35°C.

The maximum CO_2 production rate (Figure 2a) and the cumulative CO_2 production 8 days after the end of the apparent lag time (calculated from the area below the curve in Figure 2a) were higher for *M. alpina* (Table 1). *M. alpina* converted 55% of the available carbon to CO_2 during the 8 days after its apparent lag time, and *U. isabellina* converted 35% to CO_2 (the medium contained 7.1 Cmol m^{-2} glucose and 2.2 Cmol m^{-2} protein hydrolysate). This means that both strains have different

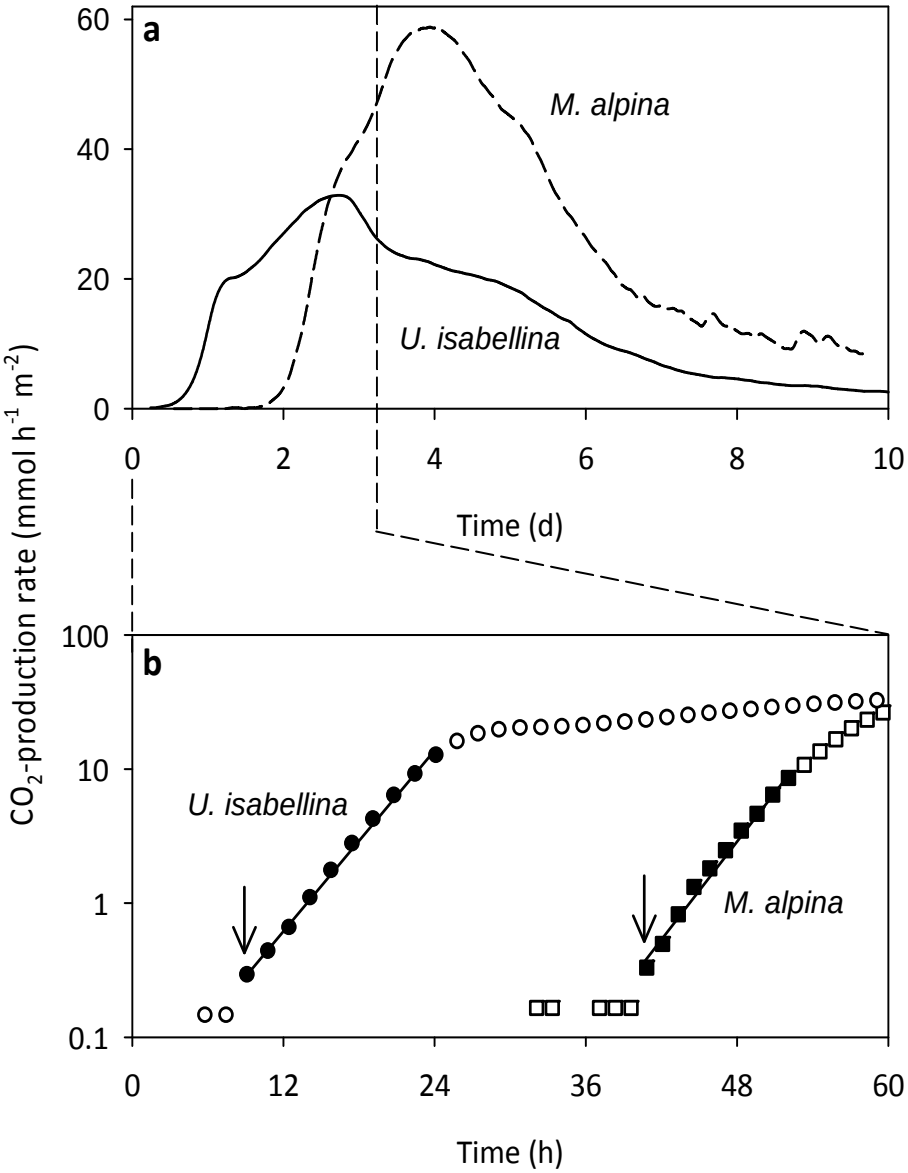

Figure 2: CO_2 production rate (mmol h^{-1} m^{-2}) of *U. isabellina* and *M. alpina* on medium with glucose as main C-source. CO_2 production was calculated per m^2 agar plate surface area. **a.** CO_2 production rate during ten days. **b.** CO_2 production rate during the first 60 hours of the cultivation with logarithmic y-axis. Arrows indicate the end of the lag phase. Filled symbols indicate data points used for linear regression analysis (r^2>0.99, n=10) to obtain the specific growth rate (Table 1).

growth patterns and different yields of CO_2 on glucose. Therefore we compare their conversion of other C-sources using their conversion of glucose as a reference, in addition to their conversion of the protein hydrolysate in the blanks.

Utilization of other substrates on agar plates

Table 1 gives the data derived from the CO_2 production on agar plates containing starch, cellulose (Solka-Floc), xylose or pectin together with protein hydrolysate and minerals. Agar plates with only protein hydrolysate and minerals were used as a blank, because the protein hydrolysate could also be used as a C-source. Only substrates for which the cumulative CO_2 production was higher than the cumulative CO_2 production in the blank were considered to be utilized by the strains.

Table 1: Kinetics and yields for cultivation of *M. alpina* (**a**) and *U. isabellina* (**b**) on agar-plates containing different C-sources.

a *M. alpina*	glucose	starch	cellulose	xylose	pectin	blank [c]
Lag time (h)	40	46	43	72	53	40
Specific growth rate[a] (h^{-1})	0.29±0.02	0.27±0.03	0.18±0.01	0.14±0.01	0.20±0.01	0.23±0.02
Maximum CO_2 production rate (mmol h^{-1} m^{-2})	59	25	19	14	16	19
Cumulative CO_2 production after 8 days[b] (mol m^{-2})	5.2	2.9	1.5	1.3	1.3	1.6[c]

b *U. isabellina*	glucose	starch	cellulose	xylose	pectin	blank [c]
Lag time (h)	11	8	12	11	10	10
Specific growth rate[a] (h^{-1})	0.26±0.01	0.31±0.03	0.37±0.05	0.27±0.02	0.24±0.01	0.37±0.07
Maximum CO_2 production rate (mmol h^{-1} m^{-2})	33	26	12	43	35	11
Cumulative CO_2 production after 8 days[b] (mol m^{-2})	3.2	3.4	0.8	4.1	3.4	1.0[c]

[a] Specific growth rate ± 95% confidence interval (r^2>0.99, n=6-16).
[b] Cumulative CO_2 production after 8 days of growth; the 8-day period starts after the lag time.
[c] Total available C-source during cultivation was approximately 2.2 Cmol m^{-2} (from protein) for the blank and 9.3 Cmol m^{-2} (from the C-source and protein) for the other media.

M. alpina only utilized glucose and starch. Its specific growth rate was comparable on glucose and starch, but its maximum CO_2 production rate and CO_2 production eight days after the apparent lag phase were considerably lower on starch. In the cultures with xylose, cellulose and pectin the cumulative CO_2 production after eight days was the same or lower than in the blank, and also the maximum specific growth rate and CO_2 production rate were the same or lower than in the blank.
U. isabellina converted all substrates except cellulose. It reached approximately the same CO_2 production on starch, pectin and glucose 8 days after the apparent lag phase, and a higher CO_2 production on xylose. Its specific growth rates on glucose, starch, xylose and pectin were approximately the same (considering the 95%-confidence interval) or lower than that in the blank.

Utilization of sugar beet pulp

Figure 3 shows the CO_2 production rate of *M. alpina* and *U. isabellina* on beet pulp, expressed in mmol h^{-1} g^{-1} initial dry matter (IDM). Results extracted from this graph are shown in Table 2. The difference in apparent lag time can largely be attributed to the difference in inoculum density of the strains. No exponential growth phase was detected; the increase in CO_2 production rate in the first phase was linear

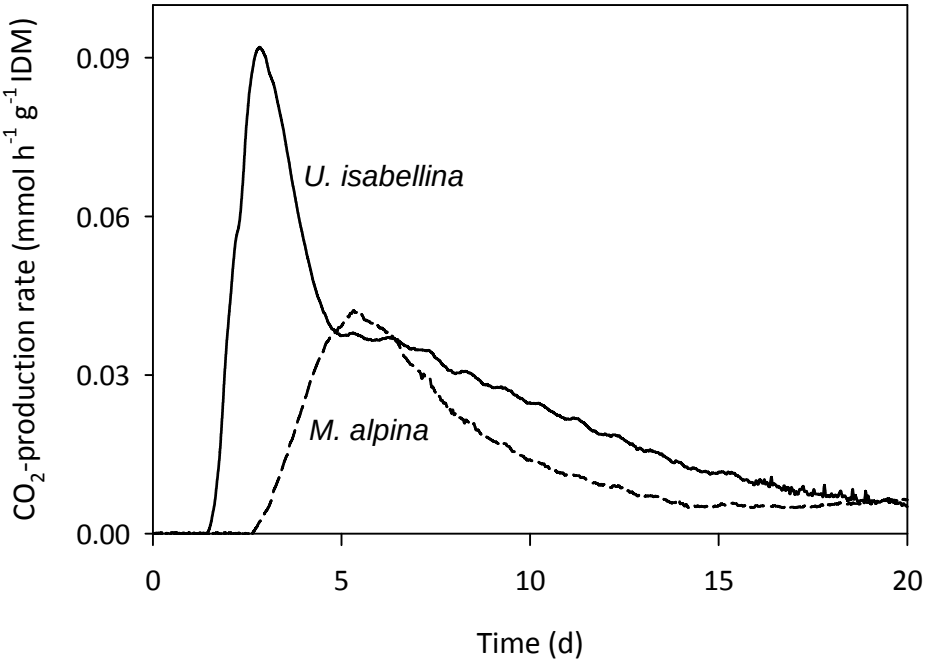

Figure 3: CO_2 production rate (mmol h^{-1} g^{-1} IDM) of *U. isabellina* and *M. alpina* in solid-state fermentation on sugar beet pulp in an aerated packed bed. IDM = initial dry matter.

Table 2: Kinetics and yields for solid-state fermentation of *M. alpina* and *U. isabellina* on sugar beet pulp in an aerated packed bed.

	M. alpina	*U. isabellina*
Lag time (h)	60	34
Maximum CO_2 production rate (mmol h^{-1} g^{-1} IDM[a])	0.042	0.092
Cumulative CO_2 production after 8 days[b] (mol g^{-1} IDM)	4.7	8.3
Cumulative CO_2 production after 20 days[b] (mol g^{-1} IDM)	6.7	11.9
Lipid fraction in remaining dry weight after 23 days (w/w)	0.5%	2.9%

[a] IDM = initial dry matter

[b] The 8-day resp. 20-day period starts after the lag time.

instead of exponential.

M. alpina had a lower maximum CO_2 production rate than *U. isabellina* and its cumulative CO_2 production 8 d and 20 d after the apparent lag phase was lower (Table 2). Furthermore, a lot more dry weight remained after 20 days. Direct measurement of remaining sugar beet pulp is impossible because the remaining substrate includes the fungal cell mass. Assuming that the CO_2 yields on converted sugar beet pulp are the same as those on glucose, and taking the carbon content of beet pulp as 30 Cmol/g (Phyllis database), *M. alpina* consumed approximately 30% of the substrate carbon after 8 days and 40% after 20 days, and *U. isabellina* consumed 75% after 8 days and 100% after 20 days.

At the end of the culture (23 d after inoculation), the lipid content of the total remaining mass was measured (Table 2). Lipid accumulation could be expected because the C/N-ratio of sugar beet pulp is approximately 30 Cmol/Nmol (Phyllis database). The average lipid content of sugar beet pulp itself was 0.5%. Therefore, no net lipids were accumulated by *M. alpina* and there was some lipid accumulation by *U. isabellina*.

Lipid accumulation by *U. isabellina* on sugar beet pulp was optimized by adding extra hydrolyzing enzymes (pectinase and cellulose). Additionally, hemp was introduced as a non-degradable carrier to keep the fermentation mass porous during the fermentation. Optimum lipid production was observed with the addition of 8-16 µl enzyme solution per g initial sugar beet pulp combined with addition of hemp at 40-50% of the total initial dry weight. A lipid content of 9% w/w on dry weight was reached after 8-10 days, which was equal to a lipid yield of 6% w/w of initial dry weight of sugar beet pulp. A representative graph of these results is shown in Figure 4. This figure also shows a decrease in lipid content after 10 days.

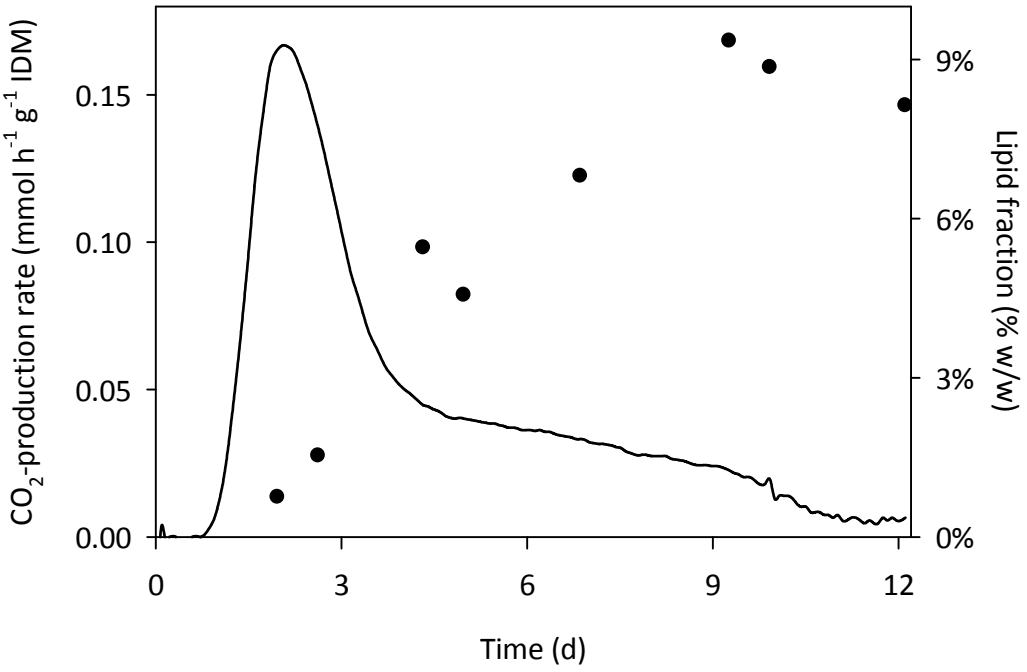

Figure 4: CO_2 production rate (line) and lipid fraction of dry weight (dots) of *U. isabellina* in solid-state fermentation on sugar beet pulp and hemp 1:1 in an aerated packed bed with addition of 8 µl/g IDM of enzyme solution as mentioned in the Materials and Methods. IDM = initial dry matter.

Discussion

M. alpina and *U. isabellina* were cultured on the monomers glucose and xylose, and the polymers starch, cellulose (Solka-Floc) and pectin. Starch, cellulose and pectin commonly occur in agro-industrial by-products or wastes that can be used in SSF. Hemicellulose, another polymer often occurring in agro-industrial waste, was not tested because of the wide variety of hemicelluloses existing. Xylose was tested instead, and the ability to utilize xylose is a condition for utilization of xylan, an important hemicellulose component. Glucose was tested as a positive control.

Pure Solka-Floc was not consumed by either of the strains. Botha et al. (1997) showed that *M. alpina* cannot utilize cellobiose, which implies that this strain will not be able to utilize any type of cellulose. Results from the culture on sugar beet pulp indicate that *U. isabellina* consumed all carbon in the pulp, including the cellulose. Therefore Solka-Floc, which is quite a crystalline material, may not be the proper type of cellulose to test a strain.

M. alpina only utilized glucose and starch, and starch was converted slowly and incompletely. This indicates that *M. alpina* does not possess a good amylase system. *M. alpina* did not convert xylose or pectin. The inability of *M. alpina* to utilize xylose was shown before by Botha et al. (1997). Xylose even seems to inhibit the utilization of the protein hydrolysate. The inability of *M. alpina* to utilize pectin could be caused by the absence of pectinases, or the inability to utilize the monomers of pectin. Although *M. alpina* consumed some of the beet pulp, it did this slowly and incompletely: We estimated that even after 20 days only 40% of the carbon was consumed. These results together indicate that *M. alpina* is not suitable for growth in SSF.

The starch hydrolysis system of *U. isabellina* slows down CO_2 production on starch compared to that on glucose, but it is much faster than the amylase system of *M. alpina*. Papanikolaou et al. (2007) also showed a minor difference between glucose and starch consumption of *U. isabellina* in SmF. In our cultures, pectin shows the same utilization rate as glucose, and xylose even has a higher rate. In literature, however, both substrates are consumed slower than glucose in SmF (Papanikolaou et al. 2007, Fakas et al. 2009b). Our cultures were carried out on agar plates, where the availability of the substrate depends on diffusion to the fungal biofilm. It is therefore possible that in our cultures, the diffusion of the substrate is limiting and not the maximum consumption rate of the fungus for these substrates.

However, this does not change the conclusion that *U. isabellina* can utilize glucose as well as starch, xylose and pectin.

The consumption of beet pulp by *U. isabellina* was not as fast as the consumption of the pure substrates, but we estimated that after 20 days all carbon was consumed. Furthermore, also a small amount of lipids was accumulated. Because of the long culture time, it is possible that lipid accumulation had already stopped at the end of the culture, and even lipid turnover could have taken place, which was indeed observed in the optimized cultures (Figure 4). The found maximum lipid yield of 9% w/w in the optimized cultures is comparable to results from literature: 12% of remaining mass on pear pomace (Fakas et al. 2009a) and 10% of remaining dry mass on sweet sorghum (Economou et al. 2010).

The addition of enzymes significantly increased lipid production. This indicates that the enzyme production of the fungus is the limiting factor. Addition of enzymes accelerated hydrolysis of the substrate, but also made the resulting substrate slurry less suitable for SSF because the decreased porosity of the substrate reduced oxygen transfer and heat removal by aeration. Addition of hemp as a carrier material at low doses of enzymes can prevent this problem; at high doses, the amount of hemp that needs to be added will be so high, that the productivity per reactor volume will decrease considerably. This shows that fast hydrolysis of the substrate in an SSF system is not always favorable.

Concluding, the limited substrate utilization capacity of *M. alpina* makes this strain not suitable for SSF on agro-industrial wastes. On the other hand, the good utilization of most of the substrates tested in this paper as well as the found growth and lipid production on sugar beet pulp and other substrates from literature make *U. isabellina* a promising fungus for this purpose.

Chapter 3

Modeling lipid accumulation in oleaginous fungi in chemostat cultures: I. Development and validation of a chemostat model for *Umbelopsis isabellina*

Meeuwse P, Tramper J, Rinzema A. 2011. Modeling lipid accumulation in oleaginous fungi in chemostat cultures. I: Development and validation of a chemostat model for *Umbelopsis isabellina*. Bioprocess Biosyst Eng 34: 939-949

Abstract

Lipid-accumulating fungi may be able to produce biodiesel precursors from agricultural wastes. As a first step in understanding and evaluating their potential, a mathematical model was developed to describe growth, lipid accumulation and substrate consumption of the oleaginous fungus *Umbelopsis isabellina* (also known as *Mortierella isabellina*) in submerged chemostat cultures. Key points of the model are: (1) If the C-source supply rate is limited, maintenance has a higher priority than growth, which has a higher priority than lipid production; (2) the maximum specific lipid production rate of the fungus is independent of the actual specific growth rate. Model parameters were obtained from chemostat cultures of *U. isabellina* grown on mineral media with glucose and NH_4^+. The model describes the results of chemostat cultures well for $D>0.04\ h^{-1}$, but it has not been validated for lower dilution rates because of practical problems with the filamentous fungus. Further validation using literature data for oleaginous yeasts is described in part II of this paper. Our model shows that not only the C/N-ratio of the feed, but also the dilution rate highly influences the lipid yield in chemostat cultures.

Introduction

As the need to replace fossil fuels increases, lipids accumulated in oleaginous organisms come into view for the production of biodiesel. Besides oleaginous microalgae, oleaginous yeasts and fungi may be a promising option, provided that these heterotrophs use biomass residues as a C-source (Li et al. 2008, Rittmann 2008, Wijffels 2008). We study the potential of oleaginous fungi to convert biomass residues to biodiesel precursors.

Previously, lipid accumulation in oleaginous yeasts and especially oleaginous fungi has been studied mainly with the aim to produce high-value poly-unsaturated fatty acids (PUFAs), such as arachidonic acid and γ-linolenic acid (Certik and Shimizu 1999), in submerged fermentation with glucose as C-source. If the aim is biodiesel production, the use of other substrates such as agricultural or industrial waste streams becomes of interest, as well as the use of cheaper production systems, such as solid-state fermentation. Lipid production on waste streams has been studied in submerged fermentation (Vamvakaki et al. 2010, Papanikolaou et al. 2007, Angerbauer et al. 2008, Fakas et al. 2009b), as well as in solid-state fermentation (Gema et al. 2002, Stredansky et al. 2000, Peng and Chen 2008, Economou et al. 2010). These studies mainly focused on maximum lipid fractions reached and less on production rates or yield on substrate. Especially in solid-state fermentation, only low yields were reached. Obviously, the product yield and formation rates are of primary importance for biodiesel production. To allow development of bioprocesses with higher yields and production rates, insight in the kinetics of lipid production has to be improved.

As a starting point to study kinetics, we chose a chemostat system. In chemostat, the supply of all substrates and the growth rate can be controlled by setting the dilution rate and the concentrations of the substrates in the feed. This makes chemostat culture a suitable tool to study lipid accumulation under different circumstances. This paper describes kinetic modeling of lipid production in submerged chemostat cultures. In part I of this paper, we develop a chemostat model and validate it with chemostat cultures of *U. isabellina*, a filamentous fungus that proved to be the most promising strain for solid-state fermentation among a large group of oleaginous fungi tested (Chapter 2 and other results, not published). In part II of this paper, we will compare our model to literature data for chemostat cultures of oleaginous yeasts, and to a previously described model for continuous culture published by Ykema et al. (1986).

Model

Figure 1 shows a simplified scheme of the metabolism of an oleaginous organism. The organism uses a C-source, an N-source and oxygen to produce lipid-free cell material (X), lipids (L), carbon dioxide and water. The compositions of lipid-free cell material and lipids given in Fig. 1 are based on the average composition of cells and lipids in our experiments (see "Results"). Symbols used in the model are listed on page 207.

The model is based on the Scheme in Fig. 1 and several assumptions:

- The C-source and/or the N-source is limiting for the production of lipid-free biomass and lipids; oxygen and other nutrients are supplied in abundance.
- No other carbon or nitrogen-containing products are produced besides lipid-free biomass, lipids and CO_2. This means that the element balances for C and N read:

$$r_S + r_X + r_L + r_C = 0 \text{ (for carbon) and } r_N + \frac{r_X}{Y_{XN}} = 0 \text{ (for nitrogen)} \qquad (1)$$

- The first priority of the fungus is to use the supplied C-source to satisfy its maintenance requirements, then to produce lipid-free biomass, and finally, only if there is C-source left, to accumulate lipids.
- The fungus always produces a basal amount of lipids for its cell membranes; the basal specific lipid production rate is proportional to the specific growth rate:

$$q_{L,\min} = \frac{f_{L0}}{1 - f_{L0}} \mu \qquad (2)$$

- If sufficient C-source is available, the specific lipid production rate increases up to a maximum value $q_{L,\max}$. This maximum specific lipid production rate is independent of the specific growth rate, as has been shown before in literature (Hansson and Dostalek 1986, Choi et al. 1982).
- Low C-source and N-source concentrations do not affect the conversion rates of these components (zero-order kinetics with respect to reactants).
- Physiological or regulatory mechanisms do not impose a maximum on the lipid content of the cells. Such a maximum has been found in batch cultures (Wynn et al. 1999), but it is not included in the model because high lipid contents were not reached in the experiments used for validation.

The model predicts the concentrations of lipid-free biomass (C_X), lipids (C_L), non-consumed C-source (C_S) and non-consumed N-source (C_N) in the culture during steady state at any combination of the dilution rate (D) and the concentrations of C-source (C_{Sin}) and N-source (C_{Nin}) in the feed. Component mass balances over the culture combined with Pirt's linear growth law, read:

Lipid-free biomass: $0 = -DC_X + \mu C_X$ (3)

Lipids: $0 = -DC_L + q_L C_X$ (4)

C-source: $0 = D(C_{Sin} - C_S) - \left(m_S + \frac{\mu}{Y_{XS}} + \frac{q_L}{Y_{LS}} \right) C_X$ (5)

N-source: $0 = D(C_{Nin} - C_N) - \frac{\mu}{Y_{XN}} C_X$ (6)

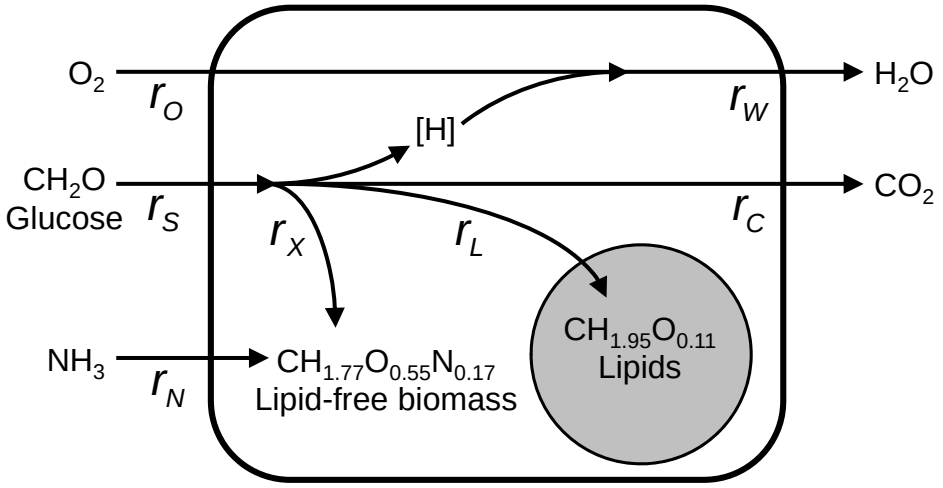

Fig. 1 Schematic representation of the carbon and nitrogen metabolism in the oleaginous fungus *U. isabellina*. The production or uptake rates of the carbon source (glucose, r_S), lipid-free biomass (r_X), lipids (r_L) and CO_2 (r_C) are expressed in Cmol m^{-3} h^{-1}, the rate of nitrogen source (NH_3, r_N) is expressed in Nmol m^{-3} h^{-1} and the rates of oxygen (r_O) and water (r_W) are expressed in mol m^{-3} h^{-1}. Compositions of lipid-free biomass and lipids are based on experimental results.

When we combine these balances, the assumptions above and the boundary conditions (all concentrations must be ≥0), we get the following set of equations:

$$C_S = C_{Sin} - \frac{C_X}{D}\left(m_S + \frac{D}{Y_{XS}} + \frac{q_L}{Y_{LS}}\right) \geq 0 \quad (7)$$

$$C_N = C_{Nin} - \frac{C_X}{Y_{XN}} \geq 0 \quad (8)$$

$$C_L = \frac{q_L}{D} C_X \quad \wedge \quad q_{L,\min} \leq q_L \leq q_{L,\max} \quad (9)$$

Three different regimes can be distinguished, depending on the concentrations of C-source (C_{Sin}) and N-source in the feed (C_{Nin}) and the dilution rate (D): single nitrogen limitation ($C_N = 0$), dual limitation ($C_N = 0$ and $C_S = 0$), and single carbon limitation ($C_S = 0$). The equations used in these regimes, all derived from Eqs. 7-9, are summarized in Table 1. Figure 2 shows the three regimes in a chemostat culture with a constant C/N-ratio of the feed and a variable dilution rate. All regimes are explained below.

Single nitrogen limitation

Single nitrogen limitation implies that the nitrogen source is the only limiting substrate. Therefore, the concentration of the N-source in the culture (C_N) is 0 according to the model, and Eq. 8 gives the lipid-free biomass concentration (C_X). The concentration of C-source in the culture (C_S) is higher than 0. Therefore, the specific lipid production rate (q_L) has its maximum value ($q_{L,\max}$), and the lipid concentration (C_L) can be calculated from Eq. 9. Eq. 7 can be used to calculate the concentration of C-source in the culture (C_S). Single nitrogen limitation occurs when the C/N-ratio of the feed is high and a high enough dilution rate (D) is applied (see Fig. 2).

Table 1 Equations used to calculate concentrations of glucose, ammonium, lipid-free biomass and lipids, and the specific lipid production rate for *U. isabellina* in a chemostat. The numbers before the arrows indicate the equation from which the shown equations were derived.

	N-limitation	Dual limitation	C-limitation
C-source	(7)→ $C_S = C_{Sin} - \frac{C_X}{D}\left(m_S + \frac{D}{Y_{XS}} + \frac{q_{L,max}}{Y_{LS}}\right)$ (10)	$C_S = 0$	$C_S = 0$
N-source	$C_N = 0$	$C_N = 0$	(8)→ $C_N = C_{Nin} - \frac{C_X}{Y_{XN}}$ (11)
Lipid-free Biomass	(8)→ $C_X = C_{Nin} Y_{XN}$ (12)	(8)→ $C_X = C_{Nin} Y_{XN}$ (12)	(7)→ $C_X = \frac{DC_{Sin}}{m_S + \frac{D}{Y_{XS}} + \frac{q_{L,min}}{Y_{LS}}}$ (13)
Lipids	$q_L = q_{L,max}$ (14) (9)→ $C_L = \frac{q_{L,max} C_X}{D}$ (15)	(7)→ $q_L = Y_{LS}\left(\frac{C_{Sin} D}{C_X} - m_S - \frac{D}{Y_{XS}}\right)$ (16) (9)→ $C_L = \frac{q_L C_X}{D}$ (17)	$q_L = q_{L,min} = \frac{f_{L0}}{1 - f_{L0}} D$ (18) (9)→ $C_L = \frac{f_{L0}}{1 - f_{L0}} C_X$ (19)
Respiration	For all limitations: (1) → $r_C = D(C_{Sin} - C_S - C_X - C_L)$ (20) and $r_O = -D(C_{Sin} - C_S - 1.04C_X - 1.43C_L)$[a] (21)		

Numbers in equation calculated from element balances of C, N, H and O (see Fig. 1).

Dual limitation

Dual limitation implies that $C_N = 0$ and $C_S = 0$ in the model. Eq. 8 gives the lipid-free biomass concentration (C_X), while Eq. 7 gives the specific lipid production rate (q_L). The N-source is limiting for lipid-free biomass production, and the C-source is limiting for lipid production because the cell will give priority to maintenance and growth. This dual limitation is known as heterologous dual limitation (Zinn et al. 2004).

Single carbon limitation

Single carbon limitation occurs when $C_S = 0$ but $C_N > 0$ in the model. As the cells give priority to growth and maintenance above lipid production, only membrane lipids will be produced and the specific lipid production rate (q_L) will have its minimum value ($q_{L,\min}$). The lipid-free biomass concentration (C_X) can be determined using Eq. 7, the remaining N-source concentration with Equation 8. Single carbon limitation occurs when the C/N-ratio in the feed is lower than the

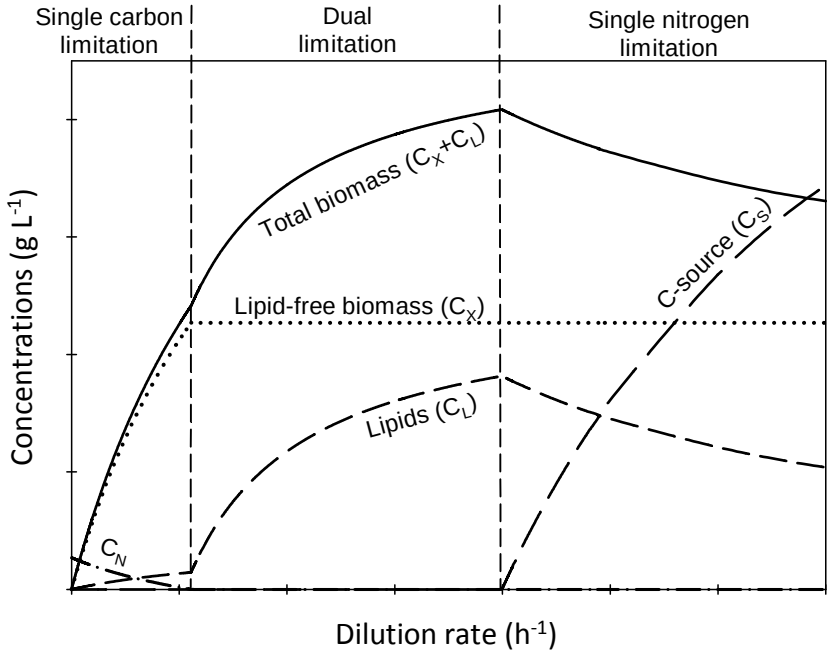

Fig. 2 Concentrations of N-source (C_N), C-source (C_S), lipid-free biomass (C_X), lipids (C_L) and total biomass (C_X+C_L) for a variable dilution rate predicted by the model (arbitrary units). Limitation regimes are indicated as described in the text. In cultures with a high C/N-ratio, the single carbon limitation area and the dual limitation area are usually very small, but are shown prominently here to give an overview of all limitation regimes possible.

C/N-ratio required for growth, but can also occur at higher C/N ratios in the feed when the dilution rate is very low (see Fig. 2), i.e. when maintenance plays an important role.

Respiration

The CO_2-production rate and the O_2-consumption rate are calculated using mass balances. From the carbon balance in Eq. 1 the CO_2-production rate is calculated. The O_2-production rate is calculated in a similar way using the oxygen and hydrogen balances, which can be calculated from the composition of all substrates and products involved. The equations for both rates are also shown in Table 1.

Materials and Methods

Inoculum

Umbelopsis isabellina CBS 194.28 was cultured on potato dextrose agar (Oxoid CM139) for 14 days at 25°C. The spores were harvested by adding 10 mL PFS-Tween (containing 1 g neutral bacterial peptone (Oxoid L34), 8.5 g NaCl and 0.5 g Tween-80 per l water) per plate and scraping with a glass spatula. The obtained spore solution was filtered through sterile glass wool to remove mycelium. Glycerol was added up to 23% v/v and the suspension was frozen at –80°C in aliquots of 1 mL. Spore counts were done on plate count agar (Oxoid CM325) after thawing and dilution of the spore suspension. The vials contained 3×10^7 CFU/mL.

Medium

Liquid medium for all cultures contained per liter: 0.5 g KCl, 0.5 g $MgSO_4 \cdot 7H_2O$, 1.5 g $Na_2HPO_4 \cdot 2H_2O$, 1 mL trace metal solution as described by Vishniac and Santer (1957), glucose as C-source and $(NH_4)_2SO_4$ as N-source. Chemostat cultures were started as a batch culture with medium containing 50 mM glucose and 25 mM NH_4^+. The different concentrations of glucose and ammonium in the feed during continuous operation are shown in Table 2. Pre-culture medium contained 100 mM glucose and 100 mM NH_4^+. The pH of all media was adjusted to 6.0 with H_2SO_4. Glucose was autoclaved separately. To all media, except for the preculture, 1 mL of antifoam (Polypropylene glycol (Sigma), 50% v/v in ethanol) was added per liter.

Pre-culture

The pre-culture was carried out in 250 mL shake flasks with 100 mL pre-culture medium. The flasks were inoculated with 1 mL spore suspension and incubated at 25°C in a shaking incubator at 225 rpm for 3 days.

Culture

The cultivation was carried out in a baffled glass bioreactor with a volume of 2.5 L and a working volume of 1 L (Applikon, The Netherlands), placed in a temperature-controlled cabinet to keep the culture at 28°C. The reactor was stirred with one 6-

blade disc turbine impeller (Applikon, The Netherlands) at 700 rpm. To reduce attachment of mycelium clumps behind the baffles, the stirring direction was reversed every 30 seconds as was done before by Song et al. (2001). The baffles were not removed because this would decrease oxygen transfer up to a factor three, according to calculations. The pH of the medium was kept at 6.0 with a pH electrode and a control system (biocontroller ADI 1030, Applikon, The Netherlands) by addition of NaOH (1M). Air was blown into the culture at a rate of 1L/min through a PTFE-filter (0.2 µm Whatman Polyvent 16), just below the stirrer. Off-gas was cooled to 4°C in a condenser, before the O_2 and CO_2 concentrations were measured with a paramagnetic O_2 analyzer (Servomex 4100, The Netherlands) and an infrared CO_2 analyzer (Servomex 1440, The Netherlands); these measurements were logged using Labview 5.1 (National Instruments, U.S.). Calculations showed that the CO_2 and O_2 dissolved in the outgoing medium could be neglected compared to the CO_2 and O_2 in the off-gas. The O_2 concentration in the liquid was not controlled because the fungus grows on the membrane of an O_2 electrode, influencing the measurements. Calculations and measurements of the oxygen transfer rate at the start of a culture showed that at the used mixing rate and air flow rate, approximately 10 mol m^{-3} h^{-1} of oxygen could be transferred from the gas phase to the liquid phase. Low substrate concentrations in the feed were used to keep the biomass concentration in the bioreactor low and therefore keep the O_2-consumption rate below 10 mol m^{-3} h^{-1}.

The cultivation was started as a batch culture by adding 50 mL preculture to 950 mL start medium. After one day the feed was started at a fixed dilution rate using a peristaltic pump with the medium as indicated in Table 2. The weight of the fresh medium vessel was registered to calculate the dilution rate. Culture broth was removed every 12 minutes via an overflow tube, using a peristaltic pump operated at high rate. The removed culture broth was collected and stored in a fraction collector kept at 5°C for a maximum of 18 hours, before separation of biomass and medium. During this storage no significant changes in the samples were observed. After a change in the dilution rate, samples were taken after at least 3 hydraulic residence times and when the CO_2-concentration in the off-gas remained stable for at least 12 hours. Samples were taken during at least 12 hours when a steady state was reached.

Dry weight measurement

Samples taken from the reactor were centrifuged (10 min, 4000 g), and the supernatant was frozen until further analysis. The pellet was washed with water once and freeze-dried to determine the dry weight. The ash content of the cell material was determined after incubation in an oven at 500°C. Elemental analysis (CHNS) of the samples was carried out with an EA1110 elemental analyzer (Thermoquest, CE Instruments, U.K.). All mass that was not determined as being ash, carbon, hydrogen, nitrogen or sulfur was assumed to be oxygen.

Lipid determination

Freeze dried mycelium was pulverized with a mortar and pestle and suspended in chloroform containing a known concentration of nonadecanoic acid (Fluka) as internal standard. The samples were incubated overnight in a head-over-tail-mixer. The chloroform was filtered through a paper filter (Whatman 595, Germany) to remove remains of the mycelium. The extracted lipids in the chloroform were transesterified by adding a small amount of trimethylsulfonium hydroxide solution (TMSH, 0.25M in methanol, Fluka) and the methyl esters formed were measured on a GC (Hewlett Packard 6890 series) with column: Supelco 25357, 30m x 530 µm, 1 µm nominal. The temperature of the column was raised from 90°C to 200°C with 10°C/min, at which it stayed for 18 min. Both the injector and the detector (FID) had a temperature of 250°C. The carrier gas was helium with a flow rate of 16.1 ml/min. We used nonadecanoic acid as an internal standard. Only C16:0, C18:0, C18:1 and C18:2 were measured, as these four fatty acids comprised more than 98% of the fatty acids present.

Medium analysis

The glucose concentration in the medium was determined using the glucose GOD-PAP test (Roche, Germany). The NH_4^+ concentration was estimated using Merckoquant ammonium test strips (Merck). Total organic carbon (TOC) was measured using the Dr. Lange TOC test (LCK 386, Hach Lange, Germany).

Table 2 Results from chemostat experiments with *U. isabellina* in a 1-L bioreactor

C/N ratio (Cmol Nmol^{-1})	dilution rate (h^{-1})	NH_4^+ in feed[a] (Nmol m^{-3})	glucose in feed (Cmol m^{-3})	glucose in culture (Cmol m^{-3})	Total biomass (kg m^{-3})	lipids in biomass (% w/w)	CO_2 production (mol m^{-3} h^{-1})	O_2 consumption (mol m^{-3} h^{-1})	Carbon recovery[d] (Cmol Cmol^{-1})
6	0.10	50[b]	300	<5	3.2 ± 0.3	4.5 ± 0.3%	6.7 ± 0.2	6.3 ± 0.2	ND
16	0.05	15	240	0.4 ± 0.1	2.6 ± 0.5	14 ± 1%	4.2 ± 0.1	3.5 ± 0.2	77 ± 8%
16	0.06	15	240	5 ± 1	3.8 ± 0.5	20 ± 1%	4.5 ± 0.2	4.4 ±0.2	98 ± 8%
16	0.08	15	240	9 ± 1	2.8 ± 0.3	15 ± 1%	5.2 ± 0.2	4.8 ± 0.2	78 ± 5%
16	0.11	15	240	75 ± 4	2.9 ± 0.1	10 ± 1%	5.7 ± 0.2	4.6 ± 0.2	96 ± 4%
16	0.16	15	240	86 ± 5	2.9 ± 0.2	4.7 ± 0.3%	5.3 ± 0.1	5.4 ± 0.2	89 ± 5%
16	0.19	15[c]	240	122 ± 15	2.3 ± 0.3	5.9 ± 0.3%	5.1 ± 0.1	4.4 ± 0.2	98 ± 11%
20	0.04	15	300	12 ± 3	3.3 ± 0.1	20 ± 1%	4.1 ± 0.1	3.8 ± 0.2	82 ± 2%
20	0.05	15	300	7 ± 3	4.0 ± 0.8	25 ± 3%	4.4 ± 0.6	3.5 ± 0.3	87 ± 12%
20	0.06	15	300	54 ± 8	3.4 ± 0.2	14 ± 1%	3.7 ± 0.1	3.7 ± 0.2	79 ± 4%
20	0.08	15	300	94 ± 5	3.1 ± 0.2	13 ± 1%	4.2 ± 0.1	4.4 ± 0.2	93 ± 4%
20	0.10	15	300	116 ± 5	3.0 ± 0.1	16 ± 1%	5.7 ± 0.1	6.0 ± 0.2	95 ± 4%
20	0.16	15	300	140 ± 6	3.0 ± 0.3	8 ± 1%	5.0 ± 0.2	3.9 ± 0.2	90 ± 7%

All measured values are ± SD

[a] Concentration of NH_4^+ in culture <0.5 mol m^{-3} unless stated otherwise

[b] Concentration of NH_4^+ in culture approximately 6 mol m^{-3}

[c] Concentration of NH_4^+ in culture approximately 1 mol m^{-3}

[d] Produced lipid-free biomass plus lipids plus CO_2 divided by consumed glucose. Missing carbon was assumed to be present as aggregates attached to the reactor wall and stirrer.

Results and Discussion

Results of chemostat cultures

Table 2 shows the results of the chemostat cultures of *U. isabellina* with glucose as C-source and NH_4^+ as N-source. For all data points with a feed C/N-ratio of 16 or 20 Cmol/Nmol, the NH_4^+ concentration in the effluent was ≤ 1 mol m^{-3}. In the experiment with a feed C/N-ratio of 6 Cmol/Nmol, approximately 6 mol m^{-3} NH_4^+ was found in the effluent.

The lipid fractions found in the experiments do not exceed 25% w/w, while *U. isabellina* is known to be capable of producing up to 55% w/w (Papanikolaou et al. 2004a). Reaching higher lipid fractions required lower dilution rates than we could use because of practical problems; this will be explained later. The fatty acid composition of the lipids depended on the lipid content of the cells (Fig. 3): 46% w/w of the lipids were C18:1 at the basal lipid fraction of 5% w/w, and this increased to 55% w/w at lipid fractions of 15% w/w or higher. All other measured fatty acids decreased with increasing lipid fraction. The lipid fraction was in most

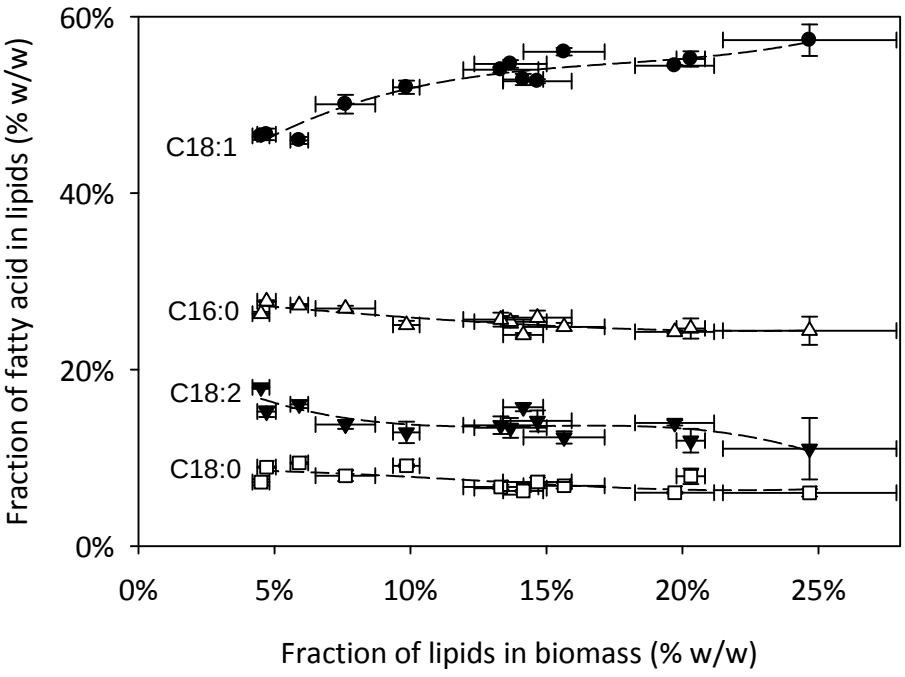

Fig. 3 Composition of lipids produced by *U. isabellina* in a chemostat as a function of the fraction of lipids in the biomass. The shown fatty acids comprised more than 98% of the total lipids. Error bars indicate standard deviation. The lines emphasize the trend that can be observed.

cases proportional to the average residence time (=1/*D*) and therefore to cell age. Fakas et al. (2009a) have shown before that similar changes in lipid composition of *U. isabellina* occur during the aging of mycelia. The composition of the lipids ($CH_{1.95}O_{0.11}$, MW=15.7 g $Cmol^{-1}$) used in the model is based on the average of the compositions shown in Fig. 3. Although *U. isabellina* is a known producer of γ-linolenic acid (Song et al. 2001), we did not detect this fatty acid in the strain we used.

The elemental composition of lipid-free biomass was $CH_{1.77}O_{0.55}N_{0.17}$; the molecular mass was 28.7±0.5 g $Cmol^{-1}$ including ash. These values were the same for all samples and independent of the dilution rate, feed C/N-ratio or lipid content of the cells.

The recovery of carbon in the culture (produced lipid-free biomass plus lipids and CO_2 divided by consumed glucose) was 88% on average (Table 2). Total organic carbon (TOC) measurements in supernatant samples showed that only a small part of the missing carbon was present in solution or as a dispersion of particles that were too small to separate during centrifuging. The largest part of the missing carbon was not found in the medium and we assume that this was present in cell aggregates attached to the baffles and stirrer.

Determination of parameter values

Data obtained with a feed C/N-ratio of 6 Cmol/Nmol were used to determine the basal lipid fraction in the cells (f_{L0}). Biomass, lipid and glucose concentrations obtained with feed C/N-ratios of 16 and 20 Cmol/Nmol were used to find the other model parameters Y_{XN}, Y_{XS}, Y_{LS}, m_S and $q_{L,\max}$. The determination of parameter values is explained below; parameter values are shown in Table 3a.

Basal lipid fraction

At a feed C/N-ratio of 6 Cmol/Nmol, approximately 6 mol m^{-3} NH_4^+ was found in the culture, while the glucose concentration in the culture was low. Therefore we assume that all measured lipids are membrane lipids. The basal lipid fraction of the cells is then 4.5% w/w, which gives f_{L0}=0.079 Cmol $Cmol^{-1}$.

Table 3 parameter values used in the model, obtained as described in the text. All values are ± SD. **a**: Summary of all parameter values. **b**: Y_{XS}, Y_{LS} and m_S obtained by linear regression analysis. Numbers indicate parameter value ± SD (p-value).

a		value
f_{L0}	(Cmol Cmol^{-1})	0.079
Y_{XN}	(Cmol Nmol^{-1})	6.1 ± 0.7
Y_{XS}	(Cmol Cmol^{-1})	0.92 ± 0.09
Y_{LS}	(Cmol Cmol^{-1})	0.59
m_S	(Cmol Cmol^{-1} h^{-1})	0.05 ± 0.01
$q_{L,\max}$	(Cmol Cmol^{-1} h^{-1})	0.023 ± 0.005
$\mu_{\max}$	(h^{-1})	0.23 ± 0.02

b		3-parameter fit	2-parameter fit
Y_{XS}	(Cmol Cmol^{-1})	0.93±0.09 (0.000)	0.92±0.09 (0.000)
Y_{LS}	(Cmol Cmol^{-1})	4±16 (0.8)	n.d. [a]
m_S	(Cmol Cmol^{-1} h^{-1})	0.09±0.02 (0.004)	0.05±0.01 (0.001)
SSE ×10^3		2.4	3.2
Degrees of freedom [b]		9	10

[a] A fixed value was used in the regression analysis: Y_{LS} = 0.59 Cmol Cmol^{-1}.

[b] n=12.

Yield of lipid-free biomass on N-source

The yield of lipid-free biomass on N-source (Y_{XN}) was determined using:

$$Y_{XN} = \left\langle \frac{C_X}{C_{Nin} - C_N} \right\rangle \qquad (22)$$

The average value found for the 12 data points is Y_{XN} = 6.1 ± 0.7 Cmol Nmol^{-1}. The value of $1/Y_{XN}$ = 0.16 ± 0.02 Nmol Cmol^{-1} agrees well with the 0.17 Nmol Cmol^{-1} found in the element analysis of the lipid-free biomass.

Maximum specific lipid production rate

The model uses a maximum specific lipid production rate ($q_{L,\max}$) when there is an excess of glucose in the medium. We took the average of the specific lipid production rates calculated with Equation 15 for all data points in the single N-limited regime ($C_N = 0$ and $C_S > 0$). First we omitted the data points with a low residual glucose concentration (< 15 Cmol m^{-3}); this gave $q_{L,\max}$ = 0.022 ± 0.006

Cmol Cmol^{-1} h^{-1} (n=7). Using this value, the model predicts that some of the data points with a low glucose concentration also fall in the single N-limitation regime. Inclusion of these data points in the calculation gave $q_{L,max}$ = 0.023 ± 0.005 Cmol Cmol^{-1} h^{-1} (n=10); this value was used in the model and will be discussed and compared to other lipid producers in part II of this article. Fig. 4 shows that this constant maximum specific lipid production rate gives an adequate description of the measurements in the single N-limitation regime.

Yields of lipid-free biomass and lipids on C-source and maintenance coefficient

In a chemostat, lipid-free biomass production, lipid production and maintenance occur simultaneously, and glucose is used for all of these processes. The specific glucose consumption rate can be described by re-arranging Equation 5:

$$q_S = \frac{D(C_{Sin} - C_S)}{C_X} = \frac{D}{Y_{XS}} + \frac{q_L}{Y_{LS}} + m_S \qquad (23)$$

Multiple linear regression analysis with q_S as dependent variable and D and q_L as independent variables gave Y_{XS} = 0.93 ± 0.09 Cmol Cmol^{-1}, Y_{LS} = 4 ± 16 Cmol

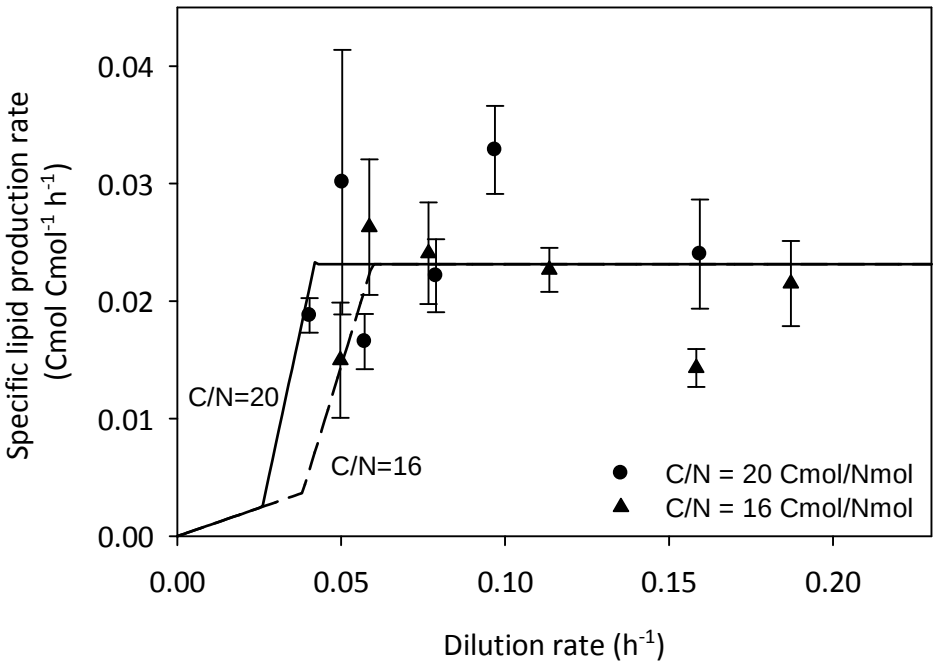

Fig. 4 Measured and modeled specific lipid production rate for *U. isabellina* in a chemostat. Symbols indicate measured values, lines indicate the model, error bars indicate standard deviation.

Cmol^{-1} and m_S = 0.09 ± 0.02 Cmol Cmol^{-1} h^{-1} (Table 3b). The value for Y_{LS} is unreliable, which is due to the low correlation coefficient of q_S and q_L (-0.046). Therefore, we repeated the regression analysis using Y_{LS} = 0.59 (the theoretical maximum according to Ratledge (1988). This gave Y_{XS} = 0.92 ± 0.09 Cmol Cmol^{-1} and m_S = 0.05 ± 0.01 Cmol Cmol^{-1} h^{-1} (Table 3b). The 3-parameter fit gave a smaller sum of squares of residuals (SSE), but the F-test showed that this is insignificant (F=2.86, p=0.125). Therefore, we used the results of the 2-parameter fit together with the assumed value Y_{LS}=0.59 in the rest of this paper (see Table 3a).

The regression analysis gave high values for Y_{XS} and m_S. For Y_{XS}, the value of 0.67 Cmol Cmol^{-1} was expected, as this is the theoretical yield of the conversion of glucose to acetylCoA, the precursor for most biomass components. For m_S, values around 0.02 Cmol Cmol^{-1} h^{-1} were found before for different fungal species (Roels 1983) on glucose. A reason for our high values could be the incomplete carbon recovery (Table 2). If we assume that all the missing carbon is present as attached cells with the same lipid content and specific growth rate as the suspended cells found in the medium, we find a lower specific glucose uptake rate (q_S) while the dilution rate and specific lipid production rate remain unchanged. As a result, the regression analysis gives lower values for Y_{XS} (0.88 ± 0.07 Cmol Cmol^{-1}) and m_S (0.026 ± 0.009 Cmol Cmol^{-1} h^{-1}). This value for the maintenance coefficient is reasonable, which means that cells attached to the baffles and stirrer can probably explain the high maintenance coefficient found in the regression analysis of uncorrected data. The cell yield, however, is still high after correcting the data for the carbon loss. In principle the cell yield can be high if the cells use anaplerotic pathways to bind CO_2. According to Wynn et al. (2001), the enzyme pyruvate decarboxylase combines CO_2 and pyruvate to oxalo-acetate in the transhydrogenase cycle in oleaginous fungi. Therefore, we can assume that this enzyme is present and active in our fungus, and that it could have contributed to a higher than normal value of Y_{XS}. However, the use of the anaplerotic route decreases the ATP production, which makes a high value for Y_{XS} still hard to explain. We have no conclusive explanation for the high value of Y_{XS}, but the parameters from Table 3a allow accurate simulation of the chemostat data as shown below.

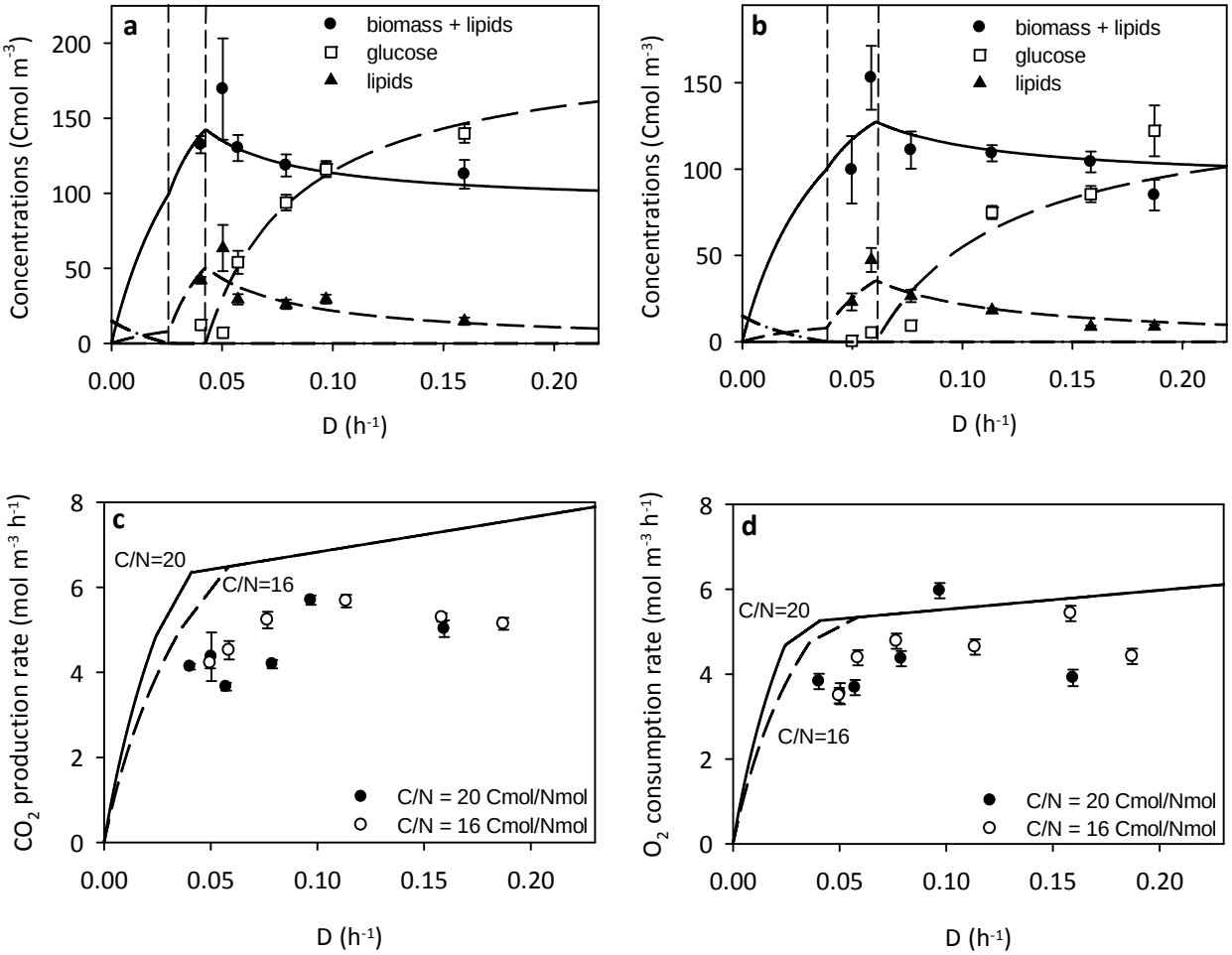

Fig. 5a C/N-ratio of the feed = 20 Cmol/Nmol, **Fig. 5b** C/N-ratio of the feed is 16 Cmol/Nmol. Vertical dashed lines indicate boundaries between C-limited regime (left), dual limited regime (middle) and N-limited regime (right). Concentrations in Cmoles, except for N-source (line only), which is expressed in Nmoles.
Fig. 5c CO_2-production rate, **Fig. 5d** O_2-consumption rate.

Fit of the model to the data

Fig. 5 shows the fitted model together with the measured concentrations of total biomass, lipids and glucose in the culture and the O_2 consumption rates and CO_2 production rates. The measured concentrations of NH_4^+ are not shown because they were very low. The same parameter values (Table 3a) were used for all graphs. Fig. 5a and 5b show that the model describes the decrease in lipids and the increase in residual glucose with increasing dilution rate very well. Furthermore, the fit for both C/N-ratios in the feed is equally good, which indicates that the model can predict the results of a change in C/N-ratio in the feed.

Fig. 5c and d show that the measured CO_2 production and O_2 consumption rates - which were not used to determine the model parameters - are not predicted accurately. The C-balance attributes the missing carbon (12% on average) to CO_2, leading to an overestimation of the CO_2-production rate. However, this error does not affect the predictions for lipid-free biomass, lipids and glucose; these are predicted well for the tested dilution rates and C/N-ratios.

In Fig. 5a and 5b the three limitation regimes described in the model section are shown: single C-limitation, dual limitation and single N-limitation. Most of the measurements fall in the single N-limitation regime, where the lipid concentration decreases with increasing dilution rate because the specific lipid production rate is constant while the specific growth rate increases. The lipid-free biomass concentration is not shown in the graph, but has an average value of 2.7 ± 0.3 g L^{-1} for all data points in the N-limitation regime, which is close to the model value of 2.6 g L^{-1}. Glucose was detected at all data points in this regime, meaning that it was not limiting.

There are only two data points in the dual limitation regime and no data points in the single C-limitation regime. For the used C/N-ratios in the feed, a very low dilution rate was required to have dual limitation or single C-limitation. Cultures at dilution rates lower than 0.04 h^{-1} were attempted, but no steady state could be reached and no reliable data could be obtained. This was due to problems associated with the filamentous form of *U. isabellina*. At high dilution rates (D >0.1 h^{-1}), the fungus grew in small pellets (<<1 mm), but at lower dilution rates free mycelium was present, which caused formation of large aggregates adhering to the baffles and stirrer. Reversing the rotation direction of the stirrer every 30 seconds reduced formation of aggregates on the baffles, but still aggregates were formed and re-suspended periodically, leading to fluctuations in the biomass concentration and therefore to large error bars in Fig. 5. Furthermore, at lipid fractions of the cells above 10 % w/w, the mycelium tended to float and clot together irreversibly at the surface of the culture, making it impossible to take representative samples. These problems make any submerged fermentation with *U. isabellina* an instable system, in which the chance of failure increases with time. As the time to reach steady state increases with decreasing dilution rate, it was not possible to get reliable results at very low dilution rates. Using other C/N-ratios than the tested ones would not have added extra information to validate the model, because for higher C/N-ratios an even lower dilution rate is required to

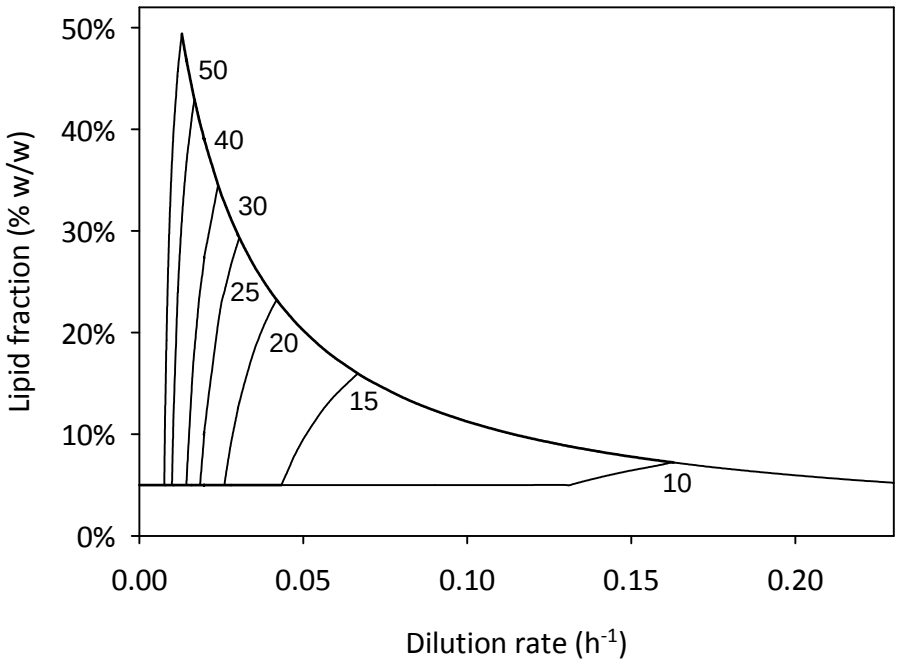

Fig. 6 Predicted lipid fraction in the cells as a function of the dilution rate. Numbers in the graph indicate C/N-ratio in the feed (Cmol/Nmol, C_{Nin}=constant).

reach high lipid concentrations, and for lower C/N-ratios the reached lipid concentration will be so low that it cannot be distinguished from the basal lipid concentration for membranes.

To validate our model also for the dual limitation regime and the single C-limitation regime, we used literature data for oleaginous yeasts, which do not have the problems that we experienced with our fungus at low dilution rates. Results of the validation with literature data can be found in part II of this paper.

Prediction of the maximum lipid content and production rate

Fig. 6 shows a prediction of the lipid fraction in the cells for several C/N-ratios in the feed and a range of dilution rates. For $D < 0.04\ h^{-1}$ this is an extrapolation, but we believe the shown pattern is correct. For a given feed C/N-ratio, the lipid fraction increases with decreasing dilution rate until it peaks.

The peak occurs at the transition from single N-limitation to dual C and N-limitation; the dilution rate at the peak can be found with Equation 10 using $C_S = 0$:

$$D_{opt} = \frac{\frac{q_{L,\max}}{Y_{LS}} + m_S}{\frac{1}{Y_{XN}}\frac{C_{Sin}}{C_{Nin}} - \frac{1}{Y_{XS}}} \tag{24}$$

Similarly, one can find the dilution rate at which no extra lipids are accumulated, by substituting $C_N = 0$ in Equation 11:

$$D_{\min} = \frac{m_S}{\frac{1}{Y_{XN}}\frac{C_{Sin}}{C_{Nin}} - \frac{1}{Y_{XS}} - \frac{f_{L0}}{1-f_{L0}}\frac{1}{Y_{LS}}} \tag{25}$$

The lipid production rate in the three regions is given by:

$$r_L = \begin{cases} q_{L,\max} Y_{XN} C_{Nin} & \text{if} \quad D \geq D_{opt} \\ Y_{LS} Y_{XN} C_{Nin} \left(\frac{C_{Sin}}{C_{Nin}} \frac{D}{Y_{XN}} - \frac{D}{Y_{XS}} - m_S \right) & \text{if} \quad D_{min} < D < D_{opt} \\ \frac{\frac{f_{L0}}{1-f_{L0}} C_{Sin} D}{\frac{m_s}{D} + \frac{1}{Y_{XS}} + \frac{f_{L0}}{1-f_{L0}}\frac{1}{Y_{LS}}} & \text{if} \quad D < D_{min} \end{cases} \tag{26}$$

In the single N-limited region ($D > D_{opt}$), the lipid production rate in the bioreactor is constant because the specific lipid production rate and the lipid-free biomass concentration are both constant (Equation 15). In the dual C and N-limited region ($D_{min} < D < D_{opt}$) the lipid production rate in the bioreactor is proportional to D because the specific lipid production rate increases with increasing glucose supply rate and the lipid-free biomass concentration is constant (Equations 16 and 17). The lipid production rate in the single C-limited region ($D < D_{min}$) is proportional to D but too low to be of interest (Equations 13 and 19).

Operating the bioreactor at D_{opt} gives the highest possible lipid production rate in the bioreactor, combined with the highest possible lipid content of the cells and the highest possible lipid yield on glucose. The lipid content of the cells can be

increased by increasing the C/N-ratio of the feed and decreasing the dilution rate accordingly. Theoretically, it should be possible to reach much higher lipid fractions than we have measured, but in practice this will be difficult for two reasons: (1) The problems with cells adhering to the bioreactor and floating on the surface described above, and (2) At higher C/N-ratio and lower D the lines in Fig. 6 are very steep, which means that a small deviation in the dilution rate has a large influence on the lipid fraction. So although the model predicts that very high lipid fractions can be reached at high C/N-ratios in the feed and low dilution rates, in practice it will not be easy to reach these high lipid fractions in a chemostat culture. The highest lipid fraction in the cells reached in our experiments was 25% w/w, at a C/N-ratio of 20 Cmol $Nmol^{-1}$ and a dilution rate of 0.04 h^{-1}. This is probably the highest lipid fraction that can be reached with *U. isabellina* in chemostat cultures.

Implications of the model

The most important insight in kinetics of lipid accumulation of *U. isabellina* is that the fungus only accumulates lipids when it has fully satisfied its carbon requirements for maintenance and growth. This can also have large implications for lipid production in other systems, such as solid-state fermentation. In solid-state fermentation, the substrate monomers are released from the solid substrate and diffuse to the fungal cells, at a certain supply rate. When this supply rate is low, for example because of diffusion limitation or low enzyme activity, we can compare the situation with a chemostat in the single-carbon limitation or dual limitation regime. As a result, even if the C/N-ratio of the 'feed' is high enough to allow for lipid production, the lipid yield on converted substrate can be very low (see Fig. 2). This may explain the low lipid yields reported in literature (Gema et al. 2002, Stredansky et al. 2000, Peng and Chen 2008, Economou et al. 2010).

Most production systems reported in the literature are batch reactors. In a chemostat, the cells grow, but in batch culture, growth stops when the nitrogen source is exhausted, and this may give other lipid production kinetics. In future work, we will extend our work to submerged batch cultivation.

Chapter 4

Modeling lipid accumulation in oleaginous fungi in chemostat cultures: II. Validation of the chemostat model using yeast culture data from literature

Meeuwse P, Tramper J, Rinzema A. 2011. Modeling lipid accumulation in oleaginous fungi in chemostat cultures. II: Validation of the chemostat model using yeast culture data from literature. Bioprocess Biosyst Eng 34: 951-961.

Abstract

A model that predicts cell growth, lipid accumulation and substrate consumption of oleaginous fungi in chemostat cultures (Meeuwse et al. 2011) was validated using published data sets for chemostat cultures of oleaginous yeasts and fungi and one published data set for a poly-hydroxyalkanoate accumulating bacterial species. The model could describe all data sets well with only minor modifications that do not affect the key assumptions, *i.e.* (1) oleaginous yeasts and fungi give the highest priority to C-source utilization for maintenance, second priority to growth and third priority to lipid accumulation, and (2) oleaginous yeasts and fungi have a growth-rate independent maximum specific lipid production rate. Analysis of all data showed that the maximum specific lipid production rate is in most cases very close to the specific production rate of membrane and other functional lipids for cells growing at their maximum specific growth rate. The limiting factor suggested by Ykema et al. (1986), *i.e.* the maximum glucose uptake rate, did not give good predictions of the maximum lipid production rate.

Introduction

In part I (Meeuwse et al. 2011) we presented a mathematical model for lipid accumulation in oleaginous fungi growing in chemostat cultures. This model describes our chemostat cultures of *U. isabellina* growing on glucose as C-source and NH_4^+ as N-source well. In the current paper we show that the model can also describe data obtained with oleaginous yeasts cultivated in chemostats using a large range of C/N-ratios and dilution rates, including the low dilution rates that could not be realized with *U. isabellina*. With the large set of data from literature, we also test hypotheses about the limiting factor for the specific lipid production rate. One of these hypotheses comes from the chemostat model published by Ykema et al. (1986), Finally, we show that our model for lipid accumulation can also predict accumulation of polyhydroxy-alkanoates (PHA), another carbon-based storage material.

Model

The model is based on component mass balances, Pirt's law and two major assumptions (Meeuwse et al. 2011):

- The first priority of the fungus is to use the supplied C-source to satisfy its maintenance requirements, then to produce lipid-free biomass including functional lipids, and finally, only if there is still C-source available, to accumulate storage lipids.
- If sufficient C-source is available, the specific lipid production rate will increase up to a maximum value $q_{L,\max}$. This maximum specific lipid production rate is independent of the specific growth rate.

These assumptions lead to three different limitation regimes:

- Single nitrogen limitation, where the N-source limits the lipid-free biomass formation and the specific lipid production rate has its maximum value;
- Dual limitation of C-source and N-source, where the N-source limits the lipid-free biomass formation and the C-source limits the lipid production;
- Single carbon limitation, where the C-source limits the lipid-free biomass formation and only membrane lipids are produced.

The equations used in the model are shown in Table 1 of part I (Meeuwse et al. 2011). For the calculations in this paper we used molecular weights of 25 g $Cmol^{-1}$ for lipid-free biomass and 15.7 g $Cmol^{-1}$ for lipids. A list of symbols can be found on page 207.

Results and discussion

Table 1 shows an overview of chemostat cultures with more than four dilution rates or C/N-ratios found in literature. In most studies one or two constant C/N-ratios and various dilution rates were used. In most studies a high C/N-ratio in the feed (>20 Cmol/Nmol) was used in order to promote lipid accumulation. Some studies also included a low C/N-ratio, which does not lead to lipid production in most cases.

Model parameters were determined for all data sets in Table 1, in most cases using all data within a set, independent of the C/N-ratio or dilution rate. Because of the large number of studies used, we will not describe all studies separately. We will discuss the fitting procedure and the predictions for all studies in general and point out some exceptions. Graphs showing the measured data points together with the model predictions for all studies are shown in the appendix; parity plots are included this article.

Chemostat cultures with filamentous fungi

Results from submerged chemostat studies with oleaginous fungi are hardly described in the literature: we only found three papers on this topic. The first (Data set 1) uses the filamentous fungus *Mucor rouxii* (Hansson et al. 1989). This fungus has a filamentous and a yeast-like morphology, and the yeast-like form was observed during most of the experiments. The filamentous form of *Mucor rouxii* is able to accumulate lipids up to 30% w/w (Somashekar et al. 2003), but in the yeast-like form less than 10% w/w lipids was found, even in the presence of residual glucose. Therefore, Data set 1 was not suitable to fit the model. In our studies with *U. isabellina* (Data set 2, Meeuwse et al. (2011)) we also observed that the filamentous fungus transformed to a yeast-like morphology when it was cultivated at a high dilution rate and exposed to the shear forces of the stirrer for at least 7 days. This yeast-like form also did not accumulate lipids and was not included in the model validation. Data set 2 has been discussed extensively in part I (Meeuwse et al. 2011), and will therefore not be discussed here. Data set 3 uses *Mucor circinelloides* (Song et al. 2001) and will be discussed together with the yeast cultures. Kendrick and Ratledge (1992) used the fungus *Entomophtora exitalis* in chemostat culture, but only used one C/N-ratio and dilution rate. As our

Table 1 Literature data used to validate the model as is described in the text

Data set	Reference	Organism	Medium C-source / N-source [a]	Number of datapoints [b]	C/N-ratio (Cmol/Nmol)	Dilution rates (h^{-1})	Reported μ_{max} (h^{-1})
	Fungi						
1	Hansson et al. (1989)	*Mucor rouxii* [c]	Glucose / NH_4Cl+YE	15	11-29	0.03-0.14	-
2	Meeuwse et al. (2011)	*Umbelopsis isabellina*	Glucose / $(NH_4)_2SO_4$	6 + 6	16 + 20	0.04-0.19	0.23
3	Song et al. (2001)	*Mucor circinelloides*	Glucose / NH_4Cl+YE	5	43	0.04-0.18	-
	Yeast						
4	Alvarez et al. (1992)	*Rhodotorula glutinis*	Molasses (both C and N)	7	25-35	0.04-0.1	-
5	Brown et al. (1989)	*Candida curvata*	Glucose / YE	20 [d]	71	0.025-0.29	0.305
6	Choi et al. (1982)	*Rhodotorula gracilis*	Glucose / $(NH_4)_2SO_4$+YE	6	53	0.02-0.09	-
7	Evans and Ratledge (1983)	*Candida curvata*	Sugars [e] / NH_4Cl+YE	16 + 16 [f]	17 + 50-52 [g]	0.02-0.3 [f]	0.3 [f]
8	Gill et al. (1977)	*Candida* 107	Glucose / NH_4Cl+YE	7 + 7	6 + 26	0.03-0.21	0.21
9	Hansson and Dostalek (1986)	*Cryptococcus albidus*	Glucose / NH_4Cl+YE	5 + 4	10 + 58	0.031-0.107	0.11
10	Hassan et al. (1993)	*Apiotrichum curvatum* UfaM3 [h,i]	Glucose / NH_4Cl+YE	11	44	0.04-0.4	-
11	Papanikolaou and Aggelis (2002)	*Yarrowia lipolytica*	Glycerol / $(NH_4)_2SO_4$+YE	5	147	0.03-0.13	0.21
12	Ratledge and Hall (1979)	*Rhodotorula glutinis*	Glucose / NH_4Cl+YE	5 + 4	6 + 25	0.02-0.1	0.12
13	Ykema et al. (1986)	*Apiotrichum curvatum* [f]	Glucose / NH_4Cl+YE	11	7-68	0.02	0.2
14	Yoon and Rhee (1983)	*Rhodotorula glutinis*	Glucose / $(NH_4)_2SO_4$+YE	7	62	0.01-0.1	0.13

Footnotes: see next page

model needs at least four data points for the determination of parameter values, this data set was not used.

Chemostat cultures with oleaginous yeasts

All studies in Table 1 report total biomass concentrations and lipid concentrations or lipid fractions in the cells, but they do not always report all substrate concentrations required to find the model parameters. For Data sets 2, 4-6 and 8-11, the C-source and N-source concentrations are reported, or the limiting (=depleted) substrate is indicated and the concentration of the non-limiting substrate is reported. For Data sets 3, 7 and 12-14, however, one or both substrate concentrations are not reported. Therefore these data sets could not be completely described by the model, as will be discussed later. None of the studies reports CO_2 production or O_2 consumption. Data set 13 was obtained under non-steady state conditions in a continuous culture with a changing C-source concentration in the feed. To describe this data set, changes in time have to be taken into account, which makes the model and the fitting procedure for this data set different from the other data sets. Therefore we decided not to use this data set for the validation of the model; however, we will discuss non-steady state situations later in this article.

Footnotes Table 1

[a] YE = yeast extract

[b] When two C/N-ratios were used as is shown in the column to the right, the number of data points is mentioned for the two C/N-ratios separately.

[c] Mainly present in a yeast-like form

[d] including duplicates; 9 different dilution rates were measured with 2-4 duplicates

[e] Glucose, sucrose, lactose and xylose, respectively. Ethanol was also used, but is not included in the modelling because it could not be modelled together with the sugars, and not enough data points are available to model it separately.

[f] Five data points per substrate were available, but at the highest dilution rate used, signs of washout were detected. These data points were therefore not used, and the highest dilution rate used was taken as μ_{max}.

[g] The same concentrations in grams were used for all sugars, which leads to different C/N-ratios in moles because of different molar weights.

[h] Mutant blocked in Δ^9-desaturase

[i] *A. curvatum* is currently also called *Candida curvata*

Table 2 Model parameters found for the literature data

Data set no.	f_{L0} (Cmol Cmol^{-1})	Y_{XN} [a] ± SD (Cmol Nmol^{-1})	$q_{L,max}$ ± SD (Cmol Cmol^{-1} h^{-1})	Y_{XS} ± SD (Cmol Cmol^{-1})	Y_{LS} ± SD (Cmol Cmol^{-1})	m_S ± SD (Cmol Cmol^{-1} h^{-1})
2	0.079	6.1 ± 0.7	0.023 ± 0.005	0.92 ± 0.10	0.59 [b]	0.05 ± 0.01
3	0.15	(12.1±0.7)-(37±5)*D	0.032 ± 0.007 [c]	ND [d]	ND [d]	ND [d]
4	0.15	(13.7±1.4)-(71±23)*D [e]	0.039 ± 0.006	0.56 ± 0.07	0.99 ± 0.36	0 [b]
5	0.12	(15.3±0.6)-(41±4)*D	0.040 ± 0.008	0.86 ± 0.11	0.65 ± 0.27	0 [b]
6	0.15	(8.5±0.7)-(70±15)*D	0.027 ± 0.006	0.25 ± 0.02	0.59 [b]	0 [b]
7a [f] 7b [f]	0.19	(22±1)-(84±11)*D ND [d]	0.037 ± 0.010 [c,g]	0.55 ± 0.02 [g,h]	0.59 [b]	0 [b]
8a [f] 8b [f]	0.15	(13.8±0.7)-(38±6)*D 5.8 ± 0.3	0.069 ± 0.009	0.62 ± 0.03	0.88 ± 0.14	0 [b]
9a [f] 9b [f]	0.15	(18±2)-(83±30)*D 6.4 ± 0.5	0.041 ± 0.004 0.032 ± 0.002	0.75 ± 0.05	0.47 ± 0.04	0 [b]
10	0.12	(16.5±0.4)-(34±2)*D	0.065 ± 0.015	0.73 ± 0.04	0.88 ± 0.18	0 [b]
11	0.12	(16.9±0.8)-(37±10)*D	0.030 ± 0.013	0.16 ± 0.01	0.97 ± 0.34	0 [b]
12a [f] 12b [f]	0.21	(9.8±0.4)-(62±6)*D ND [d]	0.031 ± 0.004 [c]	0.56 ± 0.04 [h]	0.77 ± 0.41 [h]	0 [b]
14	0.15	(8.1±0.4)-(60±8)*D	0.028 ± 0.006 [c]	ND [d]	ND [d]	ND [d]

Footnotes: see next page

Determination of parameter values

To describe the data sets with our model, values have to be found for the basal (membrane) lipid fraction in the cells (f_{L0}), the yield of lipid-free biomass on N-source (Y_{XN}), the yield of lipid-free biomass on C-source (Y_{XS}), the yield of lipids on C-source (Y_{LS}), the maintenance coefficient (m_S) and the maximum specific lipid production rate ($q_{L,\max}$). The approach used to determine these parameters has been described in detail in part I (Meeuwse et al. 2011). All parameter values found are shown in Table 2.

Basal lipid content of the cells (f_{L0})

If available, we used the reported lipid fraction in the C-limitation regime as the basal lipid content of the cells. However, not all studies report results in this regime. For these studies, we used either an estimated value of 10% w/w = 0.015 Cmol Cmol^{-1}, which is the average measured value found in literature, or the lowest reported lipid fraction if this was below 10% w/w (see Table 2).

Yield of lipid-free biomass on N-source

As was discussed before in part I (Meeuwse et al. 2011), the yield of lipid-free biomass on N-source (Y_{XN}) can be calculated with the following equation:

$$Y_{XN} = \frac{C_X}{C_{Nin} - C_N} \qquad (22)$$

Footnotes Table 2

[a] Yield of lipid-free biomass on N-source as a function of the dilution rate D (r^2>0.80 unless stated otherwise) or as a constant value (see text).

[b] estimated value

[c] Because no C-source concentration was reported, only data points where no C-source limitation ($C_S > 0$) could reasonably be assumed (see text), were used to determine these parameter values

[d] Not determined because substrate concentrations were not reported.

[e] r^2=0.66

[f] Data set a contains data points from N-limited culture (high C/N-ratio), data set b contains data points from C-limited culture (low C/N-ratio).

[g] Differences in parameter values for the different substrates were not significant and we determined one value for all sugars.

If present, yeast extract (YE) was taken into account as N-source; it was assumed to contain 10% N w/w, unless another fraction was reported in the study.

For data sets with a C/N-ratio ≤ 20 Cmol/Nmol, the overall Y_{XN} could be calculated by taking the average value for all data points. For data sets with a C/N-ratio > 20 Cmol/Nmol, however, Y_{XN} did not have a constant value, but depended on the dilution rate:

$$Y_{XN} = a - bD \qquad (27)$$

This linear dependence is shown in Fig. 1 for Data sets 8 and 10. In Data set 8, two different C/N-ratios were used: 26 Cmol/Nmol (8a) and 6 Cmol/Nmol (8 b), with the same yeast strain and substrates. In Data set 10, one C/N-ratio (44 Cmol/Nmol) was used.

Fig. 1 shows clearly that a high C/N-ratio (Data sets 8a and 10) gives a linear decrease of the yield with increasing dilution rate, while a low C/N-ratio (Data set 8b) does not. This is also the case for the other data sets; the values or equations for Y_{XN} are shown in Table 2. The dependency of the yield of lipid-free biomass on the dilution rate at a high C/N-ratio (C/N>20 Cmol/Nmol) was not reported in the original publications. As far as we know, this is the first time that this linear

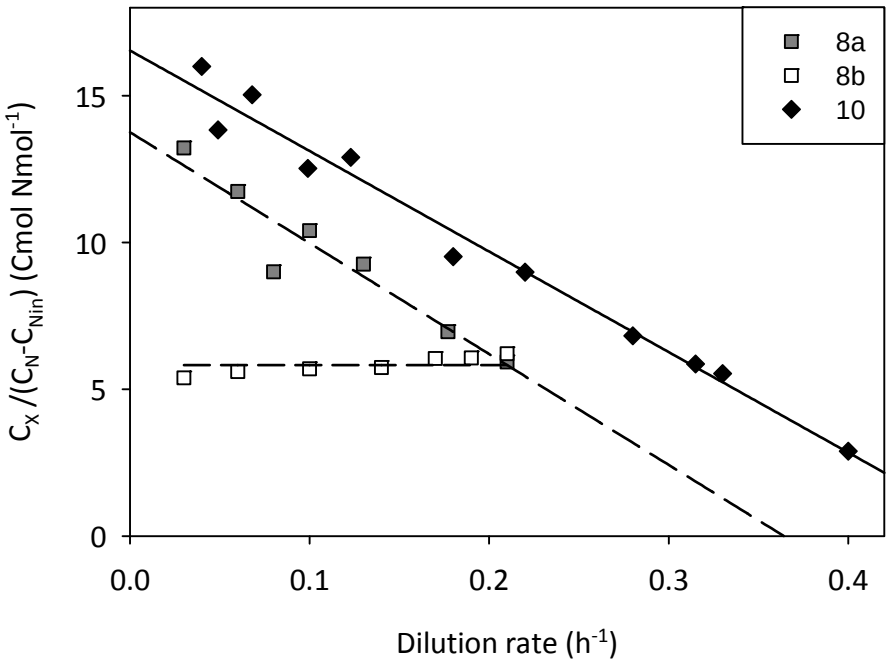

Fig. 1 The yield of lipid-free biomass on N-source as a function of the dilution rate for Data sets 8a (C/N = 26 Cmol/Nmol), 8b (C/N = 6 Cmol/Nmol) and 10 (C/N = 44 Cmol/Nmol)

dependency is reported. We assume that this change in yield is caused by accumulation of another carbon-based storage material than lipids, because it only appears at high C/N-ratios, when the C-source is in abundance. In this respect it is similar to the accumulation of lipids, which also appears at high C/N-ratios and increases with decreasing dilution rate. The accumulation of lipid precursor molecules has been reported before (Ykema et al. 1986), but a relation with the dilution rate was not found. None of the studies in Table 1 reported another storage material or (changes in) the element composition of the biomass.

The values found for the yield of lipid-free biomass on N-source (Y_{XN}) reported in Table 2 can be used to predict the lipid-free biomass concentration (C_X) during N-limitation (Equation 12, Table 1 in part I) and the N-source concentration in the fermenter (C_N) during single C-limitation (Equation 11, Table 1 in part I). Fig. 2a and 2b show two parity plots of the modeled versus the measured lipid-free biomass concentration, calculated with a constant value for Y_{XN} (Equation 22, Fig. 2a) and with a dilution rate dependent value for Y_{XN} (Equation 27, Fig. 2b), respectively. Fig. 2b shows a much better correlation between measured and modeled values than Fig. 2a, indicating that Equation 27 gives a better fit than a constant value for Y_{XN} when C/N >20 Cmol/Nmol (see Table 2). So although the reason for the linear relation between the yield of lipid-free biomass on N-source (Y_{XN}) and the dilution rate (D) is not known, Equation 27 is used in the fitting procedure because it describes the data very well.

Only very few studies applied C-limitation and reported values for the N-source concentration in the fermenter (C_N). Reported N-source concentrations are compared to the predicted values in Fig. 2c. The few data points that are depicted in this parity plot are close to the correlation line, so from this plot and Fig. 2b we can conclude that the values found for Y_{XN} are suitable for use in the model.

Maximum specific lipid production rate

Because we assume that the specific lipid production rate is constant when the C-source is not limiting, the value for the maximum specific lipid production rate ($q_{L,\max}$) was calculated by taking the average specific lipid production rate for all data points with $C_N = 0$ and $C_S > 0$. For Data sets 3, 7, 12 and 14, the C-source

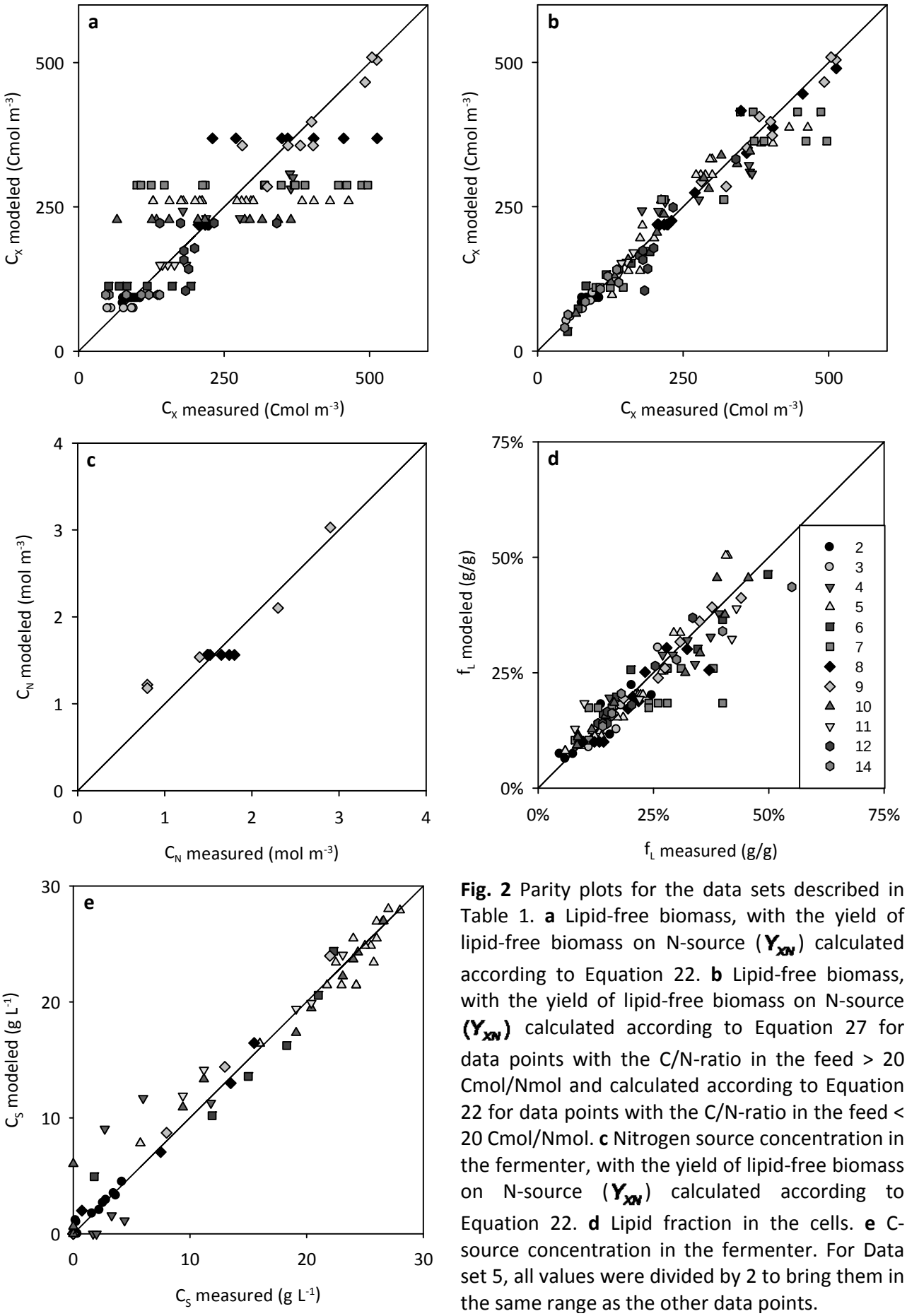

Fig. 2 Parity plots for the data sets described in Table 1. **a** Lipid-free biomass, with the yield of lipid-free biomass on N-source (Y_{XN}) calculated according to Equation 22. **b** Lipid-free biomass, with the yield of lipid-free biomass on N-source (Y_{XN}) calculated according to Equation 27 for data points with the C/N-ratio in the feed > 20 Cmol/Nmol and calculated according to Equation 22 for data points with the C/N-ratio in the feed < 20 Cmol/Nmol. **c** Nitrogen source concentration in the fermenter, with the yield of lipid-free biomass on N-source (Y_{XN}) calculated according to Equation 22. **d** Lipid fraction in the cells. **e** C-source concentration in the fermenter. For Data set 5, all values were divided by 2 to bring them in the same range as the other data points.

concentration (C_S) was not reported but the occurrence of N-limitation ($C_N = 0$) was reported. Therefore for the data points with $C_N = 0$ we did not know if the cells were subjected to single N-limitation ($C_S > 0$) or to dual limitation ($C_S = 0$). Because single N-limitation usually occurs at a higher dilution rate than dual limitation, we calculated the maximum specific lipid production rate using only data points with N-limitation and a high dilution rate for which the specific lipid production rate appeared to be constant.

All values for the maximum specific lipid production rate ($q_{L,\max}$) are shown in Table 2. The standard deviation for most values is quite small, indicating that the value of the specific lipid production rate was indeed constant for the used data points. No dependency on the dilution rate or the C/N-ratio was found. The maximum specific lipid production rate ($q_{L,\max}$) predicts the lipid concentration in the fermenter and the lipid fraction in the cells when the C-source is in abundance (Equation 15, Table 1 in part I). The parity plot in Fig. 2d shows that the lipid fraction in the cells is predicted very well.

Data set 9 has two values for the maximum specific lipid production rate ($q_{L,\max}$), depending on the limiting component (N-limitation or C-limitation). This yeast is an exception to the rule that cells have a constant lipid fraction in the cells during single C-limitation. For an unknown reason, this strain also produces lipids at a constant rate under C-limitation, i.e. it gives priority to lipid production at the expense of lipid-free biomass production. This has been described before by Boulton and Ratledge (1984). To model this phenomenon, we have to alter the model slightly. In the model described in part I, the specific lipid production rate during single C-limitation is proportional to the specific growth rate:

$$q_{L,\min} = \frac{f_{L0}}{1 - f_{L0}} D \qquad (18)$$

For Data set 9, the specific lipid production rate is constant and independent of the specific growth rate:

$$q_{L,\min} = \text{constant} \qquad (28)$$

The constant minimum specific lipid production rate ($q_{L,\min}$) for Data set 9 was calculated by taking the average of the specific lipid production rates during single C-limitation. This allowed accurate modeling of this data set, as shown in Fig. 2d.

Yields of lipid-free biomass and lipids on C-source and maintenance coefficient

The specific substrate consumption rate is divided into three parts: lipid-free biomass production, lipid production and maintenance:

$$q_S = \frac{D(C_{Sin} - C_S)}{C_X} = \frac{D}{Y_{XS}} + \frac{q_L}{Y_{LS}} + m_S \qquad (23)$$

Multiple linear regression analysis using Equation 23 was applied to find Y_{XS}, Y_{LS} and m_S. However, for none of the data sets from literature this gave a reliable value for the maintenance coefficient. In all cases, the obtained value for m_S was negative or had such a large standard deviation that it was not significantly different from zero. Therefore, the maintenance coefficient (m_S) was set to zero and values for Y_{XS} and Y_{LS} were obtained (Table 2). For Data sets 2, 6 and 7 a theoretical value of Y_{LS} = 0.59 Cmol Cmol^{-1} was used as was published by Ratledge (1988). The fitting of Data set 2 was discussed extensively in part I. Fitting of Y_{LS} for Data set 6 and 7 gave unrealistic values of Y_{LS} ± SD = 9*10^3 ± 6*10^7 Cmol Cmol^{-1} and Y_{LS} ± SD = 7*10^3 ± 9*10^7 Cmol Cmol^{-1}, respectively, and therefore we replaced Y_{LS} with the literature value of 0.59 Cmol Cmol^{-1}.

All values found for the yield of lipid-free biomass on C-source (Y_{XS}) are in the expected range when the inaccuracy is taken into account. Only the value for Data set 2 is very high; this was discussed in detail in part I. Data sets 6 and 11 have a very low value for Y_{XS}. This could be caused by the use of C-source for production of extra products that were not measured. Data set 11 does report production of small amounts of citrate, but taking this product into account did not increase the value for Y_{XS}. Therefore, other by-products may have been present. The values found for Y_{LS} are generally above the theoretical value of 0.59 Cmol Cmol^{-1}, but several values are not very accurate as is indicated by a large standard deviation, so no conclusions can be drawn here.

Because all data sets lack CO_2-production data, the carbon balance and therefore the assumption that no other products besides biomass, lipids and CO_2 were formed, could not be checked. The parameter values found are based on this assumption and are therefore only valid if the model is not extended with by-product formation.

For most data points, the parameters Y_{XS}, Y_{LS} and m_S predict the concentration of C-source in the fermenter well (Equation 10, Table 1 in part I); a parity plot is shown in Fig. 2e. For some data points that experience C-limitation, the parameters Y_{XS}, Y_{LS} and m_S are needed to predict the specific lipid production rate (Equation 16, Table 1 in part I) or the lipid-free biomass concentration (Equation 13, Table 1 in part I), as was explained in part I. Parity plots for these variables were already shown in Fig. 2b and 2d.

Fit of the model to the data sets

All parity plots in Fig. 2b-2e show that the model gives a good fit for all data sets with the parameter values from Table 2. So far, we have not been able to find chemostat results for oleaginous yeast or fungi in literature that cannot be described with the model, unless there was a clear reason for it, as was the case with Data set 1.

Graphs of the different concentrations as a function of the dilution rate for all datasets are shown in the appendix. These graphs show that our model describes the data sets very well.

Comparison with previously published model

A model for growth and lipid production in continuous culture was published before by Ykema et al. (1986). This model is similar to our model; the major differences are:

- Carbohydrates stored in the cells are included as an extra product
- The maximum specific lipid production rate of the cells is not constant, but is given by the difference between their maximum specific glucose uptake rate ($\frac{\mu_{\max}}{Y_{XS}} + \frac{q_{L,\min}}{Y_{LS}} + m_S$) and their actual specific glucose requirement for growth and maintenance ($\frac{D}{Y_{XS}} + m_S$).

Ykema et al. (1986) validated their model using a continuous culture of *Apiotrichum curvatum* with a constant dilution rate and a changing C/N-ratio of the feed. As the change in C/N-ratio was quite fast, this continuous culture was not in steady-state, while all mass balances used in the model require steady-state to be valid. Furthermore, a theoretical glucose concentration in the reactor was used

for validation instead of the glucose concentration in the feed. This theoretical glucose concentration in the reactor was calculated assuming no consumption of glucose in the reactor, but only supply and washout by the ingoing and outgoing flow, respectively. Because in reality there is consumption in the reactor, the outgoing flow will contain less glucose than is assumed using this theoretical glucose concentration in the reactor. This leads to an underestimation of the glucose consumption. We doubt that this model was properly validated; this triggered us to develop our model and to check if the assumptions used in the model of Ykema et al. (1986) are indeed valid.

Ykema's assumption that the maximum specific glucose uptake rate is limiting for lipid production leads to the following equation for the maximum specific lipid production rate:

$$\left.\begin{array}{l} D = \mu_{\max}:\ q_{S,\max} = \dfrac{\mu_{\max}}{Y_{XS}} + \dfrac{q_{L,\min}}{Y_{LS}} + m_S \\ D < \mu_{\max}:\ q_{S,\max} = \dfrac{D}{Y_{XS}} + \dfrac{q_{L,\max}}{Y_{LS}} + m_S \end{array}\right\} q_{L,\max} = \frac{Y_{LS}(\mu_{\max} - D)}{Y_{XS}} + q_{L,\min} \qquad (29)$$

To check Ykema's hypothesis, we used this equation to calculate the maximum specific lipid production rate for the data sets in Table 1, instead of the constant value in Table 2. Parity plots for the lipid content of the cells and the concentration of C-source in the fermenter obtained with Equation 29 are shown in Fig. 3. For Data sets 4, 6 and 10, no μ_{max} was reported. For these data sets we used the highest reported dilution rate without washout in Equation 29; these values are shown in Fig. 3. Data sets 3 and 14 are not shown in the figure because insufficient parameter values are available to estimate the maximum specific lipid production rate with Equation 29 (see Table 2). Fig. 3 shows that in most cases the lipid fraction in the cells is overestimated with Equation 29, and therefore the residual C-source concentration is underestimated. Comparison of Fig. 2d and 2e with Fig. 3a and 3b leads to the conclusion that a constant value for the maximum specific lipid production rate gives a much better correlation between the model and the experimental data. This shows that Ykema's assumption that the maximum specific glucose uptake rate can be used to predict lipid production in chemostat is not correct.

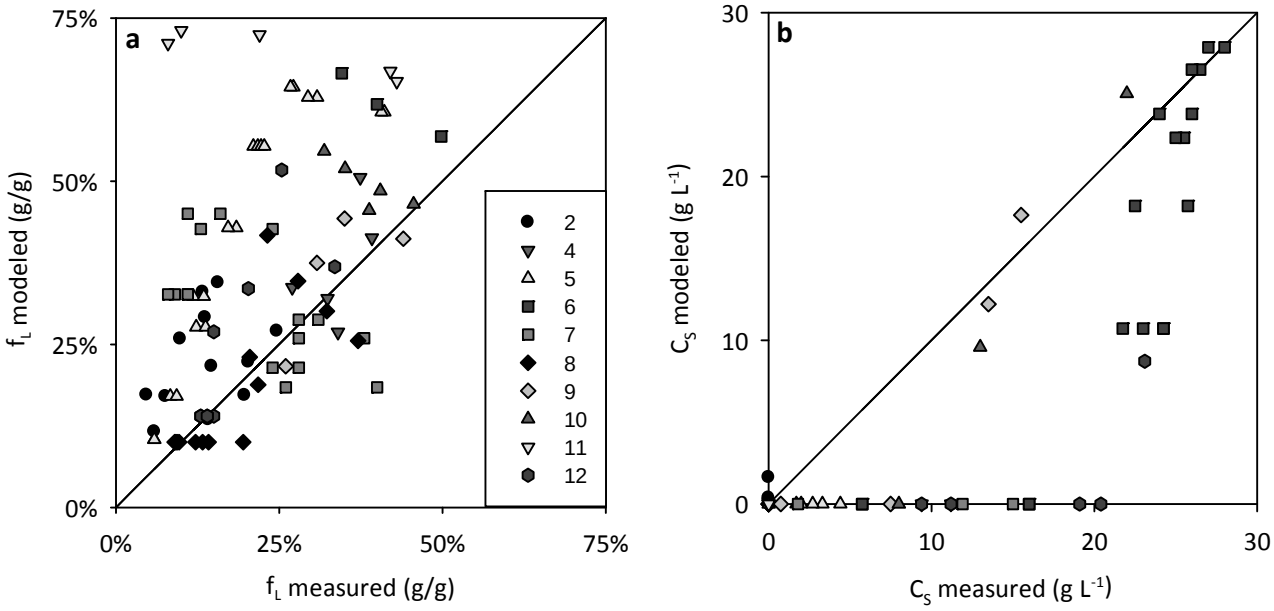

Fig. 3 Parity plots of the lipid fraction in the cells (**a**) and the C-source concentration in the fermenter (**b**), calculated with Equation 29 instead of with a constant maximum specific lipid production rate. Numbers of data sets: see Table 1.

Regulation of the maximum lipid production rate

Although the metabolic pathway and the enzymes involved in lipid production in oleaginous yeast and fungi are known (Ratledge and Wynn 2002), nothing is known about the regulation of the maximum specific lipid production rate. We showed before that the maximum glucose uptake rate, as used in the model of Ykema et al. (1986), is not limiting for the maximum specific lipid production rate. Therefore we propose another hypothesis.

Our hypothesis is that the enzyme activity of the rate limiting step in the lipid synthesis pathway determines the maximum specific lipid production rate. We assume that in chemostat the lipid accumulation pathway is not switched on by nitrogen shortage as was found by Ratledge and Wynn (2002) in batch, because nitrogen source is constantly supplied in chemostat. Therefore we assume that only the enzymes needed for membrane lipid production are available for lipid production, and that no extra enzymes are produced. The membrane lipid synthesizing enzymes reach their maximum activity at the maximum specific growth rate, when the highest specific membrane lipid production rate is needed.

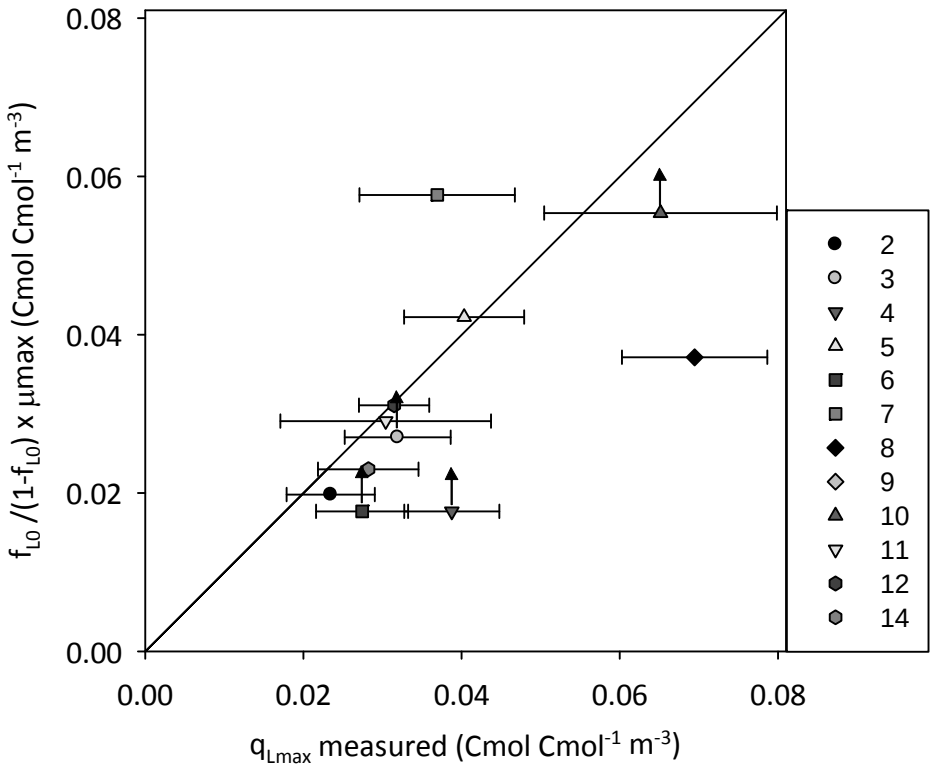

Fig. 4 Parity plot of the maximum specific lipid production rate during C-limitation versus the measured average lipid production rate during N-limitation, calculated with Equation 30. The arrows indicate that the maximum specific growth rate was not given and therefore the maximum applied dilution rate was used, which means that the calculated value can be too low. Numbers of data sets: see Table 1.

This leads to the following equation for the maximum specific lipid production rate:

$$q_{L,\max} = \frac{f_{L0}}{1-f_{L0}}\mu_{\max} \qquad (30)$$

Fig. 4 compares the maximum specific lipid production rates found with this equation to measured values. Data set 9 is not included because f_{L0} does not have a constant value for this data set. For Data sets 3, 4, 6 and 10 μ_{max} was not reported. In these cases we used the highest applied dilution rate (without washout) as μ_{max} value, as is indicated by arrows in the figure. Fig. 4 shows that all data sets except Data sets 7 and 8 are close to or just below the correlation line. This means that indeed for most data sets, the maximum specific lipid production rate is equal to or slightly higher than the specific lipid production rate in cells

growing at μ_{max}. This means that we cannot reject our hypothesis. Further research including enzyme activity measurements can give more insight in this matter.

Broader use of the model

Some micro-organisms store other forms of carbon source in their cells instead of lipids. A well-known storage product is polyhydroxy-alkanoate (PHA). We used our model to describe PHA storage in *Pseudomonas oleovorans* from the data set of Durner et al. (2000), which contains 50 data points for 5 different dilution rates and several C/N-ratios. A summary of the properties of the data set and the parameter values found for this data set is shown in Table 3. The large number of data points provided enough information to fit all parameter values. Fig. 5 shows the data points together with the model predictions. All five graphs were obtained with the same parameter values. The model describes all data well for a wide range of combinations of dilution rate and feed C/N ratio, although the prediction of C-source consumption is less good than the prediction of biomass and PHA concentrations. We conclude that our model can also describe PHA production well.

Table 3 Culture properties and parameter values for PHA-production

Reference	Durner et al. (2000)
Organism	*Pseudomonas oleovorans*
Medium C-source / N-source	octanoate / $(NH_4)_2SO_4$
Number of datapoints	50
C/N-ratio (Cmol/Nmol)	1-33
Dilution rates (h^{-1})	0.05, 0.1, 0.2, 0.3, 0.4
Y_{XN} ± SD (Cmol $Nmol^{-1}$)	4.0 ± 0.8
$q_{P\max}$ [a] ± SD (Cmol $Cmol^{-1}$ h^{-1})	0.20 ± 0.04
Y_{XS} ± SD (Cmol $Cmol^{-1}$)	0.82 ± 0.04
Y_{PS} [a] ± SD (Cmol $Cmol^{-1}$)	0.45 ± 0.02
m_S ± SD (Cmol $Cmol^{-1}$ h^{-1})	0.11 ± 0.02

[a] $q_{P,\max}$ = maximum specific PHA production rate; Y_{PS} = yield of PHA on C-source

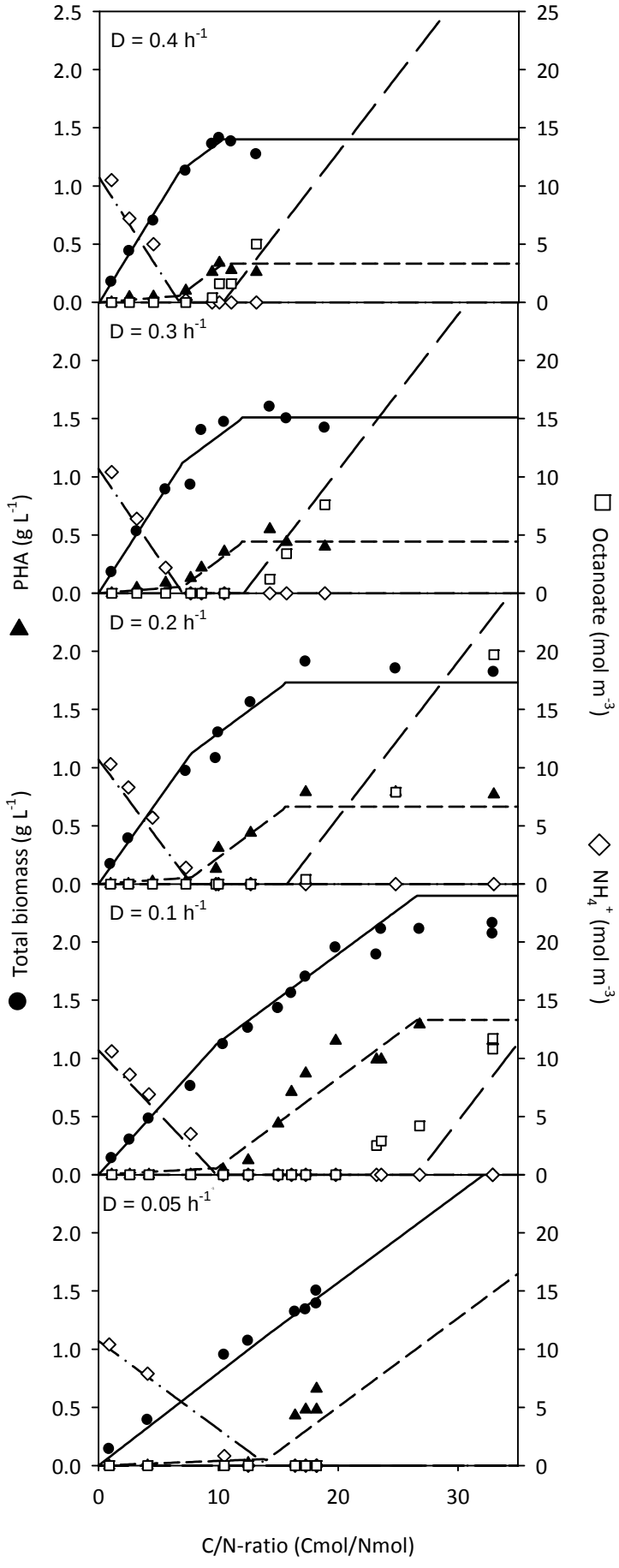

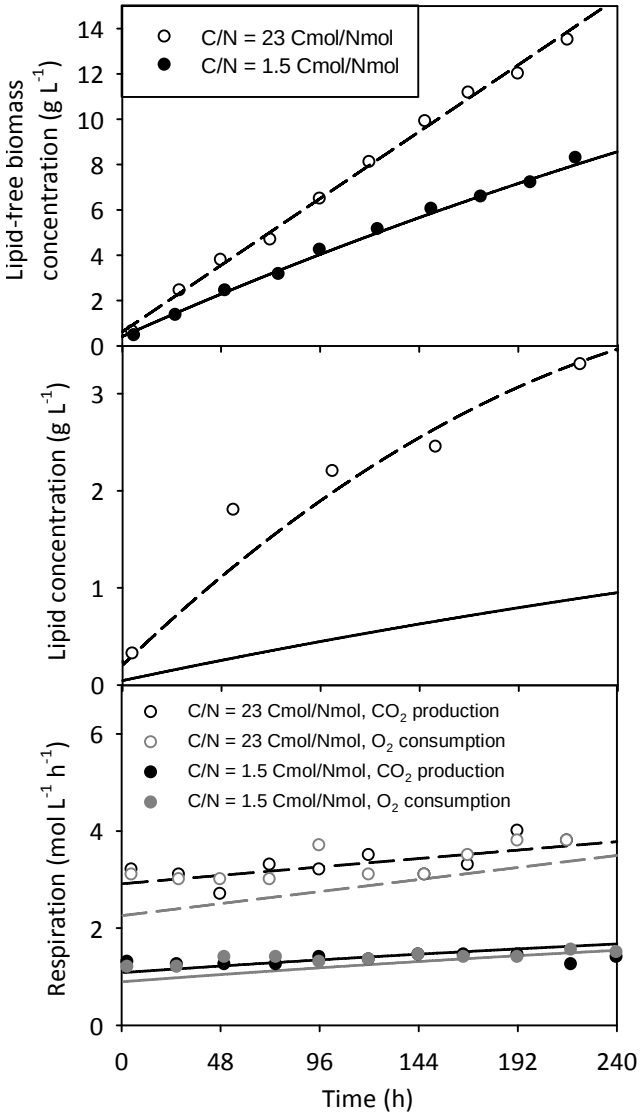

Fig. 5 (left) Model (lines) and data points for PHA accumulating cultures of *Pseudomonas oleovorans* from Durner et al. (2000).

Fig. 6 (right) Modeling of recycling cultures from Ykema et al. (1989). Parameter values found by non-linear fitting and iteration: f_{L0} = 0.015 Cmol Cmol^{-1}, Y_{XN} = 8.6 Cmol/Nmol, Y_{LS} = 0.53 Cmol Cmol^{-1}, m_S = 0.003 Cmol Cmol^{-1} h^{-1}, Y_{XS} = 0.67 Cmol Cmol^{-1} for C/N= 1.5 Cmol/Nmol and Y_{XS} = 0.59 Cmol Cmol^{-1} for C/N= 23 Cmol/Nmol.

Use of the model for non-steady state conditions

When developing the model, we assumed steady state in the culture and therefore no accumulation in the fermenter (see equations 3-6, part I). This gives linear equations which are easy to handle. However, we can adapt the model to non-steady state conditions by including accumulation terms in the mass balances over the fermenter. We fitted this adapted model to data from a non-steady state culture (Ykema et al. 1989). We did not use Data set 13, because the glucose concentration in the feed is not given and could not be calculated because some vital information is missing. Instead, we used data from a recycling culture which was not in steady state (Ykema et al. 1989). This recycling culture is a continuous culture in which the biomass is retained while the medium is refreshed continuously. As a consequence, the biomass concentration in this culture increased in time. We determined parameter values from data of two recycling cultures with different C/N-ratios with the non-steady state version of the model, assuming there is no biomass in the outgoing liquid. Fig. 6 shows the fit of the model to the data and the obtained parameter values. All graphs were calculated with the same parameter values except one parameter: we used different values of the yield of biomass on glucose for both cultures because we expected a difference in carbohydrate storage in both situations. The graphs show a good fit for all variables, and show that our model can indeed describe non-steady state cultures.

Conclusions

The model that was developed and partly validated in part I of this article Meeuwse et al. 2011) was further validated using published data sets for chemostat cultures of oleaginous yeasts and fungi and one data set for PHA accumulating micro-organisms. All data sets except one could be described well with the model, if a growth rate dependent yield of lipid-free cell mass on N-source was incorporated (Equation 27). One data set required another modification, *i.e.* the incorporation of a constant instead of a growth rate dependent minimum specific lipid production rate (Equation 28). This shows that the main assumptions in the model are valid: (1) oleaginous yeasts and fungi give the highest priority to C-source utilization for maintenance, second priority to growth and third priority to lipid accumulation, and (2) oleaginous yeasts and fungi have a growth-rate independent maximum specific lipid production rate. The maximum specific lipid production rate was in most cases very close to the lipid production rate required for synthesis of the basal (membrane and functional) lipids in cells growing at their maximum specific growth rate. This indicates that the cells use the same pathway for lipid accumulation and for production of membrane and functional lipids, and that no special pathway is switched on for lipid accumulation in chemostat cultures. The assumption that the maximum specific lipid production rate is dictated by the maximum glucose uptake rate, postulated by Ykema et al. (1986), was shown not to be correct for the tested data sets. Finally, the model proved also to be able to predict the production of PHA, another carbon-based storage product.

Appendix

Fit of the model to all datasets in Table 1.

Data set 3

Not enough information is available to model the whole range of dilution rates.

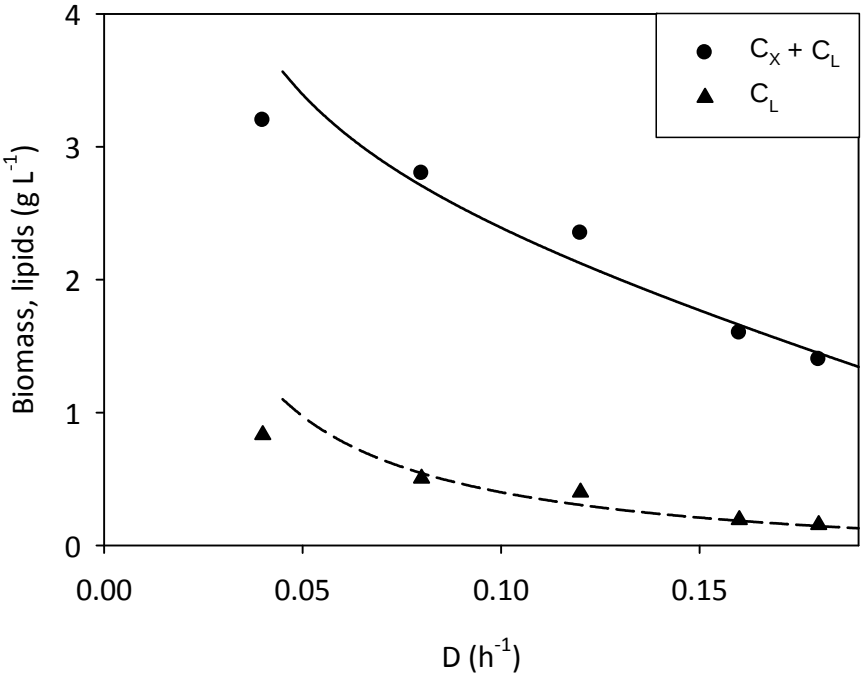

Total biomass (C_X+C_L) r^2 = 0.94 (n=5)

Lipids (C_L) r^2 = 0.94 (n=5)

Data set 4

Because in this dataset both the dilution rate and the C/N-ratio was different for each data point, it is not possible to display these data in a 2D-graph.

Total biomass (C_X+C_L)	r^2 = 0.93 (n=7)
Lipids (C_L)	r^2 = 0.90 (n=7)
C-source concentration (C_S)	r^2 = 0.48 (n=7)

Data set 5

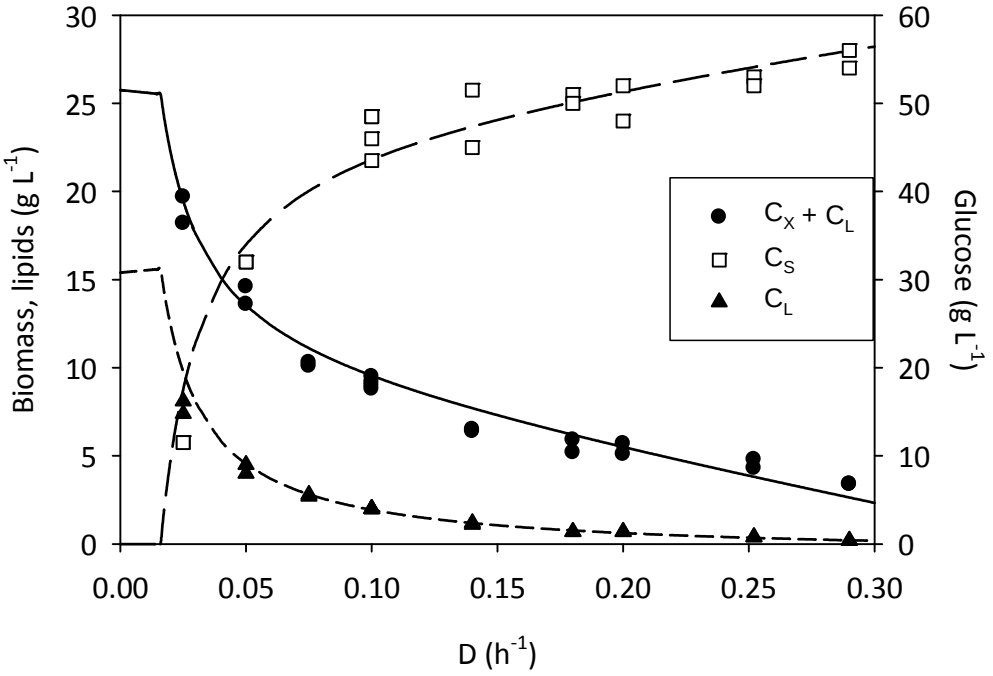

Total biomass (C_X+C_L)	r^2 = 0.85 (n=20)
Lipids (C_L)	r^2 = 0.99 (n=20)
C-source concentration (C_S)	r^2 = 0.91 (n=18)

Data set 6

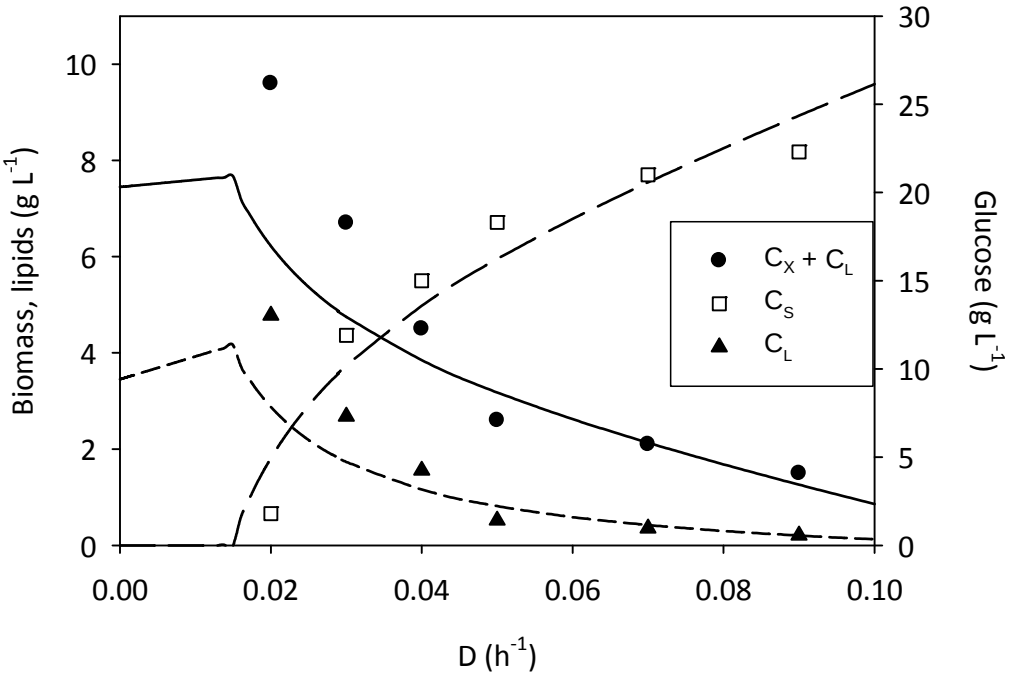

Total biomass (C_X+C_L)	r^2 = 0.88 (n=6)
Lipids (C_L)	r^2 = 0.93 (n=6)
C-source concentration (C_S)	r^2 = 0.96 (n=6)

Data set 7

Results for all four sugars were fitted together with the same parameter values in moles, but because of different molar weights of the sugars, modeling results are slightly different and shown in separate graphs.

Glucose and xylose (30 g/Cmol)

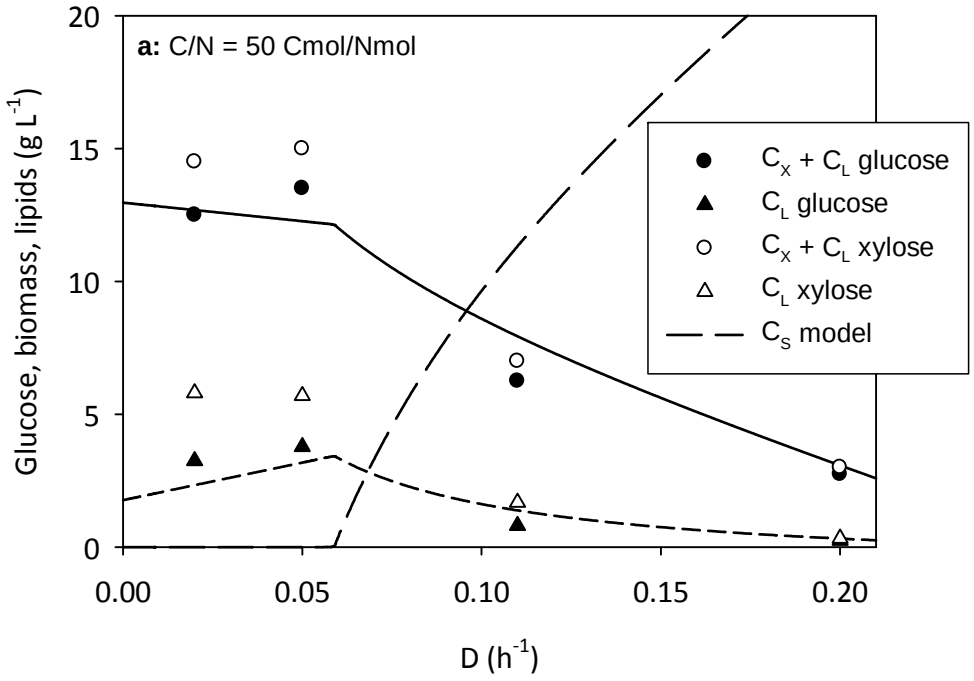

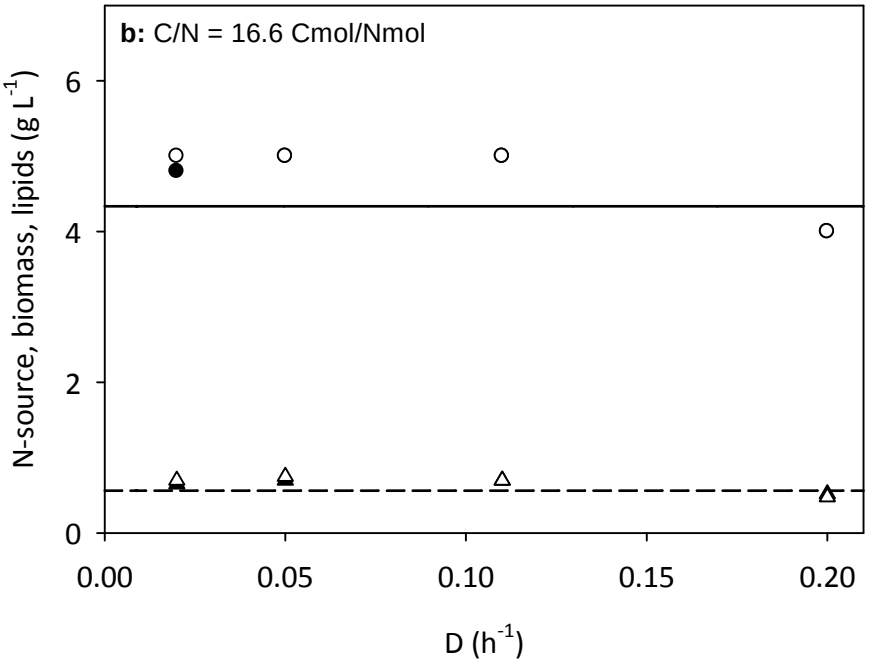

Sucrose and lactose (28.5 g/Cmol)

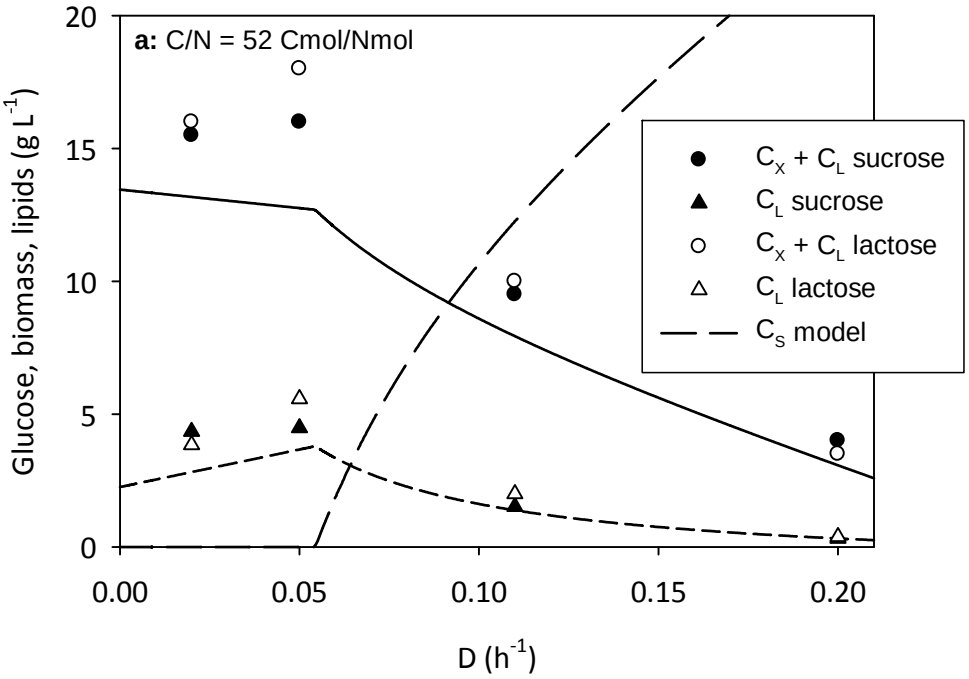

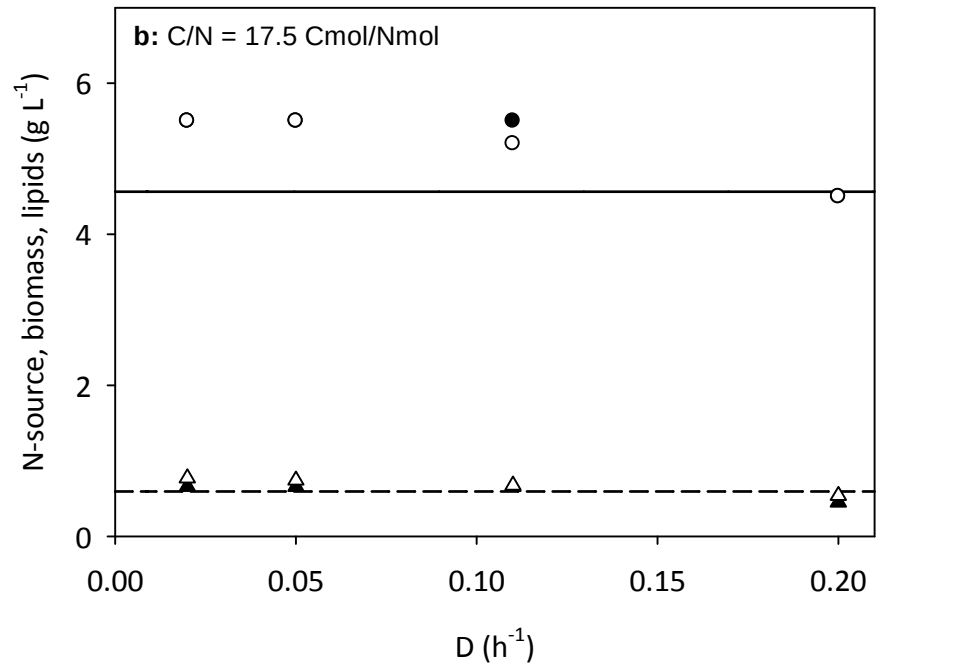

Total biomass (C_X+C_L) r^2 = 0.95 (*n*=32)

Lipids (C_L) r^2 = 0.90 (*n*=32)

Data set 8

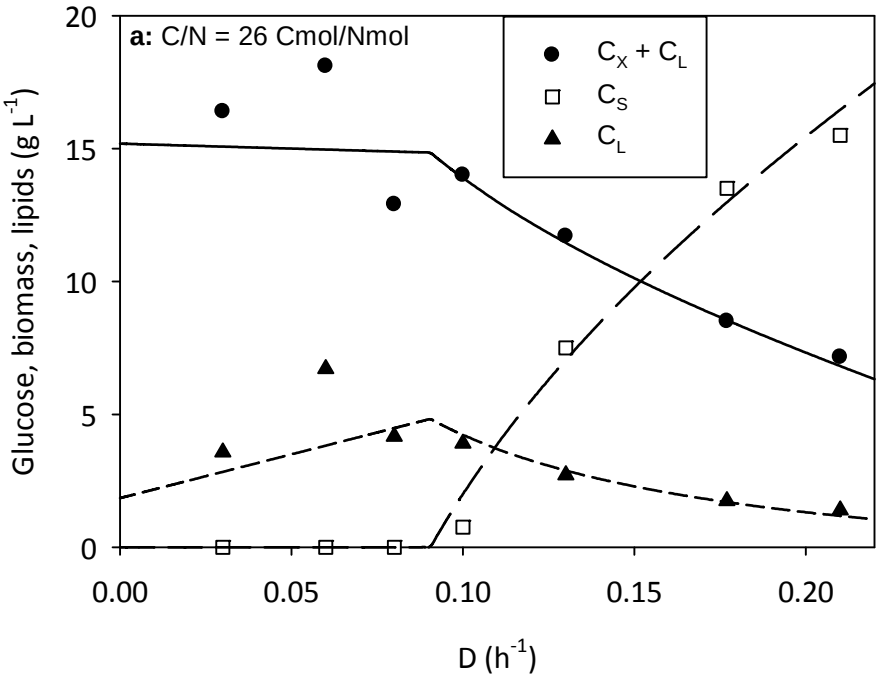

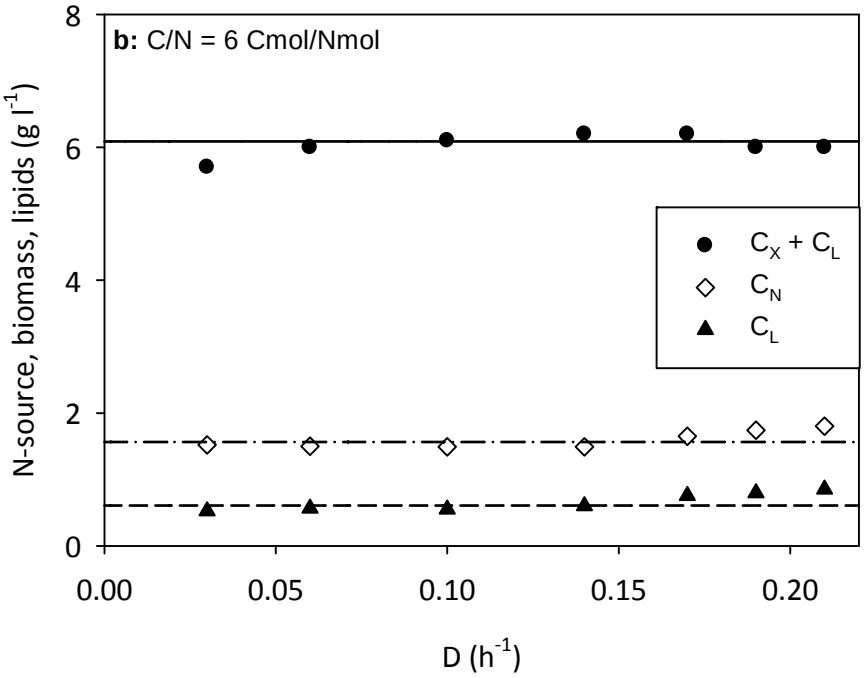

Total biomass (C_X+C_L)	r^2 = 0.94 (n=14)
Lipids (C_L)	r^2 = 0.83 (n=14)
C-source concentration (C_S)	r^2 = 0.99 (n=7)
N-source concentration (C_N)	r^2 = 0.23 (n=7)

Data set 9

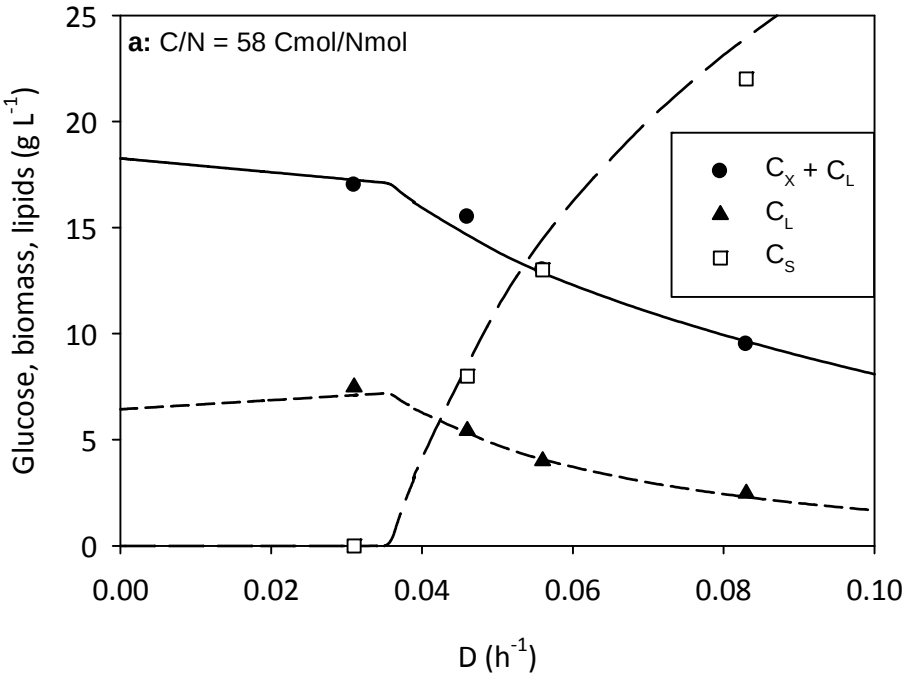

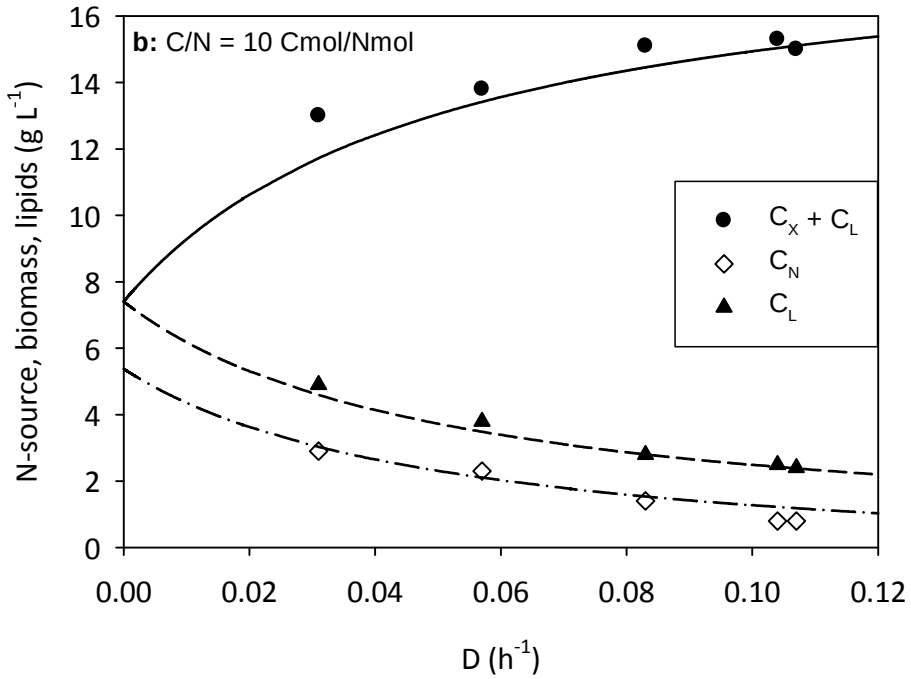

Total biomass (C_X+C_L)	r^2 = 0.95 (n=9)
Lipids (C_L)	r^2 = 0.99 (n=9)
C-source concentration (C_S)	r^2 = 0.99 (n=4)
N-source concentration (C_N)	r^2 = 0.95 (n=5)

Data set 10

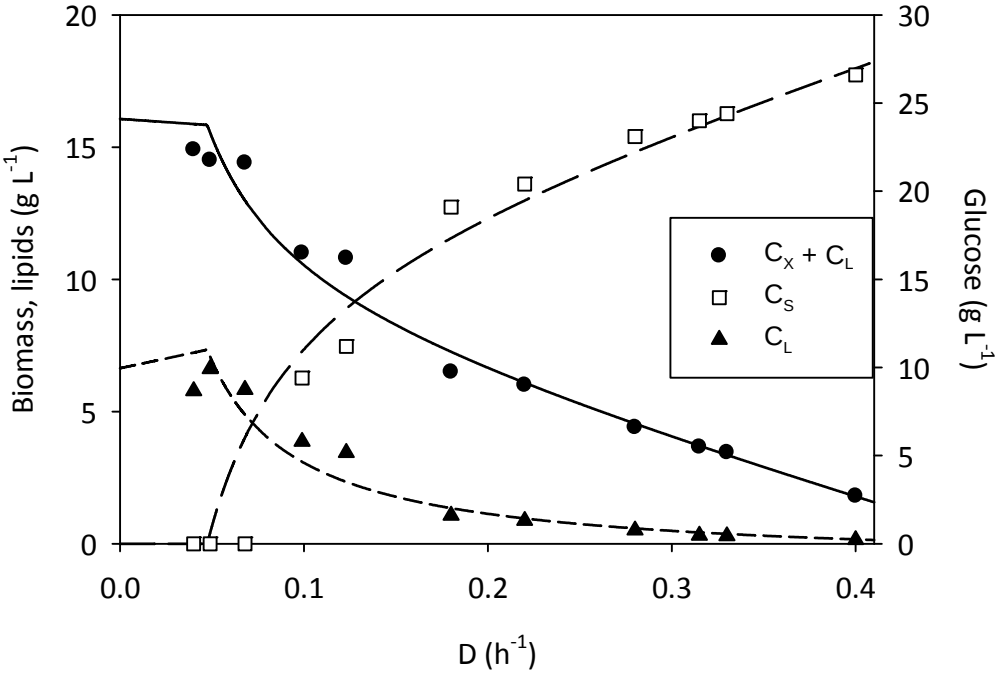

Total biomass (C_X+C_L)	r^2 = 0.97 (n=11)
Lipids (C_L)	r^2 = 0.93 (n=11)
C-source concentration (C_S)	r^2 = 0.97 (n=11)

Data set 11

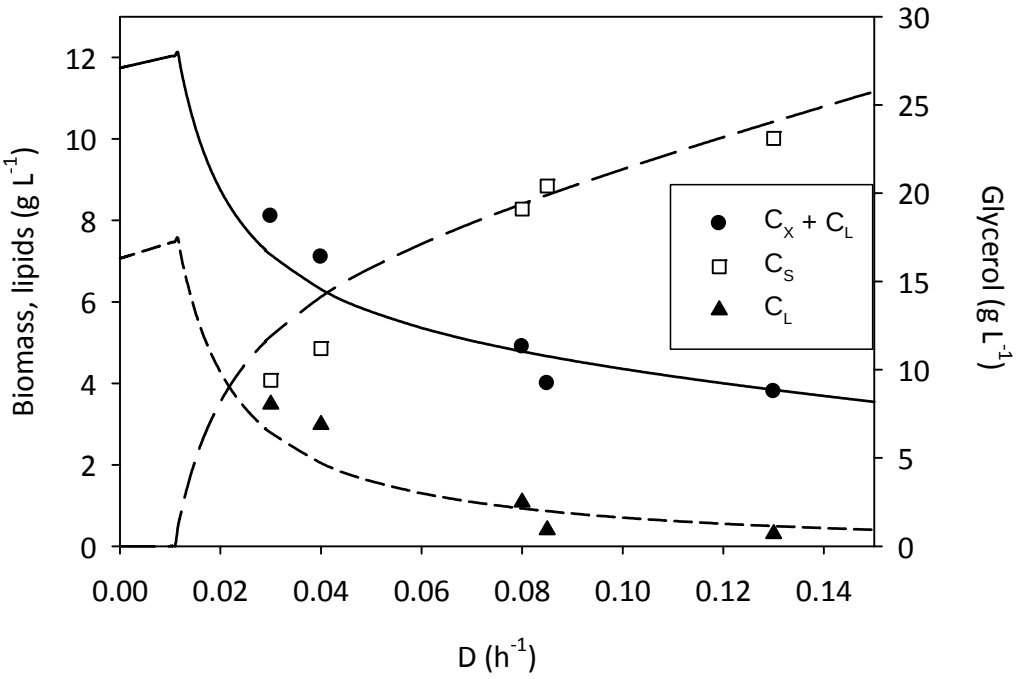

Total biomass (C_X+C_L)	r^2 = 0.96 (*n*=5)
Lipids (C_L)	r^2 = 0.95 (*n*=5)
C-source concentration (C_S)	r^2 = 0.97 (*n*=5)

Data set 12

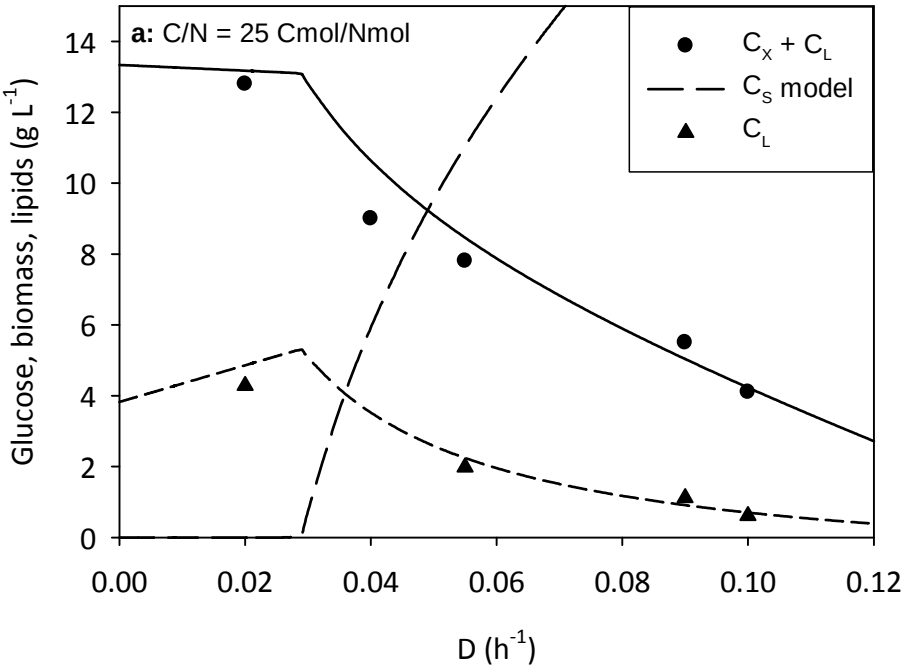

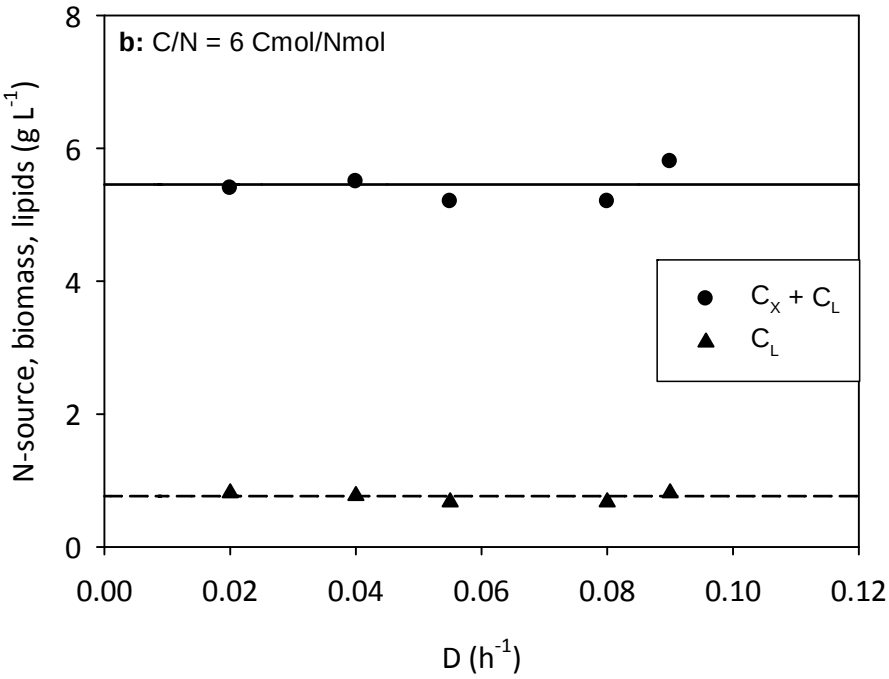

Total biomass (C_X+C_L) r^2 = 0.97 (n=10)

Lipids (C_L) r^2 = 0.99 (n=9)

Dataset 14

Not enough information is available to fit all data points.

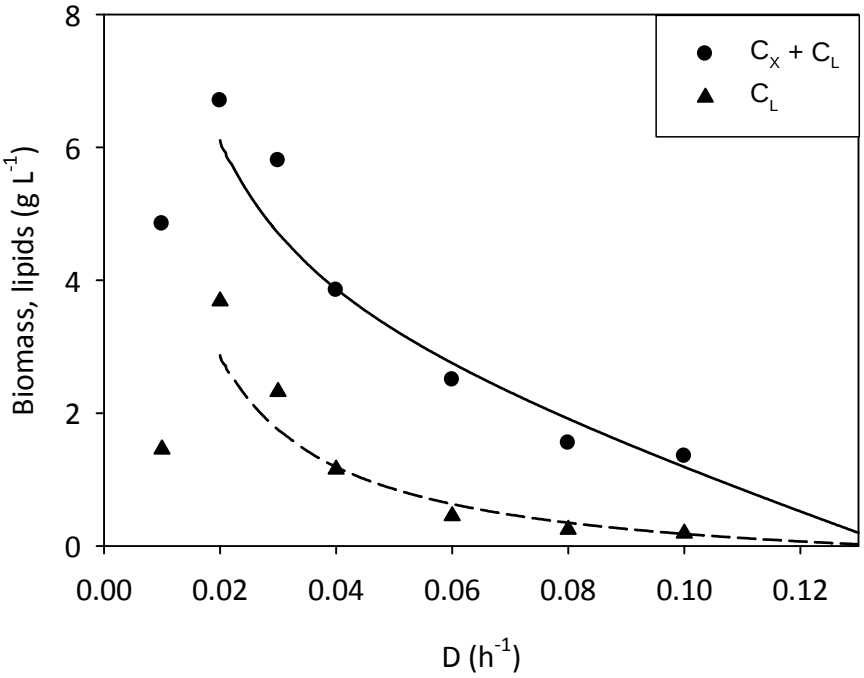

Total biomass (C_X+C_L) r^2 = 0.97 (n=6, $D \geq 0.02$)

Lipids (C_L) r^2 = 0.99 (n=6, $D \geq 0.02$)

Chapter 5

Modeling growth, lipid accumulation and lipid turnover in submerged batch cultures of *Umbelopsis isabellina*

Meeuwse P, Akbari P, Tramper J, Rinzema A. 2011. Modeling growth, lipid accumulation and lipid turnover in submerged batch cultures of *Umbelopsis isabellina.* Bioprocess Biosyst Eng DOI: 10.1007/s00449-011-0632-x

Abstract

The production of lipids by oleaginous yeast and fungi becomes more important because these lipids can be used for biodiesel production. To understand the process of lipid production better, we developed a model for growth, lipid production and lipid turnover in submerged batch fermentation. This model describes three subsequent phases: exponential growth when both a C-source and an N-source are available, carbohydrate and lipid production when the N-source is exhausted and turnover of accumulated lipids when the C-source is exhausted. The model was validated with submerged batch cultures of the fungus *Umbelopsis isabellina* (formerly known as *Mortierella isabellina*) with two different initial C/N-ratios. Comparison with chemostat cultures with the same strain showed a significant difference in lipid production: in batch cultures, the initial specific lipid production rate was almost four times higher than in chemostat cultures but it decreased exponentially in time, while the maximum specific lipid production rate in chemostat cultures was independent of residence time. This indicates different mechanisms for lipid production are active in batch and chemostat cultures. The model could also describe data for submerged batch cultures from literature well.

Introduction

Research on lipid accumulation in oleaginous yeast and fungi has long been focused on the production of poly-unsaturated fatty acids such as arachidonic acid and γ-linolenic acid (Certik and Shimizu 1999). More recently, production of lipids as a feedstock for biodiesel also gets attention (Li et al. 2008, Meng et al. 2009, Feofilova et al. 2009). Microbial lipids for biodiesel production are a bulk product and therefore have to be produced at low cost. The method used for PUFA production, i.e. cultivation of oleaginous yeast or fungi in submerged cultures on a substrate such as glucose, is expensive because bioreactor costs and substrate costs are high. Development of a new and cheaper process requires knowledge about the mechanisms involved and the kinetics. A mathematical model can help to structure this knowledge and can be used as a tool to improve the production. This paper presents a model for the bioconversion kinetics in submerged batch cultures of a lipid-accumulating fungus.

Several mathematical models for lipid production in submerged batch culture are already available in literature. Granger et al. (1993) and Sattur and Karanth (1989) developed stoichiometric models for prediction of the final lipid concentration in a batch culture from initial substrate concentrations. These models do not take reaction kinetics into account and are therefore not suitable to describe cultures in time. Sattur and Karanth (Sattur and Karanth 1991, Karanth and Sattur 1991) developed a kinetic model for growth and lipid accumulation based on the logistic law and the Luedeking-Piret model. Their models do not describe depletion of the N-source, which is an important factor for lipid production (Wynn et al. 2001). Several models of Aggelis and co-workers (Aggelis et al. 1995, Aggelis and Sourdis 1997, Papanikolaou and Aggelis 2003) describe growth and lipid production on various lipid-based substrates, but also do not take depletion of the N-source into account. Glatz et al. (1984) and Economou et al. (2011) modeled growth and lipid accumulation using Monod kinetics and a mathematical function that gives a gradual transition from growth to lipid accumulation as the N-source gets depleted. Economou et al. (2011) also included substrate inhibition and lipid turnover; substrate inhibition was observed but lipid turnover was not observed.

Our experiments show that there are two aspects of a submerged batch culture with oleaginous fungi that were not properly described in the aforementioned models. First, we observed a decrease in the lipid production rate in batch cultures

that is not caused by the decline in C-source concentration; this was reported before (Wynn et al. 1999) but not described in previous models (Glatz et al. 1984, Economou et al. 2011). Second, lipid turnover was in previous models (Aggelis et al. 1995, Aggelis and Sourdis 1997, Papanikolaou and Aggelis 2003, Economou et al. 2011) associated with growth, which is not in agreement with our results. Instead, we observed lipid turnover for maintenance.

We developed a new model for lipid accumulation in batch cultures including the two afore mentioned aspects, based on our previously developed model for lipid production in chemostat cultures (Meeuwse et al. 2011a, Meeuwse et al. 2011b). The model describes the experimental data presented in this paper as well as data from literature well, which shows that it is more generally applicable.

Model

Fig. 1 shows a simplified scheme of the metabolism of an oleaginous organism (Meeuwse et al. 2011a). The organism uses a C-source (S), an N-source (N) and oxygen (O) to produce cell material (X), lipids (L), carbohydrates (IP), carbon dioxide (C) and water (W). For calculations, the biomass is divided into lipids, carbohydrates and lipid-free, carbohydrate-free biomass; the latter is referred to as basic biomass. The composition of basic biomass ($CH_{1.77}O_{0.55}N_{0.17}$, MW=28.7 g $Cmol^{-1}$ including 13% (w/w) ash) is based on the average composition of *U. isabellina* during exponential growth in the experiments, and the composition of the lipids ($CH_{1.95}O_{0.11}$, MW=15.7 g $Cmol^{-1}$) is based on the average fatty acid composition of the accumulated triacylglycerol in *U. isabellina* during the experiments. Concentrations of all components that contain carbon are expressed in Cmoles; O_2 and NH_3 are expressed in moles and Nmoles, respectively. Used symbols can be found on page 207.

The model is based on Fig. 1 and several assumptions:

- Oxygen is not limiting.
- The N-source in the substrate is exhausted before the C-source.

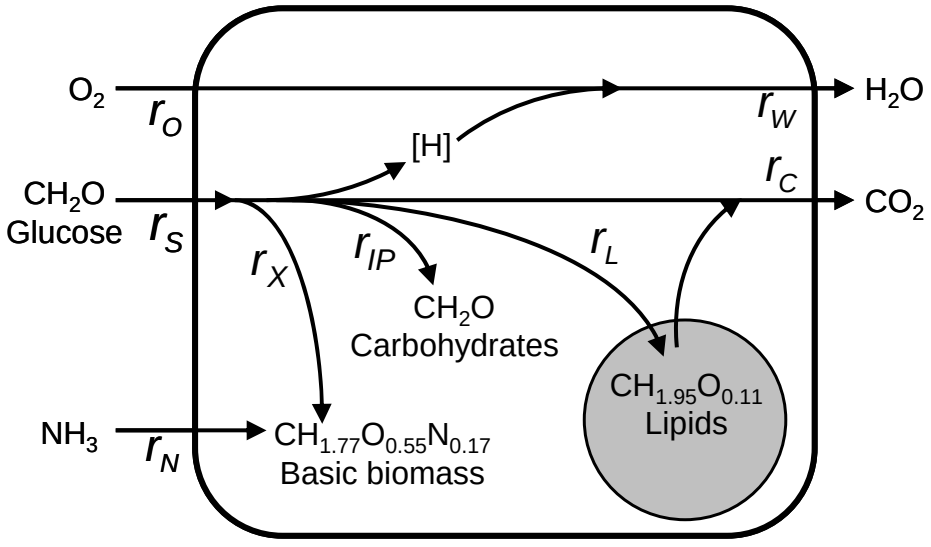

Fig. 1 Schematic overview of carbon and nitrogen metabolism of the oleaginous fungus *U. isabellina.* The substrates oxygen (r_O), glucose (r_S) and ammonium (r_N) are consumed to produce basic biomass (r_X), carbohydrates (r_{IP}), lipids (r_L), water (r_W) and CO_2 (r_C). The composition of basic biomass and lipids are based on experimental results.

- A batch culture consists of three subsequent phases: (1) As long as both N-source and C-source are available, the fungus grows and synthesizes only functional lipids (for membranes, etc.). (2) After the N-source is depleted, the fungus accumulates lipids and storage carbohydrates in its cells until the C-source is depleted. (3) After the substrate C-source is depleted, the fungus uses the lipids stored in its cells for maintenance; stored carbohydrates are shown not to be consumed.
- The C-source is a monomer and the N-source an inorganic compound; no hydrolysis of polymers is needed.
- The initial C-source and N-source concentrations are not inhibitory.
- After depletion of the N-source, the cells accumulate lipids and another storage compound, which we assume to be carbohydrates (CH_2O). Glycogen and trehalose are important storage products in many fungi (Griffin 1993, Gow and Gadd 1995) and carbohydrate storage has been demonstrated in oleaginous yeasts (Boulton and Ratledge 1983, Ykema et al. 1986). We assume that all carbon containing storage components that cannot be extracted with chloroform are carbohydrates.
- No other carbon or nitrogen containing products are produced besides basic biomass, carbohydrates, lipids and CO_2.
- The C-source and N-source concentrations do not affect the conversion rates of these components (zero-order kinetics with respect to reactants).

We will now discuss the three different phases in a batch process and further assumptions made for each phase. All balances used are differential equations, but we only show the integrated forms.

Phase 1: exponential growth phase

During the exponential growth phase, basic biomass with a basal fraction of functional lipids is formed and C-source and N-source are consumed. We assume that none of the substrates is limiting for growth in this phase. Therefore, the cells will grow exponentially with their maximum specific growth rate and the basic biomass concentration is given by:

$$C_X(t) = C_X(0)e^{\mu_{max}t} \qquad (1)$$

The cells have a constant basal lipid fraction (f_{L0}). Therefore, the lipid concentration is proportional to the basic biomass concentration:

$$C_L(t) = \frac{f_{L0}}{1-f_{L0}} C_X(t) \tag{2}$$

Carbohydrates formed during phase 1 are included in the basic biomass and not calculated separately ($C_{IP} = 0$).

We assume a linear relation between the rates of N-source conversion and basic biomass production and use Pirt's law for the conversion rate of the C-source. This gives for the concentrations of N-source and C-source:

$$C_N(t) = C_N(0) - \frac{C_X(t) - C_X(0)}{Y_{XN}} \tag{3}$$

$$C_S(t) = C_S(0) - \left(\frac{\mu_{\max}}{Y_{XS}} + \frac{f_{L0}}{1-f_{L0}} \frac{\mu_{\max}}{Y_{LS}} + m_S \right) \frac{C_X(t) - C_X(0)}{\mu_{\max}} \tag{4}$$

The CO_2-production rate is found from the C-balance:

$$r_C(t) = \left(\left(\frac{1}{Y_{XS}} - 1 + \frac{f_{L0}}{1-f_{L0}} \left(\frac{1}{Y_{LS}} - 1 \right) \right) \mu_{\max} + m_S \right) C_X(t) \tag{5}$$

An electron balance gives the O_2-consumption rate:

$$-r_O(t) = \frac{1}{-\gamma_O} \left(\left(\gamma_X - \frac{\gamma_S}{Y_{XS}} + \frac{f_{L0}}{1-f_{L0}} \left(\gamma_L - \frac{\gamma_S}{Y_{LS}} \right) \right) \mu_{\max} - \gamma_S m_S \right) C_X(t) \tag{6}$$

The exponential growth phase ends at $t = t_{12}$ when the N-source is depleted (derived from Equations 1 and 3):

$$t_{12} = \frac{1}{\mu_{\max}} \ln \left(\frac{Y_{XN} C_N(0)}{C_X(0)} + 1 \right) \tag{7}$$

The basic biomass has then reached its maximum value:

$$C_{X\max} = C_X(0) + Y_{XN} C_N(0) \tag{8}$$

Phase 2: lipid accumulation phase

After the N-source is depleted, the cells no longer grow but do continue to use the C-source for maintenance, carbohydrate production and lipid production. The experimental results show that the specific lipid production rate decreases exponentially in this phase. This gives for the lipid concentration:

$$C_L(t) = \left(\frac{f_{L0}}{1-f_{L0}} + \frac{q_{L\max}}{k_d}\left(1-e^{-k_d(t-t_{12})}\right)\right) C_{X\max} \tag{9}$$

At the beginning of phase 2, we assume accumulation of carbohydrates at a constant rate, until the maximum carbohydrate fraction in the cells is reached:

$$C_{IP}(t) = q_{IP} C_{X\max}(t-t_{12}) \le f_{IP\max} C_{X\max} \tag{10}$$

This means that phase 2 can be divided in two parts: part 2a in which carbohydrates are produced, and part 2b in which the cells have a constant maximum carbohydrate fraction. The time at which the maximum carbohydrate fraction is reached, t_{2ab}, is equal to:

$$t_{2ab} = t_{12} + \frac{f_{IP\max}}{q_{IP}} \tag{11}$$

We assume that the specific carbohydrate production rate (q_P) is limited by the maximum specific C-source uptake rate of the cells, which corresponds to the specific rate during exponential growth:

$$\frac{\mu_{\max}}{Y_{XS}} + \frac{f_{L0}}{1-f_{L0}}\frac{\mu_{\max}}{Y_{LS}} + m_S = \frac{q_L}{Y_{LS}} + \frac{q_{IP}}{Y_{IPS}} + m_S \rightarrow q_{IP} = Y_{IPS}\left(\frac{\mu_{\max}}{Y_{XS}} + \frac{f_{L0}}{1-f_{L0}}\frac{\mu_{\max}}{Y_{LS}} - \frac{q_L}{Y_{LS}} \right) \tag{12}$$

The C-source concentration in phases 2a and 2b is then obtained from Pirt's law and a mass balance for the C-source:

$$\begin{cases} t < t_{2ab} : C_S(t) = C_S(t_{12}) - \left(\frac{q_{L\max}}{Y_{LS}k_d}(1-e^{-k_d(t-t_{12})}) + \left(\frac{q_{IP}}{Y_{IPS}} + m_S \right)(t-t_{12}) \right) C_{X\max} \\ t \ge t_{2ab} : C_S(t) = C_S(t_{2ab}) - \left(\frac{q_{L\max}}{Y_{LS}k_d}(e^{-k_d(t_{2ab}-t_{12})} - e^{-k_d(t-t_{12})}) + m_S(t-t_{2ab}) \right) C_{X\max} \end{cases} \tag{13}$$

The respiration rates are again obtained from the C-balance and the electron balance, respectively:

$$r_C(t) = \left(\left(\frac{1}{Y_{LS}} - 1 \right) q_{L\max} e^{-k_d (t - t_{12})} + \left(\frac{1}{Y_{IPS}} - 1 \right) q_{IP}(t) + m_S \right) C_{X\max} \quad (14)$$

$$-r_O(t) = \frac{1}{-\gamma_O} \left(\left(\gamma_L - \frac{\gamma_S}{Y_{LS}} \right) q_{L\max} e^{-k_d (t - t_{12})} + \left(\gamma_{IP} - \frac{\gamma_S}{Y_{IPS}} \right) q_{IP}(t) - \gamma_S m_S \right) C_{X\max} \quad (15)$$

Phase 2 ends when the C-source is depleted. Equation 13 can be used to find the time of transition to phase 3, t_{23}, by iteration.

Phase 3: Lipid turnover phase

When the C-source in the medium is exhausted, the cells use the accumulated lipids for maintenance. The mass balance for lipids gives:

$$C_L(t) = C_L(t_{23}) - m_L C_{X\max} (t - t_{23}) \quad (16)$$

Lipid combustion generates 1.4 times more ATP per Cmol than glucose combustion, hence:

$$m_L = m_S / 1.4 \quad (17)$$

In contrast to our expectations, the accumulated carbohydrates were not consumed in our experiments, and we have therefore not included carbohydrate turnover in the model.

The respiration rates in phase 3 are:

$$r_C(t) = m_L C_{X\max} \quad (18)$$

$$-r_O(t) = \frac{\gamma_L}{-\gamma_O} m_L C_{X\max} \quad (19)$$

Materials and methods

Medium

Liquid medium for all cultures contained per liter 0.5 g KCl, 0.5 g $MgSO_4 \cdot 7H_2O$, 1.5 g $Na_2HPO_4 \cdot 2H_2O$, 1 mL trace metal solution as described by Vishniac and Santer (1957), glucose as C-source and $(NH_4)_2SO_4$ as N-source. Pre-culture medium contained 100 mM glucose and 100 mM NH_4^+. Culture medium contained 100 mM glucose and 20 mM NH_4^+, resulting in an initial C/N-ratio of 30 Cmol/Nmol. The pH of all media was adjusted to 6.0 by adding H_2SO_4. The glucose was autoclaved separately. To the fermentation medium, 1 mL of antifoam (Polypropylene glycol (Sigma), 50% v/v in ethanol) was added per liter.

Pre-culture

The pre-culture was carried out in 250-mL shake flasks with 100 mL pre-culture medium. The flasks were inoculated with 1 mL spore suspension of *Umbelopsis isabellina* CBS 194.28 containing 3×10^7 CFU/mL, prepared as described in Meeuwse et al. (2011a), and incubated at 25°C in a shaking incubator at 225 rpm for 3 days. To avoid transfer of non-consumed C-source or N-source to the main culture, 10-80 mL of pre-culture, depending on the desired initial amount of biomass, was centrifuged (10 min, 4000 g) and resuspended in 40 mL medium without C-source and N-source.

Batch cultures

The batch cultures were carried out in a baffled glass bioreactor at 28°C with stirring (700 rpm), aeration (1L/min), pH-control and off-gas analysis as was described before in Meeuwse et al. (2011a). Each batch culture was started by adding 40 mL of pre-culture without C-source or N-source to obtain a final volume of 2L. Six cultivations were done with different initial amounts of biomass, in order to obtain runs that were out of phase and to reduce nocturnal gaps in sampling. The phase differences were chosen to allow even distribution of sampling in time. Samples were taken every 2 hours during daytime. The bioreactor was placed on a balance and the total mass of the bioreactor was logged on-line using labview 5.1 (National Instruments, U.S.). From this mass the liquid volume in the bioreactor

was calculated, which was used to correct for changes in culture volume because of sampling, evaporation and addition of NaOH and medium.
All cultures were started at an initial glucose concentration of 100 mM (C/N-ratio 30 Cmol/Nmol). 200 mL glucose solution (1 M) was added to two out of the six cultures immediately after the exhaustion of the N-source in the medium, leading to a theoretical initial glucose concentration of 200 mM (C/N-ratio 60 Cmol/Nmol).

Analysis

Samples taken from the reactor were processed and analyzed as described in Meeuwse et al. (2011a). The biomass, dry weight, ash content, elemental composition and lipid content were determined as described before (Meeuwse et al. 2011a). The medium was analyzed for glucose and TOC as described before (Meeuwse et al. 2011a), and the NH_4^+ concentration was measured with an ammonium test kit (LCK 303, Hach Lange, Germany).

Results and discussion

Batch culture results

Six batch cultivations were carried out. In all cases the initial glucose concentration was 600 Cmol m^{-3} and the initial NH_4^+ concentration was 20 Nmol m^{-3} (C/N = 30 Cmol/Nmol). In two of the six cultures, extra glucose was added immediately after the exhaustion of NH_4^+; this resulted in a total glucose addition of 1200 Cmol m^{-3} (C/N = 60 Cmol/Nmol). The extra glucose was not added at the start of the experiments because preliminary results (not published) showed that a high initial glucose concentration (> 1000 Cmol m^{-3}) caused formation of an unknown byproduct. To avoid this, we kept the glucose concentration during exponential growth ≤600 Cmol m^{-3}.

Each batch culture was inoculated with a different amount of biomass in order to obtain different lengths of the exponential phase, as is shown by the CO_2-production rate in Fig. 2a. This made it possible to take samples covering the whole time range of the culture equally, without the need for sampling during the night. To facilitate the determination of model parameters from results of all cultures, we shifted the data points from all but one culture in time in such a way that the end of the exponential phase coincided, as is shown in Fig. 2b. Cultures with the same initial C/N-ratios gave very similar CO_2-production rates and therefore it is allowed to combine data points obtained from different cultures.

Fig. 3 shows all measured data. All data obtained before the addition of extra glucose are shown in Fig. 3a and 3b; data obtained after extra glucose addition are shown only in Fig. 3b. Arrows in Fig. 3b indicate the glucose addition. Microscopic examination showed that the biomass was present as loose filaments and very small pellets with an average size of 100-200 µm, which means that exponential growth was possible. Fig. 3 shows that the total biomass concentration indeed increased exponentially as long as NH_4^+ was present, and the lipid fraction remained constant. When NH_4^+ was exhausted, the lipid fraction started to increase. At the moment of NH_4^+-exhaustion, both the CO_2-production rate and the O_2-consumption rate suddenly decreased and then increased again. The nitrogen fraction of the cells decreased from 7.6% to 5.7% w/w, while the lipid fraction only increased from 4% to 8% w/w in the same period. Calculations show that the decrease of the nitrogen fraction cannot be explained by lipid production

alone; therefore, we assume that a second carbon-based storage product accumulated, which we assume to be carbohydrates. Accumulation of carbohydrates by oleaginous yeast has been described in literature (Boulton and Ratledge 1983, Ykema et al. 1986).

Fig. 3b shows that the lipid production rate gradually decreased in time; this is also visible in the decreasing respiration rates. The lipid fraction in the cells did not

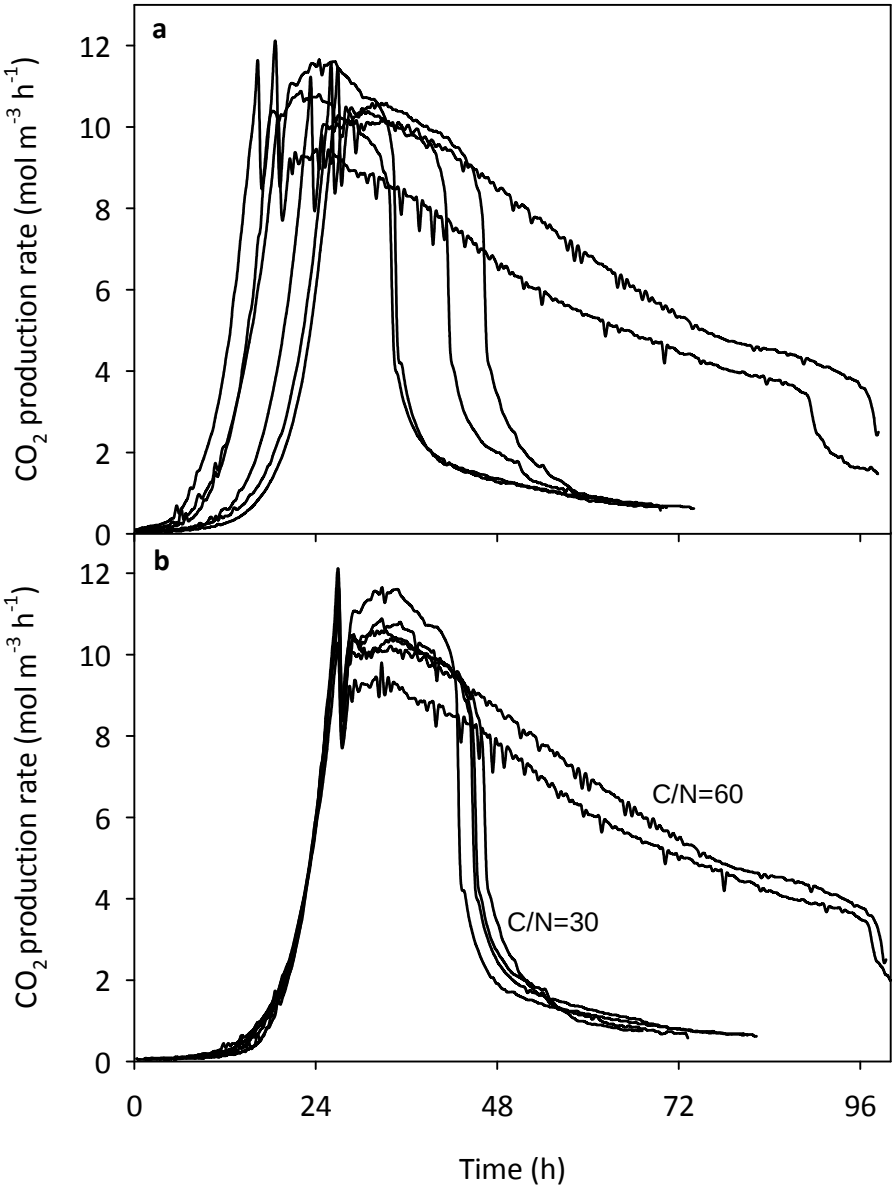

Fig. 2 CO_2-production rate during the six batch cultures (**a)** as measured in time and (**b**) after shifting of the time axis of all but one culture to let the end of the exponential phase coincide with each other. Four of the fermentations had an initial C/N-ratio of 30 Cmol/Nmol, while in two fermentations the theoretical initial C/N-ratio was increased to 60 Cmol/Nmol after the exponential growth phase.

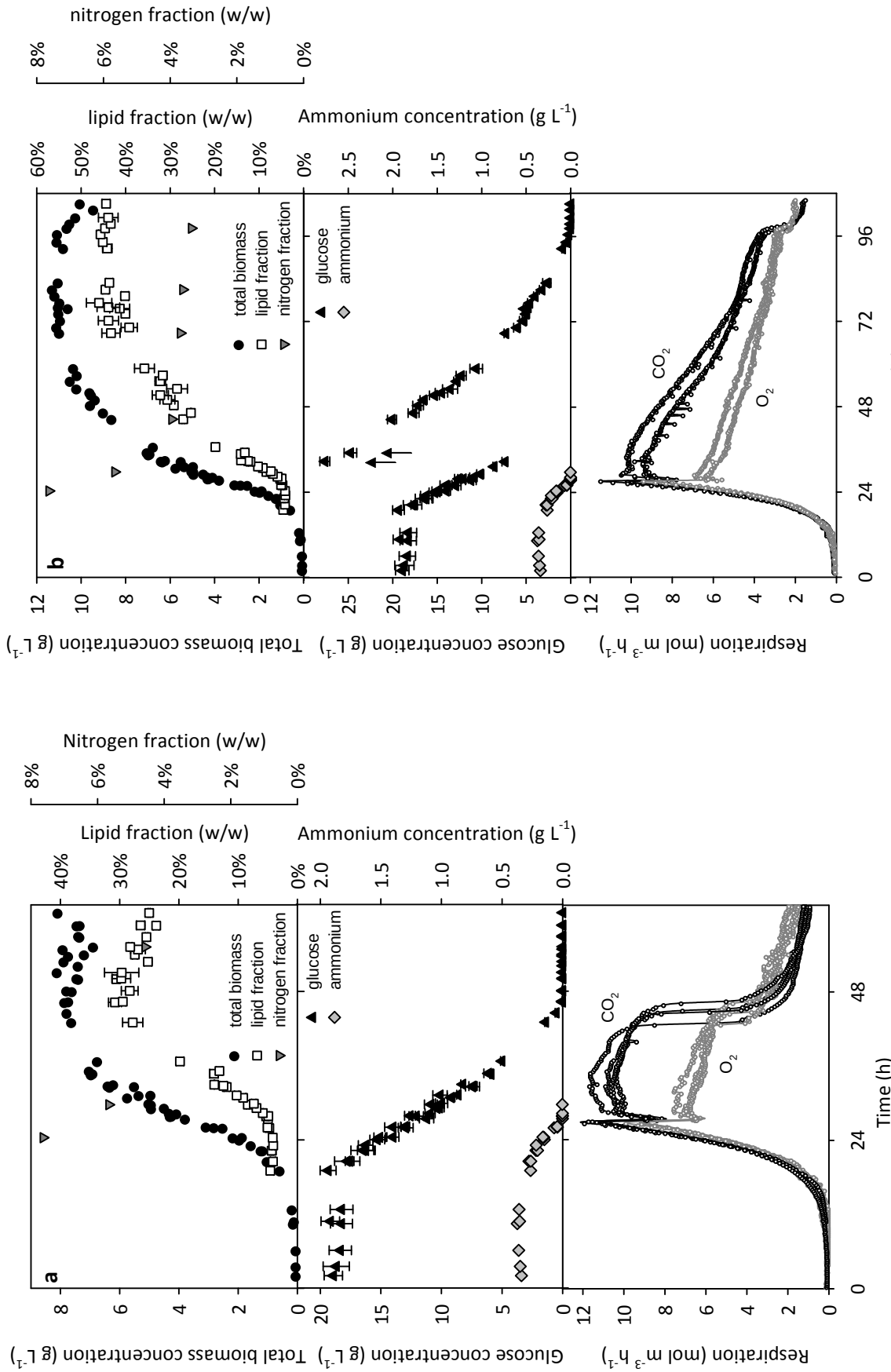

Fig. 3 Results of batch cultures with *U. isabellina* on glucose and NH_4^+. (**a**) with an initial C/N-ratio of 30 Cmol/Nmol, (**b**) with an initial C/N-ratio of 30 Cmol/Nmol and addition of extra glucose (indicated with arrows) to a theoretical initial C/N-ratio of 60 Cmol/Nmol. Error bars indicate SD.

increase significantly anymore after 72 hours, while the glucose was not yet exhausted (> 5 g L^{-1}). Addition of extra glucose after 72 hours did not have any effect on lipid production (results not shown). This shows that the lipid production was not limited by glucose, as was previously described (Glatz et al. 1984, Economou et al. 2011). The maximum lipid fraction reached was around 45% w/w (Fig. 3b), which is lower than lipid fractions reported in literature (55-74% w/w) for batch cultures with a different strain of the same species using glucose as C-source (Papanikolaou et al. 2004a, Chatzifragkou et al. 2010).

In Fig. 3a, a linear decrease of the lipid fraction is visible after glucose is exhausted. Because the cells store the lipids as a reserve material, it is reasonable to assume that they use it as an energy source when the external energy source is exhausted. We assume that the cells use the lipids for maintenance, because growth is not possible in the absence of an N-source. Growth with accumulated lipids as C-source was only observed for cultures with a low initial C/N-ratio (Aggelis et al. 1995, Aggelis and Sourdis 1997, Papanikolaou and Aggelis 2003).

Fig. 4 compares the carbon-containing products (lipid-free biomass, lipids, CO_2)

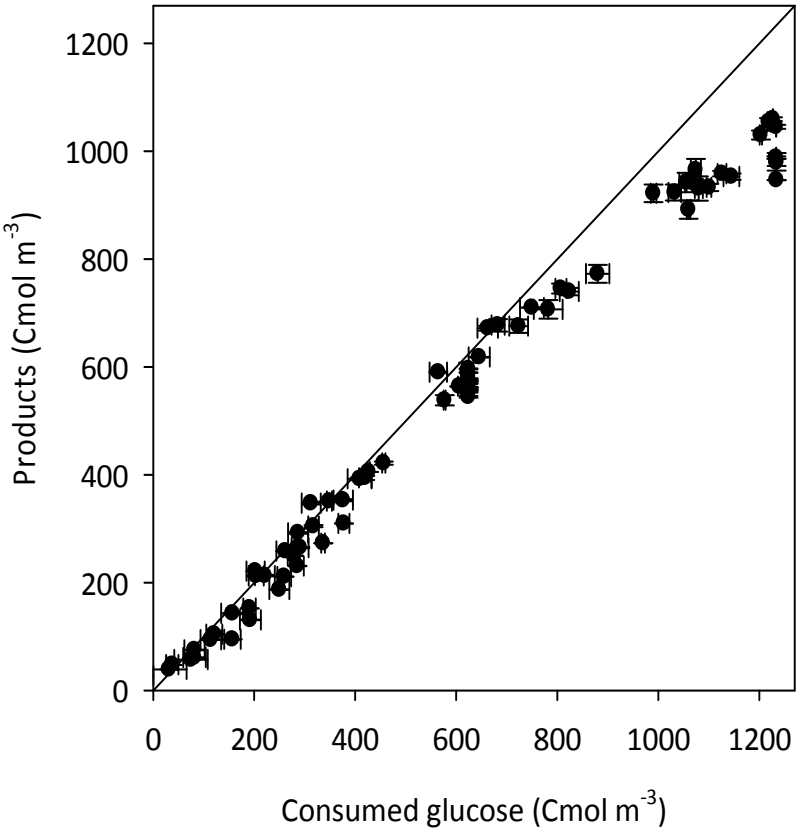

Fig. 4 Carbon recovery as a function of consumed glucose. Error bars indicate SD.

with the consumed glucose. C-recovery decreased when more than 700 Cmol m^{-3} of glucose was consumed, after approximately 50 h. Measurements of the total carbon content of the medium showed that only a minor part of the missing carbon was present in the medium as unknown product or cell debris (results not shown). We conclude that the major part of the missing carbon was present in the observed biomass aggregates attached to the walls and stirrer of the bioreactor, and was therefore not recovered in the broth samples.

Fig. 5 shows the composition of the accumulated lipids for all cultures. During exponential growth (until 27h), the lipids have an average composition of 30±1% C16:0, 1.5±0.2% C16:1, 12±2% C18:0, 39±1% C18:1 and 18±1% C18:2 fatty acids. After the exponential growth phase, the composition changes over a period of approximately 10 hours and then remains constant. The constant composition during lipid accumulation and lipid turnover was 25±1% C16:0, 1.3±0.1% C16:1, 6±1% C18:0, 54±1% C18:1 and 14±1% C18:2. This is consistent with findings in chemostat experiments with this strain (Meeuwse et al. 2011a) and with results from literature for the same species during the lipid accumulation phase in batch cultures with glucose as C-source (Chatzifragkou et al. 2010, Papanikolaou et al. 2007). The largest change between the growth phase and the lipid production phase is seen for C18:1. Fakas et al. (2009a) showed that C18:1 is more abundant

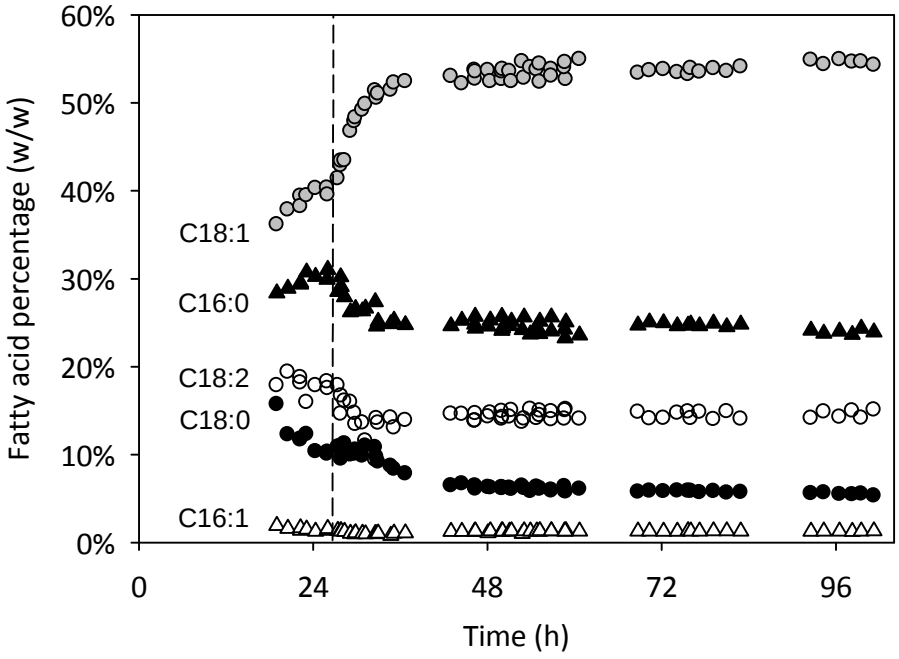

Fig. 5 Composition of the accumulated lipids in the cells in time divided into the five measured fatty acids. The vertical line at 27h indicates the end of the exponential growth phase and the start of N-source limitation.

in the neutral lipid fraction of the cell (storage lipids) than in the phospholipid fraction (membrane lipids) in the same species, which is consistent with our findings.

Fitting procedure

Ten model parameters (μ_{max}, $C_X(0)$, f_{L0}, Y_{XN}, $f_{IP\,max}$, Y_{XS}, Y_{LS}, m_L, $q_{L\,max}$, k_d) were determined by fitting the model on the data as explained below. The obtained parameter values are shown in Table 1. The initial biomass concentrations in our cultures were too low to measure accurately. Therefore, we determined values for μ_{max} and $C_X(0)$ by fitting the equation for exponential growth (Equation 1) on all data points with NH_4^+ present. The minimum lipid fraction of the cells, f_{L0}, was calculated from the average lipid fraction of cells during exponential growth. The yield of basic biomass on N-source, Y_{XN}, was determined by linear regression analysis using lipid-free biomass data and N-source consumption data in Fig. 6a. This figure shows a good correlation (r^2 = 0.97) before N-depletion. After N-depletion, the lipid-free biomass concentration increased, indicating accumulation of a storage compound which we assume to be carbohydrates. The

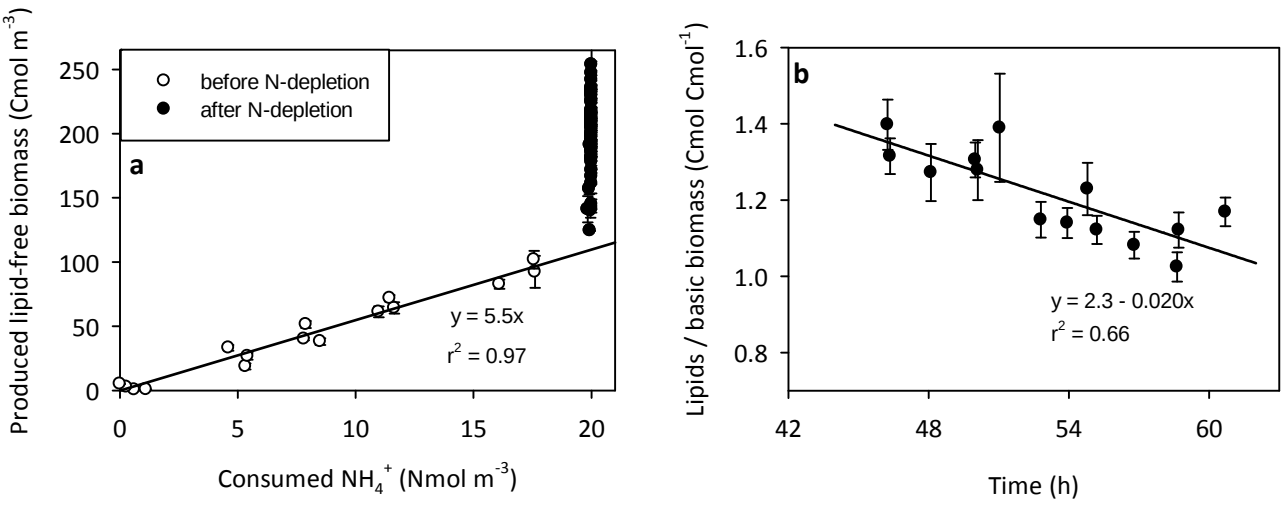

Fig. 6 Graphs for parameter value determination. Error bars indicate SD. (**a**) Lipid-free biomass including carbohydrates versus N-consumption for linear regression analysis. The slope of the curve is equal to the yield of basic biomass on N-source Y_{XN}. The increase of lipid-free biomass without extra N-consumption is assumed to be caused by carbohydrate accumulation. (**b**) The lipid concentration divided by the basic biomass concentration versus the time during lipid turnover (initial substrate ratio: C/N = 30 Cmol/Nmol).

Table 1 Parameter values used to fit our data set, and parameter values for a chemostat culture (Meeuwse et al. 2011a, [1]) and another batch culture (Economou et al. 2011 [2]) from literature, with the parameter values given in the source article, and found by fitting our model on this data set. All values are ± SD.

Parameter	Symbol		Batch (n=80) (this study)	Chemostat (n=12) [1]	Batch on sweet sorghum [2], values from literature	Batch on sweet sorghum [2], values from this study (Fig. 8)
Yield of lipid-free biomass on NH_4^+	Y_{XN}	Cmol $Nmol^{-1}$	5.5 ± 0.2	6.1±0.7	8.9 - 11.1 [a]	6.1±0.2
Yield of lipid-free biomass on glucose	Y_{XS}	Cmol $Cmol^{-1}$	0.78 ± 0.01	0.92±0.10	0.21 - 0.36 [a]	0.51±0.03 [b]
Yield of lipids on glucose	Y_{LS}	Cmol $Cmol^{-1}$	0.56 ± 0.01	(0.59) [c]	0.27 - 0.46 [a]	0.39±0.01
Yield of carbohydrates on glucose	Y_{IPS}	Cmol $Cmol^{-1}$	1 [d]	-	-	1 [d]
Maintenance on lipids	m_L	Cmol $Cmol^{-1}$ h^{-1}	0.020 ± 0.004	-	-	0 [e]
Maintenance on glucose	m_S	Cmol $Cmol^{-1}$ h^{-1}	0.028 ± 0.006	0.05±0.01	-	0 [e]
Minimum lipid fraction	f_{L0}	Cmol lipids (Cmol total biomass)$^{-1}$	0.078 ± 0.006	0.079	-	0.08 [f]
Maximum carbohydrate fraction	f_{IPmax}	Cmol carbohydrates (Cmol basic biomass)$^{-1}$	0.87 ± 0.17	-	-	ND [g]
Maximum specific growth rate	μ_{max}	h^{-1}	0.21 ± 0.01	0.23±0.02	0.566 (<0.23) [h]	0.26±0.01
Maximum specific lipid production rate	q_{Lmax}	Cmol $Cmol^{-1}$ h^{-1}	$0.090 \pm 0.003\, e^{-k_d t}$	0.023±0.006	0.785 (<0.038) [i]	$0.083 \pm 0.003\, e^{-k_d t}$
Time constant decrease lipid production rate	k_d	h^{-1}	0.016 ± 0.001	-	-	0.028±0.001
Maximum carbohydrate accumulation rate	q_{IP}	Cmol $Cmol^{-1}$ h^{-1}	0.14 ± 0.01	-	-	0.006±0.001
Initial biomass concentration	$C_X(0)$	Cmol m^{-3}	0.36 ± 0.09	NA	multiple	multiple

Footnotes: see next page

maximum carbohydrate fraction in the cells, $f_{IP\max}$, was calculated from the average lipid-free biomass concentration for $t > 35$ h divided by the maximum basic biomass concentration ($C_{X\max}$) from Equation 8. We determined the maintenance coefficient, m_L, from the decrease in the lipid fraction after glucose was exhausted, according to Equation 16. Data from the cultures with C/N = 60 Cmol/Nmol were not used. The result of this linear regression analysis is shown in Fig. 6b. The parameters Y_{XS}, Y_{LS}, $q_{L\max}$ and k_d were determined simultaneously by non-linear regression analysis using all data for the total biomass concentration, the lipid fraction of the cells, the glucose concentration and the CO_2 and O_2-production rates, *i.e.* all data shown in Fig. 3 except the nitrogen fraction in the cells. All values were divided by the median value and the number of data points for that variable to give all variables an equal weight in the fitting procedure. For the yield of carbohydrates on C-source, Y_{IPS}, we used the theoretical value of Y_{IPS} = 1 Cmol Cmol^{-1}. The two remaining parameters q_{IP} and m_S were calculated from Equations 12 and 17, respectively.

Footnotes Table 1

[a] Both an experimental value as well as a fitted value are given

[b] We assumed that only 95% of the sugars could be consumed

[c] Theoretical value (Ratledge 1988)

[d] Theoretical value

[e] No significant value above zero was found

[f] estimated to be 5% w/w because lipid measurements at low biomass concentrations were not accurate enough to fit a value

[g] assumed not to be reached in the experiments

[h] Number in parenthesis is the maximum specific growth rate possible at the initial substrate concentrations in our cultures as well as the sweet sorghum cultures used according to the used Andrews' equation for double substrate limitation and C-source inhibition.

[i] Number in parenthesis is the maximum value possible according to the used Andrews' equation for double substrate limitation and C-source inhibition.

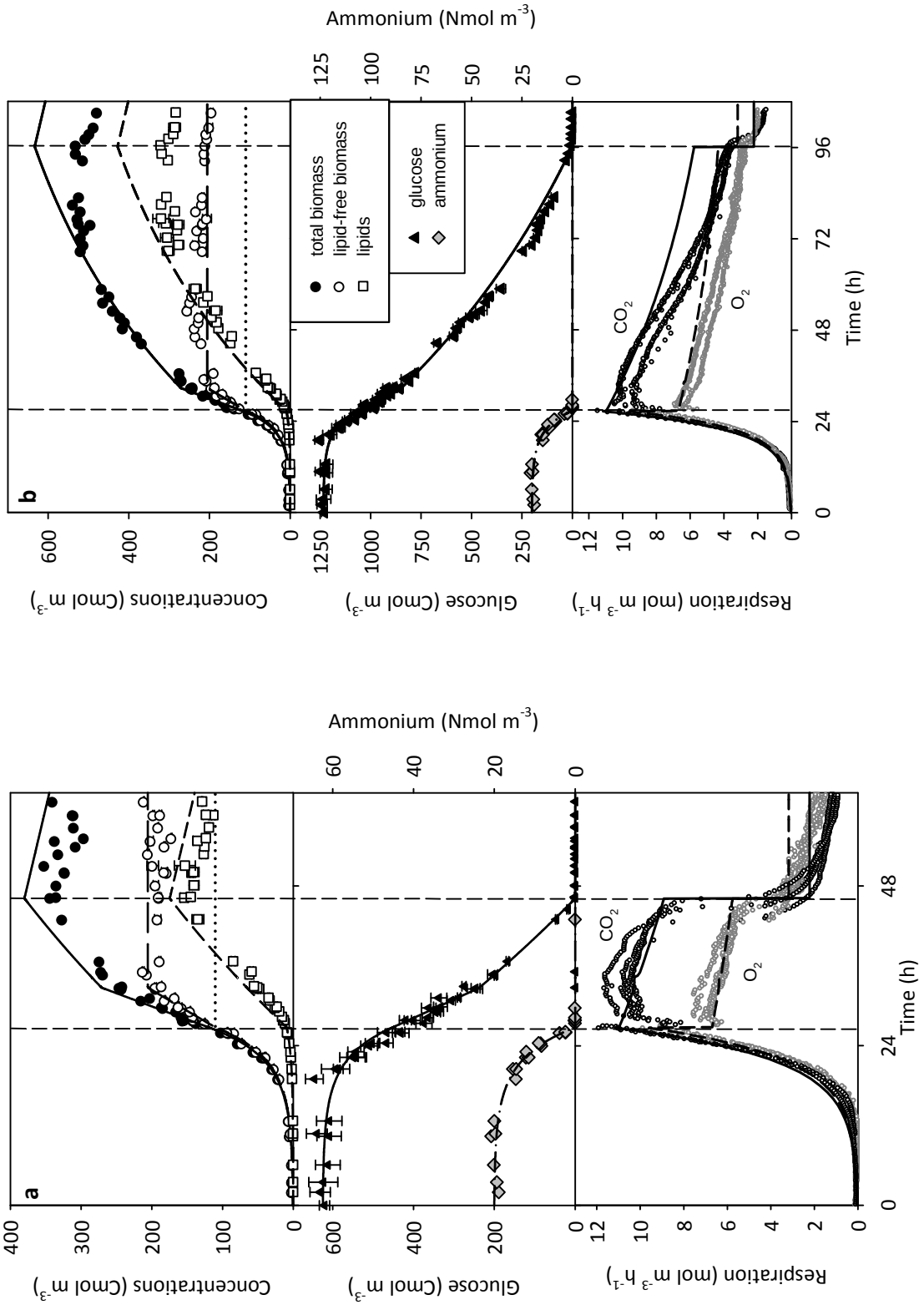

Fig. 7 Fit of the model on the results of batch cultures with *U. isabellina* on glucose and NH_4^+. (**a**) with an initial C/N-ratio of 30 Cmol/Nmol, (**b**) with a (theoretical) initial C/N-ratio of 60 Cmol/Nmol. Error bars indicate SD. Vertical lines divide the graphs in three phases in time: the growth phase, the lipid accumulation phase and the lipid turnover phase.

Fit of the model to the data

Fig. 7 compares the measurements and the results of model calculations with the parameter values in Table 1. Vertical lines divide the figures in three periods that are described in the model: growth, lipid accumulation and lipid turnover. The calculated biomass concentration is shown as total biomass, lipid-free biomass (including carbohydrates) and basic biomass. Only the model prediction is shown for the basic biomass concentration (lipid-free, carbohydrate-free biomass), because carbohydrates were not measured. In Fig. 7b, the glucose concentrations before addition of extra glucose were recalculated as if the glucose was added at the start of the culture.

In the exponential growth phase, the model describes all measured variables very well ($r^2 = 0.99$ for lipid-free biomass, basic biomass and CO_2 production rate). The substrate concentrations are predicted accurately by the model. There is no sign of deceleration in the substrate consumption at low concentrations, which shows that the assumed zero-order kinetics can be used.

In the accumulation phase, carbohydrate accumulation and the trend of lipid accumulation is predicted well, but the lipid concentrations and the respiration rates are overestimated later in the experiments, while the measured lipid-free biomass concentration is not as constant as the model predicts. These deviations are caused by the decrease in C-recovery at the end of the cultures with high C/N-ratio (Fig. 4). The model assigns the missing carbon to lipids and CO_2, which are therefore overestimated. However, the trend predicted by the model agrees with that of the data. For all experiments, the observed decrease in CO_2 production rate (Fig. 7b) from 29h (directly after the exponential phase) until 97h (when glucose is exhausted) could be fitted with exponential functions with constants of -0.016 h^{-1} ($r^2 = 0.99$, n = 225 for both experiments). This shows that the decrease in lipid production rate is indeed exponential and that the value for k_d in Table 1 is valid. Furthermore, the observed ratio between the CO_2 production rate and the O_2 consumption rate (RQ) decreases during the lipid production phase from 1.7 to 1.3 mol/mol (Fig. 7b), while the model predicts a decrease from 1.6 to 1.3 mol/mol. In our model, we assumed that the lipid accumulation starts immediately with the maximum rate and we neglected the delay in the lipid accumulation that is visible in the respiration measurements. (Boulton and Ratledge (1983) described the transition from carbon-limited to nitrogen-limited conditions for the oleaginous yeast *Lipomyces starkeyi*; they found that it takes

several hours for the culture to adapt to the new situation. Fig. 7 shows that the overall fit of the model on the data is hardly influenced by our assumption.

Fig. 7a shows a clear decrease of lipids in the turnover phase and no increase of basic biomass during this phase. The lipid turnover rate is predicted very well, even though the lipid concentration is slightly overestimated due to the over-prediction in the accumulation phase explained in the previous section. The respiration rate during the third phase is also overestimated; but the predicted RQ is correct: 0.7 mol/mol. This means that lipid turnover is taking place as predicted.

We conclude that the model describes the physiology and kinetics of the lipid accumulating fungus *U. isabellina* in batch cultures quite well. The model reveals that the low total mass yield of lipids on glucose reached (14% w/w for both cultures) is partially caused by the 'wasting' of glucose for carbohydrates (up to 20% of consumed glucose) and maintenance (up to 19% of consumed glucose). Carbohydrate storage is not a problem exclusively for the strain we used; it has been measured before (Boulton and Ratledge 1983, Ykema et al. 1986), and we found evidence for carbohydrate storage in other cultures from literature (Meeuwse et al. 2011b). It could be debated whether the stored component in our cultures was indeed a carbohydrate; fungi are also known to accumulate for example polyols (Ruijter et al. 2004). However, polyol quantities in fungi are generally small compared to for glycogen and trehalose quantities (Griffin 1993, Gow and Gadd 1995). Furthermore, Fig. 7 shows that the degree of reduction of the storage product (4 $Cmol^{-1}$) used in the calculations gives a good fit of the respiration rates. Polyols have a higher degree of reduction, which would lead to a lower O_2 consumption rate. Therefore, we believe that the assumption that the cells accumulate carbohydrates is reasonable.

Finally, the model shows how rapidly the lipids are lost due to maintenance when the external C-source is depleted. In a well-mixed batch culture, lipid turnover can be avoided by harvesting the cells at the right moment. Lipid turnover might be a problem in inhomogeneous cultures where local depletion of C-source can occur before the average concentration is zero. Repression of lipid turnover by multiple limitations as described by Papanikolaou et al. (2004b) might be an option to circumvent this, if this is feasible with the used (solid) substrate.

Lipid production mechanisms

Table 1 compares values found in batch cultures and chemostat cultures with *U. isabellina* (Meeuwse et al. 2011a). Most of the parameter values are similar, but there are some exceptions. The values found for the yield of basic biomass on glucose (Y_{XS}) and for the maintenance coefficient (m_S) in batch are lower than in chemostat. However, they are also more accurate because they are based solely on data from the exponential growth phase where the carbon recovery was complete, while in the chemostat cultures the carbon recovery was incomplete.

There is also a striking difference between the maximum specific lipid production rate, $q_{L\max}$, found in batch and chemostat cultures. The initial specific lipid production rate in batch cultures is almost four times higher than the constant value found in chemostat cultures (Meeuwse et al. 2011a). Furthermore, $q_{L\max}$ in chemostat cultures was independent of the residence time (= cell age), while there was an exponential decrease in batch cultures. The value of $q_{L\max}$ in chemostat cultures is very close to the specific functional lipid production rate, *i.e.* the production rate needed to obtain a lipid fraction f_{L0} in cells growing at μ_{max} (Meeuwse et al. 2011b). This suggests that the fungus uses the enzymes that normally produce functional or membrane lipids to accumulate lipids in chemostat cultures. The much higher initial specific lipid production rate in batch cultures, which decreases in time according to a first order decay mode, might indicate that another mechanism is used.

Ratledge and Wynn (2002) proposed that lipid accumulation in batch cultures is caused by continuation of glucose assimilation while growth slows down or stops because of nitrogen limitation. In our model, we assume that the specific glucose uptake rate after N-source depletion remains equal to the specific uptake rate during exponential growth. This gives an accurate prediction and therefore supports the proposition of Ratledge and Wynn (2002). However, part of the glucose taken up by the cell is accumulated as carbohydrates instead of being converted to citric acid and subsequently to lipids. The reason for the carbohydrate accumulation could be a kinetic bottleneck in the conversion of citric acid to fatty acids; it cannot be the conversion of glucose to citric acid or the respiration as these processes had a higher rate during exponential growth.

Wynn et al. (Wynn et al. 1999, Wynn et al. 2001) described a switch from normal growth to lipid accumulation in batch cultures of *Mucor circinelloides* and

Mortierella alpina when they encounter nitrogen limitation: a decrease in intracellular NH_4^+ inhibits the activity of the enzyme phosphofructokinase, leading to accumulation of citrate, which is the source of acetyl-CoA used for lipid production (Wynn et al. 2001). Wynn et al. (1999) also reported a decrease in lipid production rate in time, which could be attributed to a decrease in activity of malic enzyme, the rate-limiting enzyme in the lipid production route. Their limited number of data points (Wynn et al. 1999) suggest that the observed decrease in enzyme activity is exponential, as we found in our cultures. The decrease is irreversible because malic enzyme activity can only be restored by *de novo* synthesis (Wynn et al. 1999), which requires an N-source. Although we have no enzyme activity data, it seems likely that the decrease in specific lipid production rate in our batch reactors was caused by degradation of malic enzyme, which could not be synthesized because of the lack of N-source. In chemostat culture, the continuous supply of N-source would allow continuous protein synthesis, which could explain the observed constant value of the maximum specific lipid production rate (Meeuwse et al. 2011a).

Comparison to literature

Table 1 compares our parameter values to values reported by Economou et al. (2011) for batch cultures of a different strain of the same species with sweet sorghum extract as substrate. Additionally, we fitted our model on the same data; parameter values found are also shown in Table 1 and the resulting fit is shown in Fig. 8. This graph shows that our model fits the experimental data well, although the underestimation of the lipid production rate in Figure 8a could indicate that substrate inhibition was important in Figures 8b and 8c, which was not included in our model. However, the sum of squares of residuals for all fitted data points (for lipid-free biomass, lipids and sugars in the three presented graphs) was three times lower than for the original model developed for these data points (Economou et al. 2011). We also fitted our model successfully on published results (Sattur and Karanth 1991, Karanth and Sattur 1991) of batch cultures of the oleaginous yeast *Rhodotorula gracilis* (results not shown). This shows that our model is suitable for other data sets with different C/N-ratios, strains and substrates.

Table 1 shows that there are some significant differences between the parameter values for the different models and data sets. Both μ_{max} and $q_{L\,max}$ determined by Economou et al. (2011) are much higher than our values for both data sets because they used Monod kinetics and substrate inhibition in their model, which leads to very high maximum values. The actual specific rates shown in Table 1 are similar to our values. The yield values Y_{XS} and Y_{LS} are lower for the sweet sorghum batches, both the values from literature and our values; this may have been caused by differences in substrate or strain. The value for Y_{XN} obtained by Economou et al. (2011) is higher and close to the yield of lipid-free biomass including carbohydrates in our experiments (10.5 Cmol $Nmol^{-1}$). This may indicate that carbohydrates were produced in their cultures, which is also supported by the observed production of lipid-free biomass after N-depletion (Economou et al. 2011). We therefore included carbohydrate production in our fit, which results in a value for Y_{XN} similar to the value from our experiments, combined with a very low specific carbohydrate production rate (Table 1). This rate could not be described

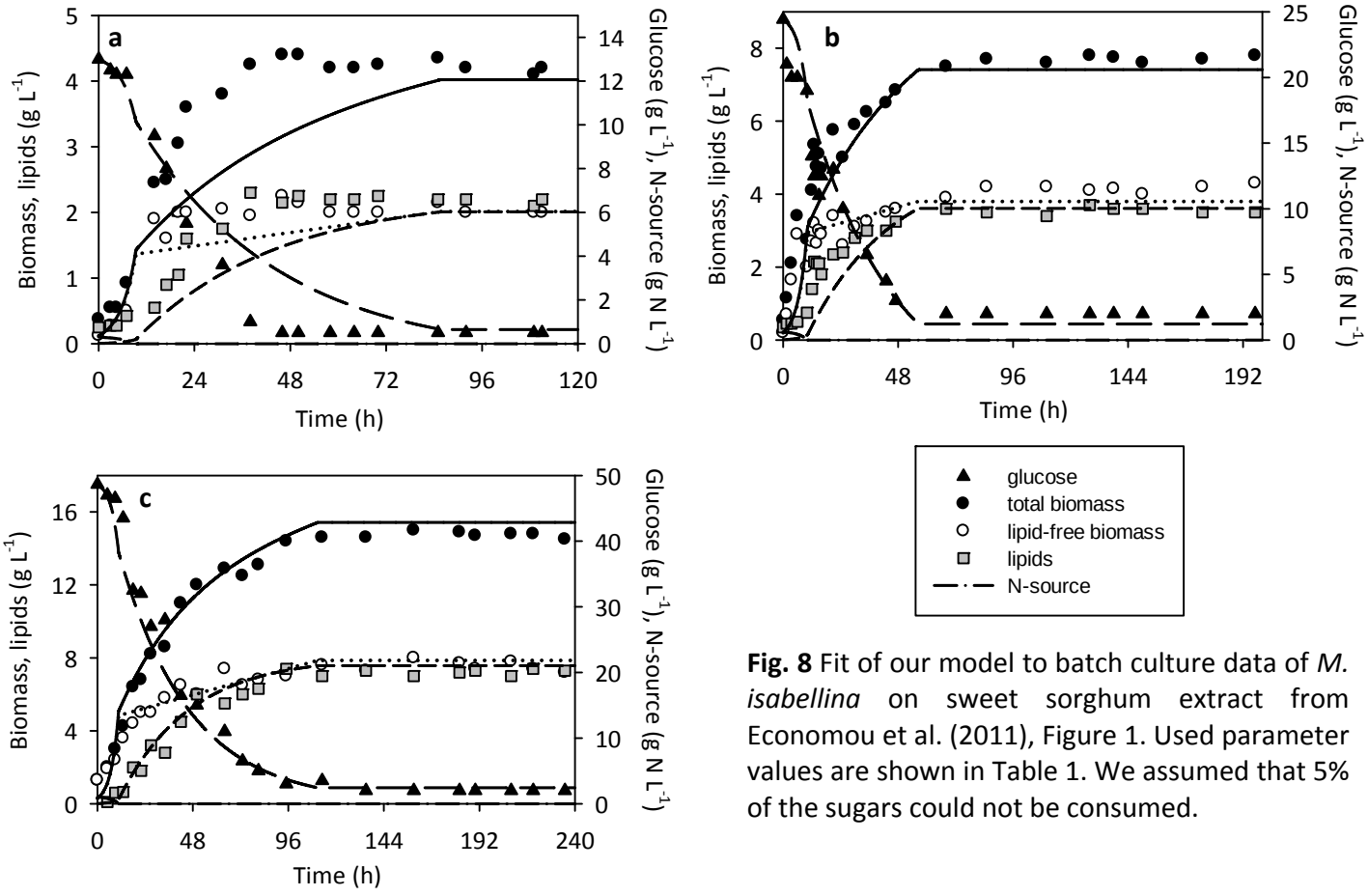

Fig. 8 Fit of our model to batch culture data of *M. isabellina* on sweet sorghum extract from Economou et al. (2011), Figure 1. Used parameter values are shown in Table 1. We assumed that 5% of the sugars could not be consumed.

by Equation 12; we used a constant fitted value instead, which leads to a good fit. The most important parameter for lipid accumulation is $q_{L\max}$. Therefore, we compared our value to literature values from other batch cultures; the large difference in $q_{L\max}$ for batch and chemostat cultures shown in the previous paragraph means that comparison to values from chemostats is not useful. Our value for $q_{L\max}$ is high compared to the values found for *R. gracilis* on glucose (0.025 Cmol Cmol^{-1} h^{-1}) (Sattur and Karanth 1991) and *C. curvata* on whey (0.040 Cmol Cmol^{-1} h^{-1}) (Glatz et al. 1984). However, all values are of the same order of magnitude and therefore our value is reasonable. Our $q_{L\max}$ value is lower than values found for batch cultures using lipid-based substrates (0.09 – 0.25 Cmol Cmol^{-1} h^{-1}) (Aggelis and Sourdis 1997, Papanikolaou and Aggelis 2003), which is not surprising because less transformations are needed when lipids are used as starting material for lipid accumulation.

Conclusions

We developed a model for submerged batch culture of oleaginous fungi and validated it with data from batch cultures of *U. isabellina* growing on glucose and NH_4^+. The deviation between model and data was small and could be explained by incomplete carbon recovery near the end of the cultures, due to aggregation of cells on baffles and stirrer. The model shows that a batch culture can be divided into three phases: the growth phase, the lipid accumulation phase and the lipid turnover phase. In the first phase, no substrate is limiting and growth occurs at the maximum specific growth rate, while only a basic lipid fraction for functional lipids is present in the cells. When the nitrogen source is exhausted, the cells accumulate carbohydrates up to a maximum fraction, and lipids with an exponentially decreasing specific rate. We showed that this decrease was not caused by the declining C-source concentration, and therefore could not be described with Monod kinetics, as was done in other models for submerged batch culture (Glatz et al. 1984, Economou et al. 2011). The specific rate of lipid production in batch cultures is much higher than in chemostat cultures, indicating that another lipid synthesis mechanism is active. Observations during the lipid production phase and results from literature (Wynn et al. 2001, Meeuwse et al. 2011a, Boulton and Ratledge 1983) indicate that in batch cultures a switch from growth to lipid accumulation takes place, while in chemostat cultures growth and lipid production occur simultaneously, which leads to different rates. When the C-source is exhausted, lipids are combusted for maintenance requirements, and not for growth as described before (Economou et al. 2011).

The model developed in this paper described all observed features of a submerged batch culture well, including turnover of lipids for maintenance and the decrease in lipid production rate that was observed to be independent of the C-source concentration. It also describes results from literature well. Therefore it is a useful addition to previously published models (Granger et al. 1993, Sattur and Karanth 1989, Sattur and Karanth 1991, Karanth and Sattur 1991, Aggelis et al. 1995, Aggelis and Sourdis 1997, Papanikolaou and Aggelis 2003, Glatz et al. 1984, Economou et al. 2011).

Chapter 6

Growth and lipid production of *Umbelopsis isabellina* on a solid substrate
Mechanistic modeling and validation

Meeuwse P, Klok AJ, Haemers S, Tramper J, Rinzema A. 2011. Growth and lipid production of *Umbelopsis isabellina* on a solid substrate – mechanistic modeling and validation.

Abstract

Microbial lipids are an interesting feedstock for biodiesel. Their production from agricultural waste streams by fungi cultivated in solid-state fermentation may be attractive, but the yield of this process is still quite low. In this article, a mechanistic model is presented that describes growth, lipid production and lipid turnover in a culture of *U. isabellina* on κ-carrageenan plates containing the monomers glucose and alanine as C-source and N-source, respectively, and improves the understanding of the complex solid-state system. The model includes reaction kinetics and diffusion of glucose, alanine and oxygen. It is validated empirically and describes the different phases of the culture very well: exponential growth, linear growth because of oxygen limitation, accumulation of lipids and carbohydrates after local N-depletion and turnover of lipids after local C-depletion. Extending the model with an unidentified extracellular product improved the fit of the model to the data considerably. The model shows that oxygen limitation is extremely important in solid-state cultures using monomers. Together with the lower specific lipid production rate found in solid-state cultures, it explains the difference in production rate with submerged cultures.

Introduction

Lipids produced by microorganisms become more and more important as feedstock for biodiesel (Li et al. 2008, Feofilova et al. 2009, Meng et al. 2009). Cultivation of oleaginous fungi in solid-state fermentation (SSF) on substrates such as agricultural waste streams is a possibility to produce lipids sustainably and at low cost. However, the yield of this process is still much lower than that of lipid production in submerged cultures (Stredansky et al. 2000, Gema et al. 2002, Peng and Chen 2008, Economou et al. 2010). Mechanistic mathematical modeling can give insight in the causes of this low yield. Previously, we modeled lipid production in submerged fermentation (SmF) (Meeuwse et al. 2011a, Meeuwse et al. 2011b, Meeuwse et al. 2011c), and in this paper we present a model for lipid production on a κ-carrageenan gel containing monomers. This model describes growth and lipid accumulation combined with diffusion of substrates.

Several mathematical models for growth in SSF have been described in literature; these have been reviewed by Mitchell et al. (2004) and Rahardjo et al. (2006). These models differ in system boundaries (substrate and/or biofilm), modeled substrates (polymers, glucose and/or oxygen) and modeled products (usually only biomass, sometimes enzymes). We will briefly discuss three of the reviewed models that are most relevant to the work presented in this paper.

The only model that includes the solid substrate as well as the biofilm is the model of Rajagopalan and Modak (1995). This model takes into account diffusion of glucose, glucoamylase and oxygen during growth of a fungus on a spherical particle containing starch. The simulations show that oxygen becomes limiting in the inner part of the biofilm, but this model was not validated. Oostra et al. (2001) measured oxygen profiles in layers of *Rhizopus oligosporus* growing on agar plates with glucose and found that oxygen was limiting in the biofilm after 36 hours of growth. They modeled the oxygen profiles in a quasi-steady state and did not describe growth. Mitchell et al. (1991) modeled growth on κ-carrageenan plates containing starch, but did not take oxygen into account. They could only validate their model by changing some of the independently measured parameter values, possibly because they neglected the influence of oxygen.

None of the described models takes into account an N-source, which is very important for lipid production, because N-source limitation is known to trigger lipid production (Wynn et al. 2001). Furthermore, none of the models describes accumulation of a product such as lipids. Therefore, we developed a model describing growth, lipid accumulation and lipid turnover during cultivation of the oleaginous fungus *U. isabellina* on a κ-carrageenan gel containing glucose and alanine as C-source and N-source, respectively. Oxygen penetrating the biofilm from the surface was also included in the model. The kinetics used in this model are based on our work on submerged cultures (Meeuwse et al. 2011a, Meeuwse et al. 2011c).

Model

Figure 1 shows a simplified scheme of the metabolism of an oleaginous organism. The organism uses a C-source (glucose, S), an N-source (alanine, N) and oxygen (O) to produce cell material (X), lipids (L), carbohydrates (intracellular product, IP), carbon dioxide (C), water (W) and an extracellular product (EP). The biomass is divided into lipids (L), carbohydrates (IP) and lipid-free, carbohydrate-free cell material, which we will refer to as basic biomass (X). The composition of basic biomass ($CH_{1.77}O_{0.55}N_{0.17}$, MW=28.7 g $Cmol^{-1}$ including ash) is based on the average composition of *U. isabellina* during exponential growth in submerged batch cultures (Meeuwse et al. 2011c) and the composition of the lipids ($CH_{1.95}O_{0.11}$, MW=15.7 g $Cmol^{-1}$) is based on the average fatty acid composition of the accumulated triacylglycerol in *U. isabellina* determined during previous experiments (Meeuwse et al. 2011a, Meeuwse et al. 2011c). For carbohydrates, we assumed the same composition as glucose. All components that contain carbon are expressed in Cmoles, except the N-source, which is expressed in Nmoles, but also acts as a C-source. Symbols used in the model are listed on page 207.

The model predicts production of basic biomass, lipids, intracellular and extracellular product, and turnover of lipids and extracellular product in a fungal biofilm growing on κ-carrageenan gel in a petri dish. Figure 2a shows our model system at an arbitrary time point including the system boundaries.

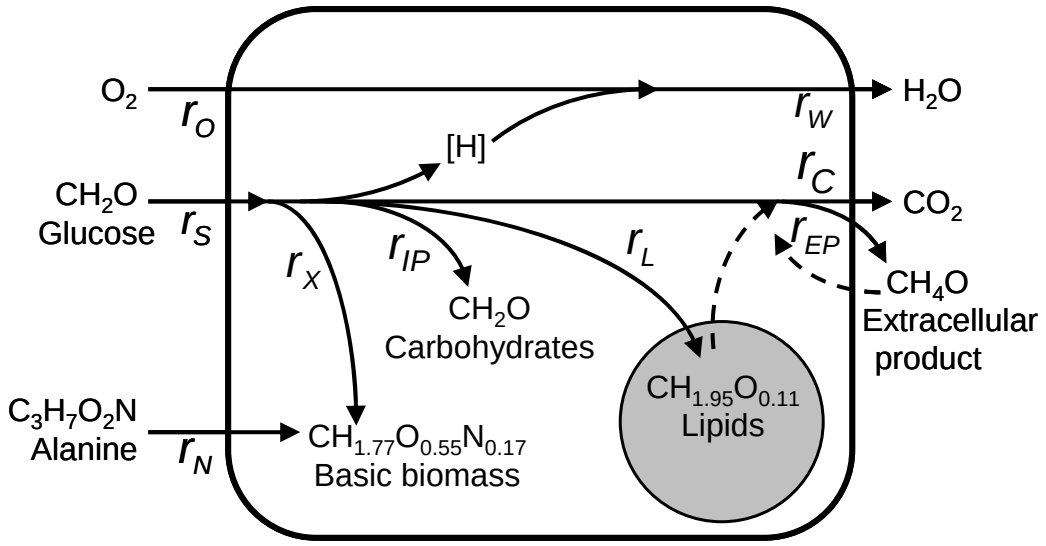

Figure 1: Schematic overview of the modeled metabolism of *U. isabellina*. Reactions indicated with dashed arrows only occur when glucose is exhausted.

We assume that the following phenomena occur:

- In the biofilm: diffusion and consumption of C-source (S), N-source (N) and oxygen (O), and production of products (X, L, IP, EP, C, W). Accumulation of substrates (S, N and O) in the biofilm is neglected; accumulation of products and uptake of water from the gel layer causes an increase in biofilm thickness at the expense of the gel layer.

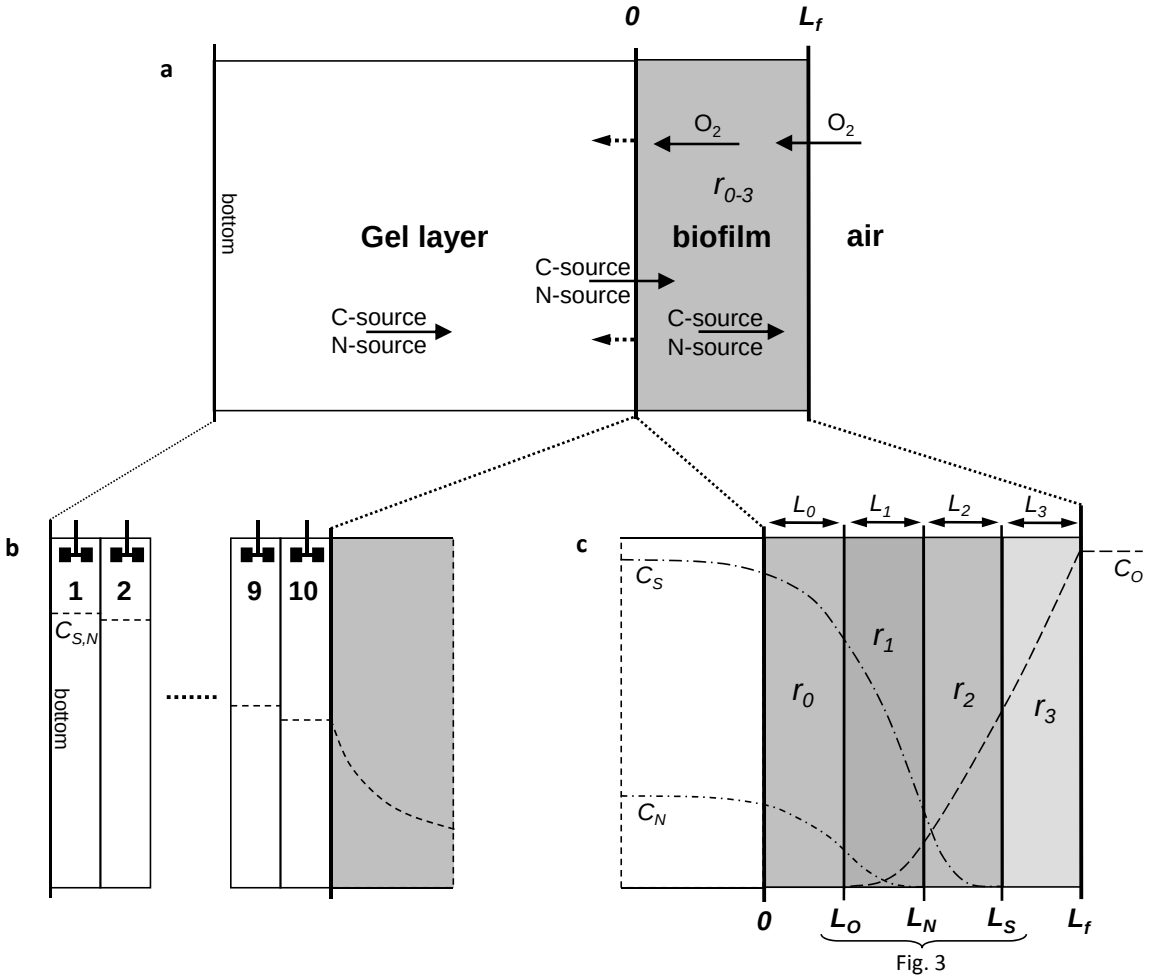

Figure 2: Schematic overview of the modeled system. Thickness of the depicted layers is arbitrary and out of scale. **Fig. 2a**: Cross-section of κ-carrageenan plate with fungal biofilm on top (right), turned 90 degrees. The model includes diffusion of C-source and N-source in both gel layer and biofilm and diffusion of oxygen and reactions (r_{0-3}) in the biofilm. Because of accumulation of products in the biofilm and transfer of water from the gel layer to the biofilm, the boundary between gel layer and biofilm, indicated with 0, shifts to the left. **Fig. 2b**: Detail of the gel layer, which is modeled as 10 ideally mixed layers with diffusion from one layer to the next. **Fig. 2c:** Detail of the biofilm. Diffusion of the different substrates (S, N and O) leads to different (sub)layers, in which different combinations of substrates are present and therefore different reactions occur, indicated with r_0-r_3.

- In the gel layer: depletion and diffusion of C-source (S) and N-source (N). Any other substrates in this layer (sulphur, phosphorus, minerals) are assumed to be present in excess and are therefore neglected. Because both water and substrates leave the gel layer, the mass and the thickness of the gel layer decrease.
- In both layers, we neglect active transport and convection of substrates with water.
- We neglect penetration of fungal hyphae into the gel layer and formation of aerial hyphae on top of the biofilm; the surface area of the fungus contacting the air is equal to the surface area of the petri dish.
- The air contacting the biofilm contains a constant oxygen concentration (constant fresh air through active aeration).
- No evaporation of water from the biofilm to the air occurs.

Model for the biofilm

We model the fungal biofilm as a continuous layer of biomass without taking into account single hyphae or cell walls. Figure 2c shows that diffusion and consumption of the three substrates can create (sub)layers within the biofilm that contain different combinations of substrates at a certain moment in time. We only modeled a situation in which the N-source is depleted before the C-source, because only in this situation lipid accumulation will occur (Wynn et al. 2001). How we calculate the position and thickness of each layer is explained in the paragraph on diffusion; which reactions occur in each layer is explained in the paragraph on reactions. We assume that the biomass (dry weight) concentration is independent of the position in the biofilm, but it can change in time. Furthermore, products produced (X, IP, EP, L) are equally distributed over the whole biofilm, independent of the layer in which they were produced. All produced CO_2 is released immediately into the air.

Reactions in the biofilm

Depending on the availability of the nutrients, four different situations are possible, indicated with r_0, r_1, r_2 and r_3 in Figure 2c. We discuss these situations below. The reactions were studied before in submerged batch culture (Meeuwse et al. 2011c). We assume zero-order kinetics with respect to substrate concentrations for all reactions. For oxygen, Rahardjo et al. (2005) showed that it is reasonable to use zero-order kinetics instead of Monod kinetics in a diffusion/reaction model for *Aspergillus oryzae* in SSF, because of the very low Monod constant of 4×10^{-3} mol m^{-3}. Other published values for the Monod constant for different *Aspergillus* species range from 6×10^{-4} to 2×10^{-2} mol m^{-3} (Kobayashi et al. 1973, Kurosawa et al. 1989, Koutinas et al. 2003), which is only 0.2 - 8% of the oxygen concentration at the interface with the air. For *M. isabellina*, no kinetic information is available in literature, but we assume that the Monod constant is low enough to use zero-order kinetics for oxygen. Because the oxygen concentration in the biofilm is much lower than the concentrations of glucose and alanine, we assume that oxygen is the limiting substrate, as was also predicted by Rajagopalan and Modak (1995). Therefore, the reaction kinetics of glucose and alanine are of minor importance and the use of zero-order kinetics for these substrates will hardly influence the modeling results.

Situation r_0: no oxygen is available

We assume that no anaerobic reactions occur. Therefore, this layer is dormant and neither metabolism (including maintenance) nor cell death takes place. Thus, this layer only acts as a diffusion barrier for the C-source and N-source. If necessary, the model can be extended to include anaerobic reactions in this layer.

Situation r_1: C-source, N-source and O_2 are available.

Submerged batch fermentation (Meeuwse et al. 2011c) has shown that the cells will grow at their maximum specific growth rate and will only produce functional lipids at a minimum lipid fraction in this situation. Based on the results of the current study, we assume that extracellular product is produced at a constant specific rate, but no storage carbohydrates are produced. The reaction rates in this situation are shown in Table 1.

Table 1 Reactions occurring in a biofilm according to the model, depending on the availability of the substrates (for X, L, IP and EP), and independent of substrate availability (for S, N, C and O).

	1: C-source, N-source and O_2 available	2: C-source and O_2 available	3: O_2 available
Basic biomass (X)	$r_{X.1} = \mu_{max} C_X$ (1a)	$r_{X.2} = 0$ (1b)	$r_{X.3} = 0$ (1c)
Lipids (L)	$r_{L.1} = \frac{f_{L0}}{1 - f_{L0}} r_{X.1}$ (2a)	$r_{L.2} = q_{L,\max} e^{-k_d t} C_X$ (2b)	$r_{L.3} = -m_L C_X$ (2c)
Carbohydrates (IP)	$r_{IP.1} = 0$ (3a)	$r_{IP.2} = q_{IP} C_X$ until $\frac{C_{IP}}{C_X} = f_{IP,\max}$ (3b)	$r_{IP.3} = 0$ (3c)
Extracellular product (EP)	$r_{EP.1} = q_{EP} C_X$ (4a)	$r_{EP.2} = q_{EP} C_X$ (4b)	$r_{EP.3} = -m_{EP} C_X$ (4c)
C-source (glucose, S)	$-r_S = \frac{r_X}{Y_{XS}} + \frac{r_L}{Y_{LS}} + \frac{r_{IP}}{Y_{IPS}} + \frac{r_{EP}}{Y_{EPS}} + m_S C_X$ (5)		
N-source (alanine, N)	$-r_N = \frac{r_X}{Y_{XN}}$ (6)		
CO_2 (C)	$r_C = -r_X - r_L - r_{IP} - r_{EP} - 3r_N - r_S$ (7)		
O_2 (O)	$r_O = 1.1675 r_X + 1.4325 r_L + r_{IP} + 1.5 r_{EP} + 3.75 r_N + r_S$ (8)		

Situation r_2: Only C-source and O_2 are available

In this situation, the cells accumulate carbohydrates and lipids, and produce extracellular product at the same specific rate as in situation r_1. Carbohydrates are stored at a constant rate until the maximum carbohydrate fraction in the cells is reached. In submerged batch culture (Meeuwse et al. 2011c), the specific carbohydrate production rate was determined by the maximum glucose uptake rate during exponential growth. This means that the maximum carbohydrate production rate is determined by the glucose used during maximum growth with a minimum lipid fraction in the cells minus the glucose used for the other products in situation r_2: lipids and extracellular product. This gives the following equation:

$$q_{IP} = Y_{IPS}\left(\frac{\mu_{\max}}{Y_{XS}} + \frac{f_{L0}}{1-f_{L0}}\frac{\mu_{\max}}{Y_{LS}} - \frac{q_L}{Y_{LS}} - \frac{q_{EP}}{Y_{EPS}}\right) \quad (9)$$

Lipids are produced at a decreasing specific rate as was observed before in submerged batch culture (Meeuwse et al. 2011c). All equations used in this situation are shown in Table 1.

Situation r_3: Only O_2 is available

In this situation, accumulated lipids and extracellular product are used for the maintenance requirements of the cells; for equations see Table 1. Carbohydrates are not consumed, as was observed in submerged batch culture (Meeuwse et al. 2011c). An adapted maintenance coefficient is used to account for the different amounts of ATP that can be produced from lipids and extracellular product compared to glucose:

$$m_S = 1.4m_L + 0.9m_{EP} \quad (10)$$

Diffusion in the biofilm

The penetration depth of the substrates in the biofilm depends on the concentrations at the boundaries of the biofilm ($C_S(0)$, $C_N(0)$ and $C_O(L_f)$) and the diffusion and consumption rates in the biofilm. As an example, we show the calculation of the penetration depth of the C-source (S) in the situation shown in Figure 2c. An enlargement of the relevant layers and fluxes for this calculation is shown in Figure 3. Calculations for other substrates (N, O) and for other situations are shown in the appendix.

We start with a balance over part of layer L_2 ranging from x_2 to L_S, as indicated in Figure 3:

$$N_S(x_2) - N_S(L_S) + r_{S.2}(L_S - x_2) = 0 \qquad (11)$$

In this equation, accumulation of substrate in the biofilm is neglected because it is negligible compared to diffusion and conversion in the biofilm. We describe the diffusion fluxes with Fick's law:

$$N_S(x) = -ID_S\left(\frac{d}{dx}C_S\right) \qquad (12)$$

By definition, $N_S(L_S) = 0$, because L_S is defined as the penetration boundary of S. To find the concentration of S at L_N, we combine equations 11 and 12 and

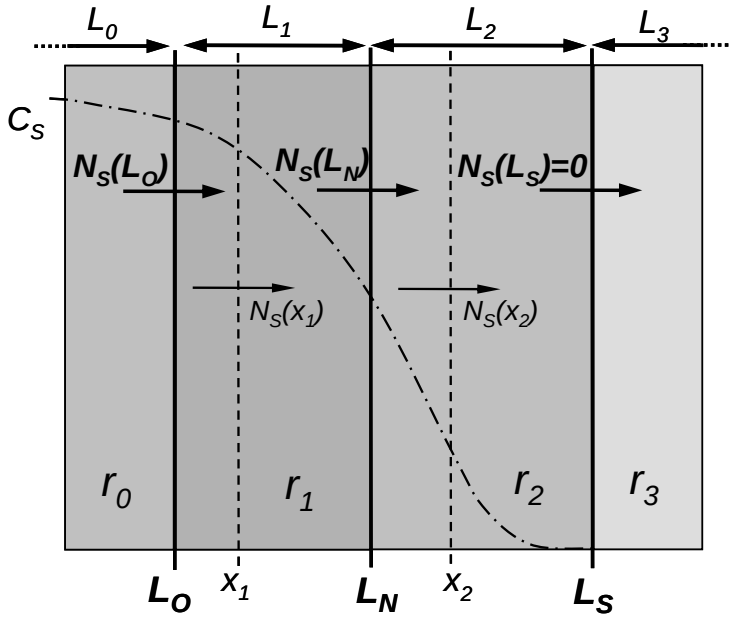

Figure 3: Detail of part of the biofilm indicated in Figure 2 with fluxes (N_S) and reactions (r_0-r_3) of the C-source used in the calculations in the text. Thickness of the layers is arbitrary.

integrate over layer L_2, assuming ID_S is constant:

$$\int_{C_S(L_N)}^{C_S(L_S)=0} ID_S dC_S = \int_{L_N}^{L_S} r_{S.2}(L_S - x_2)dx_2 \quad \rightarrow \quad C_S(L_N) = \frac{-r_{S.2}\left(L_N - L_S\right)^2}{2ID_S} \tag{13}$$

To calculate L_S with this equation, $C_S(L_N)$ and L_N have to be calculated first. The penetration depth of the N-source (L_N) is calculated from an N-source balance as is shown in the appendix, $C_S(L_N)$ can be calculated from a C-source balance over layer L_1:

$$N_S(x_1) - N_S(L_N) + r_{S.1}(L_N - x_1) = 0 \tag{14}$$

The flux through L_N is determined by the consumption beyond L_N:

$$N_S(L_N) = r_{S.2}(L_S - L_N) \tag{15}$$

Combining equations 12, 14 and 15 and including the integration boundaries, we get:

$$\int_{C_S(L_O)}^{C_S(L_N)} ID_S dC_S = \int_{L_O}^{L_N} \left(r_{S.2}(L_S - L_N) + r_{S.1}(L_N - x_1)\right)dx_1 \quad \rightarrow$$

$$C_S(L_O) = C_S(L_N) - \frac{\left(L_N - L_O\right)\left(2r_{S.2}\left(L_S - L_N\right) + r_{S.1}\left(L_N - L_O\right)\right)}{2ID_S} \tag{16}$$

Because there is no consumption or production in layer L_0, this layer can be considered a part of the gel layer when calculating diffusion in this layer. Therefore, calculating $C_S(L_O)$ is described in the paragraph on diffusion in the gel layer. The calculation of the penetration depth of oxygen (L_O) is shown in the appendix. Combining Equations 13 and 16 then gives the penetration depth of the C-source in the situation in Figure 3:

$$L_S = \sqrt{\frac{\left(L_N - L_O\right)^2\left(r_{S.1} - r_{S.2}\right) + 2ID_S C_S(L_O)}{-r_{S.2}}} + L_O \tag{18c}$$

Other situations for different combinations of layers are shown in Figure 4a-d. The calculations of the penetration depths of the C-source, the N-source and oxygen in these situations are shown in the appendix; the resulting equations are shown in Table 2. A change from one situation to the next in Figure 4 occurs when the calculated boundaries become either >0 (for L_O) or < L_f (for L_N and L_S) as is indicated in Table 2.

Table 2: Equations used to calculate penetration depth of the substrates in the biofilm and the thickness of the resulting sub-layers as shown in Figure 4. All distances are measured from the boundary between gel layer and biofilm in the direction of the biofilm.

a	b	c	d
$L_N = \sqrt{\frac{2ID_N C_N(0)}{-r_{N.1}}} > L_f$ (17a)	$L_N = \sqrt{\frac{2ID_N C_N(L_O)}{-r_{N.1}}} + L_O > L_f$ (17b)	$L_N = \sqrt{\frac{2ID_N C_N(L_O)}{-r_{N.1}}} + L_O < L_f$ (17c)	$L_N \approx L_O$ (17d)
$L_S = \sqrt{\frac{2ID_S C_S(0)}{-r_{S.1}}} > L_f$ (18a)	$L_S = \sqrt{\frac{2ID_S C_S(L_O)}{-r_{S.1}}} + L_O > L_f$ (18b)	$L_S = \sqrt{\frac{(L_N - L_O)^2 (r_{S.1} - r_{S.2}) + 2ID_S C_S(L_O)}{-r_{S.2}}} + L_O > L_f$ (18c)	$L_S = \sqrt{\frac{2ID_S C_S(L_O)}{-r_{S.2}}} + L_O < L_f$ (18d)
$L_O = L_f - \sqrt{\frac{2ID_O C_O(L_f)}{-r_{O.1}}} < 0$ (19a)	$L_O = L_f - \sqrt{\frac{2ID_O C_O(L_f)}{-r_{O.1}}} > 0$ (19b)	$L_O = L_f - \sqrt{\frac{(L_f - L_N)^2 (r_{O.2} - r_{O.1}) + 2ID_O C_O(L_f)}{-r_{O.1}}} > 0$ (19c)	$L_O = L_f - \sqrt{\frac{(L_f - L_S)^2 (r_{O.3} - r_{O.2}) + 2ID_O C_O(L_f)}{-r_{O.2}}} > 0$ (19d)
$L_0 = 0$	$L_0 = L_O$	$L_0 = L_O$	$L_0 = L_O$
$L_1 = L_f$	$L_1 = L_f - L_O$	$L_1 = L_N - L_O$	$L_1 = L_N - L_O \approx 0$
$L_2 = 0$	$L_2 = 0$	$L_2 = L_f - L_N$	$L_2 = L_S - L_N$
$L_3 = 0$	$L_3 = 0$	$L_3 = 0$	$L_3 = L_f - L_S$

Accumulation of products in the biofilm

To calculate the accumulation of any product formed in the biofilm, we add all production rates of a product over all layers present, for example for basic biomass (X):

$$\frac{d}{dt}M_X = \sum_{i=0}^{3} r_{X,i} L_i A \qquad (20)$$

This equation is also used for the other products: L, IP and EP; as said, accumulation of substrates in the biofilm is neglected.

A culture starts as a very thin biofilm in which all substrates are available, as is shown in Figure 4a. The thickness of the biofilm increases in time with the accumulation of biomass. Assuming a known basic biomass concentration inside

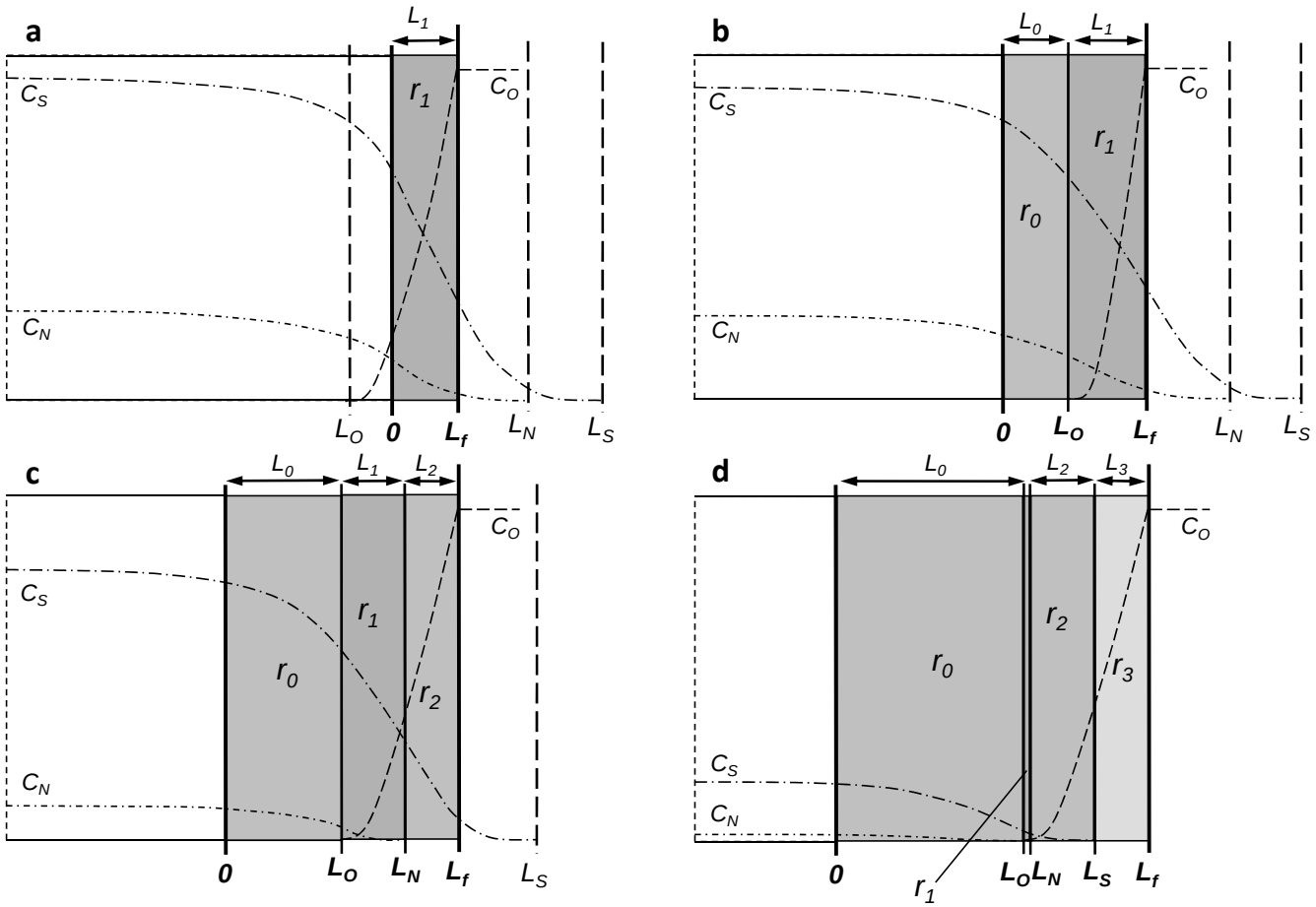

Figure 4: Occurrence of sub-layers in the biofilm in time in a κ-carrageenan culture in which the nitrogen source is exhausted before the carbon source. Calculation of the position of the boundaries and the thickness of the sub-layers is shown in Table 2. The thickness of the depicted layers is arbitrary, and the drawn diffusion profiles are the theoretical profiles used in the calculations. **a:** No limitations, **b:** Oxygen is limiting, **c:** Oxygen and N-source are limiting, **d**: Oxygen and C-source are limiting, N-source is exhausted.

the biofilm, the biofilm thickness is:

$$L_f(t) = \frac{M_X(t)}{C_X(t)A} \qquad (21)$$

As the biofilm thickness increases and the substrate concentration in the gel layer decreases, on e or more of the substrates will become limiting in a part of the biofilm. This creates the layers shown in Figure 2b in the order shown in Figures 4a-4d. Which situation in this figure is relevant, has to be checked before every time step in the calculation.

Substrate diffusion in the gel layer

The consumption of substrates by the biofilm leads to a decrease in substrate concentration at the top of the gel layer, which in turn leads to a gradient from the bottom to the top and therefore to diffusion, as was shown by Nagel et al. (2002). We divide the gel layer in ten equal sub-layers, which we assume to be ideally mixed, as is shown in Figure 2b. We chose to use ten sub-layers, each 0.8 mm thick, as this gives enough accuracy for the calculations while keeping the number of time steps in the model calculation manageable; a shorter distance requires smaller time steps to keep the used Euler method stable according to the Von Neumann criterion. For each of the ten sub-layers, a balance can be set up for both the C-source and the N-source using Fick's law for diffusion (Equation 12).
For the C-source, this results in:

Gel compartment 1 (bottom): $$0.1A\frac{d}{dt}L_g C_{S,1} = ID_S A\frac{C_{S,2} - C_{S,1}}{0.1L_g} \qquad (22)$$

Gel compartment 1<*n*<10: $$0.1A\frac{d}{dt}L_g C_{S,n} = ID_S A\frac{C_{S,n+1} - C_{S,n}}{0.1L_g} - ID_S A\frac{C_{S,n} - C_{S,n-1}}{0.1L_g} \qquad (23)$$

Gel compartment 10 (top): $$0.1A\frac{d}{dt}L_g C_{S,10} = -ID_S A\frac{C_{S,10} - C_{S,9}}{0.1L_g} + \sum_{i=0}^{3} r_{S,i} L_i A \qquad (24)$$

The same equations can be set up for the N-source. Not only the substrate concentration C_S (or C_N) changes in time, but also the thickness of the gel layer L_g changes because water is taken up by the biofilm. Therefore, the chain rule can be applied to these equations, giving for example for Equation 22:

$$0.1AL_g \frac{d}{dt}C_{S,1} + 0.1AC_{S,1}\frac{d}{dt}L_g = ID_S A\frac{C_{S,2} - C_{S,1}}{0.1L_g} \quad (25)$$

For Equations 22-24, a total of ten of these equations can be set up, which contain eleven unknown variables: $C_{S,1}$ - $C_{S,10}$ and L_g. We calculate the change in the thickness of the gel layer from a mass balance over both gel layer and biofilm; the small loss of mass by respiration is neglected:

$$\frac{d}{dt}M_g = -\frac{d}{dt}L_f \rho_X A \quad (26)$$

In the anaerobic part of the biofilm (L_0) no reactions take place; therefore, this part is similar to the gel layer. We include the anaerobic part of the biofilm in the gel layer for calculations on diffusion:

$$L_g(t) = \frac{M_g(t)}{\rho_g A} + L_0(t) \quad (27)$$

In this way, the substrate concentration in the upper layer of the gel layer ($C_{S,10}$ or $C_{N,10}$) is equal to $C_S(L_O)$ or $C_N(L_O)$, which makes an extra balance over L_0 (from 0 to L_O) redundant.

Materials and methods

Medium

The solid medium contained per liter: 4.6 g alanine (52 Nmol m^{-3} or 156 Cmol m^{-3}), 44.5 g glucose (1485 Cmol m^{-3}), 0.5 g $MgSO_4 \cdot 7H_2O$, 1.5 g KCl, 1.5 g $Na_2HPO_4 \cdot 2H_20$, 1 mL trace metal solution as described by Vishniac and Santer (1957) and 20 g κ-carrageenan (Sanofi). The pH of the medium was adjusted to 6 by addition of 2M Na_2SO_4. κ-Carrageenan solidifies by complexation with cations, in this case mainly K^+. The gel can be dissolved by heating or by dilution to an ion concentration below the critical concentration for complexation (Weber et al. 1999a). For this medium, a 10-fold dilution is sufficient to dissolve the gel for analysis. The medium was autoclaved; the glucose was autoclaved separately and added after autoclavation. Petri dishes were filled with 50 mL of medium at approximately 60-80°C using a volume pipette. Each plate contained 48.0±0.2 g medium, which leads to a layer thickness of 8.0 mm and a surface area of 5.8×10^{-3} m^2/plate.

An amino acid (alanine) was used as N-source instead of NH_4^+, which was used in previous experiments in submerged culture (Meeuwse et al. 2011a, Meeuwse et al. 2011c), despite the fact that it also acts as a carbon source. Because the solid medium used does not have pH-control, the consumption of NH_4^+ can change the pH dramatically with the low concentration of phosphate buffer (~10 mM) present (Nagel et al. 1999). A higher concentration of buffer could not be used because the increased salt concentration will result in a much higher dilution factor needed for dissolution of the gel for analysis. The amino acid alanine was used because the degree of reduction of alanine is equal to that of glucose, which means that a change in respiratory quotient (CO_2:O_2) observed will be caused by changes in metabolism and not by a change of C-source. This makes the results easier to interpret. Furthermore, previous results (not published) showed good growth of *U. isabellina* on this amino acid as single N-source.

Culture

To each κ-carrageenan plate 100 µl spore solution (6×10^6 spores mL^{-1}) of *Umbelopsis isabellina* CBS 194.28, prepared as described in Meeuwse et al. (2011a), was added and equally distributed over the surface with a glass spatula. The plates were placed on racks in four glass jars of approximately 10L. The lids of

the plates were removed to ensure that the local O_2 and CO_2 concentrations at the surface of the culture were equal to the concentrations in the whole jar. Each jar was placed in a temperature-controlled cabinet at 28°C and aerated with humidified air at 200 mL min^{-1}. The jars itself contained a small layer of water to prevent drying out. The air from the jars was led through a condenser at 2°C to remove water and was analyzed using a CO_2-analyser and an O_2-analyser. Every day for 15 days, three plates were taken from one of the jars for analysis, which were processed as separate samples.

Analysis

A plate taken for sampling was weighed and the fungal biofilm was peeled from the κ-carrageenan gel, which could be easily done after a few days of culture. In this way the biomass and the medium could be separated quantitatively. We did not use membranes because of their influence on respiration (Rahardjo et al. 2004 and own results, not published). Both the fungal biomass and the gel were weighted separately. The solid gel was diluted exactly 10-fold (v/v) with demineralized water. This mixture was stirred for approximately 30 min until all solid parts were dissolved. This diluted medium was frozen at 20°C until further analysis. The fungal biomass was dried in a freeze-dryer and weighed again to determine dry weight. Because the biofilm was not washed before drying, glucose and alanine were present in the dry weight. We calculated the amount of glucose and alanine present in the biofilm, using the average concentration measured in the gel layer. This amount was subtracted from the biofilm and added to the gel layer. This correction was carried out for all measured data: biomass, lipid fraction and substrate.

Lipid determination

After freeze drying and weighing, biomass was suspended in demineralized water and homogenized in an ultra-turrax. This suspension was freeze dried again and the obtained powder was used for lipid determination as described in Meeuwse et al. (2011a).

Medium analysis

The glucose concentration in the diluted medium was determined by the glucose GOD-PAP test (Roche, Germany). The alanine concentration in the diluted medium was determined by the primary amino nitrogen (K-PANOPA) test (Megazyme, Ireland). Several samples of the diluted medium were screened for other metabolites by gas chromatograph analysis, which could detect methanol, ethanol, acetic acid, propionic acid, butyric acid, valeric acid and hexanoic acid. Furthermore, tests for ethanol (K-ETOH), glycerol (K-GCROL) and D- and L-lactate (K-DLATE) were carried out (Megazyme, Ireland).

Numerical method

The model was solved in a spreadsheet program (Excel, Microsoft), using a forward Euler method. For equations 20, 25 and 26, this gives:

$$M_X(t+\Delta t) = M_X(t) + \sum_{i=0}^{3} r_{X,i} L_i A \Delta t \qquad (20a)$$

$$L_g(t)\frac{C_{S,1}(t+\Delta t) - C_{S,1}(t)}{\Delta t} + C_{S,1}(t)\frac{L_g(t+\Delta t) - L_g(t)}{\Delta t} = ID_S \frac{C_{S,2}(t) - C_{S,1}(t)}{0.1 L_g(t)} \qquad (25a)$$

$$M_g(t+\Delta t) = M_g(t) + \left(L_f(t) - L_f(t+\Delta t)\right)\rho_X A \qquad (26a)$$

We used time steps of 120 s and the initial values shown in Table 3.

The variable $C_X(t)$, used in Equation 21, which is the concentration of basic biomass in the biofilm, could not be measured. The fraction of solids in the biofilm (f_{solids}), which includes basic biomass, lipids and carbohydrates, was calculated from the difference between wet weight and dry weight of the biofilm. This value was used to estimate the basic biomass concentration from the previous time step in the model:

$$C_X(t+\Delta t) = \frac{M_X(t) f_{solids}(t) \rho_X}{M_X(t) + M_{IP}(t) + M_L(t)} \qquad (28)$$

Model fitting

Fitting of the model to the experimental data was carried out by iteration. Goodness of fit was evaluated by the sum of squares of residuals of experimental data and model values for all carbon containing substrates and products: C_X, C_L, C_{IP}, C_{EP}, C_S, C_N and r_C. Experimental data and model values were divided by

the median of all data points of that variable to give all reactants a similar weighing factor. Values for the following parameters were determined in this procedure: Y_{XS}, Y_{LS}, Y_{IPS}, Y_{EPS}, m_L, m_{EP}, $q_{L\max}$, k_d, q_{IP}, q_{EP}, ID_O and $L_f(0)$. The initial film thickness ($L_f(0)$) is an initial value that in theory could be chosen by the used amount of inoculum; in practice, this is not possible and therefore this value was also determined in this fitting procedure.

The fitting procedure was started by choosing initial guess values for all parameters. After that, the fitting was carried out in four steps. In each step, a group of parameters is changed until a good fit is found for a part of the culture:

1. $L_f(0)$ was changed to find a good fit for r_C during exponential growth, neglecting the germination or lag time.
2. Both ID_O and Y_{XS} were changed until a good fit was obtained for C_S and C_X and the carbon distribution for data during the growth period.
3. We used the period of lipid and carbohydrate production to determine parameter values for Y_{LS}, Y_{IPS}, Y_{EPS}, $q_{L\max}$, k_d, q_{IP} and q_{EP}. The yield factors were fitted using the carbon distribution while the rates were found using C_{IP}, C_{EP} and C_L.
4. The slopes of C_L and C_{EP} during lipid turnover give m_L and m_{EP}. From this, m_S can be calculated.

This sequence of steps has to be carried out several times because changing parameter values in later steps influences the fit for the whole culture period. Therefore, the four steps were repeated until the change in parameters was negligible.

Table 3: Initial values used in the experiment and the model.

Variable	Symbol	Value	Units
Gel mass	$M_g(0)$	4.8×10^{-2}	kg
Thickness of biofilm[a]	$L_f(0)$	1.3×10^{-8}	m
Glucose concentration in gel	$C_S(0)$	44.5; 1485	kg m^{-3}; Cmol m^{-3}
Alanine concentration in gel	$C_N(0)$	4.6; 52	kg m^{-3}; Cmol m^{-3}
Oxygen concentration at biofilm surface	$C_O(L_f)$	0.26	mol m^{-3}
Surface area of gel	A	5.8×10^{-3}	m^2

[a] This value was fitted from the experimental data, as it is not possible to set the initial biofilm thickness.

Results and discussion

Carrageenan plate culture results

Figure 5 shows wet weight, dry weight and lipid content of the biofilm, concentrations of glucose and alanine in the gel layer and the produced CO_2 and consumed O_2 for a culture of *U. isabellina* growing on κ-carrageenan. For the dry weight values in Figure 5a, both the measured value and the value corrected for substrate in the biofilm, as described in the Materials and Methods section, are shown. For all other measured variables, only the corrected values are shown in Figure 5, because the corrections are small. The corrected values were used to

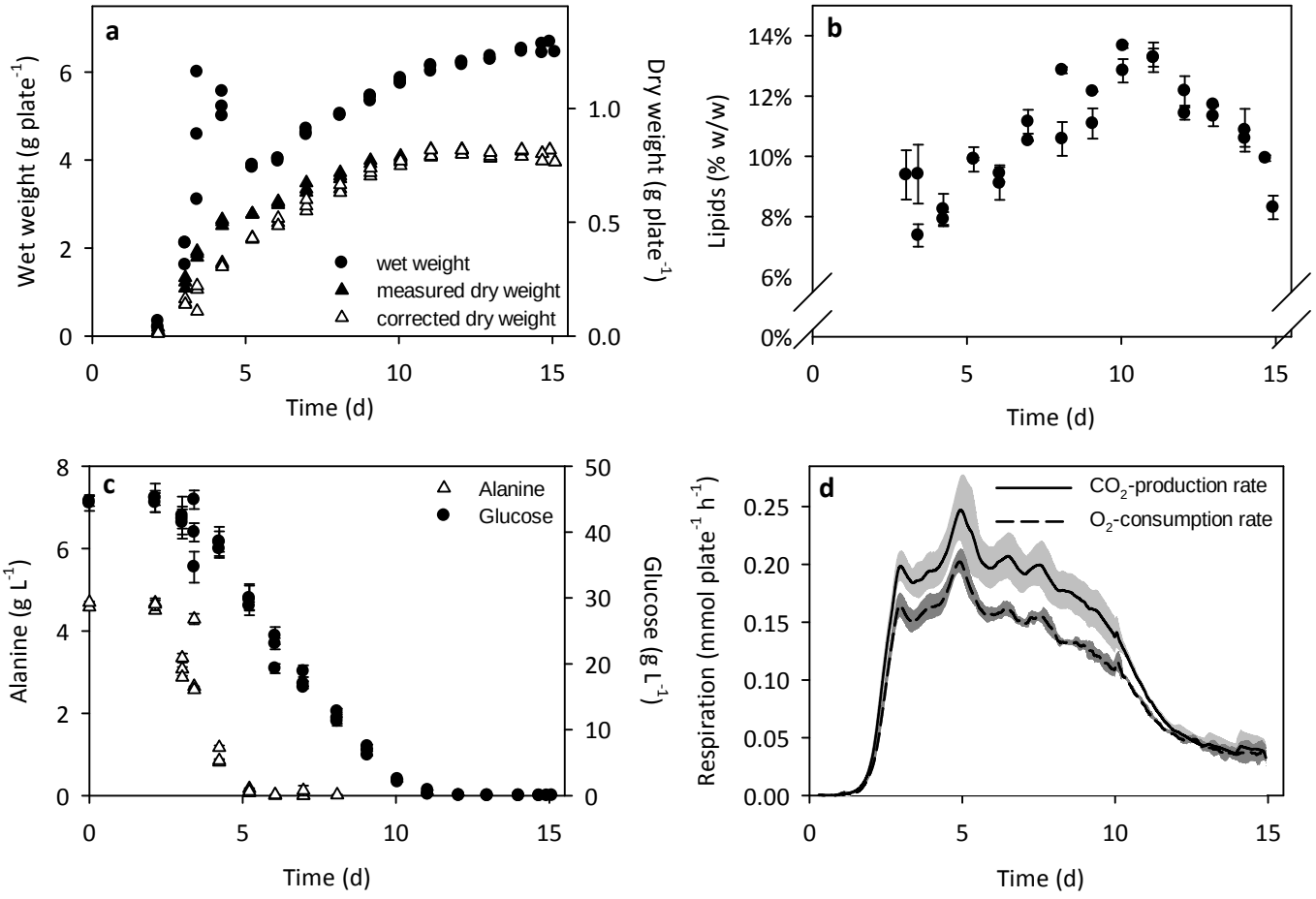

Figure 5: Results of a culture of *U. isabellina* on κ-carrageenan plates containing glucose and alanine. All shown values are corrected for substrate in the biofilm unless stated otherwise. Error bars indicate SD. **a:** Wet weight and dry weight of the biofilm. For dry weight, both the measured value and the value corrected for substrate in the biofilm are shown. **b:** Lipid fraction in the biofilm. **c:** Alanine and glucose concentrations in the gel layer. **d:** CO_2-production rate and O_2-consumption rate calculated from the concentrations of CO_2 and O_2 in the off-gas. The filled area indicates the +/- 1 SD interval from 4 glass jars with plates.

determine the model parameters.

The exponentially increasing respiration rates during the first 3 days in Figure 5d show that the fungus grows exponentially. After 3 days, the almost constant respiration rates and the linear increase in biomass indicate that the growth changes from exponential to linear. After approximately 5 days, the N-source is exhausted. At the same time, we see a decrease in fungal wet weight, while the dry weight still increases; apparently, the amount of water in the biofilm changes here. After the N-source is depleted, there is an increase in lipid fraction from 8% to 13% in the biofilm. When the C-source is exhausted after 11 days, the lipid fraction decreases.

The same increase and decrease of the lipid fraction were observed in submerged batch culture, but the maximum lipid fraction in the cells reached in the petri dish culture is low (13% of total dry weight); in submerged batch culture a maximum lipid fraction of 30% was found with the same strain and C/N-ratio (Meeuwse et al. 2011c). The produced lipids in petri dish culture consisted of 25±1% C16:0, 1.6±0.3% C16:1, 7±1% C18:0, 55±1% C18:1 and 11±1% C18:2. This is similar to the composition of the lipids produced in submerged batch culture after the exhaustion of the N-source (Meeuwse et al. 2011c).

Model assumptions

During the whole culture, hardly any aerial hyphae were observed on top of the biomass layer. Also, hardly any hyphae were found in the gel layer after removal of the fungal biofilm; samples taken from the gel showed that less than 1% of the total biomass was present in the gel. Therefore neglecting penetrative and aerial hyphae in the model is allowed for this strain.

The assumption that water diffuses from the gel layer to the biofilm without evaporation to the air was validated by weighing the gel layer before the experiment and after growth. Figure 6 shows a graph of all products (wet biomass and CO_2 minus O_2) against the amount of gel mass that disappeared during the experiment. This graph shows that indeed most of the disappeared gel mass was found back in the products. The data points above the correlation line were probably caused by water from the humidified air used for aeration, which condensed and fell into the petri dishes that had no lids to improve aeration. Only

at the end of the culture, a small part of the mass is missing; this is probably caused by evaporation of water. This water loss of approximately 2 g is less than 5% of the average initial gel mass of 48 g per plate. This shows that the assumption that all water in the biofilm is extracted from the gel layer, is valid, and that evaporation can be neglected in our system with aeration with humidified air.

By calculating the CO_2-production from the carbon balance, we assume that no other products were formed than mentioned in the model. To check this, we plotted the measured consumed carbon from glucose and alanine versus the

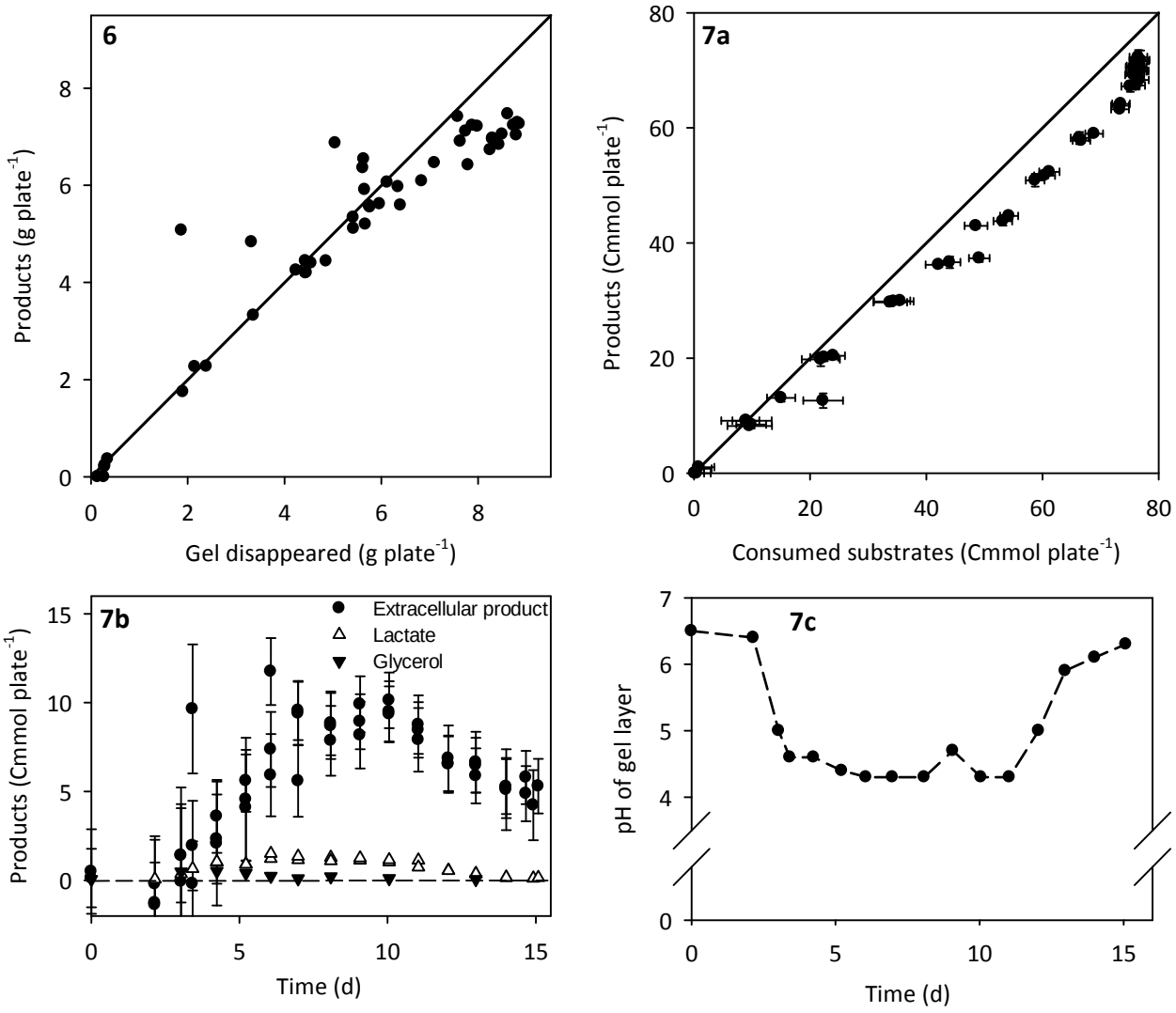

Figure 6: The total mass of products (wet biofilm and CO_2 minus O_2) versus the wet gel mass disappeared during the culture.

Figure 7: Check of carbon balance. **a:** Parity plot of measured carbon containing products (basic biomass, carbohydrates, lipids, CO_2) versus consumed carbon containing substrates (glucose and alanine). **b:** Extracellular product calculated from missing carbon in Figure 7a, and measured L-lactate and glycerol. **c:** pH of the gel layer during the culture.

produced carbon in biomass, lipids, carbohydrates and CO_2 in Figure 7a. This figure shows that up to 15% of the carbon is missing. In submerged fermentation, we observed the same problem (Meeuwse et al. 2011c), but the explanation we had for that (cell aggregates attached to the reactor wall and stirrer) cannot be valid now. Therefore we conclude that one or several other extracellular products were formed that were not yet included in the model. Figure 7b shows the quantity of the extra products in time, calculated from the difference in consumed and produced carbon. Because this product quantity is calculated from a lot of data with errors, the standard deviation is quite high, but the total amount cannot be neglected. Calculations using the degree of reduction of measured reactants showed that the extra product had an average degree of reduction of 6±1, which is for example equal to that of alcohols and some fatty acids (CH_4O). In an attempt to identify this extra product, we analyzed the gel layer for several metabolites. For methanol, ethanol, acetic acid, propionic acid, butyric acid, valeric acid, hexanoic acid and D-lactate, no significant amounts (< 0.1 Cmmol/plate) were detected. Only glycerol and L-lactate were detected in significant amounts (0.3 and 1.5 Cmmol/plate, respectively) in the gel, as is shown in Figure 7b. L-lactate shows the same pattern as the unknown product, but the concentrations were too low to be incorporated in the model (Figure 7b). However, the concentration was high enough to cause the observed pH-drop (Figure 7c) in combination with the phosphate buffer in the medium; the concentration of CO_2 in the air (<0.2%) was too low to cause this drop. The presence of glycerol can be explained by the glycerol present in the inoculum. Therefore, the extra product remains unknown, and we discuss later in the paragraph on fit of the model to the data if incorporation of this unknown product in the model is useful. Total carbon in the medium was not measured because the carbon in the carrageenan would make this very inaccurate.

Physical parameters

The physical parameters are new to this model compared to the model for submerged batch culture (Meeuwse et al. 2011c) and were measured, fitted or taken from literature. The values are shown in Table 4.

Table 4 Parameter values determined independently of the model. Values in submerged batch culture from Meeuwse et al. (2011c).

Parameter	Symbol	Value	Units	Source	Value in submerged batch[a]
Physical parameters					
Density of carrageenan	ρ_c	1030	kg m^{-3}	estimated	NA
Density of biomass	ρ_X	1030	kg m^{-3}	estimated	NA
Diffusion coefficient glucose	ID_S	6.7×10^{-10}	m^2 s^{-1}	Longsworth, 1953	NA
Diffusion coefficient alanine	ID_N	9.3×10^{-10}	m^2 s^{-1}	Umecky et al. 2006	NA
Biological parameters					
Solids in wet fungus	f_{solids}	5.7% → 12.5%	% w/w	measured: Figure 8a	NA
Maximum specific growth rate	μ_{max}	0.15±0.01	h^{-1}	fitted from CO_2 production	0.21 ± 0.01
Minimum lipid fraction of cells	f_{L0}	0.13±0.01	Cmol $Cmol^{-1}$	average value (n=5)	0.078 ± 0.006
Maximum carbohydrate fraction	f_{IPmax}	ND (>0.8)	Cmol $Cmol^{-1}$	not reached	0.87 ± 0.17
Yield of biomass on N-source	Y_{XN}	5.5±0.1 (alanine)	Cmol $Nmol^{-1}$	fitted from Figure 7b	5.5 ± 0.2 (NH_4^+)

[a] NA = not applicable

The densities of the gel layer and of the biofilm are used in the model to couple the measured weight of the layers to the volume or thickness, which is important for calculations on diffusion. Submersion of both layers in water and weighing of the replaced water gave an estimated density of 1030 kg m^{-3} for both layers, independent of the composition.

The model also needs diffusion coefficients for glucose, alanine and oxygen in carrageenan gel and in the fungal biofilm. The concentrations of glucose and alanine are much higher than the oxygen concentration during most of the culture. Therefore, the diffusion coefficients of glucose and alanine are not very important and we used literature values for diffusion in water (see Table 4). For the diffusion coefficient of oxygen in the fungal biomass, a more accurate value is needed. Different values were found in literature, which are also dependent on the biomass density in the biofilm (Beuling et al. 2000, Oostra et al. 2001, Horn and Morgenroth 2006). We used a value found by fitting on the experimental data as was explained in the Materials and Methods section, combined with a relation found by Horn and Morgenroth (2006) to correct for changing biomass concentrations in the biofilm (see Table 5).

Biological parameters independent of the model

Some of the used biological parameters could be determined directly from the experimental data, independent of the used model. These parameters were μ_{max}, f_{solids}, f_{L0} and Y_{XN}. The value for $f_{IP\max}$ can also be determined directly from the experimental data; however, it was not needed in this case because the C-source was exhausted before a maximum value was reached. The other values are shown in Table 4 and explained below.

The maximum specific growth rate μ_{max} was determined from the CO_2-production rate in Figure 5d. Between 20 and 55h, the CO_2-production rate increases exponentially. Fitting an exponential curve through the data gave μ_{max} = 0.15±0.01 h^{-1}. Because only one data point for the biomass concentration is available during that period, we could not use biomass data for μ_{max}. The value found is lower than the value in batch culture, as can be seen in Table 4. A similar specific growth rate in κ-carrageenan dish culture was found in preliminary studies

(not published) with glutamine as N-source. It is not clear if this lower growth rate is caused by the use of an amino acid as N-source instead of NH_4^+, or due to the solid substrate.

To calculate the basic biomass concentration in the biofilm as explained in the Materials and Methods section, we measured the fraction of solids in the biomass, which is shown in Figure 8a. The value changes abruptly after 5 days, which is also the moment that the N-source is exhausted. It could be that the biofilm composition changed because of the change in metabolism resulting from N-source exhaustion, but we do not have a proven explanation for the change in water content of the biofilm; further research should clarify this. The line in Figure 8a shows the value for f_{solids} that we used to calculate the basic biomass concentration (see Equation 28) in the model: 5.7% during the first 5 days and 12.5% during the rest of the time. We chose an arbitrary time of 15 h for the increase from the low to the high value to avoid problems with a step-wise increase in our Euler-based model.

The minimum lipid fraction in the cells during growth (f_{L0}) was determined by

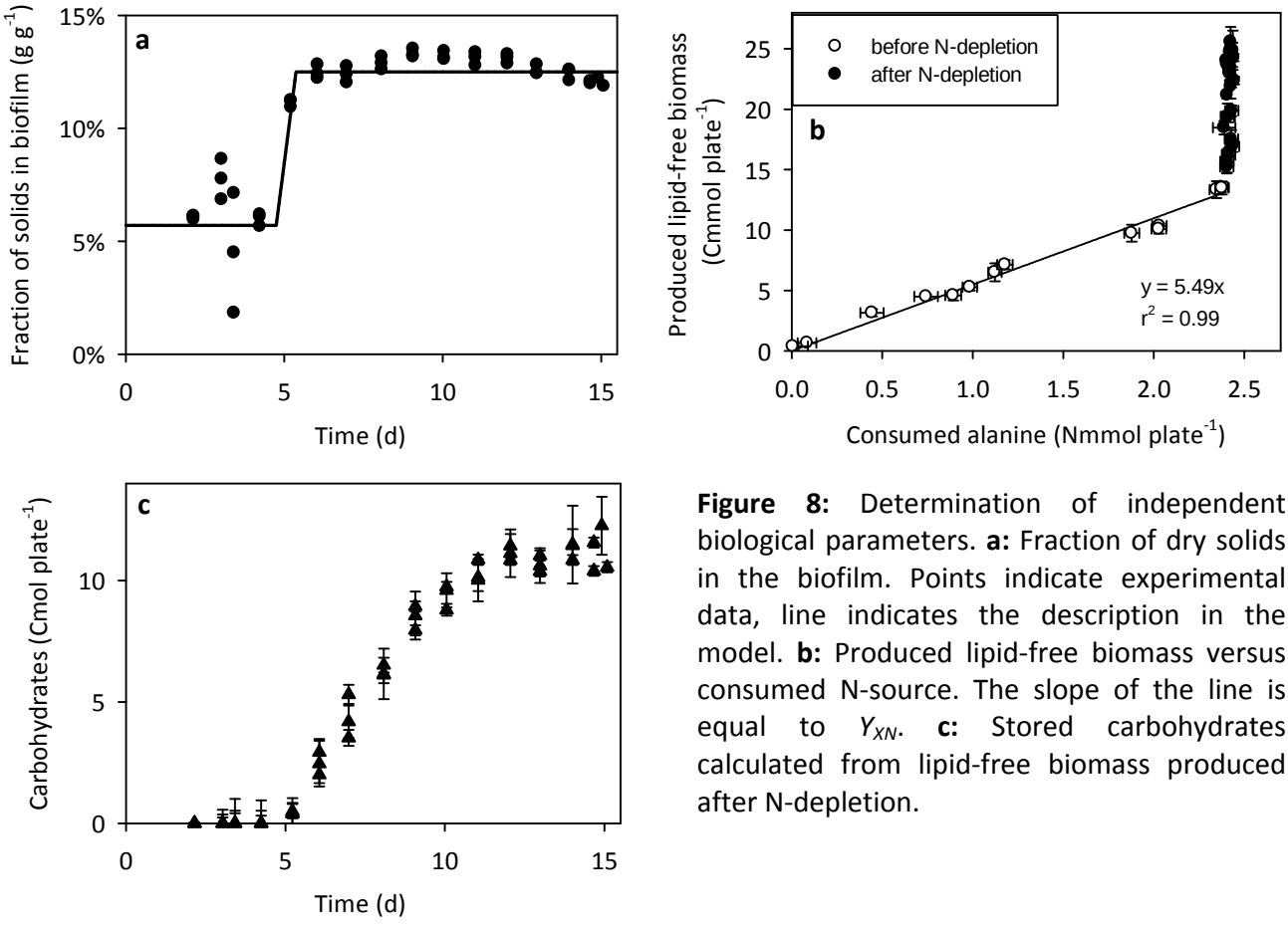

Figure 8: Determination of independent biological parameters. **a:** Fraction of dry solids in the biofilm. Points indicate experimental data, line indicates the description in the model. **b:** Produced lipid-free biomass versus consumed N-source. The slope of the line is equal to Y_{XN}. **c:** Stored carbohydrates calculated from lipid-free biomass produced after N-depletion.

taking the average lipid fraction for all biomass data points where N-source was still available. This led to an average value of 0.13 ± 0.01 Cmol Cmol^{-1}. This is higher than in submerged batch cultures (Table 4); whether this difference is caused by our corrections for substrate in the biofilm, or by differences in culture type or substrate is not clear, but also not very important as the main lipid production occurs after N-limitation.

The yield of biomass on N-source was determined from the slope of produced biomass vs. consumed N-source for the period that N-source was available, as shown in Figure 8b. The value found for Y_{XN} (Table 4) is the same as the value found in batch cultures with NH_4^+: this shows that alanine is an equally good N-source for growth as NH_4^+. We assign the further increase of the lipid-free biomass after N-exhaustion (Figure 8b) to the production of an intracellular product (IP): carbohydrates. The calculated amount of carbohydrates is shown in Figure 8c. This graphs shows that the accumulation of carbohydrates is similar to that in submerged batch culture (Meeuwse et al. 2011c): a linear increase starting at the onset of nitrogen limitation and no turnover after carbon source depletion.

Other parameters

Values for the remaining parameters (Y_{XS}, Y_{LS}, Y_{IPS}, Y_{EPS}, m_L, m_{EP}, $q_{L\max}$, k_d, q_{IP}, q_{EP}, ID_O, $L_f(0)$) could not be determined separately because they influence each other; determination of these values was done by fitting the complete model on the data. The model was fitted by stepwise iteration as is described in the Materials and Methods section.

Because no extracellular product was present in submerged batch culture (Meeuwse et al. 2011c), we initially neglected production of extracellular product in our model (r_{EP} = 0). The fit on the experimental data and the distribution of carbon over the different carbon-containing products in this case is shown in Figure 9; the found parameter values are shown in Table 5, Fit 1. The fit of the model including extracellular product is shown in Figure 10 and the parameter values in Table 5, Fit 2. Because of the high correlation between the different yield factors and production rates, we used theoretical values for Y_{LS} in Fit 1 and for both Y_{LS} and Y_{IPS} in Fit 2. For q_{IP}, we used the value calculated with Equation 9 in Fit 2, but a fitted value in Fit 1 because Equation 9 did not give a good result.

Table 5 Parameter values obtained by stepwise iteration of the model as described in the Materials and Methods section. Fit 1 indicates parameter values for the model without extracellular product formation (r_{EP} = 0), while Fit 2 indicates parameter values with extracellular product formation. Values in submerged batch culture from Meeuwse et al. (2011c).

parameter	symbol	Fit 1	Fit 2	units	value in submerged batch
Thickness of biofilm	$L_f(0)$	1.3×10^{-8}		m	NA
Diffusion coefficient O_2	ID_O	$1.6\times10^{-9} \times (1.112-1.9\times f_{solids})$		$m^2\ s^{-1}$	NA
Yield of biomass on glucose	Y_{XS}	1.0	1.8	Cmol Cmol^{-1}	0.78 ± 0.01
Yield of biomass on C-source	Y_{XC}	0.66 [b]	0.92 [b]	Cmol Cmol^{-1}	0.78 ± 0.01
Yield of lipids on C-source	Y_{LS}	0.59 [a]	0.59 [a]	Cmol Cmol^{-1}	0.56 ± 0.01
Yield of carbohydrates on C-source	Y_{IPS}	0.3	1 [a]	Cmol Cmol^{-1}	1
Yield of extracellular product on C-source	Y_{EPS}	-	0.31	Cmol Cmol^{-1}	-
Time constant decrease lipid production rate	k_d	ND	ND	Cmol Cmol^{-1} h^{-1}	0.016 ± 0.001
Maintenance on glucose	m_S	0.007 [c]	0.028 [c]	Cmol Cmol^{-1} h^{-1}	0.028 ± 0.006
Maintenance on lipids	m_L	0.005	0.007	Cmol Cmol^{-1} h^{-1}	0.020 ± 0.004
Maintenance on extracellular product	m_{EP}	-	0.020	Cmol Cmol^{-1} h^{-1}	-
Maximum lipid production rate	q_{Lmax}	0.023	0.02	Cmol Cmol^{-1} h^{-1}	$0.090\times e^{-0.016\times t}$
Carbohydrate production rate	q_{IP}	0.08	0.054 [d]	Cmol Cmol^{-1} h^{-1}	0.14 ± 0.01
Extracellular product production rate	q_{EP}	-	0.035	Cmol Cmol^{-1} h^{-1}	-

[a] theoretical value
[b] value calculated with Equation 29
[c] value calculated with Equation 10
[d] value calculated with Equation 9

For k_d, no value was found in both fits; either there was no decrease in lipid production rate, or the C-source was exhausted before it became clearly visible. Because of the iterative fitting method used, the parameter values are correlated and no standard deviations were calculated.

Fit of the model to the data

The models with and without extracellular product both show a good fit for all variables and follow the major trends (growth, lipid production, lipid turnover) well (figure 9 and 10). Using the model without extracellular product (Fit 1, Figure 9), the predictions for the total biomass, the carbohydrates and the CO_2 and O_2 are too high; this is caused by missing carbon (Figure 7b). The model with extracellular product (Fit 2, Figure 10) shows a significantly better fit than Figure 9 for dry weight, wet weight, carbohydrates, and especially CO_2, O_2 and CO_2:O_2, even when we take into account that Fit 2 uses one parameter more than Fit 1 (F-test, $p<0.01$). Also the fit for the extracellular product is good, which is an indication that the missing carbon was indeed present as an extra product as we modeled. We also tried to model the extracellular product as an anaerobic product that is produced in layer L_0 (see Figure 2), but this gave a worse fit than Fit 2 and we therefore do not discuss it further.

The models with and without extracellular product predict a maximum thickness of the total biofilm of 1.1 mm, as is shown in Figure 11 for Fit 2. Experimental estimation of the thickness of the biofilm showed an average final thickness of 1.3 mm, which shows that the thickness predicted by the model is quite accurate.

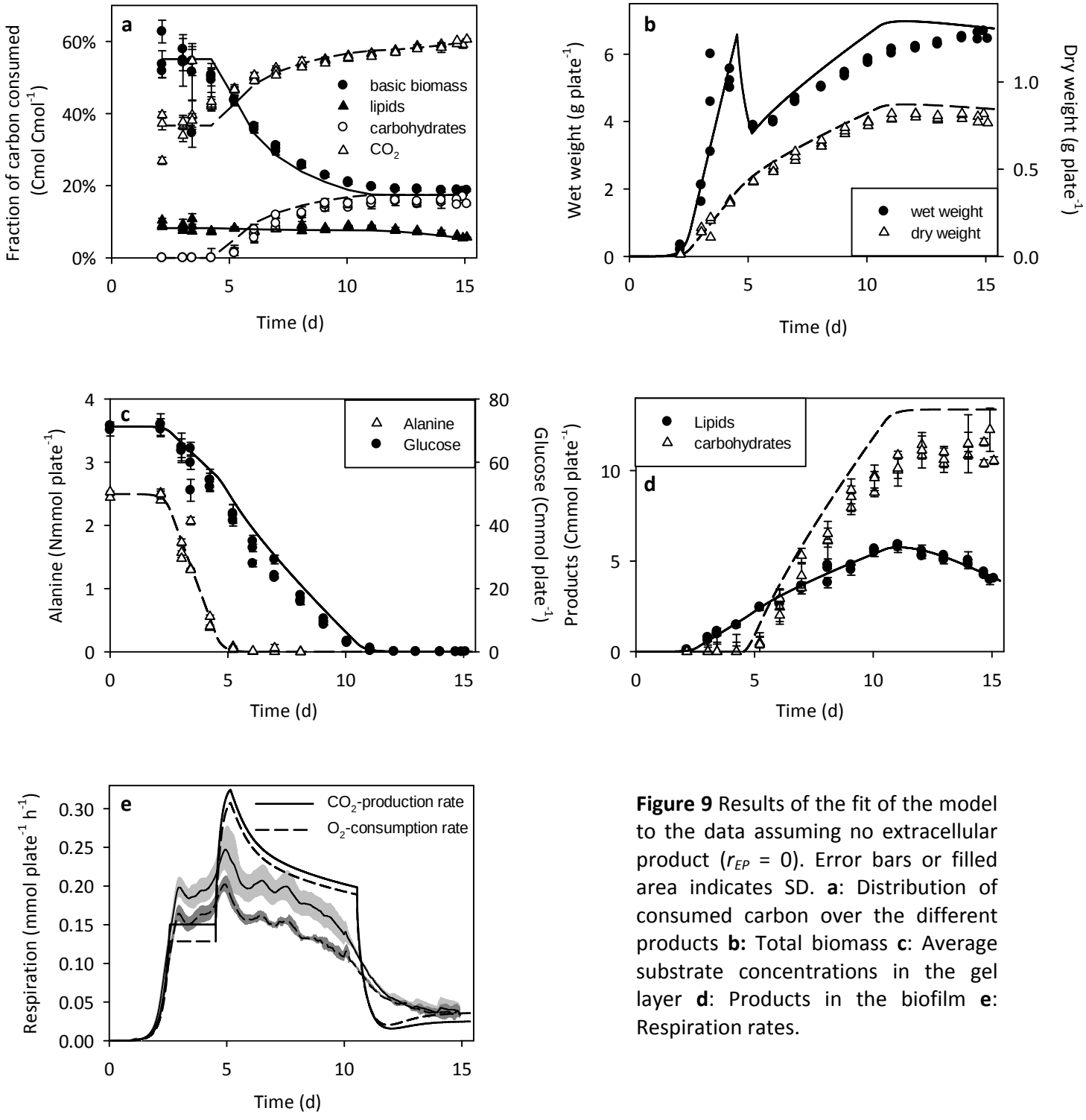

Figure 9 Results of the fit of the model to the data assuming no extracellular product (r_{EP} = 0). Error bars or filled area indicates SD. **a**: Distribution of consumed carbon over the different products **b:** Total biomass **c**: Average substrate concentrations in the gel layer **d**: Products in the biofilm **e**: Respiration rates.

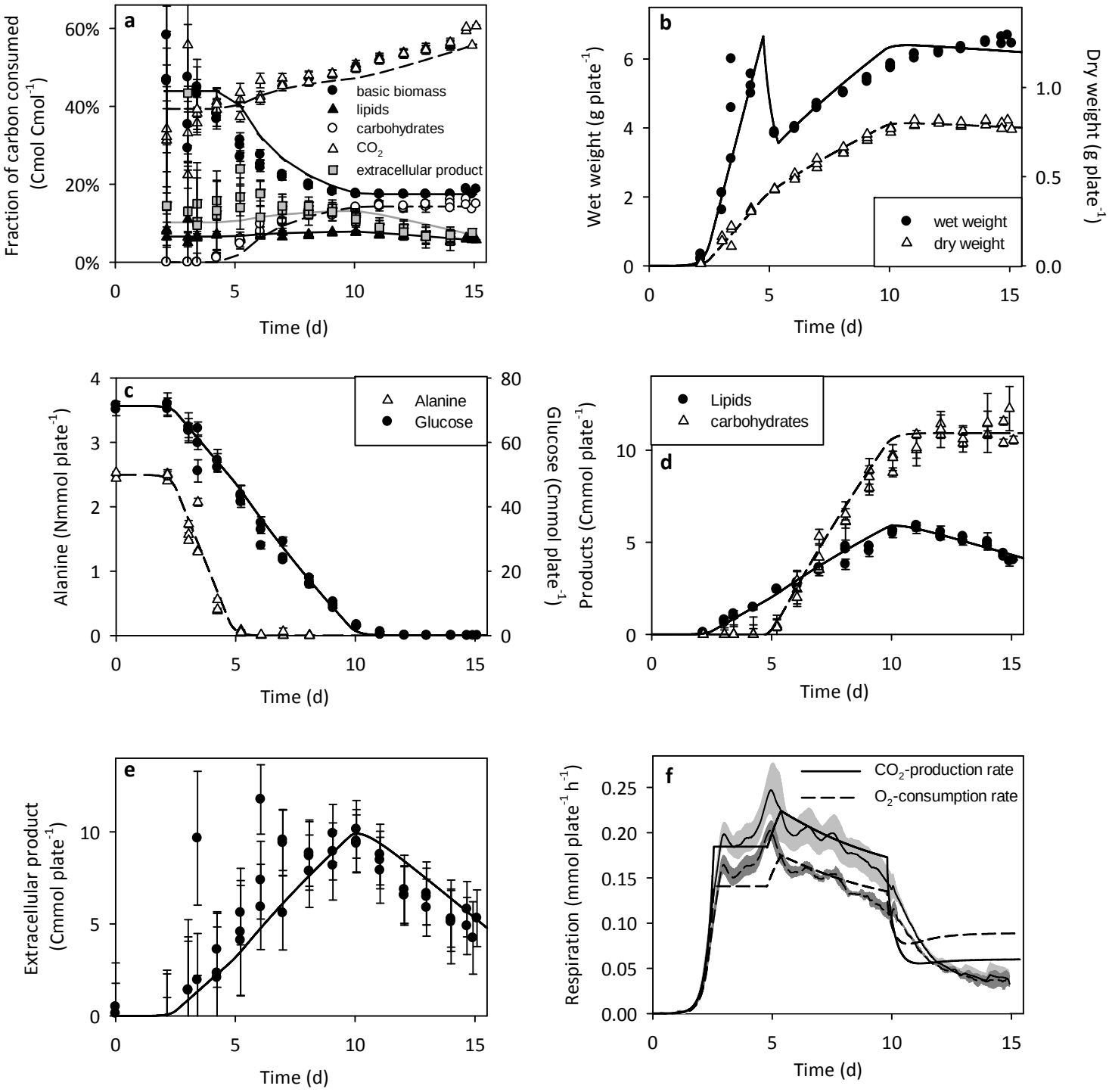

Figure 10: Results of the fit of the model to the data including extracellular product. Error bars or filled area indicates SD. **a**: Distribution of consumed carbon over the different products **b:** Total biomass **c**: Average substrate concentrations in the gel layer **d**: Products in the biofilm **e:** Extracellular product from Figure 7a **f**: Respiration rates.

Comparison with models from literature

As was mentioned in the introduction, our model is the only model that describes lipid formation in SSF besides growth. Nevertheless, other models for growth in SSF have some common features, and we compare our model with the three models mentioned in the introduction.

Oostra et al. (2001) measured and modeled penetration of oxygen in a growing biofilm, and found a penetration depth of oxygen of 60 μm into the biofilm. Figure 11 shows the development of the layers of our model in time, and shows a penetration depth of oxygen between 100 and 200 μm, depending on the metabolism. The difference can be explained by the fact that Oostra et al. (2001) used a higher biomass concentration in the biofilm (20% instead of 5.7-12.5%) and another growth rate. Oostra et al. (2001) used the same equation (Equation 19a in Table 2) to model their measured oxygen profiles successfully. The model of Rajagopalan and Modak (1995) also predicts that oxygen penetrates only partly into the biofilm, depending on the metabolism and oxygen concentration at the surface. This model only uses dimensionless depths and we can therefore not verify our modeled depths.

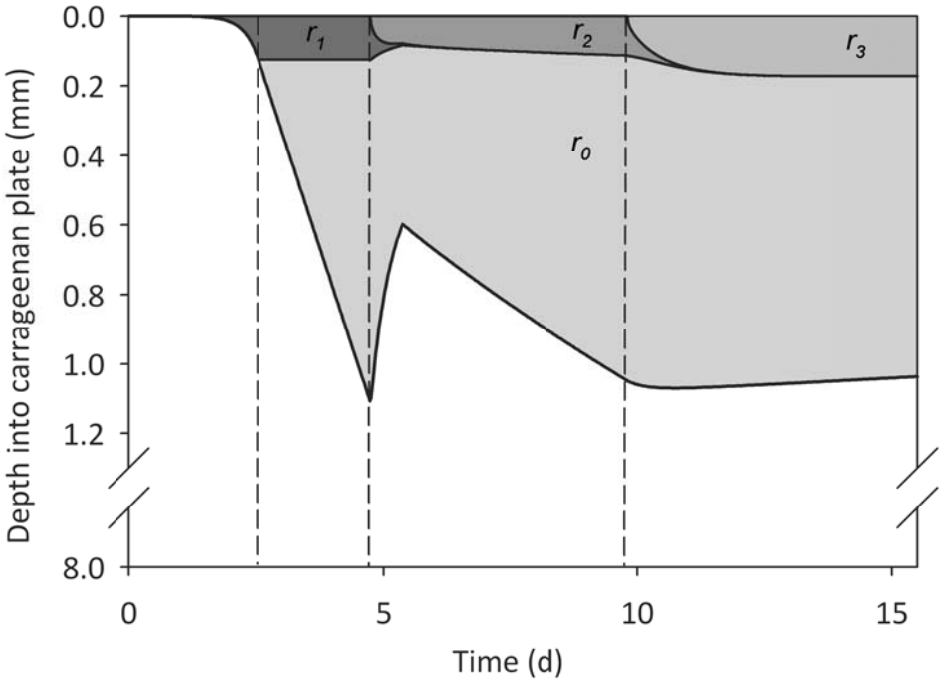

Figure 11: Model prediction of the development of the biofilm (all grey areas) in time using Fit 2. Layers as indicated in Figure 2. The 'peak' just before 5 days is caused by the sudden change in dry solids in the biofilm as was shown in Figure 8a.

Mitchell et al. (1991) did not include oxygen in their model for growth in SSF on starch. However, they found that the glucose uptake rate per unit surface area becomes constant when a certain critical biomass density per unit surface area was reached in carrageenan plate cultures. This can be explained by the constant thickness of the aerobic layer predicted by our model (L_1); the absence of oxygen in the rest of the biofilm makes the cells there inactive. The constant glucose uptake rate was reached by Mitchell et al. (1991) at a biomass density of 4.75 mg biomass cm^{-2}, while in our model the oxygen limitation starts at a biomass density of 7.4 mg biomass cm^{-2}. This difference can be caused by differences in diffusion coefficient or biomass packing density in the biofilm, considering that the glucose uptake rate in both cases is similar (0.255 mg glucose (mg biomass)$^{-1}$ h^{-1} for *R. oligosporus* in Mitchell et al. (1991) vs. 0.27 mg glucose (mg biomass)$^{-1}$ h^{-1} for *U. isabellina* in our cultures). This is proof that the prominent role of oxygen in our model is justified.

Comparison of solid-state fermentation and submerged fermentation

The model describes accurately what was also seen in the experiments: a short period of exponential growth, linear growth until the N-source is depleted, accumulation of lipids and carbohydrates and finally lipid degradation when the C-source is depleted. This is very similar to growth and lipid production in submerged batch fermentation (Meeuwse et al. 2011c). A major difference is the absence of linear growth in submerged fermentation because oxygen was not limiting there. Furthermore, the time scales of both processes are different: in the SSF culture it takes 10 days before the C-source is exhausted while in an SmF culture with the same C/N-ratio this takes two days. This is mainly caused by oxygen limitation in SSF, which caused up to 90% of the biofilm to be inactive in our κ-carrageenan system (Figure 11). The substrate in this system had a small area to volume ratio (125 m^2/m^3) because of the thick gel layer, which is unfavorable for oxygen transfer. In other SSF systems, such as an aerated packed bed, the area to volume ratio is much larger, which improves oxygen transfer to a great extent. Our model predicts that in a system with a five times higher surface area to volume ratio than our carrageenan plates, the culture will take only 4 days instead of 10 days. However, this only increases the reached lipid fraction with 0.1%, which shows

that oxygen limitation is not the main cause of the low lipid yield in our model system.

The yield of basic biomass on glucose in SSF is higher than in SmF (Table 5), but this is mainly caused by the fact that alanine is also used as C-source in SSF, which is not included in Y_{XS}. In the amino acid catabolism, alanine is converted to pyruvate by transamination without energy loss. Therefore, we assume the same energy content of the carbon in alanine as in glucose, neglecting the small difference caused by the glycolysis. With the concentrations of alanine calculated in Nmoles, the yield of biomass on all substrate carbon is then equal to:

$$Y_{XC} = \frac{1}{\frac{1}{Y_{XS}} + \frac{3}{Y_{XN}}} \qquad (29)$$

This value is also shown in Table 5. The values for the fits with and without inclusion of the extracellular product are quite different. Therefore, more information on the extracellular product is needed before conclusions can be drawn on these values.

We found quite different specific lipid production rates in SSF and SmF, as is shown in Table 5. The value found in SSF is considerably lower than the initial value in submerged batch fermentation and similar to the value found in submerged chemostat culture (Meeuwse et al. 2011a): 0.023 Cmol Cmol^{-1} h^{-1} without influence of (residence) time (k_d = 0). More research will be needed to clarify this difference. The low maximum lipid fraction reached in SSF (13% w/w of total biomass) compared to the value found previously (30% w/w of total biomass) in submerged batch culture with the same C/N-ratio (Meeuwse et al. 2011c) is caused by the lower specific lipid production rate. In SSF, the fungus channeled 15% of the glucose remaining after growth stopped to lipids, 23% to carbohydrates, 49% to the unknown extracellular product and 13% to maintenance. In SmF these percentages are 65%, 21%, 0% and 14%, respectively. Clearly, the production of the extracellular product in SSF is very important.

In literature, reported lipid yields in SSF are quite low (Stredansky et al. 2000, Gema et al. 2002, Peng and Chen 2008, Economou et al. 2010). The low specific lipid production rate on a solid substrate compared to submerged culture that we found can explain this. However, a major difference between our model system and the studies in literature is the presence of polymers. With the concentrations of alanine and glucose used in our experiment, the model shows that diffusion of

glucose and alanine can be neglected compared to diffusion of oxygen. In SSF on a polymer matrix, where monomers can be present in low concentrations because they have to be released from polymers by enzymes (Nagel et al. 2002), this could well be different. Addition of extra hydrolyzing enzymes has been shown to improve lipid yield in SSF (Peng and Chen 2008, Meeuwse, Chapter 2), which indicates that the availability of monomers can indeed be limiting. The model we presented can be extended to include polymer hydrolysis.

Conclusions

We developed a diffusion/reaction model that describes growth, lipid production and lipid turnover very well for a culture of *U. isabellina* on κ-carrageenan plates containing glucose and alanine. Including an extracellular product in the model improves the fit on our experimental data, but this product could not be identified. Furthermore, the model shows that oxygen limitation in SSF significantly increases the fermentation time compared to submerged cultures. However, the low lipid yields reached in SSF are not caused by oxygen limitation, but by the lower specific lipid production rate compared to SmF and the production of extracellular product. The developed model explains the differences found between SmF and SSF very well.

Appendix: calculation of diffusion boundaries

In the main text, the calculation of L_S in the situation shown in Figure 3 was shown; this appendix shows the calculations of the penetration depths for the N-source (N), C-source (S) and oxygen (O) for all situations in Figure 4. The resulting equations are summarized in Table 2. The variable x in all equations is set at an arbitrary position within the considered layer, as is shown in Figure 3 for layers L_1 and L_2.

Penetration depth of nitrogen source (L_N)

Because the nitrogen source is only consumed in layer L_1, one balance can be set up for all situations in Figure 4:

$$N_N(x) - N_N(L_N) + r_{N.1}(L_N - x) = 0 \text{ with } N_N(L_N) = 0 \quad \text{(A1)}$$

In situation a, we integrate between 0 and L_N:

$$\int_{C_N(0)}^{C_N(L_N)=0} ID_N dC_N = \int_0^{L_N} r_{N.1}(L_N - x)dx \quad \rightarrow \quad C_N(0) = \frac{-r_{N.1}(L_N)^2}{2ID_N} \quad \text{(A2)}$$

This results in Equation 17a in Table 2.

In situations b and c, we integrate between L_O and L_N:

$$\int_{C_N(L_O)}^{C_N(L_N)=0} ID_N dC_N = \int_{L_O}^{L_N} r_{N.1}(L_N - x)dx \quad \rightarrow \quad C_N(L_O) = \frac{-r_{N.1}(L_N - L_O)^2}{2ID_N} \quad \text{(A3)}$$

This leads to Equation 17b / 17c in Table 2. The concentrations $C_N(0)$ and $C_N(L_O)$ can be calculated from diffusion in the gel layer. In situation d, $C_N(L_O)$ is so low that $L_N = L_O$ and $L_1 \approx 0$.

Penetration depth of carbon source (L_S)

In situation a and b in Figure 4, a similar mass balance can be set up as for the nitrogen source:

$$N_S(x) - N_S(L_S) + r_{S.1}(L_S - x) = 0 \text{ with } N_S(L_S) = 0 \quad \text{(A4)}$$

Integration and solving are completely similar to the nitrogen source shown before; this results in Equations 18a and 18b in Table 2.

In situation c and d, the C-source is consumed in layers L_1 and L_2. This situation is equal to that in Figure 3, for which the calculations was shown in the main text. For situation d the Equation 18c in Table 2 can be simplified with $L_N = L_O$.

Penetration depth of oxygen (L_O)

For oxygen, the situation is different because oxygen diffuses from the air at L_f and not from the gel layer. Therefore, the direction of diffusion is reversed. For situation a and b in Figure 4 this leads to the following balance:

$$N_O(x) - N_O(L_O) + r_{O.1}(x - L_O) = 0 \text{ with } N_O(L_O) = 0 \quad \text{(A5)}$$

Integration gives:

$$\int_{C_O(L_O)=0}^{C_O(L_f)} ID_O dC_O = \int_{L_O}^{L_f} r_{O.1}(x - L_O)dx \quad \rightarrow \quad C_O(L_f) = \frac{-r_{O.1}(L_f - L_O)^2}{2ID_O} \quad \text{(A6)}$$

This results in Equation 19a / 19b in Table 2.

In situation c, the balance over layer L_1 reads:

$$N_O(x) - N_O(L_O) + r_{O.1}(x - L_O) = 0 \quad \text{(A7)}$$

Integration gives:

$$\int_{C_O(L_O)=0}^{C_O(L_N)} ID_O dC_O = \int_{L_O}^{L_N} r_{O.1}(x - L_O)dx \quad \rightarrow \quad C_O(L_N) = \frac{-r_{O.1}(L_N - L_O)^2}{2ID_O} \quad \text{(A8)}$$

For $C_O(L_N)$ we need a balance over L_2:

$$N_O(x) - N_O(L_N) + r_{O.2}(x - L_N) = 0 \text{ with } N_O(L_N) = -r_{O.1}(L_N - L_O) \quad \text{(A9)}$$

Integration gives:

$$\int_{C_O(L_N)}^{C_S(L_f)} ID_O dC_O = \int_{L_N}^{L_f} r_{O.1}(L_N - L_O) + r_{O.2}(x - L_N)dx \quad \rightarrow$$

$$C_O(L_f) = C_O(L_N) - \frac{(L_f - L_N)\left(2r_{O.1}(L_N - L_O) + r_{O.2}(L_f - L_N)\right)}{2ID_O} \quad \text{(A10)}$$

Combining equations A8 and A10, we get Equation 19c in Table 2.

In situation d, L_1 is neglected. Balances over L_2 and L_3, in a similar way as above, lead to Equation 19d in Table 2.

Chapter 7
General discussion

Lipids from yeasts and fungi:
Tomorrow's source of biodiesel?

Meeuwse P, Sanders J, Tramper J, and Rinzema A. 2011. Lipids from yeasts and fungi: tomorrow's source of biodiesel?

Abstract

In the search for new transport fuels from renewable resources, biodiesel from microbial lipids comes into view. We have evaluated the lipid yield and energy use of a process for production of biodiesel from agricultural waste using lipid-accumulating yeast and fungi. We include different bioreactors for submerged and solid-state fermentation in our evaluation. Using existing kinetic models, we predict lipid yields on substrate between 5% and 19% (w/w), depending on the culture system. According to the same models, improvement of the yield to 25-30% (w/w) is possible, for example by genetic modification of the microorganisms. The net energy ratio of the non-optimized systems varies between 0.8 and 2.5 MJ produced per MJ used; energy use for pretreatment and for oxygen transfer are most important. For the optimized systems, the net energy ratio increases to 2.9–5.5 MJ produced per MJ used, which can compete very well with other biofuels such as bioethanol or algal biodiesel. This shows that, although quite some work still has to be done, microbial lipids have the potential to be tomorrow's source of biodiesel.

Introduction

Lipid accumulation in yeasts and fungi has been studied for a long time because the lipids are rich in valuable unsaturated fatty acids such as arachidonic acid and γ-linolenic acid (Certik and Shimizu 1999). Only recently, accumulated lipids are considered as a source of feedstock for biodiesel (Li et al. 2008, Feofilova et al. 2009, Meng et al. 2009). Especially the use of waste products from agriculture and agro-industry as substrate for lipid accumulating yeasts and fungi is studied extensively (Angerbauer et al. 2008, Peng and Chen 2008, Papanikolaou and Aggelis 2009). Unlike poly-unsaturated fatty acids, which are a specialty product with a high value, lipids for biodiesel production are a bulk product with a relatively low value and therefore have to be produced at low cost. Furthermore, energy input during production should be minimized to make the process effective from an energy point of view. Literature shows that the production costs can be reduced by using cheap substrates (Angerbauer et al. 2008, Peng and Chen 2008, Papanikolaou and Aggelis 2009) and a cheaper process such as solid-state fermentation (SSF) instead of submerged fermentation (SmF) (Jang et al. 2000, Stredansky et al. 2000, Gema et al. 2002, Peng and Chen 2008, Fakas et al. 2009a). Energy input during production, however, has not been considered before.

In this paper, we estimate the energy input needed for large-scale production of lipids for biodiesel from organic waste material using lipid accumulating yeast and fungi. Lipid yields in several cultivation systems are calculated with recently developed kinetic models for the filamentous fungus *Umbelopsis isabellina* (Meeuwse et al. 2011a, Meeuwse et al. 2011c, Meeuwse et al. 2011d); two of these models can also describe data from yeasts, which shows their general applicability (Meeuwse et al. 2011b, Meeuwse et al. 2011c). Using basic engineering principles, we estimate the energy use during cultivation and part of the substrate pretreatment and down-stream processing steps.

The evaluated processes

Figure 1 gives an overview of (part of) the process for biodiesel production from a solid organic waste material. Included are a pretreatment (substrate pretreatment and sterilization), several bioreactors, a separation step and down-stream processing to obtain biodiesel. We evaluated submerged fermentation and solid-state fermentation, each with their own advantages and disadvantages.

Substrate

As a model substrate, we used sugar beet pulp, a cellulosic waste material from the European sugar industry. This material contains only a small amount of lignin, which makes it easily biodegradable (Spagnuolo et al. 1997). Although the composition of the material differs with harvest time and location, we assume that it contains 80% water and that the dry weight consists of 1/3 cellulose, 1/3 hemicellulose (mainly arabinan) and 1/3 pectin (Phyllis database, http://www.ecn.nl/phyllis). To simplify calculations, we assume that it contains only three monomers: glucose (C6), arabinose (C5) and galacturonic acid (C5). The C/N-ratio of sugar beet pulp is approximately 30 Cmol/Nmol. We also investigated

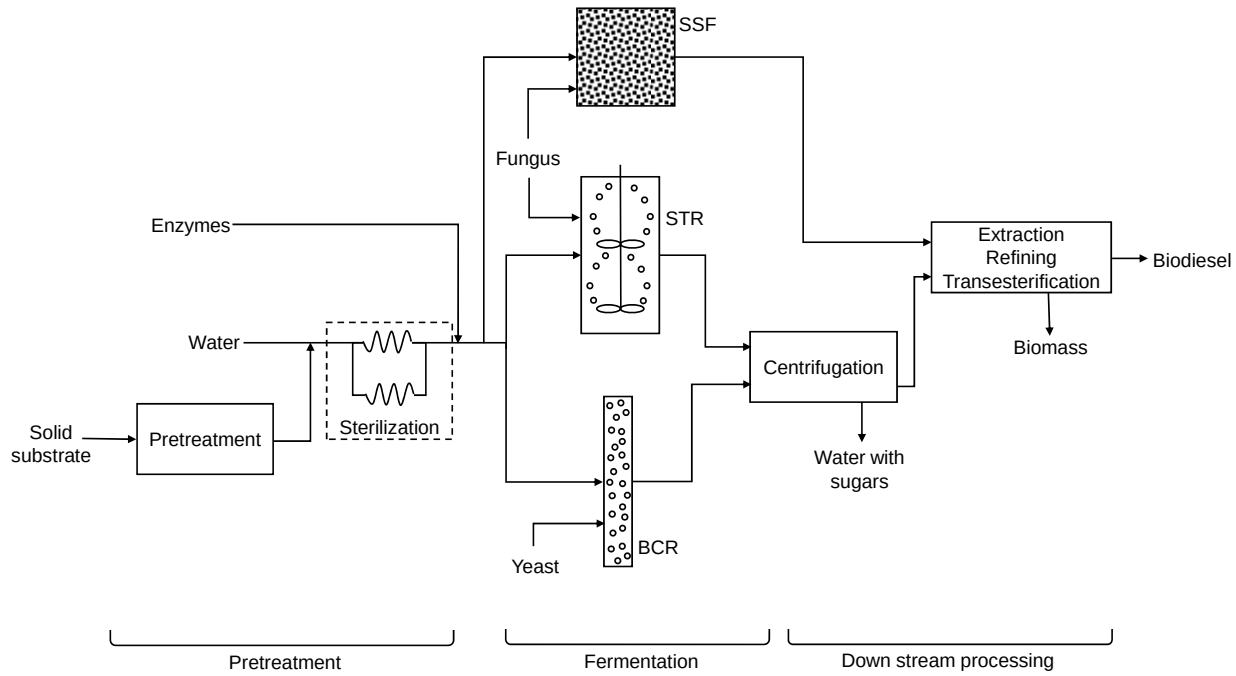

Figure 1: Schematic overview of process that is evaluated for lipid yield and energy use. STR = stirred tank reactor, BCR = bubble column reactor, SSF = solid state fermentation.

other C/N-ratios that can be obtained by either addition of N-source (for example NH_3) or addition of agricultural waste with a higher C/N-ratio. Examples of such additions are (pretreated) corn stover or wheat straw (Phyllis database, http://www.ecn.nl/phyllis), which we assume to have a C/N-ratio of 120 Cmol/Nmol.

In solid-state fermentation, the enzymatic hydrolysis takes place during the fermentation. For submerged culture, simultaneous saccharification and fermentation as well as saccharification prior to the cultivation are possible. We assume that the hydrolysis has a yield of 100%, that no inhibiting compounds are formed during pretreatment, and that the viscosity of the hydrolyzed substrate solution is equal to that of water. The substrate concentration in submerged fermentation was limited to 200 kg dry substrate/m^3 because of the water content of 80% in the main substrate (sugar beet pulp).

Microorganisms

Figure 2 shows a simplified scheme of a lipid-accumulating (oleaginous) organism (Meeuwse et al. 2011c). The organism uses an N-source and a C-source to produce cell mass, while C-source alone can also be used for lipid production, carbohydrate production and maintenance. In SSF, also the production of a yet unidentified extracellular product was found and therefore included in the model (for SSF only). All of these processes also require oxygen. The accumulated lipids are a reserve component that can be consumed when the external C-source is exhausted.

We used a yeast and a filamentous fungus as lipid-accumulating organisms in our evaluation. Two main differences between yeast and fungus were considered: broth viscosity and substrate utilization capacity. The viscosity is important for the energy needed for oxygen transfer in submerged cultures. A filamentous fungus increases the viscosity of a submerged culture already at low dry weight concentrations, while this increase is much smaller for yeast. The viscosity of all cultures was estimated using exponential functions of the cell mass concentrations as is shown in Appendix C.

As far as we know, there is no oleaginous yeast available that can convert all three monomers from sugar beet pulp. The utilization of xylose has been reported for oleaginous yeasts (He et al. 2010) as well as an oleaginous fungus (Fakas et al. 2009b), but for arabinose only a case of non-utilization is known (Glatz et al. 1984).

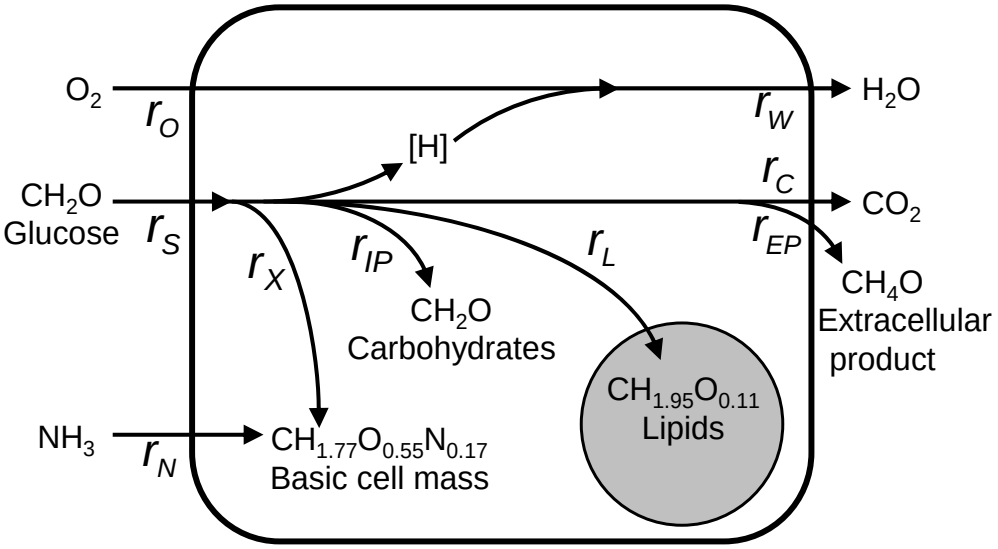

Figure 2: Schematic overview of the modeled processes in the cell (Meeuwse et al. 2011c). Carbohydrate production (r_{IP}) only occurs when no N-source is available, production of extracellular product (r_{EP}) has only been observed in SSF. A list of symbols is shown on page 207.

The utilization of pectin has been reported for fungi (Papanikolaou et al. 2007, Richard and Hilditch 2009), but not for yeasts. Additionally, we have shown before that the oleaginous fungus *Umbelopsis isabellina* can convert sugar beet pulp completely (Meeuwse, Chapter 2). Therefore, we assume that the fungus can convert all monomers from sugar beet pulp and the yeast can consume 50% (as an average between 33% for only glucose and 67% for glucose and either arabinose or galacturonic acid).

We used the same kinetic parameter values for both microorganisms (Table 2), based on experiments with the filamentous fungus *U. isabellina* in submerged batch culture (Meeuwse et al. 2011c). As these parameter values influence the outcome of our evaluation, we carried out a sensitivity analysis.

Culture system design

Submerged and solid-state fermentation were evaluated. We considered submerged batch and chemostat cultures in a stirred tank reactor and a bubble column. Submerged fermentation is widely used as a well-controlled system for cultivation. Solid-state fermentation is the culture of a microorganism, usually a filamentous fungus, on a (wet) solid matrix without free-flowing water.

Table 1: Kinetic models used for calculation of lipid yield and oxygen consumption (Meeuwse et al. 2011a, Meeuwse et al. 2011c, Meeuwse et al. 2011d), depending on the substrates available; oxygen has to be available for all reactions. A list of symbols is shown on page 207.

	C-source and N-source available	C-source available (Batch only)
Basic cell mass (X)	Chemostat: $r_X = C_{Nin} D Y_{XN}$ (1a) Batch: $r_X = \mu_{max} C_X$ (1b)	$r_X = 0$ (1c)
Lipids (L)	Chemostat: $r_L = q_L C_X$ with $\frac{f_{L0}}{1-f_{L0}} D < q_L < q_{L\max}$ (2a) Batch: $r_L = \frac{f_{L0}}{1-f_{L0}} r_X$ (2b)	$r_L = q_{L\max} e^{-k_d (t-t_N)} C_X$ (2c)
Carbohydrates (IP)	$r_{IP} = 0$ (3a)	$r_{IP} = Y_{IPS}\left(\frac{\mu_{max}}{Y_{XS}} + \frac{f_{L0}}{1-f_{L0}}\frac{\mu_{max}}{Y_{LS}} - \frac{q_L}{Y_{LS}} - \frac{q_{EP}}{Y_{EPS}}\right) C_X$ until $\frac{C_{IP}}{C_X} = f_{IP\max}$ (3b)
Extracellular product (EP), SSF only	$r_{EP} = q_{EP} C_X$ (4)	
C-source (S)	$-r_S = \frac{r_X}{Y_{XS}} + \frac{r_L}{Y_{LS}} + \frac{r_{IP}}{Y_{IPS}} + \frac{r_{EP}}{Y_{EPS}} + m_S C_X$ (5)	
N-source (N)	$-r_N = \frac{r_X}{Y_{XN}}$ (6)	
CO_2 (C)	$r_C = -r_X - r_L - r_{IP} - r_{EP} - r_S$ (7)	
O_2 (O)	$-r_O = \frac{1}{\gamma_O}\left(\gamma_X r_X + \gamma_L r_L + \gamma_{IP} r_{IP} + \gamma_{EP} r_{EP} + \gamma_S r_S\right)$ (8)	

It is less commonly used, but has several advantages (Pandey 2003, Holker and Lenz 2005, Bhargav et al. 2008). The process is cheaper, less power is needed for stirring and aeration, no centrifugation step is needed and the amount of wastewater is reduced. We assume that an aerated packed-bed reactor with evaporative cooling and without mixing can be used.

Lipid production in submerged batch and chemostat cultures and in a model system for SSF (surface culture on carrageenan gel) were modeled before in our group (Meeuwse et al. 2011a, Meeuwse et al. 2011c, Meeuwse et al. 2011d). The metabolic processes included in these models are shown in Figure 2; the kinetics are summarized in Table 1. The use of these equations in the different production systems is explained in Appendix A.

Lipid production in submerged chemostat culture

In a chemostat culture, there is constant supply of both C-source and N-source. Growth, lipid production and maintenance occur simultaneously; we found no carbohydrate production in chemostat cultures with *U. isabellina* (Meeuwse et al. 2011a). When the N-source is limiting, the cell mass production rate depends on the N-source concentration in the feed according to Equation 1a. The carbon source in the feed is used, in order of priority, for maintenance, cell mass production, and lipid production. Therefore, the maximum specific lipid production rate is only reached when the C-source supply is sufficient for all three processes. An example of a chemostat culture is shown in Figure A1 in Appendix A. The maximum yield of lipids on C-source is achieved when the maximum specific lipid production rate is reached and the C-source in the feed is completely converted ($r_L = q_{L\max} C_X$ and $r_S = r_{Sin}$ in Equation 5). This is visible in Figure A1 in Appendix A at a dilution rate of 0.016 h^{-1}. At this point, the following combination of dilution rate (D) and C/N-ratio of the feed is applicable (Meeuwse et al. 2011a):

$$D = \frac{\frac{q_{L,\max}}{Y_{LS}} + m_S}{\frac{1}{Y_{XN}}\frac{C_{Sin}}{C_{Nin}} - \frac{1}{Y_{XS}}} \qquad (9)$$

A graph of this equation is shown in Figure A2 in appendix A; this graph shows that the highest lipid fractions in the cells are reached at a low dilution rate combined with a high C/N-ratio. Figure 3 shows the lipid yield at different C/N-ratios in the

Table 2: Biological parameter values used in the models, obtained from submerged batch culture of *U. isabellina* (Meeuwse et al. 2011c).

Name	symbol	value	units
Yield of cell mass on N-source	Y_{XN}	5.5	Cmol Nmol^{-1}
Yield of cell mass on C-source	Y_{XS}	0.78	Cmol Cmol^{-1}
Yield of lipids on C-source	Y_{LS}	0.56	Cmol Cmol^{-1}
Yield of carbohydrates on C-source	Y_{IPS}	1	Cmol Cmol^{-1}
Maximum specific growth rate	$\mu_{\max}$	0.21	h^{-1}
Minimum lipid fraction	f_{L0}	7.8%	Cmol Cmol^{-1}
Maximum carbohydrate fraction	$f_{IP\max}$	87%	Cmol Cmol^{-1}
Maximum specific lipid production rate			
Chemostat	$q_{L\max}$	0.023	Cmol Cmol^{-1} h^{-1}
Submerged batch	$q_{L\max}e^{-k_d t}$	0.090e$^{-0.016t}$	Cmol Cmol^{-1} h^{-1}
SSF batch	$q_{L\max}e^{-k_d t}$	0.023e$^{-0.004t}$	Cmol Cmol^{-1} h^{-1}
Specific extracellular product production rate (SSF only)	q_{EP}	0.035	Cmol Cmol^{-1} h^{-1}
Maintenance on C-source	m_S	0.028	Cmol Cmol^{-1} h^{-1}
Solids fraction in biofilm (SSF)	f_{solids}	12.5%	w/w

feed calculated with this equation and parameter values from Table 2. This graph shows that the lipid yield increases with increasing C/N-ratio. At very high C/N-ratios, the shown curve reaches an asymptote of 20.8% w/w, but this coincides with unrealistically high lipid fractions (>90% w/w) in the cells. We therefore limited the C/N-ratio to 100 Cmol/Nmol in this graph and in our calculations.

Lipid production in submerged batch culture

Batch cultivation occurs in two phases: first, the cells grow at their maximum specific growth rate and with a minimum lipid fraction in the cells, and after depletion of the N-source, they produce lipids and carbohydrates. An example of a batch culture is shown in Figure A3 in Appendix A. The specific lipid production rate in batch culture is initially higher than in chemostat culture (Meeuwse et al. 2011a, Meeuwse et al. 2011c), but decreases exponentially in time (Meeuwse et al. 2011c). This leads to a maximum lipid fraction of approximately 60% w/w with the parameter values from Table 2. After depletion of the N-source, also carbohydrates are stored at a rate that is determined by the maximum specific

C-source uptake rate during growth (Equation 3b), until a maximum content in the cells is reached. Calculations are shown in Appendix A.

Figure 3 shows the lipid yield as a function of the initial C/N-ratio in the batch culture. The graph shows a sudden change in slope at C/N = 20 Cmol/Nmol: lower ratios lead to carbohydrate production during the entire batch culture, higher ratios allow the cells to reach their maximum carbohydrate fraction and produce only lipids during the rest of the culture. Furthermore, the mass yield decreases at C/N-ratios above 65 Cmol/Nmol because the specific lipid production rate decreases in time; this rate eventually becomes so low that maintenance reduces the lipid yield on C-source. With the parameter values from Table 2, the lipid yield in batch culture is always lower than in chemostat culture because no carbohydrates are accumulated in chemostat culture, which makes more C-source available for lipid production.

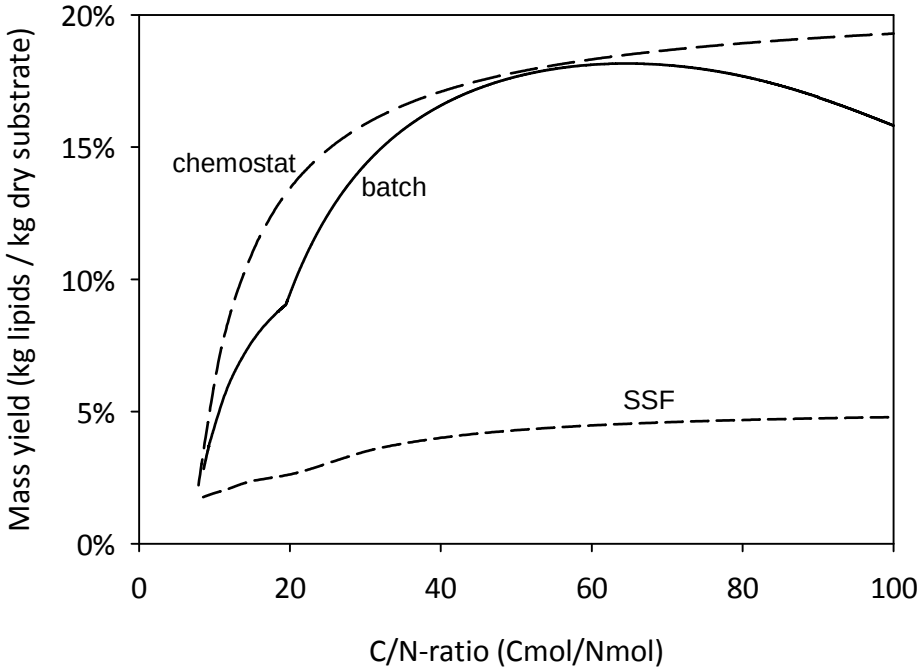

Figure 3: Mass yield of submerged batch culture, submerged chemostat culture and solid-state fermentation (SSF) according to the models from Table 1 with the parameter values from Table 2. Mass yield is on the basis of dry consumed substrate; non-consumable substrate in the case of yeast is not taken into account in this graph.

Lipid production in solid-state fermentation

In SSF, the fungus grows in a biofilm on the surface of solid substrate particles. Oxygen diffuses into the biofilm from the air, C-source and N-source monomers diffuse into the biofilm from the solid substrate. We have shown that zero-order kinetics can be used to describe the bioconversion reactions (Meeuwse et al. 2011d). Consequently, several layers can occur in the biofilm in which one or several of the substrates are depleted (Meeuwse et al. 2011d); an example of this is shown in Figure 4. Similar to the situation in submerged batch culture, the fungus grows when both C-source and N-source is available in combination with oxygen (layer L_1 in Figure 4), and starts to produce carbohydrates and lipids when the N-source is depleted while C-source and oxygen are still available (layer L_2 in Figure 4). An unidentified extracellular product is produced in both situations. Close to the substrate, there can be an anaerobic layer (L_0) where no metabolism occurs. The calculations can be found in Appendix A.

Figure 3 shows that the lipid yield in SSF is substantially lower than in submerged fermentation. This is especially caused by the low specific lipid production rate and the production of the extracellular product (Meeuwse et al. 2011d).

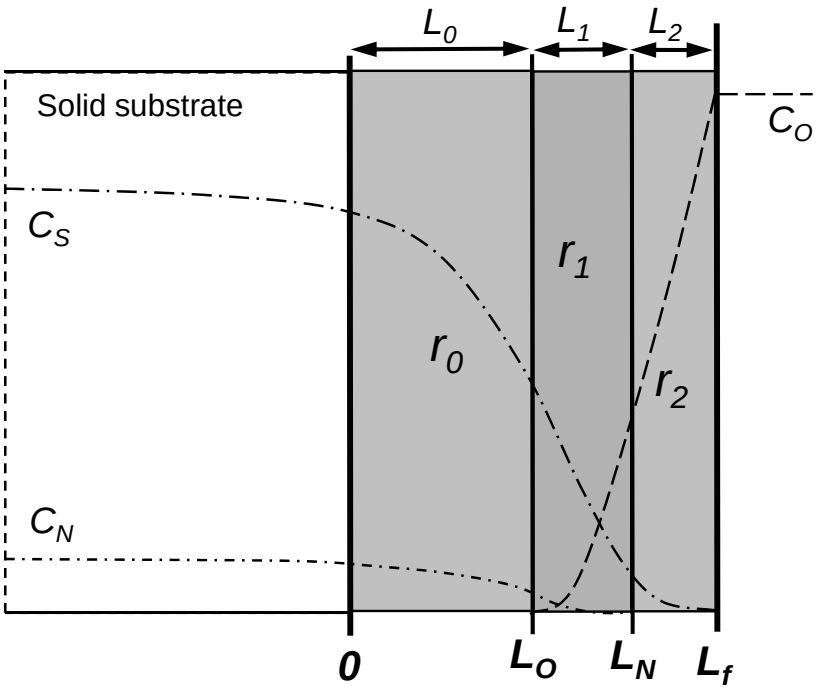

Figure 4: Schematic overview of layers in the biofilm as modeled for SSF culture (Meeuwse et al. 2011d). For the calculation of layers, see Appendix A. A list of symbols is shown on page 207.

Increasing the lipid yield

Based on the energy contents of lipids (43 MJ/kg) and substrate (16 MJ/kg), the maximum theoretical mass yield of lipids on substrate is 37% w/w. The mass yields shown in Figure 3 are considerably lower: less than 20% w/w for submerged cultures and less than 5% w/w for SSF. Experiments from literature (Gema et al. 2002, Papanikolaou et al. 2004a, Peng and Chen 2008, Zhu et al. 2008, Meeuwse et al. 2011c) show similar lipid yields (2-17% w/w, depending on the culture system), which confirms the results of our calculations. Figure 5 shows how the substrate mass is divided among the different products in both submerged systems and SSF. Bar 1 shows the mass yields for the C/N-ratio of sugar beet pulp (30 Cmol/Nmol), Bar 2 for the optimum C/N-ratio in Figure 3 (65 Cmol/Nmol for SmF batch culture, 100 Cmol/Nmol for the other two cultures). These bars show that the increase of the C/N-ratio increases the lipid yield as well as the CO_2 production; the latter because of longer culture times or average residence times and therefore higher substrate use for maintenance. Furthermore, Figure 5 also shows that a large amount of the substrate mass is converted to CO_2, but also to carbohydrates in SmF batch culture and to extracellular product in SSF.

A sensitivity analysis for the parameters in Table 2 showed that Y_{XS}, Y_{LS}, $q_{L\max}$, q_{EP} and m_S have the highest influence on the distribution of the substrate over the products; carbohydrate production is also important, but its rate depends on these parameters according to Equation 3b. Changing these parameters gives an indication which lipid yields could be reached with a microorganism optimized by selection or genetic modification. Higher values for Y_{XS} and Y_{LS} would improve the lipid yield, but both values are already close to their theoretical maximum (Meeuwse et al. 2011c, Ratledge 1988) and therefore we did not change them. We calculated the influence of changes in the other three parameters. The resulting lipid yields are shown in Figure 5 with the following bar numbers:

3. A decrease of 50% in m_S.
4. Complete replacement of carbohydrate production by lipid production. According to Equation 3b, this requires an increase of $q_{L\max}$ to 0.168 Cmol/Cmol/h for SmF (+87% for batch, +630% for chemostat) and to 0.105 Cmol/Cmol/h for SSF (+357%); the extracellular product is still formed in SSF
5. No production of extracellular product in SSF, i.e. q_{EP} = 0.
6. A combination of 3, 4 and 5.

For bars 3-6, the optimum C/N-ratio for lipid yield was used; the values are mentioned in the legend of Figure 5.

Figure 5 shows that the applied changes indeed can increase the lipid yield, up to 67% of the theoretical maximum (shown with the dashed line) for batch SmF and SSF, and up to 83% for chemostat SmF. Especially in SSF, preventing carbohydrate and extracellular product formation has a large influence on the lipid yield. Achieving these changes may not be trivial: genetic modification of suspected rate-limiting conversions has so far not led to increased lipid production in any oleaginous strain using sugars as substrate (Beopoulos et al. 2011). So although there are probably strains available that have better lipid production properties than the strain we used in our calculations, the highest yields shown in Figure 5 are not realistic yet. Nevertheless, they do show the ultimate potential of this process.

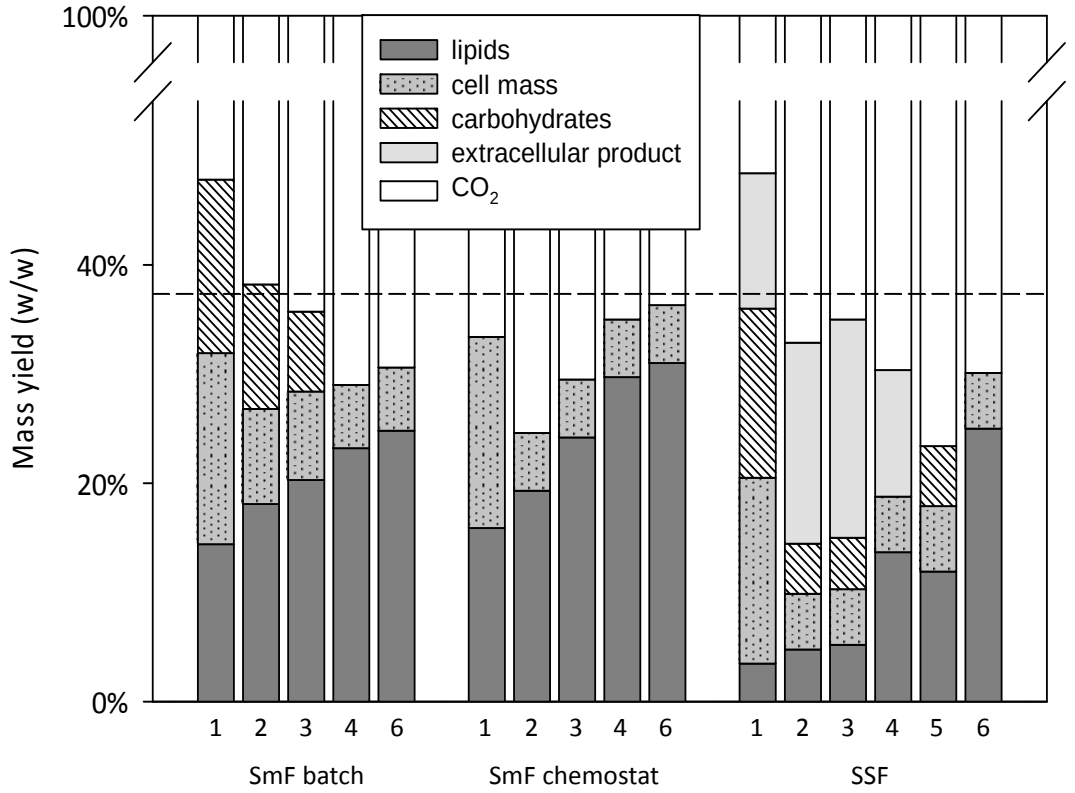

Figure 5: Distribution of used substrate over the different products in the evaluated cultivation systems. The dashed line indicates the maximum lipid yield possible based on energy content. Numbers below the bars refer to changes in parameter values (Table 2). **1**. normal values, C/N-ratio = 30 Cmol/Nmol, **2**. normal values, optimum C/N-ratio, **3**. m_S -50%, **4**. increased q_{Lmax} (+87% - +630%, see main text), **5**. q_{EP} = 0, **6**. 3-5 together. C/N-ratios used for bars 1-6: SmF batch: 30, 65, 65, 90, 90 Cmol/Nmol, SmF chemostat: 30, 100, 100, 100, 100 Cmol/Nmol, SSF: 30, 100, 100, 100, 85, 100 Cmol/Nmol. Mass yields are on the basis of dry consumed substrate; non-consumable substrate in the case of yeast is not taken into account.

Energy use

Table 3 shows the energy consumption for the process steps shown in Figure 1. Calculation of these values is explained below and in Appendices B and C.

Pretreatment and down-stream processing

Because sugar beet pulp is easily biodegradable (Spagnuolo et al. 1997), we assume that a physical or chemical pretreatment is not necessary. However, corn stover or wheat straw, which can be added to change the C/N-ratio, has to be pretreated. For pretreatment of these co-substrates, the average energy input is 10% of their energy content, which is 1.6 MJ/kg (Aden et al. 2002, Cardona and Sánchez 2006, Luo et al. 2009, Piccolo and Bezzo 2009). How much energy is needed for pretreatment therefore depends on the used C/N-ratio, as is shown in Figure C1 in Appendix C.

To avoid losing a large part of the substrate and oxygen to contaminant organisms, sterilization is necessary. We calculated energy requirements for heating of the

Table 3: Energy use for the considered steps of the process as shown in Figure 1. Values that are indicated as a range are explained in the main text and Appendix C.

Process step	Energy use	
Pretreatment steps		
Pretreatment substrate	0 – 1.5 MJ/kg	for C/N ratio's between 30 and 100 Cmol/Nmol
Sterilization	115 – 132 MJ/m^3	for medium containing 0 – 200 kg/m^3 dry substrate
	118 MJ/ton	for wet substrate SSF (containing 85% water)
Cultivation		
Oxygen transfer	0 – 2.5 kW/m^3	for submerged cultivations
	0	for SSF (oxygen provided by air used for cooling)
Cooling	neglected	for submerged cultivations
	0 – 0.2 kW/m^3	for SSF at packing densities below 85% v/v wet weight/m^3
Down-stream processing		
Centrifugation (SmF only)	5 MJ/m^3	literature value
Extraction, refining and trans-esterification	4 MJ/kg biodiesel	literature value

medium or substrate, assuming that 70% of the heat can be recovered and re-used (Soderberg 1997). The calculations are shown in Appendix C. We assume that ingoing air is filter-sterilized; the pressure drop over the filters was neglected in the calculations on aeration power.
For centrifugation, we used the average power consumption of several small scale and large scale centrifuges of different types, as reported by the manufacturers (www.uscentrifuge.com/decanter-centrifuges.htm, www.labocon.com/Centrifuge-7.html). For extraction, refining and trans-esterification, we used a literature value for production of biodiesel from rapeseed (Esteban et al. 2010). Although rapeseed does not have the same (physical) properties as fungal cell mass, we assume that differences in energy needed for extraction can be neglected.

Energy use during cultivation

We used three different bioreactor types in our calculations: a packed bed for SSF, and a stirred tank reactor (STR) and a bubble column reactor (BCR) for SmF, each with a working volume of 100 m^3.
Calculations on power consumption for the stirred tank reactor are shown in Appendices B and C. Energy use for (water) cooling can be neglected compared to stirring and aeration in submerged fermentation, both in a stirred tank reactor as well as in a bubble column reactor (calculations not shown).
In a stirred tank reactor, viscosity only has an influence on oxygen transfer above a threshold of 50×10^{-3} Nms^{-2}. This threshold is not reached in the yeast culture. In the fungal culture, it is reached at a cell mass concentration of 17 kg/m^3; above this value, the oxygen transfer coefficient decreases rapidly.
In a bubble column reactor, oxygen transfer decreases very rapidly when the viscosity of the liquid increases. Figure C2 in Appendix C shows that the power consumption for a bubble column is lower than for a stirred tank reactor for the same oxygen transfer rate, except for very high yeast concentrations and for fungal cultures. These high yeast concentrations are not reached because we limited the maximum substrate concentration in the reactor and the feed to 200 kg/m^3. We therefore chose the bubble column reactor for all yeast cultures and the stirred tank reactor for all submerged fungal cultures.
In solid-state fermentation, the packed bed is aerated to remove heat and to supply oxygen. Literature shows (Gowthaman et al. 1993, Weber et al. 1999b,

Weber et al. 2002) that if the aeration rate is sufficient for heat removal, it is also sufficient for oxygen supply. Therefore, the aeration rate is calculated from the heat production rate, which is directly proportional to the oxygen consumption rate. This is shown in Appendix B. The power consumption for aeration depends on the pressure drop over the packed bed. This pressure drop depends, amongst others, on the volume fraction of solid particles in the packed bed, which we assume to be constant during the culture. At a fraction of wet solid material below 85% v/v, the pressure drop is low (<0.05 bar); we therefore limited the wet substrate concentration to 85% v/v. These calculations are also shown in Appendices B and C.

Energy yields

Figure 6 shows the biodiesel produced and the energy used for all processes, both expressed in MJ per kg substrate. Figure 6a shows results for the normal strain with parameter values shown in Table 2. Figure 6b shows results for the optimized strains that were shown as case 6 in Figure 5. In addition, we assumed that the substrate utilization is also optimized to 100% for the yeast cultures. Biodiesel production depends on the C/N-ratio of the substrate as was shown in Figure 3. The C/N-ratio of the substrate also determines the energy use for pretreatment as shown in Figure C1 in Appendix C. The substrate concentration in the cultures also influences energy use. At low substrate concentrations, energy use for sterilization of the complete medium (including water) in SmF is relatively high; at high substrate concentrations, the viscosity of the fungal cultures increases the energy use for oxygen transfer. Figure 6 shows the results for C/N = 30 Cmol/Nmol and for the optimum C/N-ratio, in all cases at the substrate concentration giving the lowest energy use. The Net Energy Ratio (NER) shown is the produced energy in biodiesel divided by the used energy. In this calculation, energy used in the form of heat and in the form of electricity are added up without taking into account that electricity is often produced from heat with yield of approximately 40%. Therefore, the NER value for systems which need a lot of energy for oxygen transfer (electricity for stirrers and air pumps) can be lower than shown in Figure 6.

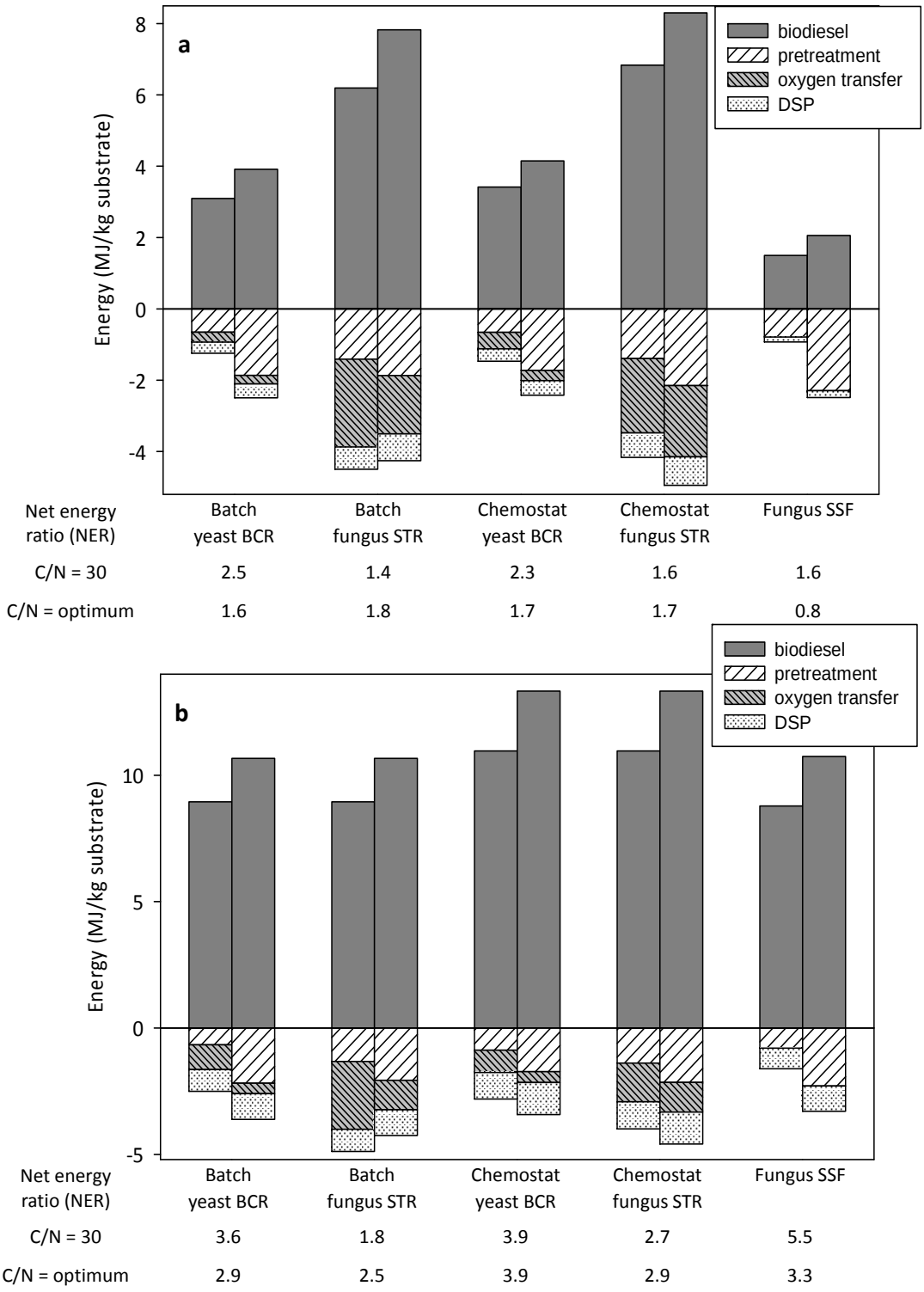

Figure 6: Biodiesel produced and energy used in the process for different production systems. Left bars are for C/N=30 Cmol/Nmol, right bars for the optimum C/N-ratio, which is 65 Cmol/Nmol for submerged batch cultures and 100 Cmol/Nmol for submerged chemostat cultures and SSF. For the SSF culture, energy use for oxygen transfer is so low that it is not visible in the graph. **a:** base case with normal parameter values (Table 2), **b:** optimized case according to case 6 in Figure 5.

The most important result shown in Figure 6 is that in many cases the higher lipid yield at the optimum C/N-ratio cannot compensate for the higher energy use at this higher C/N-ratio. In these cases, the pretreatment of the co-substrate costs more energy than is available from the extra biodiesel produced. Only for the submerged fungal cultures, a higher C/N-ratio is favorable. At a high C/N-ratio, more lipids are produced compared to biomass than at a low C/N-ratio. Therefore, relatively less oxygen transfer is needed at a high C/N-ratio, because growth needs more oxygen than lipid production. This effect is strongest for submerged fungal culture because of the high viscosity, which increases energy use for oxygen transfer. Because of the high energy use for oxygen transfer for submerged fungal culture, the NER value for yeast cultures is higher, although the biodiesel yield is lower because of the 50% substrate utilization as explained before. In SSF with the normal fungal strain, the produced energy is low because of the low lipid yields (see Figure 3). Energy use is also low, but not low enough to give a high NER value. For the optimized strain, however, SSF has the highest NER value of all processes shown. Figure 6 shows that the differences between batch culture and chemostat culture are small.

Comparison to other fuel production systems

Table 4 shows some examples of other systems that produce energy carriers from renewable resources. From our own calculations, we added both submerged batch processes (yeast BCR and fungus STR) and the SSF process. We used the values with the C/N-ratio that gave the highest NER: 30 Cmol/Nmol for SmF yeast and SSF, and the optimum C/N-ratio for SmF fungus. The base case scenario from Figure 6a as well as the optimized case from Figure 6b is shown. We compare these with two other processes that produce biodiesel and three other processes that use biomass to produce other energy carriers. As this article is not a review of all possibilities in this area, we selected a recent and representative reference for each process. We assumed in our calculations that sugar beet pulp is the substrate for all processes and we therefore included an additional 2 MJ/kg dry substrate (Lorenz and Voss 2007) for drying for the Fischer-Tropsch and combustion processes.

Table 4: Overview of systems from literature shown in Figure 7. For the anaerobic digestion, the methane yield from Kryvoruchko et al. 2009 was used with the energy use per kg substrate from Collet et al. 2011

Process	Main product	Reference	Included in calculation	Original substrate	Additional products
Yeast culture	biodiesel	This study (BCR batch)	sterilization, aeration, centrifugation, DSP [a]	sugar beet pulp (50% consumable)	cell mass and biomass to biogas
Fungal culture (SmF)	biodiesel	This study (STR batch)	sterilization, aeration, centrifugation, DSP [a]	sugar beet pulp	cell mass to biogas
Fungal culture (SSF)	biodiesel	This study (SSF)	sterilization, aeration, DSP [a]	sugar beet pulp	cell mass to biogas
Gasification + Fischer-Tropsch	biodiesel	Larson et al. 2009	complete process including drying [b]	switchgrass	gasoline, heat
Algal culture	biodiesel	Jorquera et al. 2010 (flat panel reactor)	aeration, centrifugation[c], DSP [a,c]	sunlight + CO_2	cell mass to biogas
Yeast culture	ethanol	Luo et al. 2009	complete process	corn stover	heat
Anaerobic digestion	biogas	Collet et al. 2011; Kryvoruchko et al. 2009	complete process: energy use; methane yield	algal cell mass; sugar beet pulp	-
Combustion	heat	Luo et al. 2009	complete process including drying [b]	corn stover	-

[a] DSP includes extraction, refining and transesterification

[b] Not included in literature, but added, assuming an energy consumption of 2 MJ/kg dry substrate (Lorenz and Voss 2007)

[c] Not included in literature, but added, as in our own calculations, assuming an energy consumption of 5 MJ/m^3 for centrifugation and 4 MJ/kg biodiesel for DSP (Esteban et al. 2010).

Figure 7 shows the results including energy containing by-products mentioned in Table 4. For our microbial cultures and for the algal culture, the by-products are cell mass and non-consumed substrate in the case of yeast. We assume that these by-products can be converted to biogas with the energy production and use shown

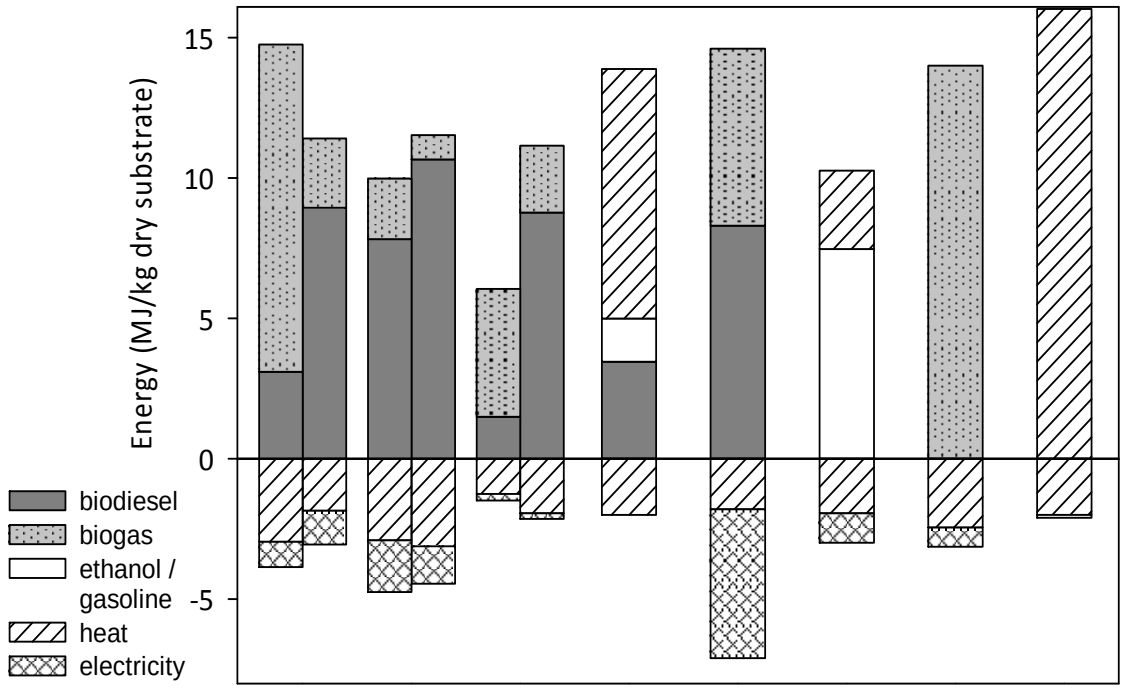

	SmF yeast	SmF fungus	SSF	Fischer-Tropsch	Algal culture [a]	Ethanol	Biogas	Combustion
Net energy ratio biodiesel	2.5 / 3.6	1.8 / 2.5	1.6 / 5.5	ND [b]	1.5	-	-	-
Net energy ratio all products	3.8 / 3.7	2.1 / 2.6	3.1 / 5.2	ND [b]	2.1	2.9	3.4	ND [b]
Net energy main product (MJ/kg substrate)	3.1[c] / 7.6	5.6 / 7.6	1.5[c] / 8.7	3.5[c]	-0.4 [d]	6.6	9.8	14

Figure 7: Comparison of different energy producing systems from Table 4. When two columns are shown: Left columns: system from Figure 6a, right column: same system from Figure 6b; batch cultures with C/N-ratio that gave the highest NER in Figure 6. Net energy ratios are calculated assuming that the energy used and produced are from different sources, the net energy main product is calculated assuming that biomass is both substrate as well as energy source (through combustion).

Footnotes:

a For the algal culture we consider the total produced algal biomass as ingoing substrate for the calculations

b Not determined because energy input and output cannot be distinguished.

c More products were produced besides the main product: 6.5 and 2.7 MJ biogas for SmF yeast and SSF, respectively, and 1.5 MJ gasoline and 6.9 MJ heat for Fischer-Tropsch

d Negative value because not enough cell mass is available to compensate for the energy use

in Figure 7. We divided the used energy in heat (such as sterilization, distillation and drying) and electricity (such as stirring, aeration and centrifugation). For the algal culture, we regarded the total produced algal biomass as substrate and assumed it has the same energy content as sugar beet pulp, although this gives a slightly distorted view because we did not include energy use for the production of sugar beet pulp in the calculations for the other cases.

To compare all different forms of energy in Figure 7, we use two different methods. The first method is the calculation of the net energy ratio (NER), which is shown below the figure, based on the assumption that the energy used (heat and electricity) is derived from other sources than the used process or substrate. For the heat-based processes (Fischer-Tropsch and combustion), the extra heat needed for drying of the substrate can be produced in the process itself, and therefore no NER was calculated. Comparison of the NER values shows that our microbial lipid processes have a higher NER than the algal culture and a similar NER as biogas and ethanol production in the base case scenario; the optimized cases give similar or better NER values than biogas or ethanol.

The second method to compare the processes is also shown below Figure 7. We calculated the net energy production when all energy needed is produced from the substrate (sugar beet pulp) or additional product (cell mass). We assume that both sugar beet pulp and cell mass can be converted to heat as is shown for the combustion case (including drying). Furthermore, we assume that the conversion from heat to electricity has an efficiency of 40%. For the algal culture, we used produced biodiesel as energy source in addition to cell mass, because insufficient cell mass is produced. The results of this calculation (Figure 7) show that the optimized cases produce a lot of net energy, even more than the ethanol process. The base cases produce less net energy, especially the submerged yeast culture and the SSF culture, because of the low lipid yield as discussed before. However, their yield is still higher than that of the algal culture, which produces no net energy.

Conclusions and perspectives

We have designed several systems for lipid production in yeasts and fungi. Lipid yields for these processes ranged from 5% w/w for SSF to 19% w/w for SmF. Optimized strains, which might be obtained by strain selection or genetic modification, can reach lipid yields of 25-30% w/w, according to the models used. To come closer to the maximum theoretical yield of 37% w/w, cell mass production should be reduced further. This would be possible if the cells would secrete the lipids, just as happens with ethanol. The yeast *Pichia pastoris* is able to secrete different polymers after genetic modification (Werten et al. 2001, Schipperus et al. 2009), which shows that there may be possibilities for secretion of large molecules such as lipids.

With sugar beet pulp as substrate (C/N = 30 Cmol/Nmol), lower lipid yields are found than with addition of wheat straw or corn stover to reach a higher C/N-ratio. However, lower C/N-ratios still give similar or higher net energy ratios (NER) because of the high energy requirements for pretreatment of straw. These NER values varied from 0.8 (for SSF because of the low lipid yield) to 2.5. For the optimized strains, the NER could be increased to 3 - 5.5; SSF has the highest NER due to the low energy costs of oxygen transfer in this system. These values can compete very well with NER values for other biofuels such as algal biodiesel and bioethanol.

The NER value might be increased further by energy savings in the process. We used separate steps for pretreatment and sterilization, while it is probably possible to combine these steps and save energy. In addition, the extraction and trans-esterification step might be combined (Vicente et al. 2010). Large energy savings could also be achieved if it would be possible to produce lipids in an anaerobic culture. However, there are no reports of lipid accumulation in yeast and fungi under anaerobic conditions and among the lipid-accumulating bacteria there are no anaerobic species (Alvarez and Steinbuchel 2002). Furthermore, intracellular lipid storage is limited by the low cell yield of anaerobic cultures. Therefore, anaerobic lipid production would only be possible when the lipids are excreted.

A topic that not has been discussed in this paper so far is the economics of this process. Submerged aerobic fermentation is known to be expensive. Rough estimates show that the costs for submerged cultivation only will be in the range of 200-1000 euro/GJ biodiesel for the non-optimized cases. This is very high

compared to the production costs for other biofuels: 7-20 euro/GJ for biodiesel from different oils (Jegannathan et al. 2011), 13-23 euro/GJ for bioethanol from straw (Gnansounou and Dauriat 2010) and 75-450 euro/GJ for biodiesel from algae (Norsker et al. 2011). For the optimized submerged cultures, the cultivation costs are a factor 10 lower, but this is still quite high. For SSF, the production price is much lower: 50-100 euro/GJ for the base case and a factor 10 lower for the optimized case, according to our estimations. Furthermore, SSF is a low-tech application, which produces less wastewater and can be used on small scale at the source of biomass production, i.e. farms and agricultural processing plants. This reduces transport costs considerably, which gives SSF an extra advantage compared to the modeled submerged systems.

Summarizing, the lipid yields found in the base case scenario are quite low, especially in SSF, but we have shown that there is a potential for higher lipid yields. The energy use of the processes is quite high, but also here there is room for improvement. Microbial lipids have only been produced commercially for high value unsaturated fatty acids so far; process development for bulk production has yet to be started. This paper shows that the potential lipid yield as well as the energy balance is promising enough to continue research on this subject. The high cultivation costs of submerged aerobic fermentation might be a serious problem, but the cultivation costs in SSF are much lower. With some improvement of lipid yield in SSF, microbial lipids produced in SSF cultures might be tomorrow's source of biodiesel.

Appendix A: Production kinetics

Production kinetics in submerged chemostat culture

In chemostat cultures, the C-source and the N-source are supplied to the reactor with a certain dilution rate. The conversion rates shown in Table 1 are equal to the dilution rate multiplied by the concentration of a reactant in the feed or reactor ($r_i = C_i D$). Figure A1 shows results for a chemostat culture with a constant C/N-ratio (30 Cmol/Nmol) in the feed at several dilution rates.

Figure A1 shows clearly that the highest lipid concentration is reached at a dilution rate of 0.016 h^{-1}. Equation 9 can be used to calculate the optimum dilution rate for every C/N-ratio. Figure A2 shows the result of this calculation. This graph shows that a low dilution rate and a high C/N-ratio lead to a high lipid concentration, a low oxygen consumption rate (and therefore low energy consumption for oxygen

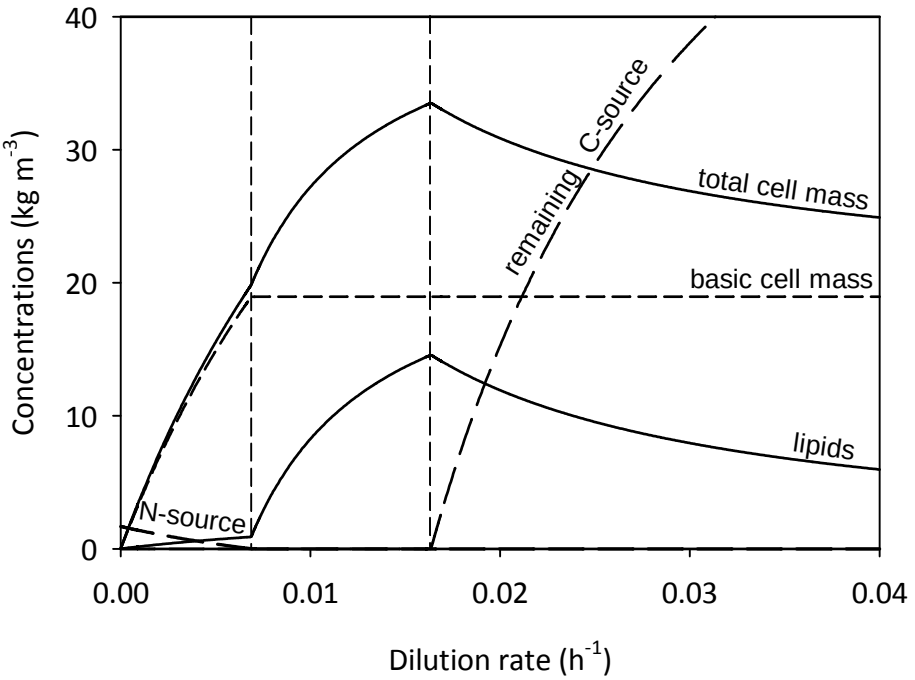

Figure A1: Chemostat culture modeled with a C/N-ratio in the feed of 30 Cmol/Nmol and parameter values from Table 2. C_{Sin} = 3600 Cmol/m^3 = 108 kg/m^3, C_{Nin} = 120 Nmol/m^3 = 6.7 kg/m^3 (based on NH_4^+). At dilution rates below 0.0066 h^{-1}, the C-source is limiting for growth; above this value, the N-source is limiting for growth. Below a dilution rate of 0.016 h^{-1} the C-source is limiting for lipid production; above this value, the C-source is in excess and the specific lipid production rate has its maximum value. Substrate concentrations can be 0 because zero-order kinetics are used in the model.

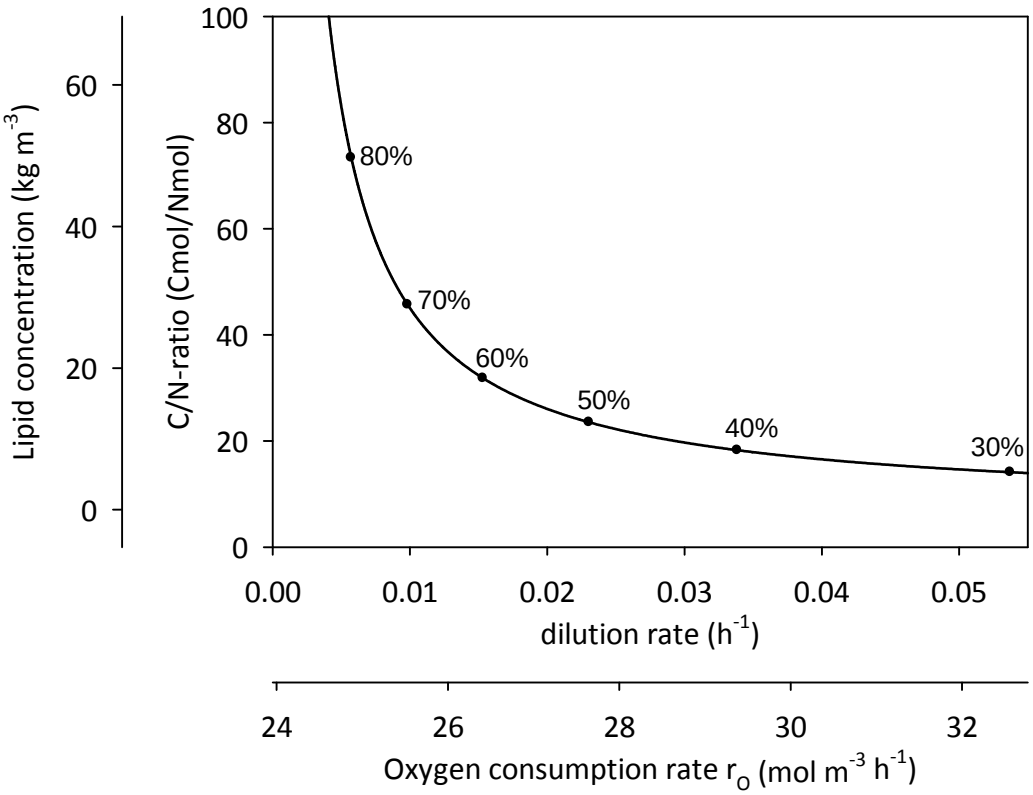

Figure A2: Result of Equation 9 with the parameter values from Table 2. The additional axes show the lipid concentration and the oxygen consumption rate (for calculation of energy use for oxygen transfer) in the bioreactor for C_{Nin} = 120 Nmol/m^3. The numbers in the graph indicate the lipid fraction in the cells at the shown combination of C/N-ratio and dilution rate.

transfer) and a high lipid fraction in the cells. The C/N-ratios used in the calculations were limited to 100 Cmol/Nmol to avoid unrealistically high lipid fractions in the cells. In Figure A2, the maximum substrate concentration of 200 kg/m^3 corresponds to a lipid concentration of 36 kg/m^3; the N-source concentration in the feed has to be decreased to obtain higher C/N-ratios.

Production kinetics in submerged batch culture

A submerged batch culture with oxygen limitation consists of two phases:

1. Exponential growth without any substrate limitation
2. Exponentially decreasing lipid production with N-source limitation

For these phases, Table 1 shows the differential equations with $r_i = \frac{dC_i}{dt}$. Below, we show the integrated forms of these equations from Meeuwse et al. 2011c. A list of symbols is shown on page 207.

1. Exponential growth without any substrate limitations

Exponential growth occurs as is shown in Table 1, which gives for cell mass production:

$$r_X = \frac{dC_X}{dt} = \mu_{\max} C_X \rightarrow C_X(t) = C_X(0) e^{\mu_{\max} t}$$

Similarly, these differential equations can be solved for lipids, N-source and C-source:

$$C_L(t) = \frac{f_{L0}}{1 - f_{L0}} C_X(t)$$

$$C_N(t) = C_N(0) - \frac{C_X(t) - C_X(0)}{Y_{XN}}$$

$$C_S(t) = C_S(0) - \left(\frac{\mu_{\max}}{Y_{XS}} + \frac{f_{L0}}{1 - f_{L0}} \frac{\mu_{\max}}{Y_{LS}} + m_S \right) \frac{C_X(t) - C_X(0)}{\mu_{\max}}$$

The oxygen consumption rate, needed to calculate energy use for oxygen transfer, is in this phase:

$$-r_O(t) = \frac{1}{-\gamma_O} \left(\left(\gamma_X - \frac{\gamma_S}{Y_{XS}} + \frac{f_{L0}}{1 - f_{L0}} \left(\gamma_L - \frac{\gamma_S}{Y_{LS}} \right) \right) \mu_{\max} - \gamma_S m_S \right) C_X(t)$$

The N-source is exhausted at the end of phase 1 at t_{12}:

$$t_{12} = \frac{1}{\mu_{\max}} \ln \left(\frac{Y_{XN} C_N(0)}{C_X(0)} + 1 \right)$$

2. Exponentially decreasing lipid production with N-source limitation

In this phase, there is no growth but carbohydrate production and lipid production; the rate of the latter decreases in time.

$$C_X(t) = C_{X\max} = C_X(0) + Y_{XN} C_N(0)$$

$$C_L(t) = \left(\frac{f_{L0}}{1 - f_{L0}} + \frac{q_{L\max}}{k_d} \left(1 - e^{-k_d (t - t_{12})} \right) \right) C_{X\max}$$

$$C_{IP}(t) = q_{IP} C_{X\max} (t - t_{12}) \leq f_{IP\max} C_{X\max}$$

Carbohydrate production stops when the maximum carbohydrate fraction is reached at t_{2ab}:

$$t_{2ab} = t_{12} + \frac{f_{IP\max}}{q_{IP}}$$

The C-source consumption during and after carbohydrate production is equal to:

$$\begin{cases} t < t_{2ab} : C_S(t) = C_S(t_{12}) - \left(\dfrac{q_{L\max}}{Y_{LS} k_d} (1 - e^{-k_d (t - t_{12})}) + \left(\dfrac{q_{IP}}{Y_{IPS}} + m_S \right) (t - t_{12}) \right) C_{X\max} \\ t \geq t_{2ab} : C_S(t) = C_S(t_{2ab}) - \left(\dfrac{q_{L\max}}{Y_{LS} k_d} (e^{-k_d (t_{2ab} - t_{12})} - e^{-k_d (t - t_{12})}) + m_S (t - t_{2ab}) \right) C_{X\max} \end{cases}$$

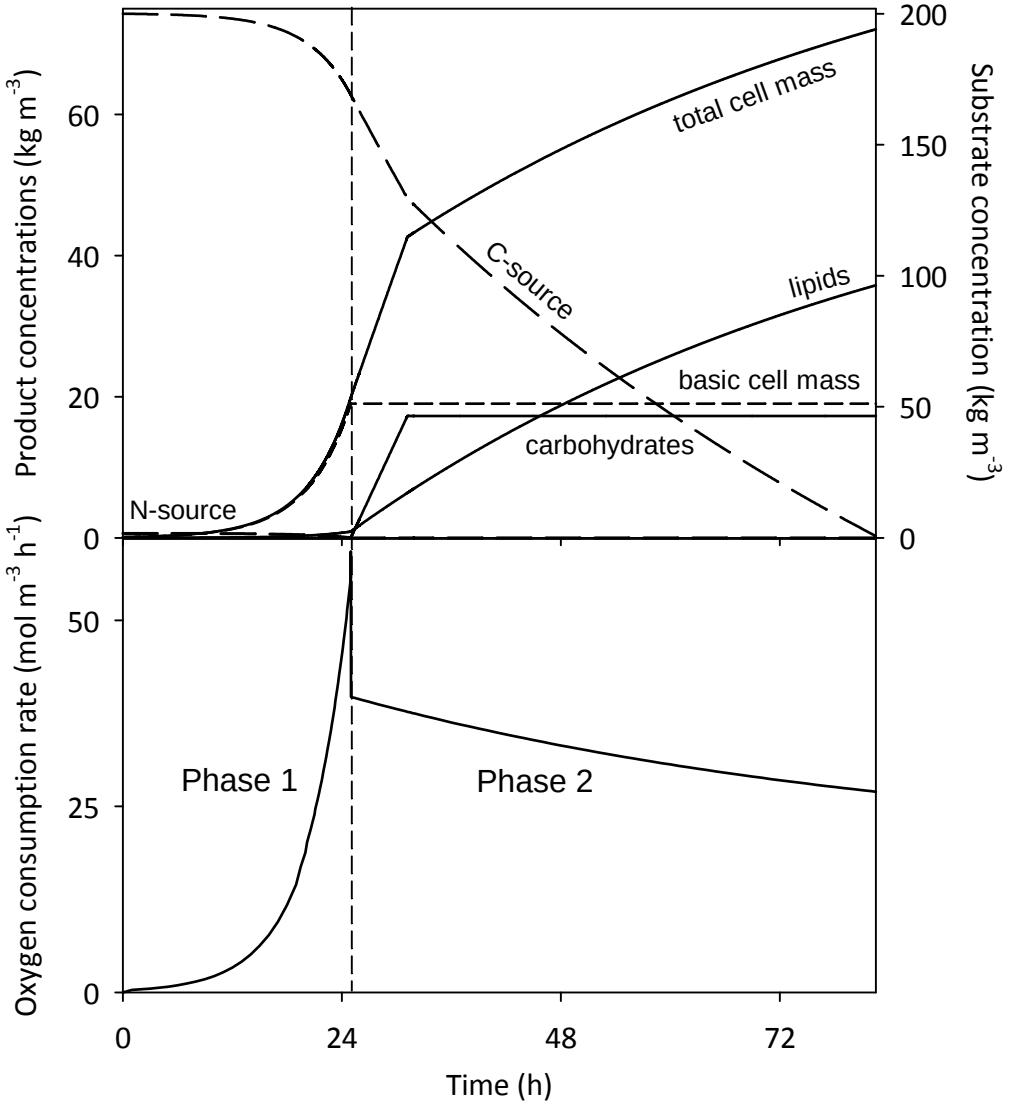

Figure A3: Submerged batch culture modeled with the phases as described in appendix A and parameter values from Table 2. Initial concentrations: $C_N(0)$ = 120 Nmol/m^3 = 6.7 kg/m^3, $C_S(0)$ = 200 kg/m^3 = 6666 Cmol/m^3, $C_X(0)$ = 0.1 kg/m^3. In Phase 1, there is no substrate limitation. Therefore, there is exponential growth with a minimum lipid fraction in the cells. In Phase 2, the N-source is exhausted and therefore there is no growth; C-source is used for lipid production and carbohydrate production. The production of carbohydrates stops at 31 h when the maximum carbohydrate fraction is reached; the lipid production continues, but the specific lipid production rate decreases exponentially in time as was found experimentally in Meeuwse et al. (2011c).

The oxygen consumption rate in this phase is equal to:

$$-r_O(t) = \frac{1}{-\gamma_O}\left(\left(\gamma_L - \frac{\gamma_S}{Y_{LS}}\right)q_{L\max}e^{-k_d(t-t_{12})} + \left(\gamma_{IP} - \frac{\gamma_S}{Y_{IPS}}\right)q_{IP}(t) - \gamma_S m_S\right)C_{X\max}$$

Figure A3 shows both phases clearly. We used the same N-source concentration as in Figure A1 and A2, and the maximum C-source concentration of 200 kg/m^3. This gives a C/N-ratio of 55 Cmol/Nmol. The final lipid fraction in the cells is 50% w/w. If more C-source had been available, a maximum lipid concentration of 59 kg/m^3 (62% w/w of total cell mass) could have been reached in this graph; more is not possible because the lipid production rate decreases in time.

Production kinetics in solid-state fermentation

This is a simplified version of the model description shown in Meeuwse et al. (2011d); for a detailed description, the source article should be consulted. A list of symbols is shown on page 207. To calculate the occurrence of the different layers shown in Figure 4, we use mass balances combined with Fick's law of diffusion. The thickness of the total biofilm can be calculated from all separate layers:

$$\frac{dL_f}{dt} = \frac{\sum_{i=0}^{2} r_{X,i}L_i}{C_X(t)}$$

The basic cell mass concentration $C_X(t)$, is calculated from the fraction of solids in the biofilm as shown in Meeuwse et al. (2011d).

Four different situations can occur in the biofilm.

1. No substrate limitation

In this case we have growth as described in the first column of Table 1 (r_1). This occurs when:

$$L_N = \sqrt{\frac{2ID_N C_N(0)}{-r_{N.1}}} > L_f \text{ and } L_O = L_f - \sqrt{\frac{2ID_O C_O(L_f)}{-r_{O.1}}} < 0$$

2. Limitation of the N-source only

There will be two layers: $L_1 = L_N$ with growth (r_1) and $L_2 = L_f - L_N$ with lipid production as described in the second column of Table 1 (r_2).

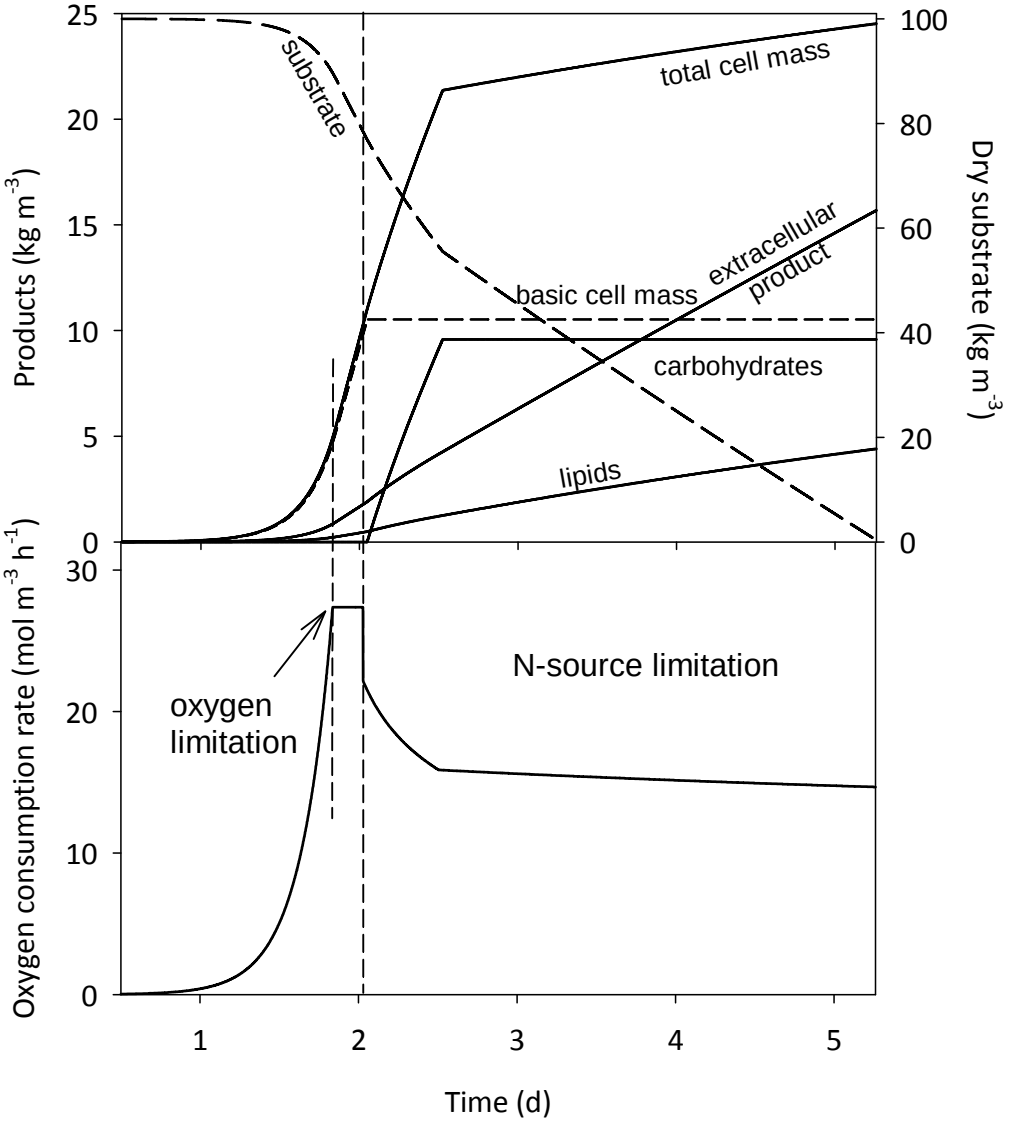

Figure A4: Solid-state fermentation with an initial dry substrate concentration of 100 kg m^{-3} = 666 kg wet substrate m^{-3}, and a C/N-ratio of 50 Cmol/Nmol.

This occurs when:

$$L_N = \sqrt{\frac{2ID_N C_N(0)}{-r_{N.1}}} < L_f \text{ and } L_O = L_f - \sqrt{\frac{2ID_O C_O(L_f)}{-r_{O.1}}} < 0$$

3. Limitation of oxygen only

In this case, there are also two layers: $L_0 = L_O$ in which no metabolism takes place and $L_1 = L_f - L_O$ with growth (r_1). This occurs when:

$$L_N = \sqrt{\frac{2ID_N C_N(L_O)}{-r_{N.1}}} + L_O > L_f \text{ and } L_O = L_f - \sqrt{\frac{2ID_O C_O(L_f)}{-r_{O.1}}} > 0$$

4. Limitation of both oxygen and N-source

This case is shown in Figure 4. There are three layers: $L_0 = L_O$, $L_1 = L_N - L_O$ and $L_2 = L_f - L_N$. This occurs when:

$$L_N = \sqrt{\frac{2ID_N C_N(L_O)}{-r_{N.1}}} + L_O > L_f \text{ and } L_O = L_f - \sqrt{\frac{(L_f - L_N)^2 (r_{O.2} - r_{O.1}) + 2ID_O C_O(L_f)}{-r_{O.1}}} > 0$$

The total amount of produced lipids was calculated with a balance over all layers:

$$\frac{dM_L}{dt} = \sum_{i=0}^{2} r_{L,i} L_i$$

Similar balances can be set up for the other products.

We assumed that the substrate particles are flat plates with a thickness of 1 mm and that extra water is added to the substrate up to 85% w/w to prevent drying out during the culture. Diffusion of C-source and N-source in the solid substrate was calculated by dividing the substrate in layers, as was explained in Meeuwse et al. (2011d). The reduction of solid substrate mass was calculated from the increase of biofilm mass.

Figure A4 shows results for a solid-state fermentation with a substrate with a C/N-ratio of 50 Cmol/Nmol. This C/N-ratio was chosen because it shows the start of oxygen limitation and N-source limitation separately; at higher C/N-ratios, these limitations start almost at the same moment. Oxygen limitation starts after 1.8 days and continues during the rest of the culture; N-source limitation starts after 2 days.

Appendix B: Oxygen transfer and cooling

All equations in this part were obtained or derived from Van 't Riet and Tramper (1991), unless mentioned otherwise. A list of parameter values is shown in Appendix D.

Oxygen transfer in a stirred tank reactor

The ungassed liquid height in the STR is 8 m and the diameter is 4 m. The tank has baffles and two 6-blade Rushton turbine impellers on one stirrer axis. We modeled it as a cascade of two 4-m high stacked tanks with one stirrer each with gas transfer from the bottom tank (no. 1) to the top tank (no. 2) and no exchange of liquid. In a stirred tank, oxygen transfer to the liquid occurs mainly near the stirrer. Oxygen supply to the rest of the tank is to a large extent achieved by the pumping action of the stirrer, which transports water with dissolved oxygen. The oxygen transfer rate (OTR) is calculated with:

$$OTR = \frac{\frac{C_{Ogi}}{m}\frac{p_{si}}{p_a} - C_{Oli}}{\frac{V_L}{mF_g}\frac{p_{si}}{p_a} + \frac{1}{k_{Ol}A} + t_c}$$

C_{Oli} is the dissolved oxygen concentration at the end of the circulation loop in tank *i*. The required air flow rate and mixing rate were calculated assuming complete exhaustion of dissolved oxygen at the end of the circulation loop in the top tank (C_{Ol2}=0). The cell mass concentration and specific conversion rates were assumed to be equal in both tanks.

The physical parameters were calculated as follows:

$$t_c = \frac{3}{2.5N_p^{1/3}}\frac{1}{N}\left(\frac{D_t}{D_s}\right)^3\frac{H_t}{D_t}$$

$$p_{s1} = p_a + 9.81\cdot\rho_l(2H_t - H_s)$$

$$p_{s2} = p_{s1} - 9.81\cdot\rho_l H_t$$

$$k_{Ol}A = 2.6x10^{-2}\left(\frac{P_s}{V_L}\right)^{0.4}\left(\frac{F_g}{0.25\pi D_t^{\,2}}\frac{p_a}{p_{si}}\right)^{0.5} \qquad \text{for } \eta_c \le 50x10^{-3}\ \text{Nsm}^{-2}$$

$$k_{Ol}A = 2.6x10^{-2}\left(\frac{P_s}{V_L}\right)^{0.4}\left(\frac{F_g}{0.25\pi D_t^{\,2}}\frac{p_a}{p_{si}}\right)^{0.5}\left(\frac{\eta_c}{0.05}\right)^{-0.7} \qquad \text{for } \eta_c > 50x10^{-3}\ \text{Nsm}^{-2}$$

$$C_{Og2} = C_{Og1} - \frac{r_O V_L}{F_g}$$

To avoid flooding of the stirrer, the stirrer speed must be high enough compared to the air flow rate according to the Froude-criterion:

$$\frac{N^3}{F_g} > \frac{9.81}{0.3D_S^{\,4}}\frac{p_{s2}}{p_a}$$

Furthermore, the gas flow rate is limited by the maximum bubble holdup of the tank:

$$0.13\left(\frac{P_S}{V_L}\right)^{0.33}\left(\frac{F_g}{0.25\pi D_t^{\,2}}\frac{p_a}{p_{s2}}\right)^{0.67} < 0.25 \qquad \text{for } \eta_c \le 50x10^{-3}\ \text{Nsm}^{-2}$$

$$0.13\left(\frac{P_S}{V_L}\right)^{0.33}\left(\frac{F_g}{0.25\pi D_t^{\,2}}\frac{p_a}{p_{s2}}\right)^{0.67}\left(\frac{\eta_c}{0.05}\right)^{-0.7} < 0.25 \qquad \text{for } \eta_c > 50x10^{-3}\ \text{Nsm}^{-2}$$

The power consumption of the stirrer and the air pump is calculated in Appendix C.

Oxygen transfer in a bubble column

In a bubble column reactor, oxygen transfer occurs in the whole reactor, although at a lower rate than in a stirred tank. The BCR used in our design is 14.7 m high (ungassed liquid height) and 2.9 m in diameter. This diameter to height ratio gave the lowest power consumption for aeration. Calculations were carried out assuming a cascade of five stacked tanks (D_txH_t =2.9mx2.9m) with gas flow from a tank to the tank above (no. 1 is lowest, no. 5 is highest) and no exchange of liquid.

The oxygen transfer rate in tank *i* is:

$$OTR = \frac{\frac{C_{Ogi}}{m}\frac{p_{ei}}{p_a} - C_{Oli}}{\frac{V_L}{mF_g}\frac{p_{ei}}{p_a} + \frac{1}{k_{Ol}A}}$$

With:

$p_{e1} = p_a + 4.5 \times 9.81 \cdot \rho_l H_t$

$p_{e2} = p_{e1} - 9.81 \cdot \rho_l H_t$; similar for p_{e3} - p_{e5}

$$k_{Ol}A = 0.32\left(\frac{F_g}{0.25\pi D_t^{\,2}}\frac{p_a}{p_e}\right)^{0.7}\left(\frac{\eta_c}{\eta_w}\right)^{-0.84}$$

The oxygen concentration in the air going from a tank to the tank above is:

$C_{Og2} = C_{Og1} - \frac{r_O V_L}{F_g}$; similar for C_{Og3} - C_{Og5}

The gas flow rate is limited by the maximum gas holdup of the tank:

$$0.6\left(\frac{F_g}{0.25\pi D_t^{\,2}}\frac{p_a}{p_{s5}}\right)^{0.7}\left(\frac{\eta_c}{\eta_w}\right)^{-0.84} < 0.25$$

The minimum required air flow rate was calculated for complete consumption of all transferred oxygen in the liquid (C_{Ol5}=0 for top tank). Power consumption of the air pump is calculated in Appendix C.

Evaporative cooling in SSF

For solid-state fermentation, we used a packed bed of LxWxH = 10mx10mx1m. Cooling is carried out by aeration, and this also provides enough oxygen for the growing cells (Gowthaman et al. 1993, Weber et al. 1999b, Weber et al. 2002). The air flow rate required for cooling was calculated with the model published by Weber et al. (1999b):

$$F_g(t) = \frac{r_O(t)\Delta H_O \rho_a(T_{in})}{h_g(T_{out}) - h_g(T_{in})}$$

The density of air depends on the pressure and the water content:

$$\rho_a(T) = \frac{p_e - p_w(T)}{287.1T} + \frac{p_w(T)}{461.5T}$$

$$p_e = p_a + \Delta p_b$$

$$p_w(T) = \exp\left(23.59 - \frac{4045}{T - 37.70}\right) \qquad (273<T<333 \text{ K})$$

The enthalpy of moist air depends on the temperature and the water content:

$$h_g(T) = c_g(T - T_{ref}) + y_w(T)\left(c_{wv}(T - T_{ref}) + \Delta H_w(T_{ref})\right)$$

$$y_w(T) = 0.622\frac{p_w(T)}{p_s - p_w(T)}$$

Water evaporates during the fermentation; the cumulative amount of water evaporated at the end of the culture should not exceed the total water content at the start of the fermentation. With the parameter values we used, a water content of 85% is enough for the whole culture time.

The pressure drop over the packed bed is estimated with the Ergun equation (Ergun 1952) for particles with a diameter of d_p:

$$\Delta p_b = 150\frac{\mu_a}{{d_p}^2}\frac{(1-\varepsilon)^2}{\varepsilon^3}v_{gs} + 1.75\frac{\rho_a}{d_p}\frac{(1-\varepsilon)}{\varepsilon^3}{v_{gs}}^2$$

With: $v_{gs} = \frac{F_g}{L \times W}$

As the air flow rate is needed to calculate the pressure drop, this set of equations was solved by iteration.

Viscosity

The viscosity of the broth was calculated with Olsvik and Kristiansen (1994):

For yeasts: $\eta_c = \eta_w e^{0.025C_x}$

For filamentous fungi: $\eta_c = \eta_w e^{0.23C_x}$

In these two equations, C_x is used in kg m^{-3}.

Appendix C: Energy use

Sterilization

For sterilization of substrate and medium, we use a temperature difference ΔT of 100K (21°C – 121°C). For water, this leads to an energy use of $\rho_l c_w \Delta T = 439$ MJ/m^3 and for substrate (assuming the properties of wood) to $c_s \Delta T = 250$ kJ/kg dry substrate. We assume that 70% of the heat needed for sterilization can be reused (Soderberg 1997).

Pretreatment

Only corn stover or wheat straw has to be pretreated at the expense of 1.6 MJ/kg (Aden et al. 2002, Cardona and Sánchez 2006, Luo et al. 2009, Piccolo and Bezzo 2009). Therefore, the energy use for pretreatment depends on the C/N-ratio. Figure C1 shows the C/N-ratio of mixtures of sugar beet pulp (C/N = 30 Cmol/Nmol) and wheat straw (C/N = 120 Cmol/Nmol) and the energy needed for pretreatment.

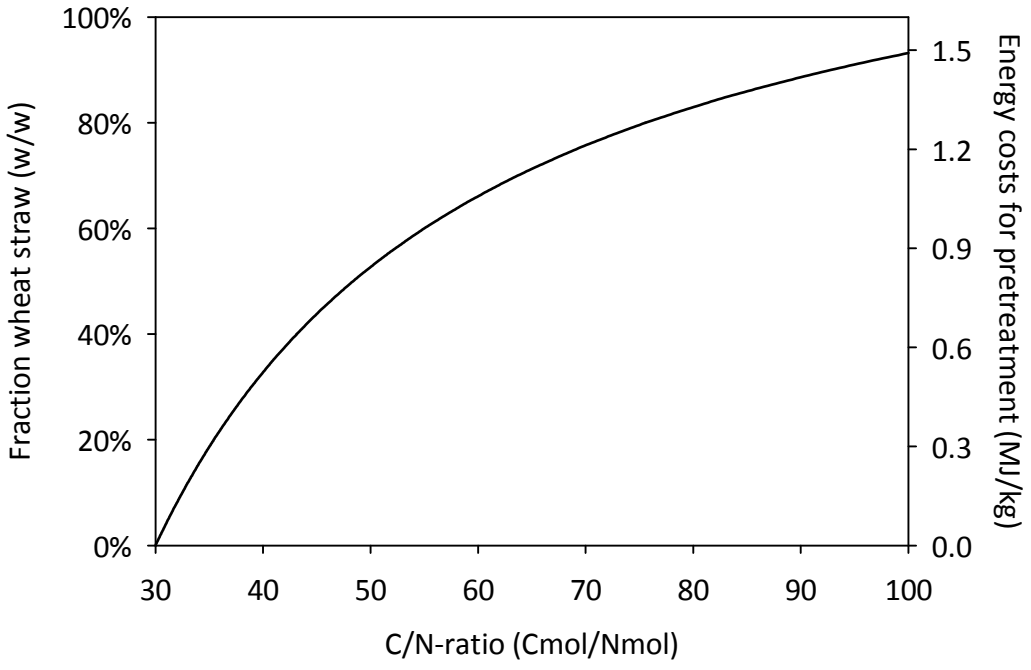

Figure C1: C/N-ratio as a function of the fraction of wheat straw in a mixture of wheat straw and sugar beet pulp, and energy use for pretreatment as a function of the C/N-ratio of this mixture.

Energy consumption cooling and aeration

For the bubble column and the packed bed, energy is needed only for aeration:

$$P_g = F_g p_a \frac{y}{y-1}\left(\left(\frac{p_e}{p_a}\right)^{\frac{y-1}{y}} - 1\right)$$

with $p_e = p_a + 9.81 \cdot \rho_l H$

For the stirred tank, energy is needed for stirring and aeration:

$$P_t = P_s + P_g$$

$$P_s = N_p \rho_l N^3 D_s^{\,5}$$

$$P_g = F_g p_a \frac{y}{y-1}\left(\left(\frac{p_s}{p_a}\right)^{\frac{y-1}{y}} - 1\right)$$

Calculation of the oxygen transfer rate in SmF and heat removal in SSF as a function of stirrer speed and aeration rate is shown in Appendix B. The ratio between stirring and aeration was optimized for minimum energy use. These calculations give the power consumption as a function of the oxygen transfer rate and as a function of viscosity and therefore as a function of yeast or fungal cell mass. Examples of results are shown in Figure C2a (with a constant cell mass concentration) and Figure C2b (with a constant oxygen transfer rate). We assume a 100% efficiency of the stirrer engine and air pumps.

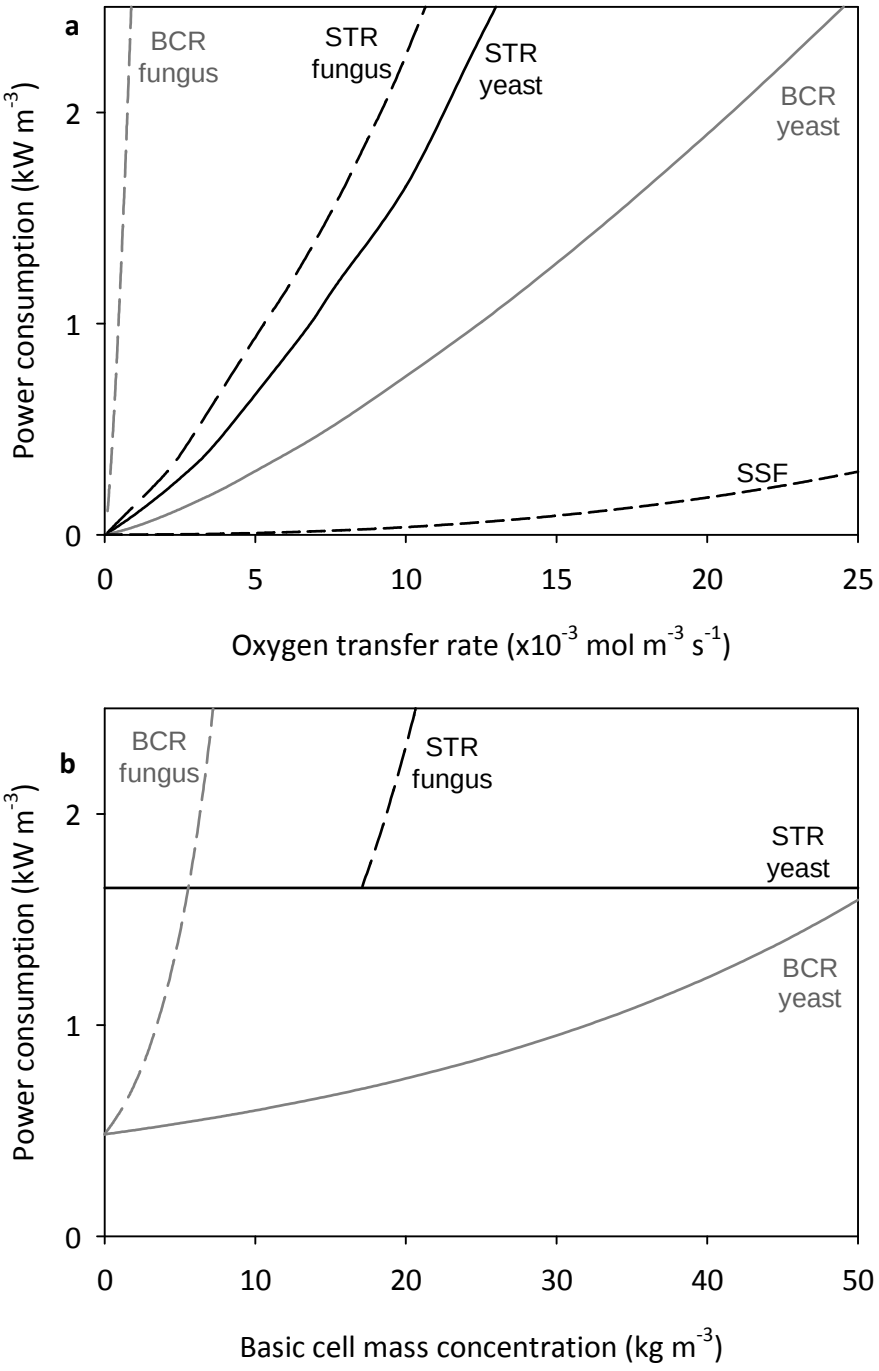

Figure C2 Power consumption for stirring and aeration **a.** with a total cell mass concentration of 20 kg/m^3 in SmF and a void fraction of 30% in SSF. **b.** as a function of cell mass concentration, which determines the viscosity of the broth, and a constant oxygen transfer rate of 1x10^{-2} mol/m^3/s

Appendix D: parameter values

Symbol	Name	value	units
c_g	specific heat dry air	1.01	kJ kg^{-1} K^{-1}
C_{Og1}	Oxygen concentration of ingoing air (21% v/v)	0.26	mol m^{-3}
C_{Ol}	Oxygen concentration in fermentation liquid	0	mol m^{-3}
c_s	specific heat solid substrate	2.5	kJ kg^{-1} K^{-1}
$C_X(0)$	Lipid-free cell mass concentration in batch t = 0	0.1	kg m^{-3}
c_w	specific heat water and medium	4.18	kJ kg^{-1} K^{-1}
c_{wv}	specific heat water vapor	1.86	kJ kg^{-1} K^{-1}
ID_N	Diffusion coefficient of N-source	$9.3x10^{-10}$	m s^{-1}
ID_O	Diffusion coefficient of oxygen	$1.4x10^{-9}$	m s^{-1}
d_p	Particle diameter in SSF	$4x10^{-3}$	m
D_s	Diameter of stirrer	1.3	m
D_t	Diameter of fermenter tank Stirred tank: Bubble column:	 4 2.9	m
f_{L0}	Minimum lipid concentration	7.8%	Cmol $Cmol^{-1}$
f_{IPmax}	Maximum carbohydrate concentration	87%	Cmol $Cmol^{-1}$
f_{solids}	Solids fraction in biofilm (SSF)	12.5%	w/w
H	Height of fermenter for Stirred tank: Bubble column: Packed bed	 8 14.7 1	m
H_s	Height of stirrer from bottom of tank	1	m
H_t	Height of fermenter tank for calculations Stirred tank: Bubble column: Packed bed	 4 2.9 1	m
k_d	Degradation rate of lipid production in batch culture	See Table 3	h^{-1}
LxW	Length x width of packed bed	10x10	m
m	Distribution coefficient oxygen air/water	32	-
m_s	Maintenance coefficient on C-source	0.028	Cmol $Cmol^{-1}$ h^{-1}
N_p	Power number stirred fermenter	2.5	-
p_a	Ambient pressure	$1x10^5$	Pa
q_{EP}	specific extracellular product production rate	0.035	Cmol $Cmol^{-1}$ h^{-1}
q_{Lmax}	Maximum specific lipid production rate	See Table 2	Cmol $Cmol^{-1}$ h^{-1}
T_{in}	temperature of ingoing air	293	K
T_{out}	temperature of outgoing air	303	K
T_{ref}	reference temperature	273	K
V_l	Liquid volume of fermenter	100	m^3

Y_{EPS}	Yield of extracellular product on C-source	0.31	Cmol Cmol^{-1}
Y_{LS}	Yield of lipids on C-source	0.56	Cmol Cmol^{-1}
Y_{IPS}	Yield of carbohydrates on C-source	1	Cmol Cmol^{-1}
Y_{XN}	Yield of cell mass on N-source	5.5	Cmol Nmol^{-1}
Y_{XS}	Yield of cell mass on C-source	0.78	Cmol Cmol^{-1}
γ	Compressibility constant of air	1.4	-
γ_{EP}	Degree of reduction extracellular product	6	-
γ_L	Degree of reduction lipids	5.73	-
γ_O	Degree of reduction oxygen	4	-
γ_{IP}	Degree of reduction carbohydrates	4	-
γ_S	Degree of reduction C-source	4	-
γ_X	Degree of reduction cell mass	4.16	-
ΔH_O	Heat production metabolism	0.46	MJ/mole O_2 produced
ΔH_w	evaporation enthalpy water at 273K	2.5	MJ kg^{-1}
η_c	Viscosity of fermentation culture		Nsm^{-2}
	Yeast:	$\eta_c = \eta_l e^{0.025 C_X}$	
	Fungus:	$\eta_c = \eta_l e^{0.23 C_X}$	
η_w	Viscosity of water	1x10^{-3}	N s m^{-2}
μ	Kinematic viscosity of air	2x10^{-5}	Pa s
μ_{max}	Maximum specific growth rate	0.21	h^{-1}
ρ_l	Density of fermentation culture	1050	kg m^{-3}
ρ_s	Density of (wet) solid substrate	1030	kg m^{-3}
	conversion factors		
	C_{EP}	32	g Cmol^{-1}
	C_{IP}	30	g Cmol^{-1}
	C_L	15.7	g Cmol^{-1}
	C_S	30	g Cmol^{-1}
	C_X	28.7	g Cmol^{-1}
	C_L	43	MJ kg^{-1}
	C_S	16	MJ kg^{-1}

References

References

Aden A, Ruth M, Ibsen K, Jechura J, Neeves K, Sheehan J, Wallace B, Montague L, Slayton A, Lukas J. 2002. Lignocellulosic biomass to ethanol process design and economics utilizing co-current dilute acid prehydrolysis an enzymatic hydrolysis for corn stover. Golden, Colorado, United States: National Renewable Energy Laboratory. Report nr NREL/TP-510-32438.

Aggelis G, Komaitis M, Papanikolaou S, Papadopoulos G. 1995. A mathematical model for the study of lipid accumulation in oleaginous microorganisms .1. Lipid accumulation during growth of *Mucor circinelloides* Cbs-172-27 on a vegetable oil. Grasas Aceites 46: 169-173.

Aggelis G, Sourdis J. 1997. Prediction of lipid accumulation-degradation in oleaginous micro-organisms growing on vegetable oils. Antonie Van Leeuwenhoek 72: 159-165.

Alvarez HM, Steinbuchel A. 2002. Triacylglycerols in prokaryotic microorganisms. Appl Microbiol Biotechnol 60: 367-376.

Alvarez RM, Rodriguez B, Romano JM, Diaz AO, Gomez E, Miro D, Navarro L, Saura G, Garcia JL. 1992. Lipid accumulation in *Rhodotorula glutinis* on sugar cane molasses in single-stage continuous culture. World J Microbiol Biotechnol 8: 214-215.

Angerbauer C, Siebenhofer M, Mittelbach M, Guebitz GM. 2008. Conversion of sewage sludge into lipids by *Lipomyces starkeyi* for biodiesel production. Bioresour Technol 99: 3051-3056.

Beopoulos A, Nicaud JM, Gaillardin C. 2011. An overview of lipid metabolism in yeasts and its impact on biotechnological processes. Appl Microbiol Biotechnol 90: 1193-1206.

Beuling EE, van den Heuvel JC, Ottengraf SPP. 2000. Diffusion coefficients of metabolites in active biofilms. Biotechnol Bioeng 67: 53-60.

Bhargav S, Panda BP, Ali M, Javed S. 2008. Solid-state fermentation: An overview. Chem Biochem Eng Q. 22: 49-70.

Botha A, Strauss T, Kock JLF, Pohl CH, Coetzee DJ. 1997. Carbon source utilization and gamma-linolenic acid production by mucoralean fungi. Syst Appl Microbiol 20: 165-170.

Boulton CA, Ratledge C. 1983. Use of transition studies in continuous cultures of *Lipomyces starkeyi*, an oleaginous yeast, to investigate the physiology of lipid accumulation. J Gen Microbiol 129: 2871-2876.

Boulton CA, Ratledge C. 1984. *Cryptococcus terricolus*, an oleaginous yeast re-appraised. Appl Microbiol Biotechnol 20: 72-76.

Brown BD, Hsu KH, Hammond EG, Glatz BA. 1989. A relationship between growth and lipid accumulation in *Candida curvata* D. J Ferment Bioeng 68: 344-352.

Cardona Alzate CA, Sánchez Toro OJ. 2006. Energy consumption analysis of integrated flowsheets for production of fuel ethanol from lignocellulosic biomass. Energy 31: 2447-2459.

Certik M, Shimizu S. 1999. Biosynthesis and regulation of microbial polyunsaturated fatty acid production. J Biosci Bioeng 87: 1-14.

Chatzifragkou A, Fakas S, Galiotou-Panayotou M, Komaitis M, Aggelis G, Papanikolaou S. 2010. Commercial sugars as substrates for lipid accumulation in *Cunninghamella echinulata* and *Mortierella isabellina* fungi. Eur J Lipid Sci Technol 112: 1048-1057.

Chen HC, Chang CC, Chen CX. 1997. Optimization of arachidonic acid production by *Mortierella alpina* Wuji-H4 isolate. J Am Oil Chem Soc 74: 569-578.

Choi SY, Ryu DDY, Rhee JS. 1982. Production of microbial lipid - Effects of growth rate and oxygen on lipid synthesis and fatty acid composition of *Rhodotorula gracilis*. Biotechnol Bioeng 24: 1165-1172.

Collet P, Hélias A, Lardon L, Ras M, Goy RA, Steyer JP. 2011. Life-cycle assessment of microalgae culture coupled to biogas production. Bioresour Technol 102: 207-214.

Desgranges C, Georges M, Vergoignan C, Durand A. 1991. Biomass estimation in solid-state fermentation .2. Online measurements. Appl Microbiol Biotechnol 35: 206-209.

Durner R, Witholt B, Egli T. 2000. Accumulation of poly[(R)-3-hydroxyalkanoates] in *Pseudomonas oleovorans* during growth with octanoate in continuous culture at different dilution rates. Appl Environ Microbiol 66: 3408-3414.

Economou CN, Makri A, Aggelis G, Pavlou S, Vayenas DV. 2010. Semi-solid state fermentation of sweet sorghum for the biotechnological production of single cell oil. Bioresour Technol 101: 1385-1388.

Economou CN, Aggelis G, Pavlou S, Vayenas DV. 2011. Modeling of Single-Cell Oil Production Under Nitrogen-Limited and Substrate Inhibition Conditions. Biotechnol Bioeng 108: 1049-1055.

Ergun S. 1952. Fluid Flow through Packed Columns. Chem Eng Prog 48: 89-94.

Esteban B, Baquero G, Puig R, Riba JR, Rius A. 2010. Is it environmentally advantageous to use vegetable oil directly as biofuel instead of converting it to biodiesel? Biomass Bioenergy 35: 1317-1328.

Evans CT, Ratledge C. 1983. A comparison of the oleaginous yeast, *Candida curvata*, grown on different carbon sources in continuous and batch culture. Lipids 18: 623-629.

Fakas S, Makri A, Mavromati M, Tselepi M, Aggelis G. 2009a. Fatty acid composition in lipid fractions lengthwise the mycelium of *Mortierella isabellina* and lipid production by solid state fermentation. Bioresour Technol 100: 6118-6120.

Fakas S, Papanikolaou S, Batsos A, Galiotou-Panayotou M, Mallouchos A, Aggelis G. 2009b. Evaluating renewable carbon sources as substrates for single cell oil production by *Cunninghamella echinulata* and *Mortierella isabellina*. Biomass Bioenergy 33: 573-580.

Feofilova EP, Sergeeva YE, Ivashechkin AA. 2009. Biodiesel-fuel: Content, production, producers, contemporary biotechnology (Review). Appl Biochem Microbiol 46: 369-378.

Gema H, Kavadia A, Dimou D, Tsagou V, Komaitis M, Aggelis G. 2002. Production of gamma-linolenic acid by *Cunninghamella echinulata* cultivated on glucose and orange peel. Appl Microbiol Biotechnol 58: 303-307.

Gill CO, Hall MJ, Ratledge C. 1977. Lipid accumulation in an oleaginous yeast (*Candida* 107) growing on glucose in single-stage continuous culture. Appl Environ Microbiol 33: 231-239.

Glatz BA, Hammond EG, Hsu KH, Baehman L, Bati N, Bednarski W, Brown D, Floetenmeyer M. 1984. Production and modification of fats and oils by yeast fermentation. In: Ratledge C, Dawson PSS, Rattray J, editors. Biotechnology for the oils and fats industry: American Oil Chemists' Society. p 163-176.

Gnansounou E, Dauriat A. 2010. Techno-economic analysis of lignocellulosic ethanol: A review. Bioresour Technol 101: 4980-4991.

Gow NAR, Gadd GM. 1995. The growing fungus. London: Chapman & Hall.

Gowthaman MK, Rao K, Ghildyal NP, Karanth NG. 1993. Gas Concentration and Temperature-Gradients in a Packed-Bed Solid-State Fermenter. Biotechnol Adv 11: 611-620.

Granger LM, Perlot P, Goma G, Pareilleux A. 1993. Efficiency of fatty acid synthesis by oleaginous yeasts - Prediction of yield and fatty acid cell content from consumed C/N ratio by a simple method. Biotechnol Bioeng 42: 1151-1156.

Griffin DH. 1993. Fungal physiology. New York: Wiley-Liss.

Hansson L, Dostalek M. 1986. Lipid formation by *Cryptococcus albidus* in nitrogen limited and in carbon limited chemostat cultures. Appl Microbiol Biotechnol 24: 187-192.

Hansson L, Dostalek M, Sorenby B. 1989. Production of gamma-linolenic acid by the fungus *Mucor rouxii* in fed-batch and continuous culture. Appl Microbiol Biotechnol 31: 223-227.

Hassan M, Blanc PJ, Granger LM, Pareilleux A, Goma G. 1993. Lipid production by an unsaturated fatty acid auxotroph of the oleaginous yeast *Apiotrichum curvatum* grown in single-stage continuous culture. Appl Microbiol Biotechnol 40: 483-488.

He MX, Hu QC, Gou XH, Liu XY, Li Q, Pan K, Zhu QL, Wu J. 2010. Screening of oleaginous yeast with xylose assimilating capacity for lipid and bio-ethanol production. Afr J Biotechnol 9: 8392-8397.

Holker U, Lenz J. 2005. Solid-state fermentation - are there any biotechnological advantages? Curr Opin Microbiol 8: 301-306.

Horn H, Morgenroth E. 2006. Transport of oxygen, sodium chloride, and sodium nitrate in biofilms. Chem Eng Sci 61: 1347-1356.

Jang HD, Lin YY, Yang SS. 2000. Polyunsaturated fatty acid production with *Mortierella alpina* by solid substrate fermentation. Bot Bull Acad Sin 41: 41-48.

Jang HD, Lin YY, Yang SS. 2005. Effect of culture media and conditions on polyunsaturated fatty acids production by *Mortierella alpina*. Bioresour Technol 96: 1633-1644.

Jegannathan KR, Eng-Seng C, Ravindra P. 2011. Economic assessment of biodiesel production: Comparison of alkali and biocatalyst processes. Renew Sust Energ Rev 15: 745-751.

Jorquera O, Kiperstok A, Sales EA, Embirucu M, Ghirardi ML. 2010. Comparative energy life-cycle analyses of microalgal biomass production in open ponds and photobioreactors. Bioresour Technol 101: 1406-1413.

Karanth NG, Sattur AP. 1991. Mathematical modeling of production microbial lipids. 2. Kinetics of lipid accumulation. Bioprocess Eng. 6: 241-248.

Kendrick A, Ratledge C. 1992. Lipid Formation in the Oleaginous Mold *Entomophthora exitalis* Grown in Continuous Culture - Effects of Growth-Rate, Temperature and Dissolved-Oxygen Tension on Polyunsaturated Fatty-Acids. Appl Microbiol Biotechnol 37: 18-22.

Kobayashi T, Vandedem G, Mooyoung M. 1973. Oxygen Transfer into Mycelial Pellets. Biotechnol Bioeng 15: 27-45.

Koutinas AA, Wang R, Kookos IK, Webb C. 2003. Kinetic parameters of *Aspergillus awamori* in submerged cultivations on whole wheat flour under oxygen limiting conditions. Biochem Eng J 16: 23-34.

Kryvoruchko V, Machmuller A, Bodiroza V, Amon B, Amon T. 2009. Anaerobic digestion of by-products of sugar beet and starch potato processing. Biomass Bioenergy 33: 620-627.

Kurosawa H, Matsumura M, Tanaka H. 1989. Oxygen Diffusivity in Gel Beads Containing Viable Cells. Biotechnol Bioeng 34: 926-932.

Larson ED, Jin HM, Celik FE. 2009. Large-scale gasification-based coproduction of fuels and electricity from switchgrass. Biofuels Bioprod Biorefining 3: 174-194.

Li Q, Du W, Liu DH. 2008. Perspectives of microbial oils for biodiesel production. Appl Microbiol Biotechnol 80: 749-756.

Longsworth LG. 1953. Diffusion Measurements, at 25-Degrees, of Aqueous Solutions of Amino Acids, Peptides and Sugars. J Am Chem Soc 75: 5705-5709.

Lorenz F, Voss C. 2007. Wie viel Energie benötigt die Verdampfungstrocknung? Zuckerind 132: 766-769.

Luo L, van der Voet E, Huppes G. 2009. An energy analysis of ethanol from cellulosic feedstock–Corn stover. Renew Sustain Energy Rev 13: 2003-2011.

Meeuwse P, Tramper J, Rinzema A. 2011a. Modeling lipid accumulation in oleaginous fungi in chemostat cultures. I: Development and validation of a chemostat model for *Umbelopsis isabellina*. Bioprocess Biosyst Eng 34: 939-949.

Meeuwse P, Tramper J, Rinzema A. 2011b. Modeling lipid accumulation in oleaginous fungi in chemostat cultures. II: Validation of the chemostat model using yeast culture data from literature. Bioprocess Biosyst Eng 34: 951-961.

Meeuwse P, Akbari P, Tramper J, Rinzema A. 2011c. Modeling growth, lipid accumulation and lipid turnover in submerged batch cultures of *Umbelopsis isabellina*. Bioprocess Biosyst Eng DOI: 10.1007/s00449-011-0632-x

Meeuwse P, Klok AJ, Haemers S, Tramper J, Rinzema A. 2011d. Growth and lipid production of *Umbelopsis isabellina* on a solid substrate - Mechanistic modeling and validation. To be submitted.

Meng X, Yang JM, Xu X, Zhang L, Nie QJ, Xian M. 2009. Biodiesel production from oleaginous microorganisms. Renew Energy 34: 1-5.

Meyer W, Gams W. 2003. Delimitation of *Umbelopsis* (*Mucorales*, *Umbelopsidaceae fam. nov*.) based on ITS sequence and RFLP data. Mycol Res 107: 339-350.

Mitchell D, Krieger N, Berovic M. 2006. Solid-state fermentation bioreactors. Fundamentals of design and operation. Berlin: Springer Verlag.

Mitchell DA, Do DD, Greenfield PF, Doelle HW. 1991. A semimechanistic mathematical model for growth of *Rhizopus oligosporus* in a model solid-state fermentation system. Biotechnol Bioeng 38: 353-362.

Mitchell DA, von Meien OF, Krieger N, Dalsenter FDH. 2004. A review of recent developments in modeling of microbial growth kinetics and intraparticle phenomena in solid-state fermentation. Biochem Eng J 17: 15-26.

Nagel F, Tramper J, Bakker MSN, Rinzema A. 2001. Model for on-line moisture-content control during solid-state fermentation. Biotechnol Bioeng 72: 231-243.

Nagel FJ, Oostra J, Tramper J, Rinzema A. 1999. Improved model system for solid-substrate fermentation: effects of pH, nutrients and buffer on fungal growth rate. Proc Biochem 35: 69-75.

Nagel FJ, Van As H, Tramper J, Rinzema A. 2002. Water and glucose gradients in the substrate measured with NMR imaging during solid-state fermentation with *Aspergillus oryzae*. Biotechnol Bioeng 79: 653-663.

Norsker NH, Barbosa MJ, Vermue MH, Wijffels RH. 2011. Microalgal production - A close look at the economics. Biotechnol Adv 29: 24-27.

Olsvik E, Kristiansen B. 1994. Rheology of filamentous fermentations. Biotechnol Adv 12: 1-39.

Oostra J, le Comte EP, van den Heuvel JC, Tramper J, Rinzema A. 2001. Intra-particle oxygen diffusion limitation in solid-state fermentation. Biotechnol Bioeng 75: 13-24.

Pandey A. 2003. Solid-state fermentation. Biochem Eng J 13: 81-84.

Papanikolaou S, Aggelis G. 2002. Lipid production by *Yarrowia lipolytica* growing on industrial glycerol in a single-stage continuous culture. Bioresour Technol 82: 43-49.

Papanikolaou S, Aggelis G. 2003. Modeling lipid accumulation and degradation in *Yarrowia lipolytica* cultivated on industrial fats. Curr Microbiol 46: 398-402.

Papanikolaou S, Komaitis M, Aggelis G. 2004a. Single cell oil (SCO) production by *Mortierella isabellina* grown on high-sugar content media. Bioresour Technol 95: 287-291.

Papanikolaou S, Sarantou S, Komaitis M, Aggelis G. 2004b. Repression of reserve lipid turnover in *Cunninghamella echinulata* and *Mortierella isabellina* cultivated in multiple-limited media. J Appl Microbiol 97: 867-875.

Papanikolaou S, Galiotou-Panayotou M, Fakas S, Komaitis M, Aggelis G. 2007. Lipid production by oleaginous *Mucorales* cultivated on renewable carbon sources. Eur J Lipid Sci Technol 109: 1060-1070.

Papanikolaou S, Aggelis G. 2009. Biotechnological valorization of biodiesel derived glycerol waste through production of single cell oil and citric acid by *Yarrowia lipolytica*. Lipid Technol 21: 83-87.

Peng X, Chen H. 2008. Single cell oil production in solid-state fermentation by *Microsphaeropsis* sp. from steam-exploded wheat straw mixed with wheat bran. Bioresour Technol 99: 3885-3889.

Piccolo C, Bezzo F. 2009. A techno-economic comparison between two technologies for bioethanol production from lignocellulose. Biomass Bioenergy 33: 478-491.

Rahardjo YSP, Korona D, Haemers S, Weber FJ, Tramper J, Rinzema A. 2004. Limitations of membrane cultures as a model solid-state fermentation system. Lett Appl Microbiol 39: 504-508.

Rahardjo YSP, Sie S, Weber FJ, Tramper J, Rinzema A. 2005. Effect of low oxygen concentrations on growth and alpha-amylase production of *Aspergillus oryzae* in model solid-state fermentation systems. Biomol Eng 21: 163-172.

Rahardjo YSP, Tramper J, Rinzema A. 2006. Modeling conversion and transport phenomena in solid-state fermentation: A review and perspectives. Biotechnol Adv 24: 161-179.

Rajagopalan S, Modak JM. 1995. Evaluation of relative growth limitation due to depletion of glucose and oxygen during fungal growth on a spherical solid particle. Chem Eng Sci 50: 803-811.

Ratledge C, Hall MJ. 1979. Accumulation of lipid by *Rhodotorula glutinis* in continuous culture. Biotechnol Lett 1: 115-120.

Ratledge C. 1988. Biochemistry, stoichiometry, substrates and economics. In: Moreton RS, editor. Single Cell Oil. London: Longman Scientific & Technical. p 33-70.

Ratledge C, Wynn JP. 2002. The biochemistry and molecular biology of lipid accumulation in oleaginous microorganisms. Adv Appl Microbiol 51: 1-51.

Ratledge C. 2004. Fatty acid biosynthesis in microorganisms being used for Single Cell Oil production. Biochimie 86: 807-815.

Richard P, Hilditch S. 2009. d-Galacturonic acid catabolism in microorganisms and its biotechnological relevance. Appl Microbiol Biotechnol 82: 597-604.

Rittmann BE. 2008. Opportunities for renewable bioenergy using microorganisms. Biotechnol Bioeng 100: 203-212.

Roels JA. 1983. Energetics and kinetics in biotechnology. Amsterdam: Elsevier.

Ruijter GJG, Visser J, Rinzema A. 2004. Polyol accumulation by *Aspergillus oryzae* at low water activity in solid-state fermentation. Microbiology 150: 1095-1101.

Sattur AP, Karanth NG. 1989. Production of microbial lipids. 1. Development of a mathematical model. Biotechnol Bioeng 34: 863-867.

Sattur AP, Karanth NG. 1991. Mathematical modeling of production of microbial lipids. 1. Kinetics of biomass growth. Bioprocess Eng. 6: 227-234.

Schipperus R, Teeuwen RLM, Werten MWT, Eggink G, de Wolf FA. 2009. Secreted production of an elastin-like polypeptide by *Pichia pastoris*. Appl Microbiol Biotechnol 85: 293-301.

Shinmen Y, Shimizu S, Akimoto K, Kawashima H, Yamada H. 1989. Production of Arachidonic-Acid by Mortierella Fungi - Selection of a Potent Producer and Optimization of Culture Conditions for Large-Scale Production. Appl Microbiol Biotechnol 31: 11-16.

Soderberg AC. 1997. Fermentation design. In: Vogel HC, Todaro CL, editors. Fermentation and biochemical engineering handbook. Westwood: Noyes Publications. p 67-121.

Somashekar D, Venkateshwaran G, Sambaiah K, Lokesh BR. 2003. Effect of culture conditions on lipid and gamma-linolenic acid production by mucoraceous fungi. Proc Biochem 38: 1719-1724.

Song YD, Wynn JP, Li YH, Grantham D, Ratledge C. 2001. A pre-genetic study of the isoforms of malic enzyme associated with lipid accumulation in *Mucor circinelloides*. Microbiology 147: 1507-1515.

Spagnuolo M, Crecchio C, Pizzigallo MDR, Ruggiero P. 1997. Synergistic effects of cellulolytic and pectinolytic enzymes in degrading sugar beet pulp. Bioresour Technol 60: 215-222.

Stredanska S, Sajbidor J. 1993. Influence of carbon and nitrogen sources on the lipid accumulation and arachidonic acid production by *Mortierella alpina*. Acta Biotechnologica 13: 185-191.

Stredanska S, Slugen D, Stredansky M, Grego J. 1993. Arachidonic acid production by *Mortierella alpina* grown on solid substrates. World J Microbiol Biotechnol 9: 511-513.

Stredansky M, Conti E, Stredanska S, Zanetti F. 2000. gamma-Linolenic acid production with *Thamnidium elegans* by solid-state fermentation on apple pomace. Bioresour Technol 73: 41-45.

Sugama S, Okazaki N. 1979. Growth Of Koji Mold On The Surface Of Steamed Rice Grains. 5. Growth Estimation Of Aspergillus-Oryzae Cultured On Solid Media. J Ferm Technol 57: 408-412.

Umecky T, Kuga T, Funazukuri T. 2006. Infinite dilution binary diffusion coefficients of several alpha-amino acids in water over a temperature range from (293.2 to 333.2) K with the Taylor dispersion technique. J Chem Eng Data 51: 1705-1710.

Vamvakaki AN, Kandarakis I, Kaminarides S, Komaitis M, Papanikolaou S. 2010. Cheese whey as a renewable substrate for microbial lipid and biomass production by *Zygomycetes*. Eng Life Sci 10: 348-360.

Van 't Riet K, Tramper J. 1991. Basic bioreactor design. New York: Marcel Dekker, INC.

Vicente G, Bautista LF, Gutierrez FJ, Rodriguez R, Martinez V, Rodriguez-Frometa RA, Ruiz-Vazquez RM, Torres-Martinez S, Garre V. 2010. Direct Transformation of Fungal Biomass from Submerged Cultures into Biodiesel. Energy Fuels 24: 3173-3178.

Vishniac W, Santer M. 1957. *Thiobacilli*. Bacteriol Rev 21: 195-213.

Walker GM. 2011. 125th Anniversary Review: Fuel Alcohol: Current Production and Future Challenges. J Inst Brew 117: 3-22.

Weber FJ, Tramper J, Rinzema A. 1999a. Quantitative recovery of fungal biomass grown on solid kappa-carrageenan media. Biotechnol Tech 13: 55-58.

Weber FJ, Tramper J, Rinzema A. 1999b. A simplified material and energy balance approach for process development and scale-up of *Coniothyrium minitans* conidia production by solid-state cultivation in a packed-bed reactor. Biotechnol Bioeng 65: 447-458.

Weber FJ, Oostra J, Tramper J, Rinzema A. 2002. Validation of a model for process development and scale-up of packed-bed solid-state bioreactors. Biotechnol Bioeng 77: 381-393.

Werten MWT, Wisselink WH, van den Bosch TJJ, de Bruin EC, de Wolf FA. 2001. Secreted production of a custom-designed, highly hydrophilic gelatin in *Pichia pastoris*. Protein Eng 14: 447-454.

Wijffels RH. 2008. Potential of sponges and microalgae for marine biotechnology. Trends Biotechnol 26: 26-31.

Wijffels RH, Barbosa MJ. 2010. An outlook on microalgal biofuels. Science 239: 796-799.

Wynn JP, Hamid ABA, Ratledge C. 1999. The role of malic enzyme in the regulation of lipid accumulation in filamentous fungi. Microbiology UK 145: 1911-1917.

Wynn JP, Hamid AA, Li YH, Ratledge C. 2001. Biochemical events leading to the diversion of carbon into storage lipids in the oleaginous fungi *Mucor circinelloides* and *Mortierella alpina*. Microbiology 147: 2857-2864.

Ykema A, Verbree EC, Vanverseveld HW, Smit H. 1986. Mathematical modeling of lipid production by oleaginous yeasts in continuous cultures. Antonie Van Leeuwenhoek 52: 491-506.

Ykema A, Bakels RHA, Verwoert I, Smit H, Vanverseveld HW. 1989. Growth yield, maintenance requirements, and lipid formation in the oleaginous yeast *Apiotrichum curvatum*. Biotechnol Bioeng 34: 1268-1276.

Yoon SH, Rhee JA. 1983. Quantitative physiology of *Rhodotorula glutinis* for microbial lipid production. Proc Biochem 18: 2-4.

Zhu LY, Zong MH, Wu H. 2008. Efficient lipid production with *Trichosporon fermentans* and its use for biodiesel preparation. Bioresour Technol 99: 7881-7885.

Zinn M, Witholt B, Egli T. 2004. Dual nutrient limited growth: models, experimental observations, and applications. J Biotechnol 113: 263-279.

List of symbols

List of symbols

A	Surface area of fungus (m^2)
C_{EP}	Concentration of extracellular product (Cmol m^{-3})
c_g	Specific heat dry air (kJ kg^{-1} K^{-1})
C_{IP}	Carbohydrate concentration (Cmol m^{-3})
C_L	Lipid concentration (Cmol m^{-3})
C_N	N-source concentration (Nmol m^{-3})
C_{Nin}	N-source concentration in feed (Nmol m^{-3})
$C_N(x)$	N-source concentration at position *x* (Nmol m^{-3})
$C_O(x)$	Oxygen concentration at position *x* (mol m^{-3})
C_{Og1}	Oxygen concentration of ingoing air (mol m^{-3})
C_{Ol}	Oxygen concentration in fermentation liquid (mol m^{-3})
C_S	C-source concentration (Cmol m^{-3})
c_S	Specific heat solid substrate (kJ kg^{-1} K^{-1})
C_{Sin}	C-source concentration in feed (Cmol m^{-3})
$C_{S,n}$	C-source concentration in sub-layer *n* of gel (Cmol m^{-3})
$C_S(x)$	C-source concentration at position *x* (Cmol m^{-3})
c_w	Specific heat water and medium (kJ kg^{-1} K^{-1})
c_{wv}	Specific heat water vapor (kJ kg^{-1} K^{-1})
C_X	Basic biomass concentration (Cmol m^{-3})
$C_{X\max}$	Maximum basic biomass concentration (Cmol m^{-3})
D	Dilution rate (h^{-1})
D_{min}	Dilution rate above which lipid accumulation starts at a certain C/N-ratio in the feed (h^{-1})
D_{opt}	Dilution rate at which the highest lipid concentration and yield is reached with a certain C/N-ratio in the feed (h^{-1})
d_p	Particle diameter in SSF (m)
D_s	Diameter of stirrer (m)
D_t	Diameter of fermenter tank (m)
F_g	Gas flow rate (m^3 s^{-1})
f_{IPmax}	Maximum fraction of carbohydrates in the cells (Cmol carbohydrates (Cmol basic biomass)$^{-1}$)
f_L	Fraction of lipids in total biomass (Cmol lipids (Cmol total biomass)$^{-1}$)
f_{L0}	Minimum fraction of lipids in total biomass (Cmol lipids (Cmol total biomass)$^{-1}$)
f_{solids}	Fraction of dry weight in biofilm (g g^{-1})

H	Height of fermenter (m)
h_g	Enthalpy of moist air (J kg^{-1})
H_s	Height of stirrer from bottom of tank (m)
H_t	Height of fermenter tank for calculations (m)
ID_N	Diffusion coefficient of N-source (m^2 s^{-1})
ID_O	Diffusion coefficient of oxygen (m^2 s^{-1})
ID_S	Diffusion coefficient of C-source (m^2 s^{-1})
k_d	Lipid production rate degradation constant (h^{-1})
k_{olA}	Oxygen transfer coefficient (s^{-1})
L_f	Thickness of biofilm (m)
L_g	Thickness of gel layer (m)
L_i	Thickness of sub-layer *i* in biofilm (m)
L_N	Penetration boundary of N-source (m)
L_O	Penetration boundary of oxygen (m)
L_S	Penetration boundary of C-source (m)
$L \times W$	Length x width of packed bed (m×m)
L_0	Thickness of anaerobic sub-layer in biofilm (m)
L_1	Thickness of sub-layer in biofilm with N-source, C-source and oxygen (m)
L_2	Thickness of sub-layer in biofilm with C-source and oxygen (m)
L_3	Thickness of sub-layer in biofilm with only oxygen (m)
m	Distribution coefficient oxygen air/water (-)
m_{EP}	Maintenance coefficient on extracellular product (Cmol $Cmol^{-1}$ h^{-1})
M_g	Mass of gel layer (kg)
M_{IP}	Amount of intracellular product produced (Cmol or kg)
M_L	Amount of lipids produced (Cmol or kg)
m_L	Maintenance coefficient on lipids (Cmol $Cmol^{-1}$ h^{-1})
m_S	Maintenance coefficient on C-source (Cmol $Cmol^{-1}$ h^{-1})
M_X	Amount of basic biomass produced (Cmol or kg)
N	Stirrer speed (s^{-1})
$N_N(x)$	Flux of N-source over *x* (Nmol m^{-2} h^{-1})
$N_O(x)$	Flux of oxygen over *x* (mol m^{-2} h^{-1})
N_p	Power number stirred fermenter (-)
$N_S(x)$	Flux of C-source over *x* (Cmol m^{-2} h^{-1})
OTR	Oxygen transfer rate (mol m^{-3} s^{-1})

p_a	Ambient pressure (Pa)
p_e	Local pressure of aeration gas at entrance of fermenter (Pa)
P_g	Power consumption for aeration (MJ m^{-3} h^{-1})
P_s	Power consumption for stirring (MJ m^{-3} h^{-1})
p_s	Local pressure of aeration gas at stirrer (MJ m^{-3} h^{-1})
P_t	Total power consumption for oxygen transfer (MJ m^{-3} h^{-1})
p_w	Partial pressure of water in air (Pa)
q_{EP}	Specific extracellular product production rate (Cmol $Cmol^{-1}$ h^{-1})
q_{IP}	Specific carbohydrate production rate (Cmol $Cmol^{-1}$ h^{-1})
q_L	Specific lipid production rate (Cmol $Cmol^{-1}$ h^{-1})
$q_{L\max}$	Maximum specific lipid production rate (Cmol $Cmol^{-1}$ h^{-1})
$q_{L\min}$	Minimum specific lipid production rate (Cmol $Cmol^{-1}$ h^{-1})
q_S	Specific C-source consumption rate (Cmol $Cmol^{-1}$ h^{-1})
$q_{S\max}$	Maximum specific C-source consumption rate (Cmol $Cmol^{-1}$ h^{-1})
r_C	CO_2-production rate (Cmol m^{-3} h^{-1})
r_{EP}	Production rate of extracellular product (Cmol m^{-3} h^{-1})
$r_{EP,i}$	Production rate of extracellular product in sub-layer *i* in biofilm (Cmol m^{-3} h^{-1})
r_{IP}	Production rate of intracellular product (Cmol m^{-3} h^{-1})
$r_{IP,i}$	Production rate of intracellular product in sub-layer *i* in biofilm (Cmol m^{-3} h^{-1})
r_L	Lipid production rate (Cmol m^{-3} h^{-1})
$r_{L,i}$	Lipid production rate in sub-layer *i* in biofilm (Cmol m^{-3} h^{-1})
r_N	N-source production rate (mol m^{-3} h^{-1})
$r_{N,i}$	N-source production rate in sub-layer *i* in biofilm (Nmol m^{-3} h^{-1})
r_O	Oxygen production rate (mol m^{-3} h^{-1})
$r_{O,i}$	Oxygen production rate in sub-layer *i* in biofilm (mol m^{-3} h^{-1})
r_S	C-source production rate (Cmol m^{-3} h^{-1})
$r_{S,i}$	C-source production rate in sub-layer *i* in biofilm (Cmol m^{-3} h^{-1})
r_W	Water production rate (mol m^{-3} h^{-1})
r_X	Basic biomass production rate (Cmol m^{-3} h^{-1})
$r_{X,i}$	Basic biomass production rate in sub-layer *i* in biofilm (Cmol m^{-3} h^{-1})
r_0	Metabolism under anaerobic conditions (Cmol m^{-3} h^{-1})
r_1	Metabolism when C-source, N-source and oxygen are available (Cmol m^{-3} h^{-1})
r_2	Metabolism when C-source and oxygen are available (Cmol m^{-3} h^{-1})
r_3	Metabolism when only oxygen is available (Cmol m^{-3} h^{-1})

T	Temperature (K)
T_{in}	Temperature of ingoing air (K)
T_{out}	Temperature of outgoing air (K)
T_{ref}	Reference temperature (K)
t	Time (h)
t_c	Circulation time of liquid in STR (s)
t_{12}	Time point of transition from growth phase to lipid production phase (h)
t_{2ab}	Time point when the maximum carbohydrate fraction is reached (h)
t_{23}	Time point of transition from lipid production phase to lipid turnover phase (h)
V_l	Liquid volume of fermenter (m^3)
v_{gs}	Superficial gas velocity (m s^{-1})
x, x_1, x_2	Arbitrary position in biofilm (m)
y	Compressibility constant of air (-)
Y_{EPS}	Yield of extracellular product on C-source (Cmol $Cmol^{-1}$)
Y_{IPS}	Yield of carbohydrates on C-source (Cmol $Cmol^{-1}$)
Y_{LS}	Yield of lipids on C-source (Cmol $Cmol^{-1}$)
Y_{XC}	Yield of basic biomass on all carbon sources (Cmol $Cmol^{-1}$)
Y_{XN}	Yield of basic biomass on nitrogen source (Cmol $Nmol^{-1}$)
Y_{XS}	Yield of basic biomass on carbon source (Cmol $Cmol^{-1}$)
y_w	Water content air (kg water/kg dry air)
γ_{EP}	Degree of reduction of extracellular product (6 $Cmol^{-1}$)
γ_L	Degree of reduction of lipids (5.73 $Cmol^{-1}$)
γ_O	Degree of reduction of oxygen (-4 mol^{-1})
γ_{IP}	Degree of reduction of carbohydrates (4 $Cmol^{-1}$)
γ_N	Degree of reduction of alanine (4 $Cmol^{-1}$)
γ_S	Degree of reduction of C-source (4 $Cmol^{-1}$)
γ_X	Degree of reduction of basic biomass (4.16 $Cmol^{-1}$)
ΔH_0	Heat production metabolism (MJ/mole O_2 produced)
ΔH_w	Evaporation enthalpy water (MJ kg^{-1})
Δp_b	Pressure drop over packed bed (Pa)
ΔT	Temperature difference (K)
Δt	Time step in Euler method (s or h)
ε	Void fraction of reactor (-)
η_c	Viscosity of fermentation culture (N s m^{-2})
η_w	Viscosity of water (N s m^{-2})

μ	Specific growth rate (h^{-1})
μ_a	Kinematic viscosity of air (Pa s)
μ_{max}	Maximum specific growth rate (h^{-1})
ρ_a	Density of moist air (kg m^{-3})
ρ_f	Density of fermentation culture (kg m^{-3})
ρ_g	Density of gel layer (kg m^{-3})
ρ_s	Density of (wet) solid substrate (kg m^{-3})
ρ_X	Density of biofilm (kg m^{-3})

Subscripts

C	CO_2
EP	Extracellular product
i	Number of sub-layer in biofilm, can be 0-3
IP	Intracellular product; carbohydrates
L	Lipids
n	Number of sub-layer in gel, can be 1-10
N	Nitrogen source
O	Oxygen
S	Carbon source
W	Water
x	Position in biofilm, can be x, 0, L_N, L_S, L_O, L_f
X	Basic biomass; total biomass minus intracellular product and lipids

Summary

Summary

Finding alternatives for fossil fuels is currently urgent. One of the new processes in this field is the production of biodiesel from lipids accumulated by microorganisms. Some yeasts and fungi accumulate lipids when a component needed for growth, usually the N-source, is limiting while the C-source is in excess. These oleaginous yeasts and fungi were previously mainly used for unsaturated fatty acid production, but now also come into view for production of lipids as a source of biodiesel.

This thesis takes the first steps in the development of a new process to produce lipids with an oleaginous fungus in solid-state fermentation on agro-industrial waste. Solid-state fermentation is the cultivation on solid substrate particles without (free) flowing water, and has several advantages over submerged fermentation such as less waste water production, less energy use for oxygen transfer and lower production costs. In this thesis, we focused on growth and lipid production kinetics in submerged as well as solid-state fermentation. The models developed for these systems provide insight in the lipid production mechanism, needed to develop the new process based on solid-state fermentation.

The thesis starts with the selection of a model strain (Chapter 2). With this strain, the kinetics of growth and lipid accumulation were studied and modeled. We started with a steady-state model (Chapter 3 and 4) in submerged chemostat culture, and extended this to a dynamic model for submerged batch culture (Chapter 5). As the next step towards solid-state fermentation, we developed a model for growth and lipid accumulation on κ-carrageenan plates with monomers (Chapter 6). These three models were finally used to calculate potential lipid yield and energy use in a biodiesel production system (Chapter 7).

For the system we want to develop, we need a fungus that can utilize different substrates and can produce lipids. For this purpose, we tested two oleaginous fungi: *Mortierella alpina* and *Umbelopsis isabellina*, which is described in **Chapter 2.** We cultivated both fungi on agar plates containing glucose, xylose, starch, cellulose or pectin, and on sugar beet pulp in a packed bed. *M. alpina* did not utilize xylose, cellulose and pectin, utilized starch much slower than glucose and only consumed approximately 40% of the sugar beet pulp in 20 days. This shows that *M. alpina* is not a suitable organism for our production system. *U. isabellina*

utilized pectin and xylose with the same rate as glucose, but used starch slower and (crystalline) cellulose not at all. It consumed approximately 75% of the sugar beet pulp after 8 days and approximately 100% after 20 days. Also, it accumulated some lipids (3% of remaining dry mass) in the culture on sugar beet pulp; optimization of this process by addition of enzymes increased the lipid content to 9% of remaining dry mass. This shows that *U. isabellina* is a promising strain for lipid production from agro-industrial waste, and is therefore a good strain to use in our research.

The lipid concentrations found in SSF culture were quite low; we therefore decided to look in more depth into the kinetics of lipid production in different model systems. The first model system was a submerged chemostat culture, because the substrate supply rates can be varied in this system by varying the dilution rate as well as the concentrations in the feed. **Chapter 3** describes the development of a mathematical model that includes growth, lipid accumulation and substrate consumption of oleaginous fungi in submerged chemostat cultures. Key points of the model are: (1) If the C-source supply rate is limited, maintenance has a higher priority than growth, which has a higher priority than lipid production; (2) the maximum specific lipid production rate of the fungus is independent of the actual specific growth rate. This model was validated with chemostat cultures of *U. isabellina* grown on mineral media with glucose and NH_4^+. Because of practical problems at low dilution rates, the model could only be validated for $D>0.04\ h^{-1}$. For further validation, published data sets for chemostat cultures of oleaginous yeasts and a published data set for a poly-hydroxyalkanoate accumulating bacterial species were used, which is described in **Chapter 4**. All data sets could be described well by the model. Analysis of all data showed that the maximum specific lipid production rate is in most cases very close to the specific production rate of membrane and other functional lipids for cells growing at their maximum specific growth rate. The limiting factor suggested by Ykema et al. (1986), *i.e.* the maximum glucose uptake rate, did not give good predictions of the maximum lipid production rate. The model shows that both the C/N-ratio of the feed as well as the dilution rate has a large influence on the lipid production rate. When these data are translated to SSF, it means that a low substrate supply rate can prevent lipid production, even when the C/N-ratio of the substrate is high.

The next step towards understanding lipid accumulation was a model that also describes changes in time. Therefore, we developed a model for growth, lipid production and lipid turnover in submerged batch fermentation, which is shown in **Chapter 5**. This model describes three subsequent phases: exponential growth when both a C-source and an N-source are available, carbohydrate and lipid production when the N-source is exhausted, and turnover of accumulated lipids when the C-source is exhausted. The model was validated with submerged batch cultures of *U. isabellina* with two different initial C/N-ratios. In batch culture, the specific lipid production rate was almost four times higher than in chemostat cultures and it decreased exponentially in time. This indicates that different mechanisms for lipid production are active in batch and chemostat cultures. The model could also describe several data sets from literature very well. Furthermore, the model shows that local limitation of C-source in SSF can cause lipid turnover before the average C-source concentration in the substrate is zero.

The next step towards an SSF system is the inclusion of diffusion in the batch model. We did this by developing a model that describes growth, lipid production and lipid turnover in a culture on κ-carrageenan plates containing the monomers glucose and alanine as C-source and N-source, respectively. This is described in **Chapter 6**. The model includes reaction kinetics and diffusion of glucose, alanine and oxygen. It was validated with *U. isabellina* and describes the different phases of the culture very well: exponential growth, linear growth because of oxygen limitation, accumulation of lipids and carbohydrates after local N-depletion and turnover of lipids after local C-depletion. Extending the model with an unidentified extracellular product improved the fit of the model to the data. The model shows that oxygen limitation is extremely important in solid-state cultures using monomers. Together with the low specific lipid production rate found in SSF, it explains the difference in production rate with submerged cultures.

In **Chapter 7**, we used the models from Chapter 3, 5 and 6 together with basic engineering principles to calculate lipid yield and energy use in the modeled systems. We evaluated a process including pretreatment, cultivation and down-stream processing with sugar beet pulp and wheat straw as substrate, described different reactor types, and considered both a yeast and a fungus as

microorganisms. According to the models, lipid yields on substrate were between 5% w/w and 19% w/w, depending on the culture system. With the same models, improvement of the yield to 25-30% w/w was shown to be possible, for example by genetic modification of the microorganism. The net energy ratio of the non-optimized systems varied between 0.8 and 2.5 MJ produced per MJ used; energy use for pretreatment and for oxygen transfer were most important. For the optimized systems, the net energy ratio increased to 2.9 – 5.5 MJ produced per MJ used, which can compete very well with other biofuels such as bioethanol or algal biodiesel. So although there is still quite some work to be done, microbial lipids have the potential to be tomorrow's source of biodiesel.

Samenvatting

Samenvatting

Het vinden van alternatieven voor fossiele brandstoffen wordt steeds urgenter. Een nieuw proces op dit gebied is de productie van biodiesel uit vetten die door micro-organismen worden geproduceerd. Sommige schimmels en gisten slaan vetten op in hun cellen als één van de componenten voor groei (meestal de stikstofbron) limiterend is terwijl de koolstofbron in overmaat aanwezig is. Deze vetophopende gisten en schimmels werden tot nu toe vooral gebruikt voor de productie van onverzadigde vetzuren, maar komen nu ook in beeld voor de productie van vetten als grondstof voor biodiesel.

Dit proefschrift beschrijft de eerste stappen in de ontwikkeling van een nieuw proces om uit agro-industrieel afval vetten te produceren met een vetophopende schimmel in vaste stoffermenatie. Vaste stoffermentatie is het kweken van (filamenteuze) organismen op vaste substraatdeeltjes zonder (vrij) water, en heeft verschillende voordelen ten opzichte van vloeistoffermentatie zoals minder afvalwater, minder energiegebruik voor zuurstofoverdracht en lagere productiekosten. In dit proefschrift ligt de nadruk op het modelleren van groei- en vetproductiekinetiek in vloeistoffermentatie en vaste stoffermentatie. De modellen die beschreven zijn in dit proefschrift voor deze systemen geven inzicht in het vetproductiemechanisme, op basis waarvan een nieuw proces ontwikkeld kan worden op basis van vaste stoffermentatie.

Het onderzoek beschreven in dit proefschrift begint met de selectie van een modelschimmel (hoofdstuk 2). Met deze schimmel zijn de groei- en vetproductiekinetiek bepaald en gemodelleerd. We zijn begonnen met een steady-state model (hoofdstukken 3 en 4) voor chemostaat in vloeistoffermentatie, en hebben dit uitgebreid naar een dynamisch model voor batch cultuur in vloeistoffermentatie (hoofdstuk 5). Als de volgende stap naar vaste stoffermentatie hebben we een model voor groei en vetproductie ontwikkeld op κ-carrageenplaten met monomeren als substraat (hoofdstuk 6). Deze drie modellen zijn uiteindelijk gecombineerd om de mogelijke vetopbrengst en het energieverbruik te berekenen in een productiesysteem voor biodiesel (hoofdstuk 7).

Voor het system dat we willen ontwikkelen hebben we een schimmel nodig die verschillende substraten kan gebruiken en vet kan produceren. Voor dit doel hebben we twee vetophopende schimmels getest: *Mortierella alpina* en *Umbelopsis isabellina*. Dit is beschreven in **Hoofdstuk 2**. We hebben beide schimmels gekweekt op agarplaten met glucose, xylose, zetmeel, cellulose of pectine, en op suikerbietenpulp in een gepakt bed. *M. alpina* gebruikte xylose, cellulose en pectine niet, gebruikte zetmeel veel langzamer dan glucose en consumeerde maar ongeveer 40% van de suikerbietenpulp in 20 dagen. Dit laat zien dat *M. alpina* niet geschikt is voor ons productiesysteem. *U. isabellina* gebruikte pectine en xylose met dezelfde snelheid als glucose, maar gebruikte zetmeel langzamer en (kristallijne) cellulose helemaal niet. Hij consumeerde ongeveer 75% van de suikerbietenpulp in 8 dagen en ongeveer 100% in 20 dagen. Daarnaast hoopte hij een beetje vetten op (3% van de resterende droge massa) in de kweek op suikerbietenpulp. Optimalisatie van dit proces door de toevoeging van enzymen deed het vetgehalte toenemen tot 9% van de resterende droge massa. Dit laat zien dat *U. isabellina* een veelbelovende schimmel is voor vetproductie op agro-industrieel afval, en daarom een goede schimmel voor ons onderzoek.

The vetconcentraties die gehaald werden in vaste stoffermentatie waren nogal laag (in hoofdstuk 2). Daarom besloten we om de vetproductiekinetiek in meer detail the gaan bekijken in verschillende modelsystemen. Het eerste modelsysteem was een chemostaat vloeistofcultuur omdat in dat systeem de substraat toevoersnelheden kunnen worden gevarieerd door zowel de verdunningssnelheid als de concentraties in de toevoerstroom te variëren. **Hoofdstuk 3** beschrijft de ontwikkeling van een wiskundig model dat groei, vetproductie en substraatconsumptie beschrijft voor vetophopende schimmels in chemostaat vloeistofcultuur. De belangrijkste punten in dit model zijn: (1) Als de toevoersnelheid van de koolstofbron limiterend is, krijgt maintenance een hogere prioriteit dan groei, wat weer een hogere prioriteit krijgt dan vetproductie; (2) De maximale specifieke vetproductiesnelheid van de schimmel is onafhankelijk van de actuele specifieke groeisnelheid. Dit model werd gevalideerd met chemostaat cultures met *U. isabellina* op mineraal medium met glucose en NH_4^+. Vanwege praktische problemen bij lage verdunningssnelheden kon het model alleen gevalideerd worden voor D>0.04 h^{-1}. In **Hoofdstuk 4** is een verdere validatie

beschreven door gepubliceerde datasets van chemostaatcultures met vetophopende gisten en een dataset voor een PHA-ophopende bacterie te gebruiken. Alle datasets konden goed beschreven worden door het model. De analyse van alle data liet zien dat de maximale specifieke vetproductiesnelheid in de meeste gevallen dichtbij de productiesnelheid ligt van membraanlipiden en andere functionele vetten die aanwezig is tijdens maximale groei. De limiterende factor die gesuggereerd werd door Ykema et al. (1986), namelijk de maximale glucose opnamesnelheid, gaf geen goede voorspellingen voor de maximale specifieke vetproductiesnelheid. Het model laat zien dat zowel de C/N-ratio in de toevoer als de verdunningssnelheid invloed hebben op de vetproductiesnelheid. Als deze data worden vertaald naar vaste stoffermentatie, betekent dit dat een lage aanvoersnelheid van substraat de vetproductie kan tegenhouden, zelfs als de C/N-ratio van het substraat hoog is.

De volgende stap in het begrijpen van vetproductie is een model dat ook veranderingen in de tijd beschrijft. Daarom ontwikkelden we een model voor groei, vetproductie en vetafbraak in batch vloeistofcultuur, dat beschreven is in **Hoofdstuk 5**. Dit model beschrijft drie opeenvolgende fasen: 1) exponentiële groei als zowel de koolstofbron als de stikstofbron aanwezig zijn, 2) de productie van vetten en koolhydraten wanneer de stikstofbron op is, en 3) vetafbraak wanneer de koolstofbron op is. Het model werd gevalideerd met een batch vloeistofcultuur van *U. isabellina* met twee verschillende initiële C/N-ratios. In batch cultuur was de initiële specifieke vetproductie snelheid bijna vier keer hoger dan in chemostaat cultuur, maar deze verminderde exponentieel in de tijd. Dit wijst op verschillende mechanismes in batch en chemostaat cultuur. Het model kon ook verschillende datasets uit de literatuur beschrijven. Verder laat het model zien dat lokale limitatie van de koolstofbron in vaste stoffermentatie kan leiden tot vetafbraak voordat de gemiddelde koolstofbronconcentratie nul is.

De volgende stap naar vaste stoffermentatie was het inbouwen van diffusie in het batch model. We deden dit door het ontwikkelen van een model dat groei, vetproductie en vetafbraak beschrijft in een cultuur op κ-carrageenplaten met de monomeren glucose als C-bron en alanine als N-bron. Dit is beschreven in **Hoofdstuk 6**. Het model omvat reactiekinetiek en diffusie van glucose, alanine en zuurstof. Het werd gevalideerd met *U. isabellina* en beschrijft de verschillende

fases van de cultuur goed: exponentiele groei, lineaire groei vanwege zuurstoflimitatie, ophoping van vetten een koolhydraten na lokale N-depletie en vetafbraak na lokale C-depletie. Het uitbreiden van het model met een ongeïdentificeerd extracellulair product maakte de fit van het model op de data beter. Het model laat zien dat zuurstoflimitatie erg belangrijk is in vaste stoffermentatie op monomeren. Samen met de lage specifieke vetproductiesnelheid in vaste stoffermentatie verklaart dit het verschil in productiesnelheid met vloeistoffermentaties.

In **Hoofstuk 7** gebruikten we de modellen van Hoofdstuk 3, 5 en 6 samen met technologische principes om de vetopbrengst en het energiegebruik van de gemodelleerde systemen te berekenen. We evalueerden een proces inclusief voorbehandeling, kweek en opwerking met suikerbietenpulp en tarwestro als substraten met daarin verschillende reactortypes, en namen zowel een gist als een schimmel mee in ons ontwerp. Volgens de modellen liggen de vetopbrengsten tussen de 5% en 19% g/g, afhankelijk van het cultuursysteem. Met dezelfde modellen kon de opbrengst verbeterd worden tot 25-30% g/g, bijvoorbeeld door genetische modificatie van het micro-organisme. De netto energie ratio van de niet-geoptimaliseerde systemen varieerde tussen 0.8 en 2.5 MJ geproduceerde energie per MJ gebruikte energie, waarin energiegebruik voor voorbehandeling en zuurstofoverdracht de belangrijkste energieconsumerende processen waren. Voor de geoptimaliseerde systemen was de netto energie ratio 2.9 – 5.5 MJ geproduceerd per MJ gebruikt, wat goed kan concurreren met andere biobrandstoffen zoals bioethanol of algen biodiesel. Dus hoewel er nog veel werk te doen is, zijn microbiële vetten een potentiële grondstof voor de biodiesel van de toekomst.

Samenvatting

voor gewone mensen

Biodiesel voor dummies

Zoals bijna niemand ontgaan kan zijn, wordt er hard gezocht naar alternatieven voor aardolieproducten. Of het nu is omdat het steeds moeilijker (en dus duurder) wordt om olie uit de grond te halen, om niet meer afhankelijk te zijn van olie-producerende landen, of vanwege de klimaatverandering, er wordt volop onderzoek gedaan naar alternatieve brandstoffen voor onder andere onze auto's. Het onderzoek beschreven in dit boekje hoort daar ook bij: het gaat over een nieuwe manier om biodiesel te maken.

Biodiesel wordt op dit moment voornamelijk gemaakt van plantaardige olie, zoals bijvoorbeeld palmolie, koolzaadolie en zonnebloemolie, of uit gerecycled (frituur)vet uit restaurants, snackbars en vetinleverpunten bij supermarkten. Vooral het recyclen van vet is redelijk milleuvriendelijk, maar er wordt niet genoeg frituurvet gebruikt in Nederland om alle dieselauto's op te laten rijden. Biodiesel uit plantaardige olie is een stuk minder mileuvriendelijk: voor het verbouwen van de oliegewassen zoals oliepalmen of koolzaad wordt flink wat energie (vooral diesel voor landbouwmachines) gebruikt, en bovendien wordt er veel landbouwgrond voor gebruikt, waarop ook iets anders zoals voedselgewassen of regenwoud had kunnen groeien. Daarom wordt er onderzoek gedaan naar andere 'organismen' die ook 'plantaardige' olie kunnen maken: algen en schimmels. Algen zijn een soort hele kleine plantjes die je kan kweken in een bak met water of in zee: er is dus geen landbouwgrond voor nodig, maar het kweken kost nog wel erg veel energie. Dit proefschrift gaat over schimmels die 'schimmelolie' (*fungal lipids*) maken.

Schimmels zijn zogenaamde 'micro-organismen': hele kleine 'beestjes' net als bacteriën. Schimmels ken je waarschijnlijk als zwarte plekken in de badkamer, groene vlekken op beschimmeld brood of fruit, paddestoelen in het bos of mooie donzige kluwens in de groenbak. Schimmels kunnen op bijna alle soorten plantaardig materiaal groeien als het maar een beetje vochtig is: als je lang genoeg wacht, kunnen ze zelfs een boom helemaal verteren. Ze kunnen dus verschillende soorten voedingsstoffen aan: de soorten die wij ook kunnen eten (suiker, zetmeel) maar ook verschillende vezels (zoals cellulose en pectine).

Sommige schimmels kunnen 'schimmelolie' (vet) in hun cellen opslaan, eigenlijk net zoals mensen die (te) dik worden. Een schimmel gebruikt zijn voedsel om te kunnen groeien en voor wat onderhoud (*maintenance*) genoemd wordt: alles om in leven te blijven, zoals ademhalen, voedsel verteren, enzovoorts. Zolang hij genoeg voedsel heeft, zal hij blijven groeien. Om dat te kunnen doen, heeft hij net als mensen verschillende voedingsstoffen nodig: koolhydraten, eiwitten, en wat vitaminen en mineralen die we voor het gemak maar even vergeten. Alle vetten die hij nodig heeft, kan hij zelf maken uit de koolhydraten. De koolhydraten worden koolstofbron of C-bron (*C-source*) genoemd, omdat ze voor een groot deel bestaan uit het element koolstof (*Carbon*). De eiwitten worden stikstofbron of N-bron (*N-source*) genoemd, naar het Engelse woord voor het element stikstof (*Nitrogen*). Voor onderhoud heeft hij eigenlijk alleen maar energie nodig, en die haalt hij uit de koolhydraten oftewel de C-bron. Als een schimmel niet genoeg N-bron krijgt om te groeien, maar wel meer C-bron dan hij nodig heeft voor onderhoud, kan hij die extra hoeveelheid C-bron opslaan als vet, zodat hij dat later kan gebruiken als de C-bron op is. Vetproductie gebeurt dus vooral als er veel C-bron is ten opzichte van de N-bron: bij een hoge *C/N-ratio*. Een schimmel kan maar een bepaalde hoeveelheid vet opslaan. Als je dus veel vet wilt maken, moet je ook veel schimmel maken. Je hebt daarom altijd zowel N-bron als C-bron nodig.

Dan komen we nu bij het doel van mijn werk: een proces ontwikkelen om schimmelolie (voor biodiesel) te produceren. Omdat schimmels vrijwel alles kunnen eten, kunnen we ze afval voeren, zoals GFT-afval, suikerbietenpulp, stro, enzovoorts. Die bestaan vooral uit vezels die wij niet kunnen verteren, maar de schimmel wel. En hoe moet dat proces er dan uitzien? Schimmels groeien het liefst op vaste vochtige dingen, zoals rottende blaadjes, oud brood (vochtig, dus in een zak!), vochtig graan, enzovoorts. Je kunt ze dus het handigste kweken in een grote bak of op een grote hoop met vaste vochtige voedseldeeltjes. Je moet dan wel zorgen dat ze genoeg zuurstof krijgen en het niet te warm wordt, bijvoorbeeld door er lucht doorheen te blazen. Deze methode wordt vaste stoffermentatie (*solid-state fermentation*) genoemd. Een bekend voorbeeld daarvan is composteren. Het lijkt misschien heel logisch om schimmels zo te kweken, maar toch wordt het in de industrie en vooral in het onderzoek maar erg weinig gedaan. Daar wordt namelijk gebruik gemaakt van zogenaamde vloeistoffermentatie (*submerged fermentation*). Dat is het kweken van schimmels, gisten of bacteriën in

een groot vat met water waarin je het voedsel, meestal suiker, oplost. Om zuurstof in het water te krijgen, moet je flink roeren en lucht erdoor bubbelen. Deze methode is erg handig voor onderzoek, want je kunt erg goed in de gaten houden wat er gebeurt. je kunt bijvoorbeeld apart meten hoeveel micro-organisme en hoeveel suiker je hebt. Vloeistofcultuur is vooral erg handig voor gisten of bacteriën, maar minder handig voor schimmels, want de schimmeldraden zorgen ervoor dat de vloeistof erg stroperig wordt, waardoor roeren lastig is en je snel klonten krijgt. Maar aan de andere kant lukt het in vaste stoffermentatie nooit om de schimmeldraden tussen de voedseldeeltjes uit te pulken om ze apart te wegen als je wilt weten hoeveel schimmel je al hebt voor je onderzoek, dus dan is vloeistoffermentatie wel een optie.
Samengevat: ik wil dus een proces ontwikkelen voor het produceren van zoveel mogelijk schimmelolie met afval als voedsel in vaste-stoffermentatie, omdat de schimmel zich daar het beste in thuisvoelt en het bovendien stukken goedkoper is dan vloeistoffermentatie. Maar omdat je moeilijk onderzoek kunt doen in vaste stoffermentatie, heb ik daarvoor vooral vloeistoffermentatie gebruikt.

Ik ben mijn onderzoek begonnen met het zoeken naar een geschikte schimmel voor mijn experimenten: eentje die vet (schimmelolie) kan maken, en goed kan groeien op verschillende voedingsstoffen. De experimenten om die te vinden staan in hoofdstuk 2. Daar heb ik twee soorten schimmels getest die ik heb laten groeien op verschillende suikers, koolhydraten en vezels. De ene schimmel kon bijna niks opeten, de andere deed het een stuk beter. Die schimmel, *Umbelopsis isabellina*, werd dus mijn ‘proef’schimmel. Daarna heb ik hem op suikerbietenpulp laten groeien in vaste stoffermentatie. Dat deed hij ook prima, maar helaas zette hij maar een paar procent van de bietenpulp om in vet, zelfs nadat ik allerlei trucjes had geprobeerd. Bovendien hadden andere onderzoekers eerder al gevonden dat deze schimmel in vloeistoffermentatie op glucose (een soort suiker) veel meer vet kan maken. Blijkbaar gebeurt er iets anders in vaste stoffermentatie dan in vloeistoffermentatie: tijd om dat uit te gaan zoeken!

Daarom ben ik mijn schimmel gaan kweken in vloeistoffermentatie. Daarbij ben ik precies gaan kijken wat er gebeurt als je hem bepaalde hoeveelheden C-bron en N-bron geeft. Zoals verwacht maakt de schimmel inderdaad meer vet als hij veel meer C-bron dan N-bron krijgt (dus bij een hoge *C/N-ratio*), maar er zijn toch nogal

wat addertjes onder het gras. Zo vond ik dat als je de schimmel constant een klein beetje N-bron voert terwijl er heel veel C-bron is, hij veel minder snel vet maakt dan wanneer hij helemaal geen N-bron meer heeft (en wel C-bron). En dat hij zonder N-bron steeds langzamer vet gaat maken, en zijn vet weer gaat opeten als de C-bron op is. Verder vond ik dat als je schimmels heel langzaam voert met voedsel met een hoge C/N-ratio, ze bijna geen vet maken omdat ze bijna alle C-bron gebruiken voor onderhoud. Met al deze resultaten heb ik modellen gemaakt. Dat zijn wiskundige formules die beschrijven hoeveel schimmel en hoeveel vet je krijgt als je een bepaalde hoeveelheid C-bron en N-bron voert. Ik heb dat gedaan voor een constante toevoer van voedingsstoffen (*chemostat culture*) in hoofdstuk 3 en 4, en in hoofdstuk 5 voor een experiment waarbij je alles in het begin toevoegt en dan kijkt wat er gebeurt (*batch culture*). En ik heb experimenten gedaan om te laten zien dat mijn modellen kloppen. Daarna heb ik een model gemaakt voor het kweken van schimmel op schaaltjes met daarin een soort gelatine (*carrageenan*) waarin de voedingsstoffen zaten. Dat is dus een soort vaste stoffermentatie, maar met suikers als C-bron in plaats van vezels. Resultaten van deze experimenten en bijbehorend model staan in hoofdstuk 6. Hieruit bleek dat de schimmel een stuk langzamer vet ging maken dan in vloeistoffermentatie, maar waarom weet ik niet precies. Helaas was er geen tijd meer om nog verder uit te zoeken waarom vetproductie in vaste stoffermentatie zo moeilijk gaat. Maar dankzij mijn resultaten weten we nu een stuk beter hoe schimmels vet maken.

De modellen die ik gemaakt heb, heb ik gebruikt om te berekenen hoeveel biodiesel je eigenlijk kunt maken van afval, en hoeveel energie dat kost. Dat heb ik gedaan in hoofdstuk 7. Daar kwam uit dat ik met mijn ‘proef’schimmel van 100 kg bietenpulp ongeveer 5 tot 19 kg biodiesel kan maken, afhankelijk van welke manier ik gebruik (vaste stoffermentatie of vloeistoffermentatie). Dat is niet echt veel. Met mijn modellen heb ik ook bekeken hoeveel je maximaal kan maken met de beste schimmel die er maar bestaat: dat is 25-30 kg biodiesel uit 100 kg bietenpulp. Het proces kost wel flink wat energie, maar uiteindelijk kan er tot 5x zoveel energie gemaakt worden dan dat je nodig hebt voor de productie. Je hebt wel een superschimmel nodig om dit productieproces rendabel te maken, en er is dus nog meer onderzoek nodig. Met dit proefschrift heb ik de eerste stap gezet naar biodiesel uit schimmels, dus wie weet wat je over 20 jaar tankt…

Dankwoord

Dankwoord

Hoewel alleen mijn naam op de voorkant van dit boekje staat, heb ik de inhoud van dit boekje natuurlijk niet alleen voor elkaar gekregen. Daarom wil ik van deze gelegenheid gebruik maken om een aantal mensen te bedanken, want zonder hen had dit boekje hier niet gelegen.

Allereerst natuurlijk Arjen. Heel erg bedankt voor het vertrouwen dat je in me had, en dat je mijn project, wat oorspronkelijk maar voor twee jaar gefinancieerd was, hebt verlengd tot een volledig AIO-project zodat ik toch kon promoveren. En dat je vervolgens voor nog een half jaar verlenging hebt gezorgd, wat geresulteerd heeft in hoofdstuk 6. Dank je wel voor de vrijheid om zelf mijn project richting te geven, en voor de vele(!) kritische opmerkingen op mijn artikelen, waardoor er nu een proefschrift ligt om trots op te zijn.
Hans, jij kwam pas wat later in beeld omdat ik in het begin nog geen AIO was, maar daarna heb je me op je altijd positieve manier gesteund en de zwakke plekken uit mijn artikelen gehaald. Ik vond het prettig om met je samen te werken, ook tijdens mijn onderwijstaken.

Sebastiaan, ja, wat moest ik zonder jou? Jij zorgde ervoor dat mijn opstellingen altijd werkten, was de extra handjes als ik die nodig had en ving het werk op als ik weer eens ziek was. Daarnaast was je er ook voor een goed gesprek over zowel mijn plannen in het lab als over allerlei andere onderwerpen, voor heerlijk relativerende opmerkingen en voor een oppeppend woord als het een keer tegenzat. En dat is toch wel meer dan dat er in je taakomschrijving stond. Dankjewel dat je je voor mij wilt scheren en me in pinguinpak wilt bijstaan op mijn promotie.
Fred, dankjewel dat ik je reactoren mocht lenen, en voor het gratis advies erbij tijdens mijn experimenten. Jij was altijd wel in voor een praatje op het bordes, en dat hielp mij de moed erin te houden na het zoveelste mislukte chemostaat experiment.

The four students that I supervised during my thesis played a major role in achieving my results. Mirte, zowel voor jou als voor mij was het het eerste afstudeervak, en helaas heeft jouw werk zijn weg niet kunnen vinden naar dit

proefschrift. Toch heb ik veel van je geleerd, en hopelijk jij ook van mij. Payman, dankzij jouw (voorbereidende) werk had ik hoofdstuk 5 zo voor elkaar, en hoewel er in dat hoofdstuk niet direct resultaten van jou staan, heb je wat mij betreft het mede-auteurschap van het resulterende artikel zeker verdiend. Cristina, you did an enormous amount of work, for which I want to thank you, and I am glad that I managed to get some of your results into Chapter 2. Anne, zonder jou was hoofdstuk 6 er niet geweest. Jij was met je model mijn modelleerkunsten ver vooruit, en het heeft me best wat moeite gekost om dat in te halen. Ik vind het erg leuk dat jij nu als AIO weer gebruik maakt van mijn modellen.

Mijn project is begonnen als onderdeel van MACHT: Microbiële AfvalConversie naar Hoogwaardige Transportbrandstoffen. Daarom wil ik ook graag de andere mensen binnen dit project bedanken voor hun samenwerking: Kelly Chan, Leo de Graaff, Jan Springer en Johan Sanders. Hoewel ik uiteindelijk een andere weg ben ingeslagen dan oorspronkelijk de bedoeling was, vond ik het leuk om binnen een breder project te werken. Kelly, en ook Nicky Pansters, dank jullie wel voor de stammen die we hebben kunnen testen. Johan, dankjewel voor je input voor hoofdstuk 7. Daarnaast wil ik ook de leden van de klankbordgroep bedanken die ons vanuit de praktijk van tips hebben voorzien.

Packo, Maartje en Marjoleine, vier jaar lang hebben wij een kamer gedeeld, en samen met dat ook vele goede gesprekken over begeleiders, statistiek, modellen en allerlei onzin. Het vond het ook erg leuk om samen het sinterkerstdiner te organiseren. Ik ben nu de derde (en helaas laatste) van ons die promoveert. Dank jullie wel voor het goede gezelschap! Anne en Lenneke, jullie ook dankjewel voor het gezellige laatste half jaar, hoewel ik toen alleen nog maar over zwangerschap kon praten…

Iedereen van proceskunde, zowel BPE als FPE, dank jullie wel voor de gezelligheid tijdens de koffiepauzes, lunches, labuitjes, AIO-reizen en andere activiteiten. Ik wil geen namen noemen omdat ik bang ben om mensen te vergeten, dus bij deze iedereen bedankt! Ik heb me al die jaren prima thuisgevoeld op de zesde. Frank and Mgeni, although we did not really share our topic, we shared the lab, Sebastiaan and Arjen, which made me feel very connected to you. Thank you both for that. Mgeni, thank you for being my witness at my wedding, and I hope we will

stay friends for a long time. Annette, dank je wel voor het zingen op mijn bruiloft, en het organiseren van mijn vrijgezellenfeestje.

Geen resultaten zonder ontspanning af en toe, en die vond ik vooral bij muziekvereniging Fidelio. Dank jullie wel voor de muziek en de gezelligheid. En natuurlijk wil ik ook Anne, Gerard, Renée en Iris bedanken dat zij het het afgelopen jaar mogelijk hebben gemaakt dat Martin en ik allebei konden gaan toeteren door op de babyfoon te passen. Beter een goede buur dan een verre vriend!

Ook mijn familie en schoonfamilie wil ik bedanken voor hun interesse en steun, en voor het passen op Sander zodat ik weer eens aan mijn proefschrift kon werken. Marco, bedankt dat je mijn paranimf wilt zijn.

En last but not least natuurlijk Martin en Sander. Sander, jij hebt de afgelopen anderhalf jaar papa en mama weinig samen gezien omdat mama steeds moest typen als papa er was, maar hopelijk wordt dat nu anders. Martin, ik kan je niet genoeg bedanken, vooral voor de laatste anderhalf jaar. Door dat proefschrift van mij moest jij al het huishoudelijke werk doen naast je baan, elke keer maar weer wat verzinnen met Sander, en intussen hopen dat ik een beetje op ging schieten. Dankjewel voor je geduld, en voor je hulp met de laatste loodjes toen mijn RSI toch weer terug kwam door de stress van de deadlines. Ik hoop dat we nu weer tijd hebben voor elkaar. Ik hou van jullie!

Curriculum vitae

Petra Meeuwse was born in The Hague on March 9th 1979. She attended the Buys Ballot College in Goes, from which she graduated (Gymnasium/VWO) in 1997. Subsequently, she started the study bioprocess technology at Wageningen University. During this study, she did three master theses. The first thesis was carried out at IsoTis N.V. and the process engineering group of Wageningen University, in which she investigated the influence of oxygen on the proliferation and redifferentiation of bovine chondrocytes. In her second master thesis, she studied the activity of epoxide hydrolase from *Rhodotorula glutinis* on methyl-substituted oxaspiro-octanes at the organic chemistry group of Wageningen University. Both of these theses resulted in an article in a peer-reviewed journal. For her third master thesis, she went to Trondheim, Norway to study carotenoid production by mutants of *Phaffia rhodozyma* at SINTEF and the Norwegian University of Technology (NTNU). She graduated in November 2004. In March 2005, she started her PhD project at Bioprocess Engineering, Wageningen University, which resulted in this thesis.

List of Publications

Malda J, Van den Brink P, Meeuwse P, Grojec M, Martens DE, Tramper J, Riesle J, Van Blitterswijk CA, 2004. Effect of oxygen tension on adult articular chondrocytes in microcarrier bioreactor culture. Tissue Eng 10: 987-994.

Weijers C, Meeuwse P, Herpers R, Franssen MCR, Sudholter EJR, 2005. Stereoselectivity and substrate specificity in the kinetic resolution of methyl-substituted 1-oxaspiro[2.5]octanes by *Rhodotorula glutinis* epoxide hydrolase. J Org Chem 70: 6639-6646.

Meeuwse P, Tramper J, Rinzema A, 2011. Modeling lipid accumulation in oleaginous fungi in chemostat cultures. I: Development and validation of a chemostat model for *Umbelopsis isabellina*. Bioprocess Biosyst Eng 34: 939-949

Meeuwse P, Tramper J, Rinzema A, 2011. Modeling lipid accumulation in oleaginous fungi in chemostat cultures. II: Validation of the chemostat model using yeast culture data from literature. Bioprocess Biosyst Eng 34: 951-961

Meeuwse P, Akbari P, Tramper J, Rinzema A. Modeling growth, lipid accumulation and lipid turnover in submerged batch cultures of *Umbelopsis isabellina*. Bioprocess Biosyst Eng DOI: 10.1007/s00449-011-0632-x.

Meeuwse P, Klok AJ, Haemers S, Tramper J, Rinzema A. Growth and lipid production of *Umbelopsis isabellina* on a solid substrate - Mechanistic modeling and validation. Submitted

Meeuwse P, Sanders J, Tramper J, Rinzema A. Lipids from yeasts and fungi: tomorrow's source of biodiesel? To be submitted.

Overview of completed training activities

Discipline specific courses

Bioreactor design and operation (2006)
Reaction kinetics in food science (2006)
Sustainable process, product and systems design (2007)
A unified approach to mass transfer (2007)
Downstream processing (2007)

General courses

PhD competence assessment (2006)
Avatar^{TM} self-management (2006)
Supervising BSc and MSc theses (2005)
Techniques for writing and presenting a scientific paper (2006)
Scientific writing (2008)
Career perspectives (2008)

Congresses

Netherlands Process Technology Symposium (2005, 2008)
Netherlands Biotechnology Congress (2006, 2008)
BSDL symposium (2006, 2007)
Renewable Resources and Biorefineries Conference (2008)

Optionals

Preparation of research proposal (2005)
Brainstormweek Process engineering (2005)
PhD excursion to Denmark and Sweden (2006)
PhD excursion to Japan (2008)

Part of the work presented in this thesis was financed by the DEN program of SenterNovem under project number 2020-03-12-14-006.

Cover: Microscopic picture of pellets of *U. isabellina* in submerged culture.
P Meeuwse, 2006